NOVEL MODALITIES OF T AND B LYMPHOCYTE MIGRATION

Ervin Kara, B. Sc. (Hons)

A thesis submitted for the fulfillment of the Degree of Doctor of Philosophy

School of Biological Sciences

University of Adelaide

Adelaide, South Australia, Australia

TABLE OF CONTENTS

DECLARATION

I certify that this work contains no material which has been accepted for the award of any other degree or diploma in my name, in any university or other tertiary institution and, to the best of my knowledge and belief, contains no material previously published or written by another person, except where due reference has been made in the text. In addition, I certify that no part of this work will, in the future, be used in a submission in my name, for any other degree or diploma in any university or other tertiary institution without the prior approval of the University of Adelaide and where applicable, any partner institution responsible for the joint-award of this degree.

I give consent to this copy of my thesis when deposited in the University Library, being made available for loan and photocopying, subject to the provisions of the Copyright Act 1968. The author acknowledges that copyright of published works contained within this thesis resides with the copyright holder(s) of those works.

I also give permission for the digital version of my thesis to be made available on the web, via the University's digital research repository, the Library Search and also through web search engines, unless permission has been granted by the University to restrict access for a period of time.

Ervin Kara

For a thesis that contains publications:

I certify that this work contains no material which has been accepted for the award of any other degree or diploma in my name, in any university or other tertiary institution and, to the best of my knowledge and belief, contains no material previously published or written by another person, except where due reference has been made in the text. In addition, I certify that no part of this work will, in the future, be used in a submission in my name, for any other degree or diploma in any university or other tertiary institution without the prior approval of the University of Adelaide and where applicable, any partner institution responsible for the joint-award of this degree.

I acknowledge that copyright of published works contained within this thesis resides with the copyright holder(s) of those works.

I also give permission for the digital version of my thesis to be made available on the web, via the University's digital research repository, the Library Search and also through web search engines, unless permission has been granted by the University to restrict access for a period of time.

I acknowledge the support I have received for my research through the provision of an Australian Government Research Training Program Scholarship.

Ervin Kara

ACKNOWLEDGMENTS

A very special thank you to Prof. Shaun McColl and Dr. Iain Comerford for everything that you have taught me and to the amazing opportunities that you afforded me during my PhD. I am very thankful to have had the chance to be trained by the both of you. I have been a student of yours since the second year of my bachelor degree. I am deeply grateful to have had you both as a mentor for the entirety of my undergraduate and postgraduate scientific training. I thank you for all of the advice you have given me on all topics ranging from all things science to personal matters. I hope to get the chance to collaborate with you both as long into the future as you will allow.

Big thank you to the McColl lab members in particular Cameron, Duncan, Kevin and Carly for the discussions, laughs and general horseplay. Thank you in particular to Adriana (the lab mum) for everything you do have done for me and the lab.

To my mother Frida Kara, my father Neal Kara, my brother Emren and sisters Denise and Ela, this thesis is dedicated to you. Mum, you are a saint of a human being. Emren, thank you for all of your advice growing up and for everything you have taught me from a young age.

Biggest thanks is reserved to my girlfriend Rachelle. Through all of the long days and nights that come with doing a PhD, you remained by my side. Looks like many more years together which I assure you is your problem and not mine.

ABBREVIATIONS

ACKR4 – Atypical chemokine receptor 4

AHR – Aryl hydrocarbon receptor

BATF – Basic leucine zipper transcription factor

CKR – Chemokine receptor

CNS – Central nervous system

DZ – Dark zone

EAE – Experimental autoimmune encephalomyelitis

EBI2 – Epstein-Barr virus-induced G-protein coupled receptor 2

EBM – Early memory B cell

Eomes – Eomesodermin

Fo – Follicular

GC – Germinal center

GM-CSF – Granulocyte-macrophage colony stimulating factor

HEL – Hen egg lysozyme

IFN – Interferon

IL – Interleukin

IRF – Interferon regulatory factor

KLH – Keyhole limpet hemocyanin

LZ – Light zone

MHC – Major histocompatibility complex

MOG – Myelin oligodendrocyte glycoprotein

MS – Multiple sclerosis

MZ – Marginal zone

NP – (4-hydroxy-3-nitrophenyl)acetyl

PB – Plasmablast

PLP – Proteolipid protein

ROR – RAR-related orphan receptor

SRBC – Sheep red blood cell

T-bet – T-box transcription factor

TFH – T follicular helper

TFR – T follicular regulatory

TGF – Transforming growth factor

Th – T helper

TNF – Tumor necrosis factor

Treg – Regulatory T cell

WT – wild-type

ABSTRACT

IL-17-producing helper T (Th17) cells are critical for host defense against extracellular pathogens but also drive numerous autoimmune diseases. Th17 cells that differ in their inflammatory potential have been described including IL-10-producing Th17 cells that are weak inducers of inflammation and highly inflammatory, IL-23-driven, GM-CSF/IFNγ-producing Th17 cells. However, their distinct developmental requirements, functions and trafficking mechanisms *in vivo* were poorly understood. The results presented in chapter two of this thesis describe a temporally regulated IL-23-dependent switch from CCR6 to CCR2 usage by developing Th17 cells that is critical for pathogenic Th17 cell-driven inflammation in experimental autoimmune encephalomyelitis (EAE). This switch defines a unique *in vivo* cell surface signature (CCR6(-)CCR2(+)) of GM-CSF/IFNγ-producing Th17 cells in EAE and experimental persistent extracellular bacterial infection, and in humans. Using this signature, this work describes an IL-23/IL-1/IFNγ/TNFα/T-bet/Eomesodermin-driven circuit driving GM-CSF/IFNγ-producing Th17 cell formation *in vivo*. Thus, these results identify a unique cell surface signature, trafficking mechanism and T-cell intrinsic regulators of GM-CSF/IFNγ-producing Th17 cells.

Activated B cells can initially differentiate into three functionally distinct fates-early plasmablasts (PBs), germinal center (GC) B cells, or early memory B cells by mechanisms that remain poorly understood. Here, the results presented in chapter three of this thesis identify atypical chemokine receptor 4 (ACKR4), a decoy receptor that binds and degrades CCR7 ligands CCL19/CCL21, as a regulator of early activated B cell differentiation. By restricting initial access to splenic interfollicular zones (IFZs), ACKR4 limits the early proliferation of activated B cells, reducing the numbers available for subsequent differentiation. Consequently, ACKR4 deficiency enhanced early PB and GC B cell responses in a CCL19/CCL21-dependent and B cell-intrinsic manner. Further, aberrant localization of ACKR4-deficient activated B cells to the IFZ was associated with their preferential commitment to the early PB linage. These results reveal a regulatory mechanism of B cell trafficking via an atypical chemokine receptor that shapes activated B cell fate.

CHAPTER ONE:

INTRODUCTION

1.1 Introduction

The adaptive immune system mobilizes highly specific and tailored humoral and cellular defense mechanisms to defend the threat to homeostasis posed by invading pathogens. The ability of this system to respond against a theoretically infinite number of pathogens broadly stems from the diversity of V, (D) and J gene segments that encode antigen-specific receptors and the randomness by which these genes are recombined in the germline during B and T lymphocyte development. These processes give rise to a diverse, clonally-distinct repertoire of B and T lymphocytes which express unique antigen receptors, known as the B cell receptor (BCR) and T cell receptor (TCR) respectively, specific for a single antigenic epitope. Upon pathogen encounter, B and T cell clones that bear an antigen receptor specific to foreign antigens are selectively activated and expanded. The diversity generated as a result of V(D)J recombination coupled with the processes of selection and expansion of rare clones specific to the invading pathogen broadly underlies the ability of this system to elicit these defense mechanisms against pathogens in an incredibly specific manner. Adaptive humoral and cell-mediated immune responses are not only specific in nature but can be tailored in their functional properties to efficiently and appropriately deal with the nature of the pathogenic threat encountered. For example, antibody responses can be tailored via the mechanism of class switch recombination which genetically combines the clonally-selected paratope of an antibody with a specific class of antibody isotype, which tailors the physiological outcome of this response to the nature of threat encountered. Further, pathogen-specific $CD4^+$ T cells orchestrate immune responses by differentiating into discrete subsets of effector T helper cells defined by their production of distinct cytokine signatures that elicit pathogen-tailored innate immune responses. The tailored nature of adaptive immunity results from a complex web of bidirectional intercellular communication events between innate and adaptive immune cells. Activation and fate of clonally selected adaptive immune cells is strongly influenced by innate effector cells, and orchestration of adaptive responses to pathogens require synergistic collaboration with the innate immune system to efficiently resolve infection.

Success of adaptive immunity relies on seemingly statistically improbable cellular encounters between rare antigen-specific lymphocytes and cells of the innate immune system. Complex mechanisms of cellular migration have evolved to facilitate these rare cellular encounters. These mechanisms operate both at the level of immune priming in secondary lymphoid organs, to guide the processes of clonal selection and enable innate immune cell-mediated control over the developing adaptive response; and at site of infectious encounter where antibodies and cell-mediated immunity execute their effector function (*1*). Central to the molecular mechanisms that coordinate immune cell trafficking are chemokines, a family of structurally related cytokines specific for G-protein-coupled serpentine transmembrane receptors predominantly expressed on the surface of immune cells. The chemokine and chemokine receptor system apparently displays a large degree of functional redundancy, with multiple ligands for several receptors, and some receptors able to respond to multiple chemokine ligands. In humans 18 signaling chemokine receptors and over 50 chemokine ligands are present to provide robust co-ordination of the vast array of cellular trafficking events in the immune system (*2*). How this family of molecules controls the complex migration patterns of multiple leukocyte subsets in both homeostasis and during immune responses remains a key question in immunology.

1.2 Th17 cell differentiation, migration and function

Th17 cells were first described in 2005 when the research of two independent laboratories identified a population of effector Th cells that developed independently of Th1 and Th2 cell lineages and expressed the inflammatory cytokines IL-17A and IL-17F (*3, 4*). Th17 cells are characterized by the expression of their master transcriptional regulator RORγt (*5, 6*) and have since been described to possess a diverse cytokine-secreting potential including IL-2, IL-9, IL-10, IL-22, IFNγ, GM-CSF and TNF (*7*). Th17 cells have been shown to form an important component of protective immunity in the context of extracellular bacterial and fungal pathogens. Through the induction of the inflammatory chemotactic factors CXCL1, CXCL2, CXCL5, and CXCL8 at sites of inflammation via production of IL-17A/F, IL-22, and GM-CSF, Th17 cell-mediated responses are dominated by the inflammatory and phagocytic functions of neutrophils (*8*). Other Th17 cell-mediated functions include induction of antimicrobial peptides (including S100 proteins and β-defensins), promotion of granulopoiesis via induction of G-CSF, and enhancement of monocyte and neutrophil activation to promote their phagocytic activity. However, when misdirected, Th17 cells have been shown to be key drivers of pathogenesis in numerous models of autoimmune pathology including experimental autoimmune encephalomyelitis (EAE) and collagen-induced arthritis (CIA), mouse models of multiple sclerosis (MS) and rheumatoid arthritis, respectively, where production of Th17 cell-derived inflammatory factors promotes pathological destruction of host tissue (*2*).

An emerging concept in the field of Th17 cell biology is the existence of a spectrum of Th17 cell phenotypes that differ in their inflammatory potential and differentiation requirements (*9*). Differentiation of Th17 cells from naïve $CD4^+$ T cell precursors *in vitro* can be induced by the polarizing cytokines IL-6 and transforming growth factor (TGF)-β1 (*10-12*). Signal transduction downstream of these cytokines, including nuclear translocation of STAT3 and induction of transcription factors IRF4 and BATF, ultimately induces expression of RORγt which directly transcribes *Il17a* and *Il17f* (*5, 6, 13-15*). IL-6 mediated induction of IL-21 during Th17 cell differentiation reinforces Th17 lineage commitment via amplification of STAT3 activation via IL-21 receptor signaling in an autocrine manner (*16, 17*). TGF-β1/IL-6-driven Th17 cells co-express the immunoregulatory cytokine IL-10 via the transcription factors c-Maf and aryl hydrocarbon receptor (AHR) (*18-21*), are relatively weak inducers of inflammation (*18-20*) and can possess regulatory function (*18, 22*). Conversely, differentiation of highly inflammatory subsets of Th17 cells is critically dependent on the function of IL-23 (*19, 20, 23-28*) which induces expression of the inflammatory cytokines GM-CSF and IFNγ (*23, 25, 27-29*). Numerous lines of evidence have demonstrated that IL-23-driven Th17 cells drive pathogenesis of $CD4^+$ T cell driven autoimmune pathologies in mice including EAE and CIA (*7*). Specifically, IL-23-dependent induction of GM-CSF in Th17 cells was recently identified as the critical disease-initiating cytokine in EAE via the mobilization of inflammatory $CCR2^+Ly6C^+$ monocyte responses in the CNS (*23, 25, 27, 30*). In humans, Th17 cells that express GM-CSF or IFNγ are enriched in CNS lesions of patients with multiple sclerosis, suggesting that these cells are relevant in the context of human autoimmunity (*31, 32*). Th17 cells with pathogenic function can be generated *in vitro* from naïve $CD4^+$ T cell precursors in the absence of TGF-β1, in an IL-6-, IL-1β- and IL-23-dependent manner (*19*). Using IL-23R-deficient antigen-specific $CD4^+$ T cells, McGeachy et al. demonstrated that IL-23 was not required for the initial specification of Th17 cells from naïve precursors *in vivo* (*33*). Instead, absence of IL-23 signaling limited their subsequent expansion, maturation and acquisition of an inflammatory cytokine-secreting repertoire (*33*). These data support a step-wise model of inflammatory Th17 cell differentiation wherein initial commitment to the Th17 cell lineage differentiation occurs independently of IL-23, which subsequently drives committed Th17 cell precursor expansion and amplification of inflammatory function. Thus, it is likely that Th17 cells in any given response may comprise a heterogeneous population of distinct types of Th17 cells that arise in discrete cytokine microenvironments, possess distinct but similar transcriptomes, and subsequently possess distinct cytokine-secreting repertoires and functions. Th17 cells of differing inflammatory potential have been studied predominantly using *in vitro*-based systems in the context of autoimmune reactions. Thus, evidence for the existence of these Th17 cell phenotypes *in vivo* is limited. Further, how Th17 cells with distinct phenotypes contribute to protective immunity remains poorly defined.

Consistent with the recent description of a spectrum of activities ranging from regulatory to highly inflammatory, Th17 cells migrate to diverse functional sites within the body ranging from anatomical barriers to sites of chronic infection/inflammation. Migratory properties of effector Th cells are imprinted during differentiation with induction of chemokine receptors that enable their trafficking from secondary lymphoid tissue to effector sites. Th17 cells, together with regulatory T cells (Treg) characteristically express the chemokine receptor CCR6, which binds its sole ligand CCL20 that is present at mucosal surfaces including skin and intestine at rest, but is also rapidly induced in the context of inflammation (*34*). CCR6 induction is closely linked with TGFβ1/IL-6-driven Th17 cell differentiation and has been shown to be transcriptionally regulated by RORγt in both mice and human (*35, 36*). In EAE, a two-wave model for Th17 cell migration to the CNS has been described where, in the first wave, CCR6 facilitates the entry of Th17 cells into the uninflamed CNS via CCL20 that is constitutively expressed in the lateral ventricles of the choroid plexus, followed by subsequent waves of CCR6-independent Th17 cell trafficking into the inflamed CNS (*37*). In that study, CCR6-deficient mice were shown to be resistant to the induction of EAE, suggesting that CCR6/CCL20 is the sole and critical chemokine receptor axis driving Th17 cell trafficking to the CNS in this model. However, more recent evidence has revealed that CCR6 is largely dispensable for EAE pathogenesis (*38, 39*), with a report indicating that absence of CCR6 results in the exacerbation of disease due to defective CCR6-dependent Treg CNS infiltration (*39*). These studies indicate the existence of other, perhaps more critical, trafficking receptors that coordinate Th17 cell trafficking to sites of inflammation *in vivo*. At the time this research was conducted, the molecular basis of CCR6-indepednent mechanisms of Th17 cell trafficking was unknown and migratory receptors that differentially recruited Th17 and Treg cells were not yet identified. These questions were addressed in chapter 2 of this thesis.

1.3 B cell migration after antigen encounter

Upon encounter with their cognate antigen, B cells dynamically regulate expression of chemoattractant receptors, coordinating their migration to distinct lymphoid niches that promote their expansion and differentiation (*40, 41*). Experimental evidence, flowing predominantly from the study of monoclonal immunoglobulin (Ig) transgenic B cell responses to model antigens of defined initiating affinities and avidities, has indicated that the coordinated movements of B cells within lymphoid organs following antigen-engagement are regulated by their spatio-temporal responsiveness to ligands of the chemoattractant receptors EBI2, CCR7 and CXCR5.

Within an hour of BCR-engagement, *Ebi2* transcript is upregulated resulting in the initial migration of B cells toward the oxysterol-rich outer regions of the B cell follicle (*42-47*). EBI2-dependent positioning in the outer follicle occurs as early as 3 hours after antigen-engagement and is hypothesized to draw cells nearer the source of antigen to consolidate their activation (marginal sinuses in the spleen where blood flows; supcapsular sinus conduits where antigen drains) (*42, 43, 48*). Within 6 hours, CCR7 is induced, driving the migration of antigen-engaged B cells toward the T cell zone where an FRC-derived CCL21 gradient emanates into the B cell follicle from the T cell zones (*49, 50*). EBI2, CXCR5 and CCR7 function in concert to promote the lateral spreading of activated B cells along the T cell zone/B cell zone (T/B) boundary, hypothesized to maximize their interactions with cognate pre-T follicular helper (TFH) cells (*42, 43, 46, 47, 49, 50*) which have localized to this boundary via CXCR5 and EBI2 following DC-mediated activation in the T cell zones (*51-54*). Cognate interactions with T cells at this boundary results in CD40-dependent and EBI2-driven migration of B cells to the outer regions of the follicle and within interfollicular zones (in LN defined as the lateral poles of B cell follicles; in spleen the lateral poles of B cell follicles that are proximal to marginal zone bridging channels) within 48 hours of antigen encounter (*42, 43, 46, 47*). Intravital microscopy and detailed histological mapping of activated B cell migration during the early stages after activation have indicated that responding B cells initiate their proliferation in this region of the follicle (*47, 50, 55*). Proliferating B cells then trifurcate their differentiation trajectories down early plasmablast (PB), germinal center (GC) B cell and/or GC-independent early memory (EM) B cell pathways (*56-58*). Differentiation into these cell fates is coupled with the induction of a unique migratory program that facilitates their movement to defined microenvironments in the SLOs that support their effector function.

1.3.1 Germinal center B cells

Differentiation of GC B cells from activated B cell precursors is coupled with the downregulation of EBI2, drawing cells from the interfollicular zones and outer follicular regions into the follicle center (*46, 47*). *Ebi2* downregulation is mediated by the transcriptional repressor B cell lymphoma (BCL)6 (*59*), a critical transcriptional regulator of the GC B cell program (*60*). Expression of BCL6 can be detected in blasting B cells localized in interfollicular and outer follicular areas (*61, 62*), suggesting that cells committed to the GC B cell fate reduce their ability to respond to oxysterol ligands present in this zone (*44, 45*), and subsequently migrate toward the FDC-rich follicle center via CXCR5, S1PR2 and CXCR4 (*63, 64*). This event marks the formation of the GC structure.

GCs are the site of antibody affinity maturation, a process that results in an increase in affinity of serum antibody to the initiating antigen over time (*65-68*). GCs can be separated into two anatomically-distinct compartments: i) the light zone (LZ), the site of T cell-mediated affinity-based selection of GC B cells; and ii) the dark zone (DZ), where GC B cells rapidly proliferate and diversify their Ig genes via the processes of activation-induced cytidine deaminase (AID)-mediated somatic hypermutation (*65, 68*). Contemporary views of GC dynamics describe a T cell-centric governance of affinity maturation in a model known as ‘cyclic re-entry’ described below.

In the LZ of the GC, B cells compete for antigen displayed in the context of immune complexes on the surface of follicular dendritic cells (*69-71*). The amount of antigen captured by a LZ B cell clone reflects their intrinsic BCR affinity to the initiating antigen, wherein high affinity B cells capture, endocytose, process and present more peptide in the context of MHC-II than neighboring LZ B cells of lower affinity (*72, 73*). Tfh cells, which localize to the GC LZ following further upregulation of CXCR5 and S1PR2 as a result of B cell interactions at the T/B boundary (*51, 74*), are limiting in the GC and preferentially interact with LZ B cells with high surface peptide-MHC-II abundance (*75-78*). B-T-cell interactions in the LZ occur through feed-forward receptor-ligand interactions and T cell secretion of cytokines (*79-81*), prompting selected B cells to enter the cell cycle and migrate to the DZ of the GC (*78, 82-84*). Here, selected cells randomly introduce mutation(s) in their Ig genes and rapidly proliferate in a manner that is proportional to the strength of T cell help received (*82, 83*). As a result, daughter cells of DZ B cells express variations of their parental Ig and re-enter the LZ to test their new BCR (*75, 78*). Iterative rounds of Darwinian-like selection of high affinity mutants in the LZ, and further Ig diversification of selected cells as a result of SHM in the DZ increases the net affinity of B cell clones per GC with time (*65*). Though the cues governing post-GC fate decisions remain unclear, GC B cells can exit this reaction as long-lived plasma cells, which seed bone marrow niches and elicit long-term antibody with increased neutralization properties, or GC-dependent memory B cells, which possess the ability to rapidly form plasma cells or re-enter GCs for further antibody diversification upon re-exposure to antigen (*85*).

1.3.2 Early plasmablasts

Commitment of activated B cells to the early PB fate is coupled with the downregulation of CXCR5 and induction of CXCR4 (*86*). As a result, antigen-engaged B cells committed to the early PB lineage lose responsiveness to CXCL13-rich follicle retention cues and migrate toward a CXCL12 gradient that emanates from the splenic red pulp via marginal zone bridging channels, or the medullary chords of reactive LNs via the T cell zone (*86, 87*). Early PBs are short-lived and elicit the first line of antigen-specific antibody (*57*). In the majority of cases, early PB-elicited antibody is germline-encoded and is qualitatively of lower affinity to somatically-mutated GC-dependent antibody (*57*).

Differentiation of early PBs have been shown to be critically dependent on EBI2 (*40, 47*). EBI2-deficient monoclonal Ig transgenic B cells, which are defective in their ability to access splenic interfollicular zones and bridging channels, fail to form early PBs, whereas activation of B cells that transgenically overexpress EBI2 cells greatly enhances this response (*47*). The cellular and molecular events that promote early PB responses in this niche remain poorly defined, although DCIR2^{+} dendritic cells which localize to splenic interfollicular zones are implicated as potential regulators of this process (*88, 89*).

1.3.3 Early memory B cells

More recently it has been shown that activated B cells can exit the reaction at an early stage of the response as GC-independent early memory (EM) B cells (*56*). These cells have been shown to have proliferated extensively but have exited the cell cycle, lack Ig mutations or class switch recombination, exit the reaction independently of BCL6 expression (i.e. are of non-GC origin) and can be found in distal lymph nodes after immunization (*55, 90-93*). Little is known about the migratory receptors expressed by these cells, but it is thought that EMB cells adopt a similar trafficking receptor expression profile to naïve follicular B cells, enabling their recirculation through lymphoid organs. To date, the role of EMB cells in the context of memory responses remains to be definitively determined as these cells have been shown to expand and differentiate with similar kinetics to *bona fide* naïve Fo B cells upon antigen re-encounter (*94, 95*).

1.3.4 Atypical chemokine receptor 4 (ACKR4)

A subfamily of chemokine receptors known as 'atypical' or 'decoy' receptors has been described (*96*). These atypical chemokine receptors lack demonstrable signaling function and do not mediate chemotactic migration (*96*). The reported function of these receptors is chemokine scavenging or transportation (*96, 97*). The focus of chapter 3 of this thesis is ACKR4 (gene name: *Ccrl1*), the least well characterized member of this family. Ligands for ACKR4 are the homeostatic chemokines CCL19, CCL21 and CCL25, which collectively, control leukocyte homing to, and within SLOs, direct thymocyte migration, and direct leukocyte migration to the small intestine through interactions with one of their signaling chemokine receptors CCR7 (CCL19/21) or CCR9 (CCL25) (*2, 98*). Unlike most typical chemokine receptors, ACKR4 is expressed primarily by stromal, epithelial and endothelial cells and has been reported to be absent on hematopoietic lineages in unimmunized mice (*99*).

ACKR4 constitutively internalizes and degrades CCL19 *in vitro* (*100*), regulates CCL19/CCL21 abundance *in vivo* (*101*), plays an important role in thymocyte development (*102*), alters adaptive immune responses in EAE (*101*), shapes skin CCL19/CCL21 abundance required for activated DC migration into lymphatic vessels (*103*) and establishes a functional CCL21 gradient in LNs facilitating the emigration of DCs (*104*). Despite a previous study indicating that ACKR4 is exclusively expressed in cells of non-hematopoietic origin from unimmunized mice (*99*), genome wide comparisons of gene expression between FoB cells and GCB cells revealed *Ccrl1* as one of the most strongly induced genes in GCB cells (*105, 106*). However, despite the important role of CCR7 on B cells in the development of T-dependent antibody responses, at the time research presented in chapter 3 of this thesis was conducted, the function of ACKR4 in this context was unknown.

1.4 Summary and rationale for this study:

The goal of the research presented in this thesis is to ascertain a more complete understanding of trafficking mechanisms utilized by two important cells of the adaptive immune system: i) a subset of effector helper T (Th) cells known as Th17 cells which form an important component of antigen-specific cellular immunity to extracellular pathogens, but when misdirected can drive pathogenic inflammation; and ii) B cells, which elicit pathogen-specific antibody responses. Questions regarding the migratory mechanisms of these cell types were incompletely understood at the time research presented in this thesis was conducted. Specifically, i) trafficking mechanisms of Th17 cells from sites of immune priming to sites of inflammation, in particular, the CNS during ongoing autoimmune neuro-inflammation were poorly understood, and ii) whether atypical chemokine receptor 4, a receptor identified in this study to be expressed in the B cell compartment, shaped humoral immunity was unknown. These questions were addressed in chapters 2 and 3 of this chapter respectively with the following aims:

Chapter 2: ***To determine which chemokine receptor(s) coordinate Th17 cell migration during inflammation.***

Chapter 3: ***To determine the function of ACKR4 in humoral immunity.***

CHAPTER TWO:

RESULTS -

‘CCR2 defines *in vivo* development and homing of IL-23-driven GM-CSF-producing Th17 cells’

Kara EE *et al*. CCR2 defines *in vivo* development and homing of IL-23-driven GM-CSF-producing Th17 cells. *Nat. Commun*. 6:8644 doi: 10.1038/ncomms9644 (2015)

Statement of Authorship

Title of Paper	CCR2 defines in vivo development and homing of IL-23-driven GM-CSF-proudcing Th17 cells
Publication Status	☑ Published
Publication Details	Published in Nature Communications: Kara, E. E. *et al.* CCR2 defines *in vivo* development and homing of IL-23-driven GM-CSF-producing Th17 cells. *Nat. Commun.* 6:8644 doi: 10.1038/ncomms9644 (2015).

Principal Author

Name of Principal Author (Candidate)	Ervin E. Kara
Contribution to the Paper	Conceived the study, designed all experiments, performed most experiments, analysed all data, interpreted all data, wrote the manuscript
Overall percentage (%)	80%
Certification:	This paper reports on original research I conducted during the period of my Higher Degree by Research candidature and is not subject to any obligations or contractual agreements with a third party that would constrain its inclusion in this thesis. I am the primary author of this paper.
Signature	Date 04/04/2018

Co-Author Contributions

By signing the Statement of Authorship, each author certifies that:

i. the candidate's stated contribution to the publication is accurate (as detailed above);

ii. permission is granted for the candidate in include the publication in the thesis; and

iii. the sum of all co-author contributions is equal to 100% less the candidate's stated contribution.

Name of Co-Author	Duncan R. McKenzie
Contribution to the Paper	Performed experiments
Signature	Date 27/4/2018

Name of Co-Author	Cameron R. Bastow
Contribution to the Paper	Performed experiments
Signature	Date 29/5/2018

Name of Co-Author	Carly E. Gregor

Contribution to the Paper	Performed experiments		
Signature		Date	27/4/18

Name of Co-Author	Kevin A. Fenix		
Contribution to the Paper	Performed experiments		
Signature		Date	29/5/18

Name of Co-Author	Abiodun Ogunniyi		
Contribution to the Paper	Performed experiments		
Signature		Date	27/4/18

Name of Co-Author	James C. Paton		
Contribution to the Paper	Provided reagents		
Signature		Date	27/4/18

Name of Co-Author	Matthias Mack		
Contribution to the Paper	Provided reagents		
Signature		Date	27/4/2018

Name of Co-Author	Diana R. Pombal		
Contribution to the Paper	Performed experiments		
Signature		Date	27/4/2018

Name of Co-Author	Cyrill Seillet

Contribution to the Paper	Provided mice and performed experiments		
Signature		Date	27/4/2018

Name of Co-Author	Bénédicte Dubois		
Contribution to the Paper	Provided human samples		
Signature		Date	27/4/2018

Name of Co-Author	Adrian Liston		
Contribution to the Paper	Supervised human Th17 experiments, critical discussions		
Signature		Date	27/4/2018

Name of Co-Author	Kelli P. A. MacDonald		
Contribution to the Paper	Provided reagents		
Signature		Date	27/4/2018

Name of Co-Author	Gabrielle T. Belz		
Contribution to the Paper	Provided mice		
Signature		Date	27/4/2018

Name of Co-Author	Mark J. Smyth		
Contribution to the Paper	Provided mice, critical discussions		
Signature		Date	27/4/2018

Name of Co-Author	Geoffrey R. Hill

Contribution to the Paper	Provided mice, critical discussions		
Signature		Date	27/4/2018

Name of Co-Author	Iain Comerford		
Contribution to the Paper	Co-supervised the study, analysed, designed and interpreted experiments, wrote the manuscript		
Signature		Date	27/4/18

Name of Co-Author	Shaun R. McColl		
Contribution to the Paper	Co-supervised the study, analysed, designed and interpreted experiments, wrote the manuscript		
Signature		Date	27/4/18

nature COMMUNICATIONS

ARTICLE

Received 13 Aug 2015 | Accepted 15 Sep 2015 | Published 29 Oct 2015

DOI: 10.1038/ncomms9644

OPEN

CCR2 defines *in vivo* development and homing of IL-23-driven GM-CSF-producing Th17 cells

Ervin E. Kara[1], Duncan R. McKenzie[1], Cameron R. Bastow[1], Carly E. Gregor[1], Kevin A. Fenix[1], Abiodun D. Ogunniyi[1,2], James C. Paton[1,2], Matthias Mack[3], Diana R. Pombal[4], Cyrill Seillet[5], Bénédicte Dubois[6], Adrian Liston[4], Kelli P.A. MacDonald[7], Gabrielle T. Belz[5,8], Mark J. Smyth[7,9], Geoffrey R. Hill[7,10], Iain Comerford[1,*] & Shaun R. McColl[1,11,*]

IL-17-producing helper T (Th17) cells are critical for host defense against extracellular pathogens but also drive numerous autoimmune diseases. Th17 cells that differ in their inflammatory potential have been described including IL-10-producing Th17 cells that are weak inducers of inflammation and highly inflammatory, IL-23-driven, GM-CSF/IFNγ-producing Th17 cells. However, their distinct developmental requirements, functions and trafficking mechanisms *in vivo* remain poorly understood. Here we identify a temporally regulated IL-23-dependent switch from CCR6 to CCR2 usage by developing Th17 cells that is critical for pathogenic Th17 cell-driven inflammation in experimental autoimmune encephalomyelitis (EAE). This switch defines a unique *in vivo* cell surface signature (CCR6 CCR2^{+}) of GM-CSF/IFNγ-producing Th17 cells in EAE and experimental persistent extracellular bacterial infection, and in humans. Using this signature, we identify an IL-23/IL-1/IFNγ/TNFα/T-bet/Eomesodermin-driven circuit driving GM-CSF/IFNγ-producing Th17 cell formation *in vivo*. Thus, our data identify a unique cell surface signature, trafficking mechanism and T-cell intrinsic regulators of GM-CSF/IFNγ-producing Th17 cells.

[1] Department of Molecular and Cellular Biology, School of Biological Sciences, University of Adelaide, Adelaide, South Australia 5005, Australia. [2] Research Centre for Infectious Diseases, School of Biological Sciences, University of Adelaide, Adelaide, South Australia 5005, Australia. [3] Department of Internal Medicine II, University Hospital Regensburg, Regensburg 93042, Germany. [4] Department of Microbiology and Immunology, VIB and University of Leuven, B 3000 Leuven, Belgium. [5] Division of Molecular Immunology, Walter and Eliza Hall Institute of Medical Research, Parkville, Victoria 3052, Australia. [6] Department of Neurosciences, KU Leuven University of Leuven, B 3000 Leuven, Belgium. [7] QIMR Berghofer Medical Research Institute, Herston, Queensland 4006, Australia. [8] Department of Medical Biology, University of Melbourne, Parkville, Victoria 3010, Australia. [9] School of Medicine, University of Queensland, Herston, Queensland 4006, Australia. [10] The Royal Brisbane and Women's Hospital, Herston, Queensland 4029, Australia. [11] Centre for Molecular Pathology, School of Biological Sciences, University of Adelaide, Adelaide, South Australia 5005, Australia. * These authors jointly supervised this work. Correspondence and requests for materials should be addressed to I.C. (email: iain.comerford@adelaide.edu.au) or to S.R.M. (email: shaun.mccoll@adelaide.edu.au).

An emerging concept in inflammatory T cell biology is the existence of a spectrum of T helper 17 (Th17) phenotypes that vary in inflammatory potential. In autoimmunity, Th17 cell subsets that differ both in their developmental requirements and function have been described[1]. Transforming growth factor β1 (TGFβ1) and interleukin 6 (IL 6) drive differentiation of IL 10 producing Th17 cells[2 4], which are weak inducers of inflammation[2 4] and can possess regulatory function[2,5]. Conversely, differentiation and effector function of Th17 cells with pathogenic function is dependent on IL 23 (refs 3,4,6 10), which induces expression of the effector cytokines granulocyte macrophage stimulating factor (GM CSF) and interferon γ (IFNγ)[6,7,11]. It is widely appreciated that IL 23 dependent Th17 cell responses orchestrate numerous $CD4^+$ T cell driven pathologies including experimental autoimmune encephalomyelitis (EAE), the mouse model of multiple sclerosis (MS)[6,7,12]. It has been hypothesized that these two arms of the Th17 cell response evolved to coordinate different domains of protective immunity[12] wherein Th17 cells with a more limited inflammatory potential mediate maintenance of barrier tissue integrity[2,5,13], whereas more inflammatory subsets of Th17 cells amplify inflammation during persistent extracellular bacterial/fungal infection[14,15]. Although these models of Th17 cell biology are a useful construct for conceptualizing how different Th17 cell phenotypes participate in protective/pathological immune responses, present knowledge of distinct Th17 cell phenotypes has predominantly flowed from *in vitro* based systems and is therefore limited. Understanding mechanisms governing development and trafficking of Th17 cells with pathogenic function during autoimmune inflammation is of critical importance as intervention of these processes presents as a tractable target for novel therapeutics.

Migratory properties of effector Th cells are imprinted during differentiation with induction of chemokine receptors that enable their differential trafficking to inflammatory lesions. CCR6 is a homing receptor shared by Th17 and regulatory T cells (Tregs)[16], hypothesized to ensure that Th17 cell responses are closely regulated by Tregs to limit superfluous, and potentially damaging, inflammation[17]. However, emerging evidence suggests the existence of additional, more critical receptors in Th17 migration. In EAE, a 'two wave' model for encephalitogenic Th17 cell recruitment to the central nervous system (CNS) has been proposed where, in the first wave, CCR6 facilitates entry into the uninflamed CNS, followed by subsequent waves of CCR6 independent Th17 cell trafficking into the inflamed CNS[18]. Conversely, more recent studies have demonstrated that CCR6 is largely dispensable for EAE pathogenesis[19,20], suggesting that recruitment of encephalitogenic Th17 cells to the CNS is CCR6 independent. However, the molecular basis for CCR6 independent trafficking of Th17 cells is unknown and migratory receptors that differentially recruit Th17 and Tregs to inflammatory lesions have not been identified.

Here we demonstrate that CCR2, not CCR6, is a key driver of encephalitogenic Th17 cell recruitment into the CNS. Further, we identify GM CSF/IFNγ producing Th17 cells in EAE and persistent extracellular bacterial infection as bearing a CCR6 $CCR2^+$ phenotype in mice and in humans. Conversely, Th17 cells with an IL 10^+ and IL 9^+ cytokine profile, consistent with published descriptions of Th17 cells of more limited pathogenic potential, bear a $CCR6^+CCR2^+$ phenotype *in vivo*. Using these signatures, we demonstrate that an IL 23/IL 1/IFNγ/tumour necrosis factor α (TNFα)/T bet/Eomesodermin driven circuit drives GM CSF/IFNγ producing Th17 cell development *in vivo*. Thus, we report a unique cell surface signature and novel developmental features of GM CSF/IFNγ producing Th17 cells *in vivo* and resolve the outstanding question regarding the molecular control of encephalitogenic Th17 cell trafficking to the CNS in EAE.

Results

Th17 cells express functional CCR2 during inflammation. To identify CCR6 independent mechanisms mediating recruitment of Th17 cells and to compare migratory potential of Th17 and Tregs, we screened for the expression of all known chemokine receptors in $CCR6^+$ and CCR6 subsets of Tregs from B6.*Foxp3*^{GFP} mice and IL 17A $eYFP^+CD4^+$ T cells from B6.*Il17a*^{Cre}*Rosa26*^{eYFP} mice, in which Cre recombinase is driven by *Il17a* promoter activity to permanently mark cells that are currently producing or have previously expressed IL 17A (IL $17A^{+/ex}$) with enhanced yellow fluorescent protein (eYFP)[11] (Supplementary Fig. 1). Notably, high levels of *Ccr2* messenger RNA were apparent in CCR6 $CD4^+$IL $17A^{+/ex}$ cells (Fig. 1a). CCR2 protein was minimally expressed by naive, Th1 and Treg populations from EAE induced wild type (WT) mice, whereas IL 17A producing $CD4^+$ T cells, hereafter termed Th17 cells, expressed either CCR6 and/or CCR2 ($CCR6^+$CCR2 , $CCR6^+CCR2^+$ or CCR6 $CCR2^+$) (Fig. 1b). Functionally, *ex vivo* transmigration assays demonstrated that Th17 cells were the most CCL2 responsive $CD4^+$ T cell subset from EAE mice (Fig. 1c). In the CNS during EAE, the first detectable Th17 cells (day (d)5 post immunization) were predominantly

Figure 1 | Th17 cell recruitment to the CNS is temporally regulated by CCR6 and CCR2. (**a**) Quantitative PCR of *Ccr6* and *Ccr2* transcript in $CCR6^+$ and $CCR6^-$ subsets of $CD4^+$IL-$17A^{+/ex}$ (currently, or previously Th17) cells ($CD3^+CD4^+CD44^{hi}$IL-17AeYFP$^+$–B6.*Il17a*^{Cre}*Rosa26*^{eYFP} mice) and Tregs ($CD3^+CD4^+$Foxp3GFP$^+$–B6.*Foxp3*^{GFP} mice) from the spleen/draining lymph node (dLN) of 5–6 mice d10 post MOG/CFA immunization. Data presented relative to *Rplp0* (mean ± s.d.). (**b**) Representative flow cytometric analysis of CCR6/CCR2 staining on naive $CD4^+$ ($CD3^+CD4^+CD44^{lo}$), Th1 ($CD3^+CD4^+CD44^{hi}$IL-$17A^-$ IFNγ^+), Th17 ($CD3^+CD4^+CD44^{hi}$IL-$17A^+$) and Tregs ($CD3^+CD4^+$Foxp3^+) from the spleen of B6 mice d10 post MOG/CFA immunization. Data are representative of three independent experiments with *n* 3–4 mice per experiment. (**c**) Transwell chemotaxis to CCL20 and CCL2 by indicated T-cell subsets from d10 MOG/CFA-immunized B6 mice. Th17 cells from B6.*Ccr6*$^{-/-}$ and B6.*Ccr2*$^{-/-}$ mice served as CCL20 and CCL2 controls, respectively. Data are representative of two independent experiments with *n* 4 mice per experiment. (**d**) Representative flow cytometric analysis of CCR6/CCR2 staining on Th17 cells ($CD3^+CD4^+CD44^{hi}$IL-$17A^+$) in the dLN, spleen and CNS on d5, 10 and 15 post EAE induction. Data are representative of four independent experiments with *n* 4–6 mice per timepoint. (**e**,**f**) EAE-immunized B6 mice were administered 100 μg of $CCL2_{ala}$ (scrambled peptide control; *n* 5), $CCL20_{6-70}$ (CCR6 antagonist; *n* 4) or $CCL2_{9-76}$ (CCR2 antagonist; *n* 5) i.p. on days 2, 4, 6 and 7 (**e**) or days 8, 10, 12 and 13 (**f**). CNS-infiltrating Th17 cells were quantified 24 h after the final antagonist treatment. (**g**) Schematic of Th17 cell transfer system. (**h**) Number of transferred Th17 cells ($CD3^+CD4^+$IL-$17A^+$CD45.2^+) in CNS 48 h post transfer from $CCL20_{6-70}$ (*n* 5), $CCL2_{9-76}$ (*n* 5) or $CCL2_{ala}$ (*n* 5) treated B6.Ly5.1 recipients pre-immunized for EAE 5 (left) or 15 (right) days prior. (**i**) Number of transferred CD45.2^+ B6 (*n* 5) or B6.*Ccr6*$^{-/-}$ Th17 cells in CNS 48 h post transfer of $CCL2_{ala}$ (*n* 6)- or $CCL2_{9-76}$ (*n* 6)-treated B6.Ly5.1 recipients pre-immunized for EAE 15 days prior. (**j**) Number of transferred CD45.2^+ Th17 cells in CNS 48 h post transfer of PBS (*n* 5)- or anti-CCL2 (*n* 5)-treated B6.Ly5.1 recipients pre-immunized for EAE 15 days prior. (**c**,**e**,**f**,**h**,**i**,**j**) Data are presented as mean ± s.e.m. (**e**,**f**,**h**–**j**) $*P \leq 0.05$, $**P \leq 0.01$; (**e**,**f**,**h**) one-way analysis of variance (ANOVA) with Dunnett's multiple comparisons test relative to control $CCL2_{ala}$-treated group; (**i**) one-way ANOVA with Bonferroni multiple comparisons test; (**j**) unpaired two-tailed Student's *t*-test.

CCR6$^+$CCR2 ; however, as disease progressed, CCR2 expressing Th17 cells bearing CCR6$^+$CCR2$^+$ or CCR6 CCR2$^+$ phenotypes substantially increased in frequency (Fig. 1d). This was mirrored in secondary lymphoid organs (SLOs), as Th17 cells on d5 in the lymph node and spleen were predominantly CCR6$^+$CCR2 , followed by the emergence of CCR6$^+$CCR2$^+$ and CCR6 CCR2$^+$ Th17 cells by d10 post immunization (Fig. 1d). Thus, among the major CD4$^+$ T cell subsets in EAE, functional CCR2 expression is restricted to Th17 cells that arise following emergence of CCR6$^+$ Th17 cells.

CCR2 drives Th17 recruitment to the inflamed CNS. To map the role of CCR6 and CCR2 in temporal regulation of Th17 cell recruitment to the CNS during EAE, we treated mice with peptide antagonists for CCR6 ($CCL20_{6-70}$)[21,22] or CCR2 ($CCL2_{9-76}$)[23]

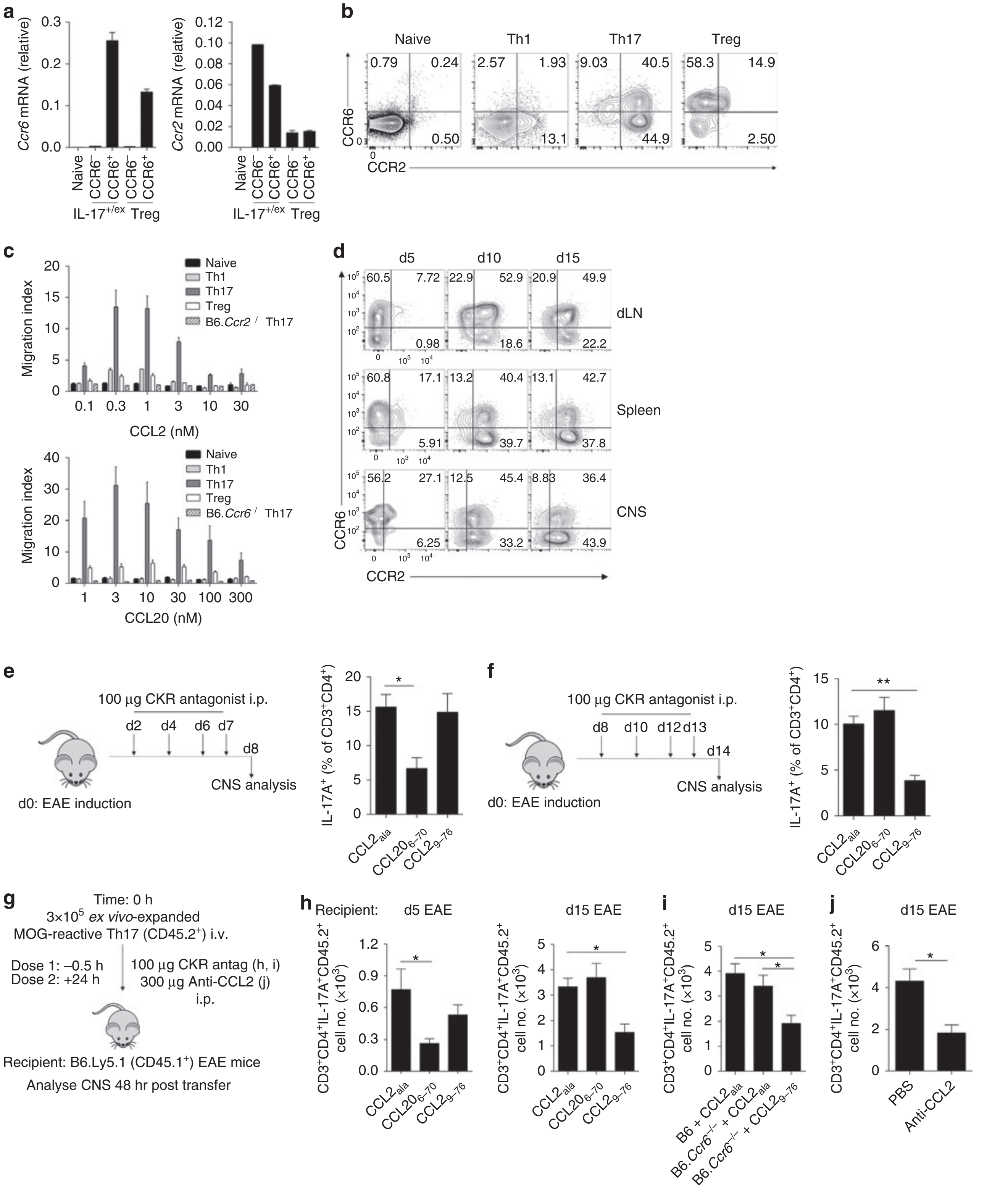

during the pre clinical or effector phases of disease. CCR6 antagonism reduced CNS accumulation of Th17 cells when administered during the pre clinical phase, but did not alter Th17 cell population of the CNS when administered during the effector phase of disease (Fig. 1e,f). Conversely, CCR2 antagonism administered during the effector phase, but not the pre clinical phase of disease, reduced Th17 cell population of the CNS (Fig. 1e,f). To extend these observations, we transferred *ex vivo* expanded myelin oligodendrocyte glycoprotein (MOG) reactive Th17 cells into B6.Ly5.1 recipients pre immunized for EAE either 5 (pre clinical) or 15 (chronic) days prior and concomitantly antagonized CCR6 or CCR2 (Fig. 1g). CCR6 antagonism inhibited CNS accumulation of transferred Th17 cells during the pre clinical but not the chronic phase of EAE, whereas CCR2 antagonism only reduced transferred Th17 cell population of the CNS when administered during the chronic phase of disease (Fig. 1h). Furthermore, transferred *Ccr6* deficient Th17 cells accumulated normally in the CNS of d15 pre immunized recipients, but this was inhibited by concomitant antagonism of CCR2 (Fig. 1i). It has been reported that CCL2 levels in the CNS increase as EAE pathology transitions from pre clinical to peak disease[24], and CCL2 plays an important role in Th17 accumulation in the inflamed CNS, as transferred Th17 cells were less abundant in the CNS of CCL2 neutralized recipients (Fig. 1j). Collectively, these data indicate that CCR6 promotes recruitment of Th17 cells into the CNS at early phases of EAE, whereas CCR2/CCL2 drives Th17 cells into the CNS at later time points, during a CCR6 independent phase of their trafficking.

Having identified CCR2, and not CCR6, as a key receptor driving Th17 cell recruitment to the inflamed CNS in chronic EAE, we next assessed CCR6 and CCR2 function in a model of relapsing remitting EAE. CCL20 was detectable in the CNS at homeostasis, increased during acute disease and remained abundant during remission and relapse (Fig. 2a). Conversely, CCL2 was undetectable in the uninflamed CNS and low during remission, and was most abundant during acute disease and in EAE relapse (Fig. 2a). In keeping with CNS chemokine expression, frequencies of CCR6 $CCR2^+$ Th17 cells were highest during peak acute disease and relapse, whereas CCR6 expressing populations of Th17 cells were more abundant during remission (Fig. 2b). To assess the function of CCR6 and CCR2 in relapse, we treated mice during EAE remission with CCR6 or CCR2 peptide antagonists and assessed molecular, cellular and clinical manifestations of disease relapse. Notably, CCR6 antagonism did not alter the incidence or severity of EAE relapse (Fig. 2c) and led to reduced CNS levels of IL 10, fewer CNS infiltrating Tregs and augmented CNS infiltrating Th17 cells and $Gr1^+$ leukocytes (mostly neutrophils based on scatter analysis) (Fig. 2d f). In contrast, CCR2 antagonism dampened EAE relapse severity (Fig. 2c) with less IL 17A in the CNS and reduced CNS infiltrating Th17 cells (Fig. 2d f). Fewer CNS infiltrating $Gr1^+$ leukocytes and other $CD11b^+$ myeloid cells were also detected in CCR2 antagonized mice (Fig. 2f). Thus, CCR2 drives EAE relapse and promotes Th17 cell responses in the CNS, whereas CCR6 supports optimal Treg responses in these settings.

CCR2 drives GM-CSF-producing Th17 cell homing to the CNS. CCR2 has been previously shown to drive EAE patho genesis[24 26]; however, a T cell intrinsic role for CCR2 has not been clearly demonstrated. Thus, to specifically examine T cell intrinsic functions of CCR6 and CCR2 in T cell trafficking during EAE, we constructed bone marrow (BM) chimeras, reconstituting lethally irradiated B6.Ly5.1 recipients with 80% BM from B6.*Tcra* / donors and 20% BM from either B6, B6.*Ccr6* / , B6.*Ccr2* / or B6.*Ccr6* / .*Ccr2* / donors. Notably, T cell specific deletion of *Ccr2* reduced CNS infiltrating Th17 cells and diminished EAE severity (Table 1 and Fig. 3a,b). In contrast, deletion of *Ccr6* delayed, but ultimately exacerbated EAE without substantially altering CNS infiltrating Th17 cells, but reduced CNS infiltrating Tregs at peak (d14) and chronic (d25) disease (Table 1 and Fig. 3a c). Deletion of both *Ccr6* and *Ccr2* in T cells substantially delayed disease onset (Fig. 3a). However, akin to *Ccr6* deficient T cell chimeras, *Ccr6* / *Ccr2* / T cell chimeric mice ultimately manifest EAE, associated with fewer CNS infiltrating Th17 cells at peak disease, but also reduced frequencies of CNS infiltrating Treg cells at all time points assessed (Table 1 and Fig. 3a c). Fewer CNS infiltrating $Gr1^+$ leukocytes were present in *Ccr2* deficient and *Ccr6*/*Ccr2* deficient T cell chimeras at peak disease, consistent with diminished CNS Th17 cell responses in these mice (Fig. 3d). These data indicate that CCR2 plays a key role in mediating trafficking of T cells with pathogenic function to the CNS during EAE, whereas CCR6 functions as an important axis for Treg function in this model. Recent data have shown that encephalitogenic Th17 cells in EAE produce the inflammatory cytokine GM CSF[6,7]. In keeping with this, T cell specific deletion of *Ccr2* reduced GM CSF^+ Th17 cell abundance in the CNS without altering their development in SLOs (Fig. 3e). Further, GM CSF producing Th17 cells were more abundant in circulation, suggesting that CCR2 drives circulation to CNS trafficking of encephalitogenic Th17 cells (Fig. 3e). To more definitively address this point, we transferred purified *Ccr2* deficient $CD4^+$ T cells into B6.*Rag1* / recipients and induced EAE. In this model, Th17 cells with pathogenic function that arise from transferred $CD4^+$ T cells represent the critical disease initiating cell type[7]. Strikingly, recipient mice receiving *Ccr2* deficient T cells were resistant to EAE (Table 2 and Fig. 3f), exemplifying the critical requirement for CCR2 in encephalitogenic T cell function in this model. Furthermore, although Th17 cell frequencies were equivalent in SLOs (Supplementary Fig. 2), Th17 cells and GM CSF^+ $CD4^+$ T cells were markedly

Figure 2 | CCR2 promotes Th17 cell responses in EAE relapse. (**a**) CCL20 and CCL2 protein abundance in the CNS at indicated stages of EAE in SJL/J mice as determined by ELISA (*n* 5 mice per group). (**b**) Representative flow cytometric analysis and quantification of CCR6/CCR2 staining on CNS-infiltrating Th17 cells ($CD3^+CD4^+IL\text{-}17A^+$) at peak acute disease (left), remission (middle) and relapse (right) of EAE-induced SJL/J mice. Data are representative of two independent experiments with *n* 6 per experiment. (**c**) Clinical disease scores of EAE relapse in SJL/J mice treated with $CCL20_{6\text{–}70}$ (*n* 10), $CCL2_{9\text{–}76}$ (*n* 10) or $CCL2_{ala}$ (*n* 10) i.p. on days indicated by black arrows. Treatment began on the fourth day of remission (disease score ≤ 1 after reaching ≥ 2 prior; d0 on graph). (**d**) IL-17A, IFNγ and IL-10 protein abundance in the CNS of mice on d8 following treatment in **c** as determined by ELISA (*n* 6 per group). (**e**) Representative flow cytometric analysis of IL-17A and IFNγ staining on CNS-infiltrating $CD3^+CD4^+$ cells on d8 following treatment in **c** (*n* 6 per group). Right, quantification of IL-$17A^+$ (Th17), IL-$17A^-$ $IFN\gamma^+$ (Th1) and $Foxp3^+$ (Tregs) cells among CNS-infiltrating $CD3^+CD4^+$ cells. (**f**) Total number of CNS-infiltrating Th17, Th1, Treg cells, $Gr1^+$ leukocytes and other myeloid cells ($CD11b^+Gr1^{lo/-}$) on d8 following treatment in **c** (*n* 6 per group). (**a–f**) Data are presented as mean ± s.e.m.; *$P \leq 0.05$, **$P \leq 0.01$, ***$P \leq 0.001$. (**d–f**) Each dot represents an individual mouse. (**b**) One-way analysis of variance (ANOVA) with Bonferroni multiple comparisons test. (**c**) Two-way ANOVA with multiple comparisons test. (**d–f**) One-way ANOVA with Dunnett's multiple comparisons test relative to control $CCL2_{ala}$-treated group.

reduced in the CNS of B6.*Rag1* $^{/}$ recipients reconstituted with *Ccr2* deficient $CD4^{+}$ T cells (Fig. 3g). Accordingly, fewer CNS infiltrating $Gr1^{+}$ and $Gr1^{lo/}$ $F4/80^{+}$ leukocytes were present in these mice (Fig. 3h). Importantly, GM CSF producing Th17 cells were substantially reduced in the CNS in the absence of CCR2 (Fig. 3i). Collectively, these data indicate that CCR2 drives CNS accumulation of Th17 cells with pathogenic function.

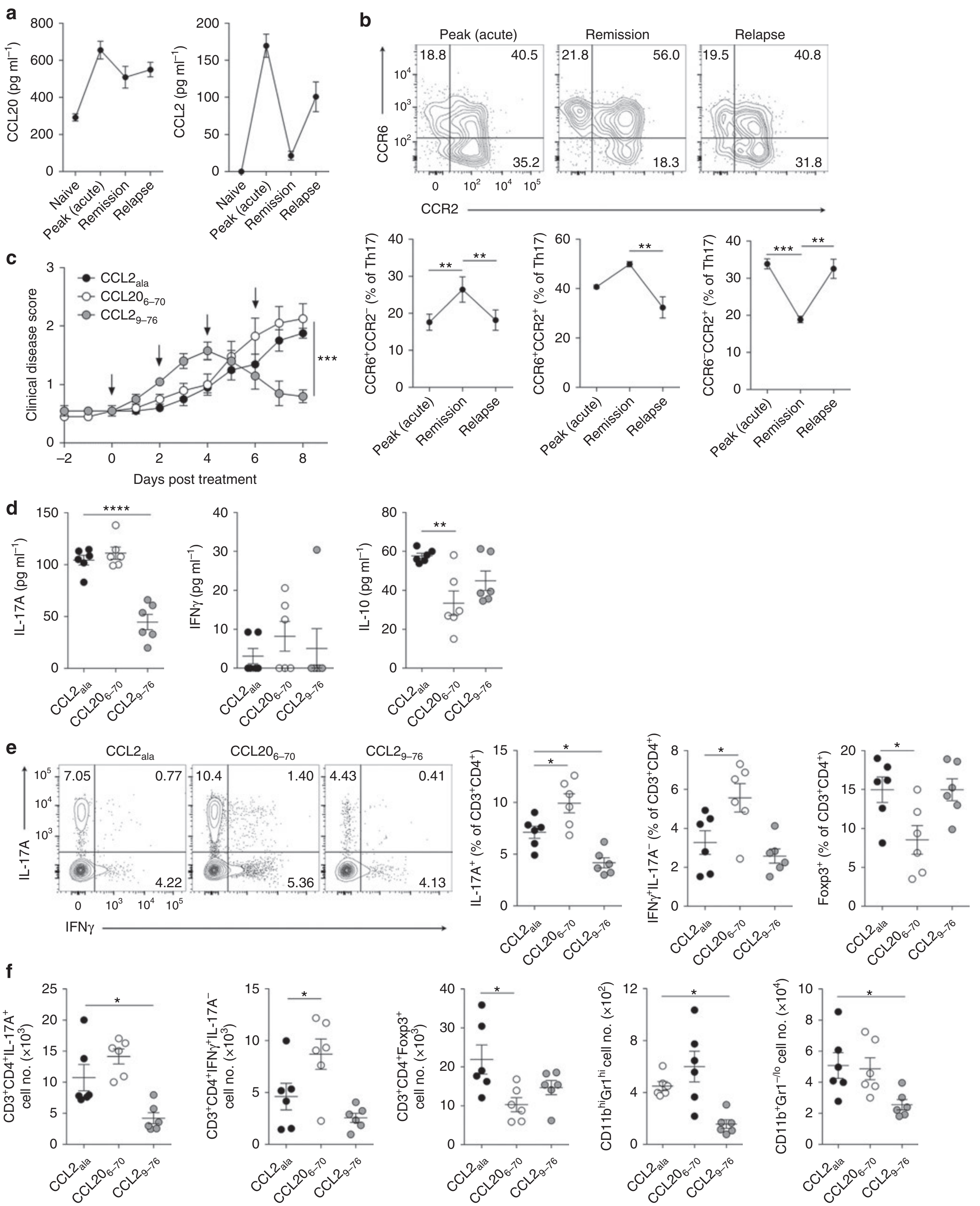

CCR6 CCR2$^+$ defines GM-CSF/IFNγ-producing Th17 cells. Recent work has demonstrated that a shift to GM CSF and IFNγ secreting capability enhances the pathogenicity of Th17 cells[3,6,7,11,27]. Having identified CCR2 as a key receptor driving GM CSF producing encephalitogenic Th17 cell trafficking in EAE, we next examined a possible relationship between the cytokine secreting repertoire of Th17 cells and CCR6/CCR2 expressing Th17 cell types. Strikingly, expression of GM CSF and IFNγ was most abundant in CCR6 CCR2$^+$ Th17 cells (Fig. 4a), which also expressed the highest level of TNFα in the CNS (Fig. 4b). Conversely, IL 10 and IL 9 were confined to CCR6 expressing Th17 cells (Fig. 4a,b). IL 2 was most abundant in CCR6$^+$ Th17 cells in the spleen, although expression in the CNS at peak disease was equally distributed between CCR6$^+$CCR2$^+$ and CCR6 CCR2$^+$ populations (Fig. 4a,b). CCR6 CCR2$^+$ Th17 cells expressed less IL 22 and IL 17F than CCR6$^+$ popu lations (Fig. 4a,b). These data indicate that Th17 cell CCR6/CCR2 expression status can delineate distinct cytokine secreting phenotypes of Th17 cells *in vivo*. Specifically, CCR6 CCR2$^+$ defines GM CSF/IFNγ producing Th17 cells *in vivo* previously described to possess pathogenic function in EAE[3,6,7,27], whereas CCR6$^+$CCR2$^+$ Th17 cells express a distinct cytokine secreting repertoire, including IL 10 and IL 9, consistent with descriptions of Th17 cells with a more limited pathogenic potential[2 5]. CCR6$^+$CCR2 Th17 cells that predominate in the early stages of EAE express a diverse cytokine profile including both inflammatory (IL 17A/F, TNFα, IL 22 and IL 2) and regulatory (IL 10) cytokines.

To determine whether these observations also applied in infectious settings, we examined Th17 cells generated in a model of persistent *Streptococcus pneumoniae* nasopharyngeal coloniza tion. Colonization using *S. pneumoniae* strain EF3030 induces long term focal infection that resolves in B6 mice by 4 weeks post inoculation[28]. Importantly, protection against *S. pneumoniae* nasopharyngeal colonization has been shown to require Th17 cells[29] and GM CSF producing T cells are also produced in response to this infection[30]. *S. pneumoniae* induced Th17 cells were detectable in the spleen by day 7, peaked at d21, remained above baseline 84 days post primary infection and were substantially expanded 5 days post reinfection (Supplementary Fig. 3). The majority of initial (d7 post inoculation) Th17 cells generated in response to infection expressed CCR6 and were followed by the later emergence of CCR6 CCR2$^+$ Th17 cells by d21 post infection (Fig. 4c). CCR6 CCR2$^+$ Th17 cells were still detectable 84 days post primary infection and were substantially expanded 5 days post secondary infection (Fig. 4c), indicating that CCR6 CCR2$^+$ Th17 cells contribute to the memory compartment in this model. Importantly, Th17 populations generated in response to persistent bacterial infection displayed similar cytokine secreting repertoires as observed in EAE, as GM CSF$^+$ or IFNγ$^+$ Th17 cells were found almost exclusively in the CCR6 CCR2$^+$ population (Fig. 4d). Thus, CCR6 CCR2$^+$ defines the GM CSF/IFNγ producing population of Th17 cells that arise in a model of persistent extracellular bacterial infection.

GM CSF or IFNγ producing Th17 cells are enriched in active MS brain lesions[31,32]. Thus, we next examined whether a similar relationship between expression of these cytokines and CCR2/CCR6 cell surface status existed in human Th17 cells from healthy and MS patients. CCR6 and/or CCR2 positive populations of Th17 cells were detected in the peripheral blood of both healthy and MS patients, with the majority of these cells bearing a CCR6 CCR2$^+$ phenotype (Fig. 4e). As in mice, human Th17 cell expression of GM CSF and IFNγ was confined to CCR6 CCR2$^+$ populations in both healthy subjects and MS patients (Fig. 4f). The presence of CCR6 CCR2$^+$ Th17 cells in healthy subjects was not unexpected given the ability of this subset to enter memory in response to infection (Fig. 4c,d). Thus, the CCR6 CCR2$^+$ signature also defines human GM CSF/IFNγ producing Th17 cells.

Differentiation of CCR6 CCR2$^+$ Th17 cells *in vivo*. Our data suggested that the 'switch' from CCR6 to CCR2 usage by developing Th17 cells was coupled with induction of a

Table 1 | EAE disease parameters in T-cell-specific chemokine receptor-deficient BM chimeras.

Group	Incidence	Mean day onset (± s.e.m.)	Mean max disease (± s.e.m.)	Mean cumulative disease (± s.e.m.)
B6.*Tcra*$^{-/-}$:B6	16/16	8.56 ± 0.74	2.02 ± 0.10	28.14 ± 2.00
B6.*Tcra*$^{-/-}$:B6.*Ccr6*$^{-/-}$	18/18	11.83 ± 0.37	2.67 ± 0.17	26.75 ± 2.76
B6.*Tcra*$^{-/-}$:B6.*Ccr2*$^{-/-}$	15/16	10.53 ± 0.60	1.17 ± 0.17	14.47 ± 2.71
B6.*Tcra*$^{-/-}$:B6.*Ccr6*$^{-/-}$.*Ccr2*$^{-/-}$	17/18	14.88 ± 0.41	2.64 ± 0.23	23.44 ± 1.84

BM, bone marrow; EAE, experimental autoimmune encephalomyelitis

Figure 3 | CCR2 drives recruitment of Th17 cells with pathogenic function into the inflamed CNS. (**a**) EAE clinical disease scores of T-cell-specific chemokine receptor-deficient bone marrow (BM) chimeras. T-cell-specific knockout (KO) chimeric mice were generated by transferring BM derived from B6.*Tcra*$^{-/-}$ (80%) and B6 (*n* 16), B6.*Ccr6*$^{-/-}$ (*n* 18), B6.*Ccr2*$^{-/-}$ (*n* 16) or B6.*Ccr6*$^{-/-}$.*Ccr2*$^{-/-}$ (*n* 18) (20%) into lethally irradiated B6.Ly5.1 recipients. Data are pooled from two independent experiments. (**b**) Representative flow cytometric analysis and quantification of CNS-infiltrating Th17 cell frequencies in T-cell-specific KO chimeras on d14 EAE. B6 (*n* 9), B6.*Ccr6*$^{-/-}$ (*n* 10), B6.*Ccr2*$^{-/-}$ (*n* 9) and B6.*Ccr6*$^{-/-}$.*Ccr2*$^{-/-}$ (*n* 9). (**c**) Frequency and total number of CNS-infiltrating Tregs in T-cell-specific KO chimeras on d14 (top) and d25 (bottom) EAE. B6 (d14: *n* 9; d25: *n* 7), B6.*Ccr6*$^{-/-}$ (d14: *n* 10; d25: *n* 8), B6.*Ccr2*$^{-/-}$ (d14: *n* 9; d25: *n* 7) and B6.*Ccr6*$^{-/-}$.*Ccr2*$^{-/-}$ (d14: *n* 9; d25: *n* 9). (**d**) Number of Gr1$^+$ leukocytes (top) and Gr1^{lo}/-F4/80$^+$ leukocytes (bottom) in the CNS of T-cell-specific KO chimeras on d14 EAE. B6 (*n* 9), B6.*Ccr6*$^{-/-}$ (*n* 10), B6.*Ccr2*$^{-/-}$ (*n* 9) and B6.*Ccr6*$^{-/-}$.*Ccr2*$^{-/-}$ (*n* 9). (**e**) Representative flow cytometric analysis and quantification of GM-CSF-producing Th17 cells (CD3$^+$CD4$^+$IL-17A$^+$) in the draining lymph node (dLN), spleen, blood and CNS of B6 (*n* 9) and B6.*Ccr2*$^{-/-}$ (*n* 9) T-cell chimeras 14 days post EAE induction. (**f**) EAE clinical disease score of B6.*Rag1*$^{-/-}$ reconstituted with 8×10^6 purified CD4$^+$ T cells from B6 (*n* 5) or B6.*Ccr2*$^{-/-}$ mice (*n* 5). Number of CNS-infiltrating (**g**) IL-17A$^+$GM-CSF$^-$, IL-17A$^+$GM-CSF$^+$ and IL-17A$^-$GM-CSF$^+$ CD4$^+$ T cells, and (**h**) Gr1$^+$ and Gr1$^{lo/-}$F4/80$^+$ leukocytes on d25 EAE in B6.*Rag1*$^{-/-}$ reconstituted mice (black bars, B6; white bars, B6.*Ccr2*$^{-/-}$). (**i**) Representative flow cytometric analysis and quantitation of GM-CSF-producing cells among CNS-infiltrated Th17 cells on d25 EAE of B6.*Rag1*$^{-/-}$ reconstituted mice (black bars, B6; white bars, B6.*Ccr2*$^{-/-}$). (**a–i**) Data are presented as mean ± s.e.m.; $^*P \le 0.05$, $^{**}P \le 0.01$, $^{***}P \le 0.001$, $^{****}P \le 0.0001$. (**b–d**) One-way analysis of variance (ANOVA) with Bonferroni multiple comparisons test. (**e**,**g–i**) Unpaired two-tailed Student's *t*-test. (**f**) Two-way ANOVA with multiple comparisons test.

cytokine secreting profile reported to promote Th17 cell patho genicity in EAE[3,6,7,27]. Differentiation of Th17 cells from naive precursors and their subsequent acquisition of pathogenicity are coordinated by various distinct cytokine signals[12]. It has been reported that initial Th17 cell differentiation *in vivo* occurs independently of IL 23 (ref. 8); however, this cytokine is critical for their subsequent survival, expansion and consequent acquisition of pathogenicity[6 8]. Thus, we first examined the role of IL 23, in relation to TGFβ1 and IL 6, in regulation of CCR2 + Th17 cell development by stimulating splenocytes from d5 EAE mice *ex vivo* with MOG_{35-55} in the presence or absence of these cytokines. *Ex vivo* stimulation with MOG_{35-55} promoted generation of Th17 cells displaying a CCR6 + CCR2 + phenotype, whereas addition of IL 23, and not TGFβ1/IL 6, drove development of CCR6 CCR2 + Th17 cells (Fig. 5a and Supplementary Fig. 4). To interrogate the role of IL 23 in CCR2 + Th17 cell development *in vivo*, we assessed mice deficient in IL 23 (B6.*Il23p19* /) or its receptor (B6.*Il23r*$^{gfp/gfp}$). As expected[8,9,33], Th17 cell frequency was reduced in B6.*Il23p19* / and B6.*Il23r*$^{gfp/gfp}$ spleen (Fig. 5b,d). Notably, this reduction could essentially be accounted for by the absence of Th17 cells bearing the CCR6 CCR2 + phenotype (Fig. 5c,e). Similar results were obtained using *Il12p40* deficient mice (Supplementary Fig. 5a,b). These processes were independent of IL 12, as B6.*Il12p35* /

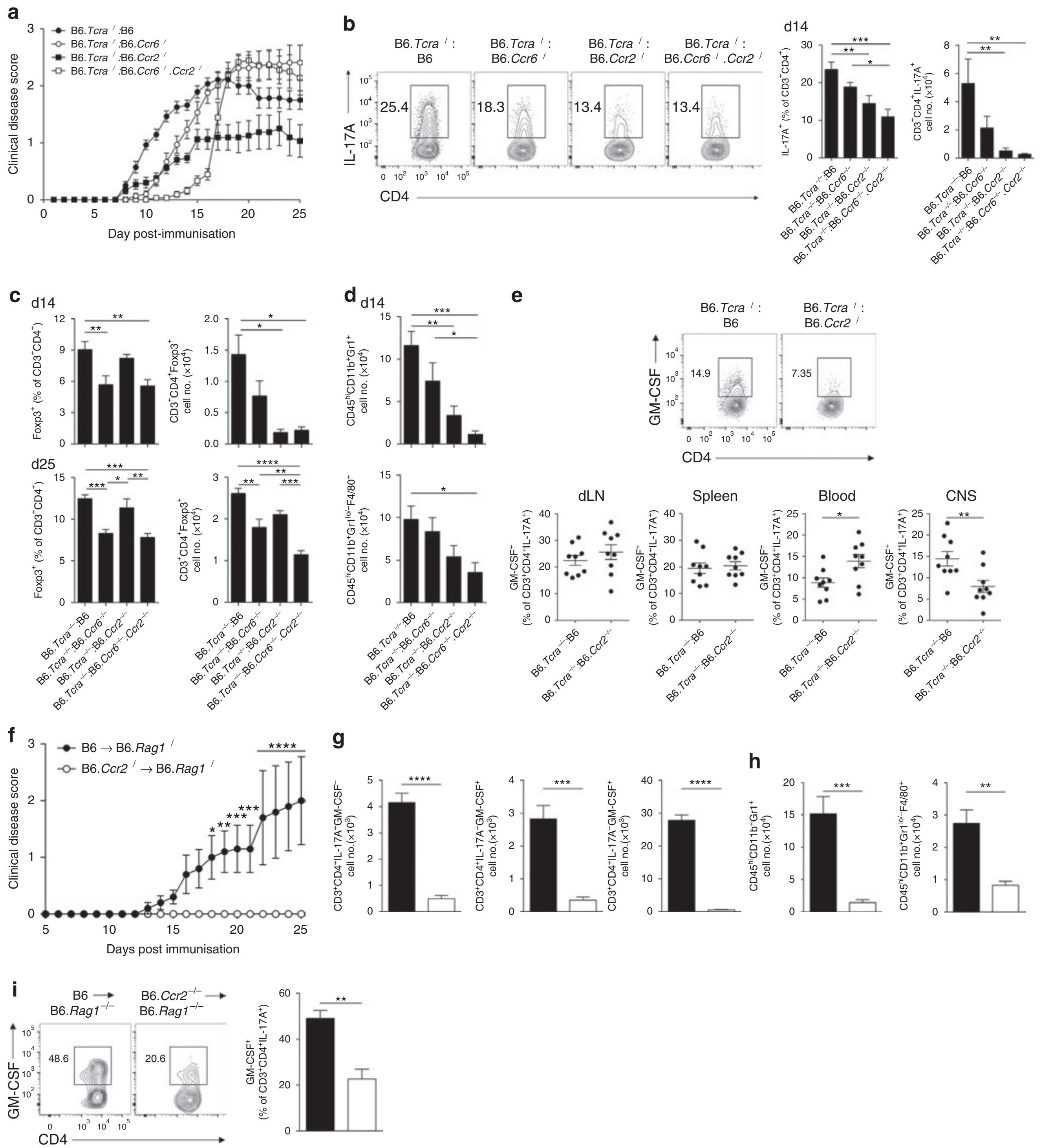

mice retained WT frequencies of CCR6 CCR2^{+} Th17 cells (Supplementary Fig. 5c,d). To determine whether these effects of IL 23 were intrinsic to CD4^{+} T cells, we generated B6.*Il23r*$^{gfp/gfp}$ mixed BM chimeric mice. In these mice, *Il23r* deficient CD4^{+} T cells with a Th17 phenotype were profoundly reduced (Fig. 5f), of which those bearing a CCR6 CCR2^{+} profile were selectively curtailed (Fig. 5g). Furthermore, in agreement with previous reports that GM CSF expression in T cells relies on IL 23/IL 23R[6,7], *Il23r* deficiency ablated GM CSF production by CCR6 CCR2^{+} Th17 cells, which was not compensated for in CCR6 expressing Th17 cell populations (Fig. 5h). Thus, our data demonstrate that CCR6 CCR2^{+} Th17 cell development is reliant on IL 23 and encompass GM CSF/IFNγ secreting Th17 cells.

Taking advantage of our novel strategy to map IL 23 driven, GM CSF/IFNγ producing Th17 cells *in vivo*, we next assessed the importance of key cytokines reported to shape both Th17 cell development and pathogenicity in EAE. A dual role for IL 1 in Th17 cell biology has been described: functioning as a polarizing factor for initial Th17 cell differentiation[34] and acting on Th17 cells to promote their inflammatory potential[6]. Accordingly, neutralization of IL 1R1 inhibited Th17 cell generation (Supplementary Fig. 6a) and shifted the balance towards the CCR6^{+}CCR2^{+} phenotype and away from the CCR6 CCR2^{+} phenotype (Supplementary Fig. 6b).

TNFα plays little to no role in Th17 lineage commitment[35], but is reported to promote *in vitro* generation of GM CSF^{+} Th17 cells[6]. *Tnf* deficiency reduced Th17 cell development (Supple mentary Fig. 7a), with a modest defect in CCR6 CCR2^{+} Th17 cell frequency (Supplementary Fig. 7b). Mixed BM chimera experiments revealed that this reduction in Th17 cell development was not due to T cell intrinsic TNF receptor (TNFR)1 or TNFR2 function (Supplementary Fig. 7c,e); however, CCR6 CCR2^{+} Th17 cell development required T cell intrinsic TNFR1, but not TNFR2 signalling (Supplementary Fig. 6d,f). Further, TNFR1 signalling was shown to promote CCR6 CCR2^{+} Th17 expression of GM CSF, although conversely TNFR1 or TNFR2 signalling inhibited IFNγ expression (Supplementary Fig. 7g,h).

IFNγ is reported to inhibit Th17 cell differentiation from naive precursors[36,37], but has also been shown to promote development of IFNγ^{+}T bet^{+} Th17 cells from committed Th17 cells[38]. *Ifngr* deficiency enhanced Th17 cell differentiation (Supplementary Fig. 8a), with a specific increase in generation of CCR6 CCR2^{+} Th17 cells (Supplementary Fig. 8b). Similar results were obtained using neutralizing antibodies to IFNγ (Supplementary Fig. 8c), suggesting that IFNγ selectively suppresses CCR6 CCR2^{+} Th17 cell generation *in vivo*. However, assessment of *Ifngr* deficient Th17 cells in mixed BM chimeras revealed that IFNγ promotes the development of CCR6 CCR2^{+} Th17 cells in a T cell intrinsic manner (Supplementary Fig. 8d,e). In line with this, IFNγ expression in CCR6 CCR2^{+} Th17 cells was also promoted by T cell intrinsic IFNγ/IFNγR signalling (Supplementary Fig. 8f).

Together, these experiments demonstrate that IL 23 drives the later emergence of the CCR6 CCR2^{+} Th17 cell population, that the CCR6 CCR2^{+} signature defines IL 23 driven GM CSF/ IFNγ producing Th17 cell development, that IL 1 and TNFα play important accessory roles in CCR6 CCR2^{+} Th17 cell differ entiation, and that IFNγ plays a dual role in Th17 biology, acting on non CD4^{+} T cells to indirectly inhibit CCR6 CCR2^{+} Th17 differentiation, while also directly promoting their development in a T cell intrinsic manner.

T-bet and Eomes drive CCR6 CCR2^{+} Th17 cell formation. To provide new insights into the transcriptional regulation of these distinct Th17 cell phenotypes *in vivo*, we screened for the expression of key transcription factors reported to direct Th17 cell differentiation in CCR6/CCR2 expressing Th17 types. A defining feature of *in vitro* generated pathogenic Th17 cells is expression of T bet[3,27], whereas the transcriptional activators of *Il10*, c Maf and AHR are abundant in TGFβ1/IL 6 induced *in vitro* generated IL 10 producing Th17 cells[3,4,39]. Accordingly, high expression of T bet was apparent in CCR6 CCR2^{+} Th17 cells (Fig. 6a), whereas c Maf and Aryl hydrocarbon receptor (AHR) were abundant in the CCR6^{+}CCR2^{+} Th17 population (Supplementary Fig. 9). Moreover, the expression of IRF4 and BATF, essential mediators of early specification of Th17 cells from naive precursors[40], was highest in CCR6^{+}CCR2^{+} Th17 cells (Supplementary Fig. 9). RORγt expression was marginally lower in CCR6 CCR2^{+} Th17 cells than other Th17 populations (Supplementary Fig. 8). Notably, novel *Eomes* Cherry reporter

Table 2 | EAE disease parameters in CD4^{+} T cell reconstituted *Rag1*-deficient mice.

Group	Incidence	Mean day onset (± s.e.m.)	Mean max disease (± s.e.m.)	Mean cumulative disease (± s.e.m.)
B6→B6.*Rag1*$^{-/-}$	5/5	15.2 ± 0.86	2.0 ± 0.77	13.8 ± 5.29
B6.*Ccr2*$^{-/-}$→B6.*Rag1*$^{-/-}$	0/5	NA	0.0 ± 0.00	0.0 ± 0.00

NA, not applicable.

Figure 4 | The CCR6^{-}CCR2^{+} signature defines murine and human GM-CSF/IFNγ-producing Th17 cells *in vivo*. (**a**) Representative flow cytometric analysis and quantification of GM-CSF, IFNγ, TNFα, IL-2, IL-9, IL-10, IL-17F and IL-22 staining in naive CD4^{+} (CD3^{+}CD4^{+}CD44^{lo}), CCR6^{+}CCR2^{-}, CCR6^{+}CCR2^{+} and CCR6^{-}CCR2^{+} Th17 cell populations (CD3^{+}CD4^{+}CD44^{hi}IL-17A^{+}) from the spleen of mice immunized for EAE 10 days prior. Data representative of three independent experiments with n 4–5 mice per experiment. (**b**) Percent cytokine positive among CCR6^{+}CCR2^{+} and CCR6^{-}CCR2^{+} Th17 cells (CD3^{+}CD4^{+}CD44^{hi}IL-17A^{+}) in the CNS d15 post EAE induction. Data are pooled from three independent experiments with n 8 CNS pooled per experiment. (**c**) Representative flow cytometric analysis of CCR6/CCR2 staining on Th17 cells (CD3^{+}CD4^{+}IL-17A^{+}) in the spleen of B6 mice colonized in the nasopharynx with *S. pneumoniae* strain EF3030 7, 21 and 84 days post primary (1^{o}) immunization and 5 days (d89) post secondary (2^{o}) immunization. Data are representative of n 5–6 mice per timepoint. (**d**) Expression of GM-CSF and IFNγ among CCR6^{+}CCR2^{-}, CCR6^{+}CCR2^{+} and CCR6^{-}CCR2^{+} Th17 cell populations (CD3^{+}CD4^{+}IL-17A^{+}) from the spleen of B6 mice 21 days post 1^{o} *S. pneumoniae* strain EF3030 nasopharyngeal colonization (n 4). (**e**) Representative flow cytometric analysis of CCR6/CCR2 staining on circulating human Th17 cells (CD4^{+}CD8^{-}IL-17A^{+}) from an MS patient. (**f**) Representative flow cytometric analysis and quantification of IFNγ and GM-CSF staining on CCR6^{+}CCR2^{-}, CCR6^{+}CCR2^{+} and CCR6^{-}CCR2^{+} human Th17 cell subsets from the peripheral blood of healthy (n 7) and MS patients (n 12). (**a**,**b**,**d**,**f**) Data are presented as mean ± s.e.m.; *$P \leq 0.05$; **$P \leq 0.01$; ***$P \leq 0.001$; ****$P \leq 0.0001$; one-way analysis of variance with Bonferroni multiple comparisons test.

mice (Supplementary Fig. 10) revealed that, among Th17 cells, the expression of Eomesodermin was confined to CCR6 expressing Th17 cell populations (Fig. 6b).

Given that T bet and Eomesodermin were differentially expressed in CCR6+ and CCR6 CCR2+ Th17 cells, we examined the T cell intrinsic function of these transcription factors using mixed BM chimeras. T bet negatively regulates Th17 cell development from naive precursors[41] but its function in pathogenic Th17 cell biology is contentious[27,42]. Consistent with prior reports[27,41], we found that *Tbx21* deficiency increased Th17 cell frequency in a T cell intrinsic manner (Fig. 6c). Assessment of CCR6/CCR2 expression on *Tbx21* deficient Th17 cells revealed

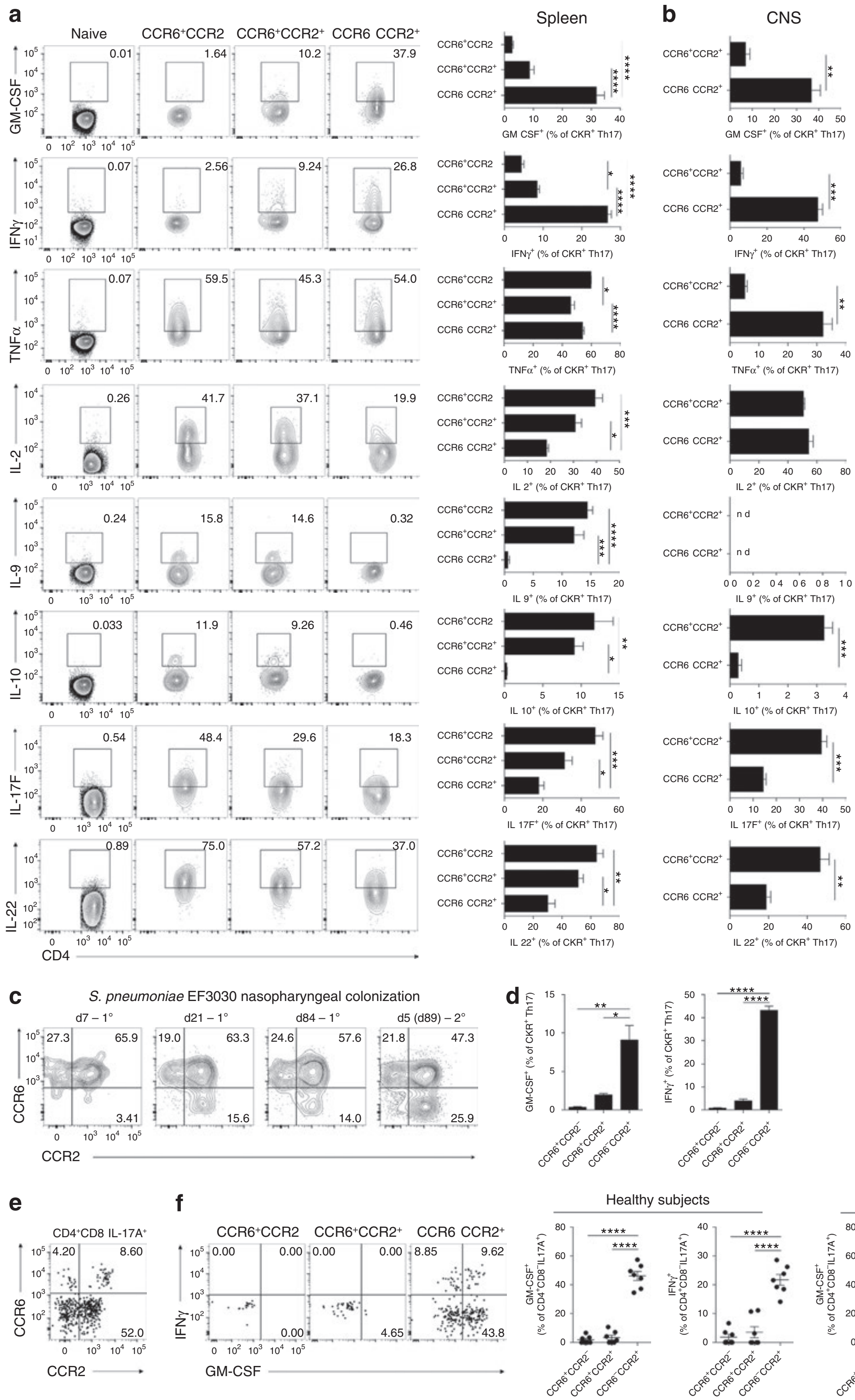

that T bet is critical for the development of CCR6 CCR2$^+$ Th17 cells (Fig. 6d). Moreover, *Tbx21* deficiency ablated IFNγ production and reduced GM CSF expression by CCR6 CCR2$^+$ Th17 cells (Fig. 6e), implicating T bet as a crucial regulator of CCR6 CCR2$^+$ GM CSF/IFNγ producing Th17 cell development *in vivo*.

The function of Eomesodermin in Th17 cell differentiation *in vivo*, to our knowledge, is unknown. *Eomes* deficiency in CD4$^+$ T cells using B6.*Cd4*^{Cre}*Eomes*$^{fl/fl}$ mixed BM chimeras reduced Th17 cell generation in a T cell intrinsic manner (Fig. 6f), identifying Eomesodermin as a novel regulator of Th17 cell development *in vivo*. Strikingly, despite abundant

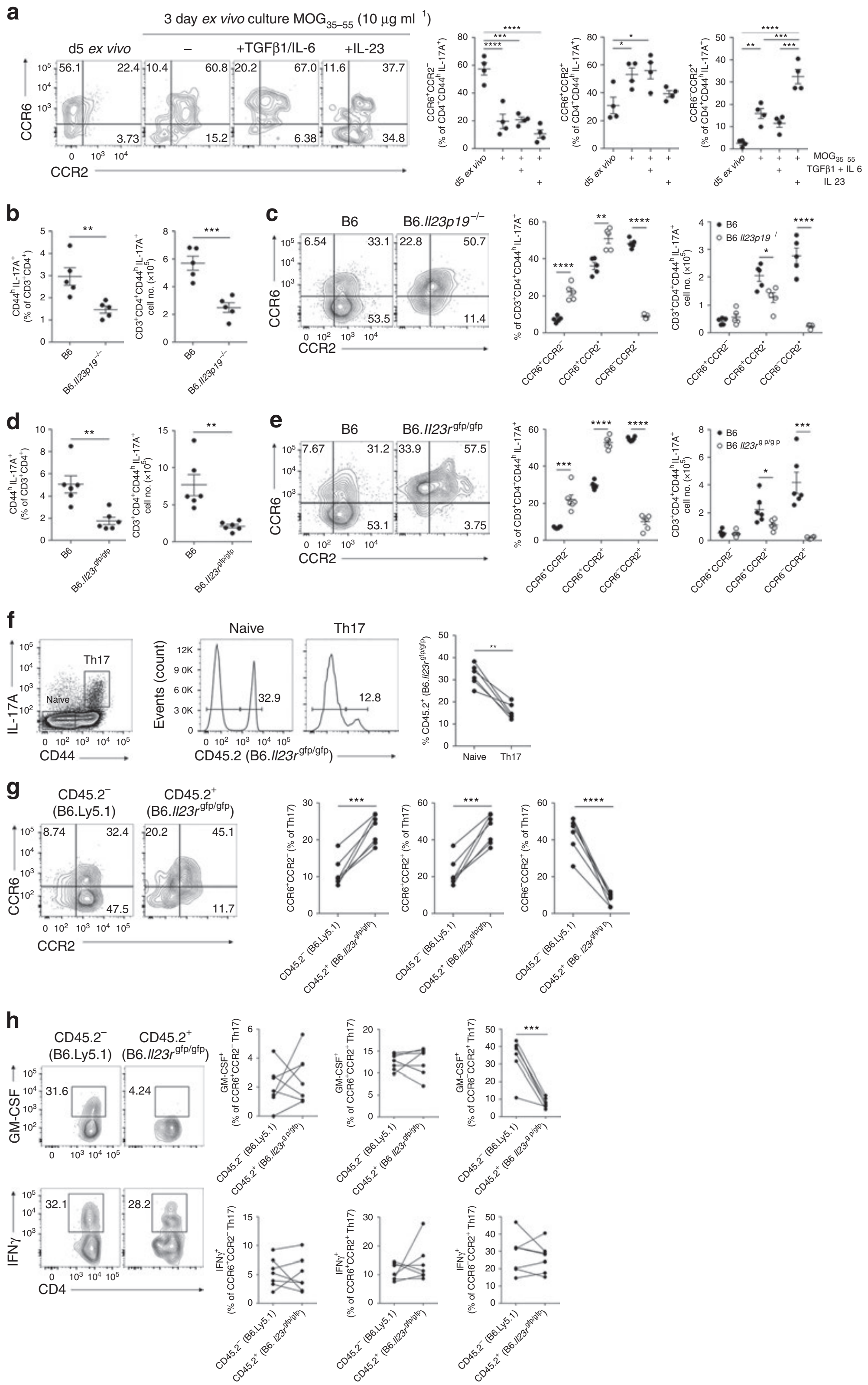

expression in CCR6 expressing Th17 cells, deletion of *Eomes* curtailed the development of CCR6 CCR2+ Th17 cells (Fig. 6g), but did not alter IFNγ or GM CSF production by these cells (Fig. 6h). Collectively, these data indicate that T bet negatively regulates differentiation of IL 17 secreting CD4+ T cells, but is required for the ontogeny of GM CSF/IFNγ producing CCR6 CCR2+ Th17 cells, whereas Eomesodermin is required for Th17 cell differentiation *in vivo* by promoting CCR6 CCR2+ Th17 cell development.

Discussion

In the present study, we demonstrate that CCR2 is a critical driver of encephalitogenic GM CSF producing Th17 cell recruitment to the CNS in EAE. Further, we show that CCR6 functions to promote homing of Th17 cells only during initial phases of inflammation and is more critically required for Treg trafficking. This 'switch' from CCR6 to CCR2 usage by Th17 cells appeared to be temporally regulated during priming as the earliest Th17 cells predominantly expressed CCR6, followed by later emergence of CCR6+CCR2+ and CCR6 CCR2+ populations in SLOs. The latter population required IL 23 and, to a lesser extent, IL 1, TNFα and IFNγ, and the transcriptional regulators T bet and Eomesodermin for development. Assessment of cytokine expres sion among Th17 populations in humans and in murine models of autoimmunity and persistent bacterial infection revealed that CCR6 CCR2+ Th17 cells align with previously described GM CSF+/IFNγ+ pathogenic Th17 cells, while CCR6+CCR2+ Th17 cells resemble previously reported Th17 cells with a more limited pathogenic potential. Thus, we define a molecular mechanism governing encephalitogenic Th17 cell recruitment to the CNS and identify unique cell surface signatures and differen tiation requirements of phenotypically distinct Th17 cells *in vivo*.

Manipulation of the chemokine system has been considered a tractable target for therapeutic intervention in CD4+ T cell driven immunopathologies for many years[43]. Central to the rational design of such approaches is a detailed understanding of unique spatio temporal homing signals used by inflammatory and regulatory subsets of T cells to infiltrate lesions. Although CCR2 has been reported to be expressed on subsets of T cells previously[44,45], until now the functional significance of this was unknown. With regard to Th17 migration, most focus has fallen on CCR6 with an early report demonstrating a critical requirement for this receptor in encephalitogenic T cell migration in EAE[18]. However, this has been challenged with the results of more recent studies demonstrating a largely redundant role for CCR6 in EAE pathogenesis[19,20]. Our data demonstrate that CCR6 promotes early infiltration of Th17 cells, but this is dispensable for the development of EAE, which is driven by CCR2 dependent recruitment of encephalitogenic Th17 cells. However, our experiments using mice with *Ccr6* / *Ccr2* / T cells indicate that when T cells lack CCR6, pathological inflammation ensues even in the absence of CCR2 on T cells. This indicates that although CCR2 strongly promotes encephalitogenic T cell recruitment to the CNS, a degree of CCR2 independent recruitment of encephalitogenic T cells must also occur, but these cells are constrained from causing disease in a CCR6 dependent manner, probably by CCR6+ Tregs. From a clinical perspective, our data, and those of others[19,20], suggest that therapeutic targeting of CCR6 will have detrimental effects on Treg function without restraining pathogenic T cells and emphasize CCR2 as a prospective target for the treatment of inflammatory T cell driven pathologies such as MS. This notion is strengthened by our findings that GM CSF and IFNγ producing Th17 cells bear a CCR6 CCR2+ phenotype in humans, other studies demonstrating that IFNγ producing Th17 cells are preferentially recruited in MS lesions[31], the observation that IL 17A/GM CSF co expressing CD4+ T cells are enriched in MS brain lesions[32] and the well established dependency on CCR2 for monocyte infiltration of the CNS[46].

Our data indicate that initial Th17 cells differentiate in an IL 23 independent manner, bear a CCR6+CCR2 phenotype and are recruited to the uninflamed CNS via CCR6. Reboldi *et al.*[18] proposed that an early CCR6 dependent wave of Th17 cells initiates CNS inflammation in EAE. CCR6+CCR2 Th17 cells express a unique cytokine profile including IL 17A/F, IL 22, IL 2, TNFα and IL 10, and although mice deficient in *Il17a*, *Il17f*, *Il22* or *Tnf* do not display substantial defects in EAE patho genesis[47 49], it is possible that these CCR6+CCR2 Th17 cell derived factors may synergistically contribute to the initiation of CNS inflammation. Importantly however, our data clearly demonstrate that the absence of this CCR6 driven wave of Th17 cells does not prevent subsequent CCR2 driven population of the CNS by encephalitogenic Th17 cells or the development of clinical EAE, challenging notions that these cells form an essential component of EAE pathogenesis.

Subsequent to the generation of CCR6+CCR2 Th17 cells is the emergence of CCR2 expressing Th17 cell populations. CCR6+CCR2+ Th17 cells express IL 10 and IL 9, consistent with published descriptions of Th17 cells with a more limited pathogenic potential[2 5]. Conversely, CCR6 CCR2+ Th17 cells express abundant GM CSF and IFNγ, and probably constitute the previously described pathogenic Th17 cell[3,4,6,7,11]. Th17 cells with pathogenic function are reported to derive from committed TGFβ1/IL 6 driven Th17 precursors in the presence of IL 23 (refs 6 8) and from naive precursors via TGFβ3 and IL 6 (ref. 4), or independently of TGFβ1 in an IL 6 , IL 1β and IL 23 dependent manner[3]. Here we demonstrate that the absence

Figure 5 | IL-23 drives differentiation of CCR6$^-$CCR2$^+$ Th17 cells *in vivo*. (**a**) Representative flow cytometric analysis and quantification of CCR6/CCR2 staining on Th17 cells (CD3$^+$CD4$^+$CD44^{hi}IL-17A$^+$) 5 days post MOG/CFA immunization (d5 *ex vivo*) and after 3 days *ex-vivo* culture with MOG$_{35–55}$ in the presence of either no cytokines ( ), TGFβ1/IL-6 or IL-23. Data are representative of two independent experiments, *n* 4. (**b**,**c**) Analysis of B6 (*n* 5) and B6.*Il23p19*$^{-/-}$ (*n* 5) mice d10 post MOG/CFA immunization. (**b**) Frequency and total number of Th17 cells in the spleen; (**c**) representative flow cytometric analysis and quantification of CCR6/CCR2 staining on Th17 cells. (**d**,**e**) Analysis of B6 (*n* 6) and B6.*Il23r*$^{gfp/gfp}$ (*n* 6) mice d10 post MOG/CFA immunization. (**d**) Frequency and total number of Th17 cells in the spleen; (**e**) representative flow cytometric analysis and quantification of CCR6 and CCR2 staining on Th17 cells. (**f**) Representative flow cytometric analysis and quantification of CD45.2$^+$ (B6.*Il23r*$^{gfp/gfp}$) cells (right) within naive CD4$^+$ (CD3$^+$CD4$^+$CD44^{lo}) and Th17 cells (CD3$^+$CD4$^+$CD44^{hi}IL-17A$^+$) (left) in the spleen of B6.*Il23r*$^{gfp/gfp}$ mixed BM chimeric mice immunized with MOG/CFA 10 days prior (*n* 7). (**g**) Representative flow cytometric analysis and quantification of CCR6/CCR2 staining on CD45.2$^-$ (B6.Ly5.1) and CD45.2$^+$ (B6.*Il23r*$^{gfp/gfp}$) Th17 cells in mixed BM chimeras immunized with MOG/CFA 10 days prior (*n* 7). (**h**) Representative flow cytometric analysis of GM-CSF and IFNγ staining among CD45.2$^-$ (B6.Ly5.1) and CD45.2$^+$ (B6.*Il23r*$^{gfp/gfp}$) CCR6$^-$CCR2$^+$ Th17 cells in B6.*Il23r*$^{gfp/gfp}$ (*n* 7) mixed BM chimeric mice 10 days post MOG/CFA immunization. Right, GM-CSF and IFNγ expression among CCR6/CCR2-expressing Th17 cell populations in B6.*Il23r*$^{gfp/gfp}$ mixed BM chimeras. (**a**–**h**) Each dot represents an individual mouse; *$P \leq 0.05$; **$P \leq 0.01$, ***$P \leq 0.001$, ****$P \leq 0.0001$. (**a**–**d**) Data are presented as mean ± s.e.m. (**a**) One-way analysis of variance with Bonferroni multiple comparisons test. (**b**–**e**) Unpaired two-tailed Student's *t*-test. (**f**–**h**) Paired two-tailed Student's *t*-test.

of the IL 23/IL 23R axis specifically curtails the development of GM CSF producing CCR6 CCR2$^+$ Th17 cells, suggesting that the CCR6 CCR2$^+$ signature defines the IL 23 driven pathogenic/inflammatory Th17 cell subset *in vivo* that may represent an advanced differentiated state of Th17 cells that arise from early CCR6$^+$ precursors. Recent reports have demonstrated that the fate of Th17 cells in chronic inflammatory settings includes transdifferentiation to an IL 17A IFNγ$^+$ Th1 like phenotype (termed Th1$^{ex\text{-}Th17}$ cells) via IL 23 (ref. 11) or an IL 10 secreting, anti inflammatory T regulatory type 1 cell (termed Tr1$^{ex\text{-}Th17}$ cells) via TGFβ1 (ref. 50). Our data suggest that this phenotypic segregation of Th17 cells may arise before transdifferentiation, although the relationship between IL 10 producing CCR6$^+$CCR2$^+$ Th17 cells, IL 23 driven GM CSF/IFNγ producing CCR6 CCR2$^+$ Th17 cells and Tr1$^{ex\text{-}Th17}$/Th1$^{ex\text{-}Th17}$ cells remains to be determined.

Our data indicate that the transcriptional regulators T bet and Eomesodermin drive CCR6 CCR2$^+$ Th17 cell development *in vivo*. TGFβ1 mediated repression of Eomesodermin is required for *in vitro* Th17 differentiation[51]; however, although *Eomes* can be induced in committed TGFβ1/IL 6 driven Th17 cells by inflammatory cytokines[27], ectopic *Eomes* expression did not promote IL 12 driven IFNγ$^+$ Th17 cell development *in vitro*[27]. We found that among Th17 cells, Eomesodermin expression is restricted to CCR6 expressing Th17 cell populations but is not required for their development *in vivo*. Instead, *Eomes* deficiency led to a selective defect in CCR6 CCR2$^+$ Th17 cell generation, implicating Eomesodermin as a key regulator of the switch from CCR6 to CCR2 expression during Th17 cell development. T bet function in pathogenic Th17 cell biology is controversial with data indicating that these cells develop independently of T bet[42] and reports demonstrating that IL 23/IL 12 induce T bet[11,27], which, in collaboration with Runx1, promote conversion of Th17 precursors into pathogenic IFNγ producing Th17 cells[27]. Our data demonstrate that in the absence of T bet, Th17 cell development is amplified but arrested at an early developmental stage with a selective defect in CCR6 CCR2$^+$ GM CSF/IFNγ producing Th17 cell formation. T bet interactions with Runx1 suppress Runx1 mediated transactivation of *Rorc* and sequester 'available' Runx1 that would otherwise form transcriptionally active Runx1:RORγt complexes required for *Il17a* and *Il17f* induction in CD4$^+$ T cells[41]. Further, Eomesodermin directly represses *Rorc* and *Il17a* transcription[51]. Thus, we speculate that Eomesodermin and T bet shape Th17 differentiation and plasticity by implementing changes to the transcriptional landscape of Th17 cells, such as repression of *Rorc* and *Il17a*, and induction of *Ifng* and *Csf2* (directly or indirectly), as they differentiate from IL 17A$^+$ CCR6$^+$CCR2$^{+/}$ Th17 cells, through IL 17A$^+$ CCR6 CCR2$^+$ GM CSF/IFNγ producing Th17 cells and perhaps towards an 'ex Th17' phenotype in chronic inflammation[11].

Taken together, our data support a step wise model of Th17 cell differentiation and homing (Fig. 7). Initial CCR6$^+$CCR2 Th17 cells develop independently of IL 23 and migrate to effector sites via CCR6. Continuing antigen exposure in SLOs drives transition of CCR6$^+$CCR2 Th17 cells to CCR2$^+$ Th17 cell populations. More specifically, persistent antigen drives the development of CCR6$^+$CCR2$^+$ Th17 cells and the cytokines IL 23, IL 1, IFNγ and TNFα promote CCR6 CCR2$^+$ GM CSF/IFNγ producing Th17 cells that develop in a T bet and Eomesodermin dependent manner. CCR2 drives subsequent waves of Th17 cell recruitment to inflammatory sites where it is likely to be that a balance between CCR6 CCR2$^+$ GM CSF/IFNγ producing Th17 cells, CCR6$^+$CCR2$^+$ IL 10 producing Th17 cells, other effector T cell populations and CCR6$^+$ Tregs dictates whether amplification or resolution of inflammation results. This switch from CCR6 to CCR2 as Th17 cells develop greater inflammatory potential identifies a novel temporally regulated recruitment mechanism that amplifies T cell dependent inflammation, a finding that has important implications for understanding regulation of auto immune inflammation and protective immunity.

Methods

Mice. C57Bl/6 (B6), SJL/J, B6.Ly5.1 and B6.*Rag1*$^{-/-}$ mice were purchased from the Animal Resource Center (WA, Australia) or bred and maintained in-house at the University of Adelaide Animal Facility. B6.*Il17a*^{Cre}*Rosa26*^{eYFP} (ref. 11), B6.*Foxp3*^{GFP} (ref. 52), B6.*Ccr6*$^{-/-}$ (ref. 53) and B6.*Ccr2*$^{-/-}$ (ref. 54) mice were bred and maintained in-house. B6.*Il23p19*$^{-/-}$ (ref. 55), B6.*Il23r*$^{gfp/gfp}$ (ref. 33), B6.*Il12p40*$^{-/-}$ (ref. 56), B6.*Il12p35*$^{-/-}$ (ref. 57) and B6.*Ifngr*$^{-/-}$ (ref. 58) mice were bred in-house at QIMR Berghofer Medical Research Institute, Herston, Australia. B6.*Tnf*$^{-/-}$ (ref. 59), B6.*Tnfrsf1a*$^{-/-}$ (ref. 60) and B6.*Tnfrsf1b*$^{-/-}$ (ref. 61) mice were kindly provided by Professor Bernhard Baune (University of Adelaide, Adelaide, Australia). B6.*Tbx21*$^{-/-}$ (ref. 62) and B6.*Cd4*^{Cre}*Eomes*$^{fl/fl}$ (ref. 63) mice were bred in-house at The Walter and Eliza Hall Institute of Medical Research, Parkville, Australia. B6.*Eomes*^{Cherry} reporter mice were generated (validation in Supplementary Fig. 10) at The Walter and Eliza Hall Institute of Medical Research, Parkville, Australia. B6.*Tcra*$^{-/-}$ (ref. 64) mice were kindly provided by Professor Carola Vinuesa (John Curtin School of Medical Research, Canberra, Australia). B6.*Ccr6*$^{-/-}$. *Ccr2*$^{-/-}$ mice were generated and maintained in-house. All B6 lines were on the C57Bl/6J background. Male and female mice between the ages of 6 12 weeks were used in experiments. Mice in each experiment were age and gender matched. All experiments were conducted in accordance to the guidelines outlined by the Animal Ethics Committee at the University of Adelaide.

Generation of B6.*Eomes*^{Cherry} reporter mice. The *Eomes* targeting construct used the pKW11 vector consisting of a splice acceptor, stop codons in all reading frames, an IRES, mCherry complementary DNA, an SV40 polyadenylation signal and a *PGK-Neor* gene. Genomic DNA containing loxP flanked *Eomes* exons 2 3, containing the entire *Eomes* coding region was cloned in front of the pKW11 insert.

Figure 6 | T-bet and Eomesodermin promote CCR6$^-$CCR2$^+$ Th17 cell differentiation *in vivo*. (**a**) Representative flow cytometric analysis and quantification (geometric MFI) of T-bet expression in naive CD4$^+$ T cells (grey, filled; CD3$^+$CD4$^+$CD44^{lo}) and CCR6$^+$CCR2$^-$ (red, open), CCR6$^+$CCR2$^+$ (blue, open) and CCR6$^-$CCR2$^+$ (black, open) Th17 cells (CD3$^+$CD4$^+$CD44^{hi}IL-17A$^+$) from the spleen d10 post MOG/CFA immunization. Geometric MFI (gMFI) of T-bet expression in Th17 cell populations is presented after subtraction from concurrent naive CD4$^+$ T-cell T-bet gMFI. Data are representative of two independent experiments with n 4–5 mice per experiment. (**b**) Representative flow cytometric analysis of Eomes-Cherry expression in naive CD4$^+$ T cells, CCR6$^+$CCR2$^-$, CCR6$^+$CCR2$^+$ and CCR6$^-$CCR2$^+$ Th17 cells (all gated and presented as in **a**) from the spleen of B6.*Eomes*$^{Cherry/+}$ reporter mice d10 post MOG/CFA immunization. Data are representative of two independent experiments with n 4 mice per experiment. (**c**,**f**) Representative flow cytometric analysis and quantification of CD45.2$^+$ cells within naive CD4$^+$ (CD3$^+$CD4$^+$CD44^{lo}) and Th17 cells (CD3$^+$CD4$^+$CD44^{hi}IL-17A$^+$) in the spleen of B6.*Tbx21*$^{-/-}$ (n 5) (**c**) and B6.*Cd4*^{Cre}*Eomes*$^{fl/fl}$ (n 6) (**f**) mixed BM chimeric mice immunized with MOG/CFA 10 days prior. Data are representative of two independent experiments. (**d**,**g**) Representative flow cytometric analysis and quantification of CCR6/CCR2 staining on CD45.2$^-$ (B6.Ly5.1) and CD45.2$^+$ (indicated KO) Th17 cells in B6.*Tbx21*$^{-/-}$ (**d**) and B6.*Cd4*^{Cre}*Eomes*$^{fl/fl}$ (**g**) mixed BM chimeras d10 post MOG/CFA immunization. Data are representative of two independent experiments. (**e**,**h**) Representative flow cytometric analysis and quantification of IFNγ and GM-CSF staining within CD45.2$^-$ (B6.Ly5.1) and CD45.2$^+$ (indicated KO) CCR6$^-$CCR2$^+$ Th17 cells (CD3$^+$CD4$^+$CD44^{hi}IL-17A$^+$) in B6.*Tbx21*$^{-/-}$ (**e**) and B6.*Cd4*^{Cre}*Eomes*$^{fl/fl}$ (**h**) mixed BM chimeras d10 post MOG/CFA immunization. Data are representative of two independent experiments. (**b**–**h**) *$P\leq0.05$, **$P\leq0.01$, ***$P\leq0.001$, ****$P\leq0.0001$. (**b**,**c**) Data are presented as mean ± s.e.m.; one-way analysis of variance with Bonferroni multiple comparisons test. (**d**–**h**) Each dot represents an individual mouse; paired two-tailed Student's *t*-test.

Homology arms of 5,700 bp (5′) and 2,667 bp (3′) were amplified from an *Eomes*-containing bacterial artificial chromosome and cloned into the final targeting vector. The linear targeting vector was introduced into the *Eomes* locus by homologous recombination in C57Bl/6 embryonic stem (ES) cells. Neomycin-resistant clones were screened by Southern hybridization using 5′ (digested with Sph1, giving WT 12,293 kb and *Eomes*fl^{mCherry} 9,198 kb) probes. Targeted ES cell clones were injected into BALB/c blastocysts, to obtain chimeric founders. Germline transmission was achieved with two clones resulting in the generation of two independent lines. Founders for the reporter lines lacked the 5′ loxP site and were designated as *Eomes* reporter (*Eomes*$^{mCherry/+}$).

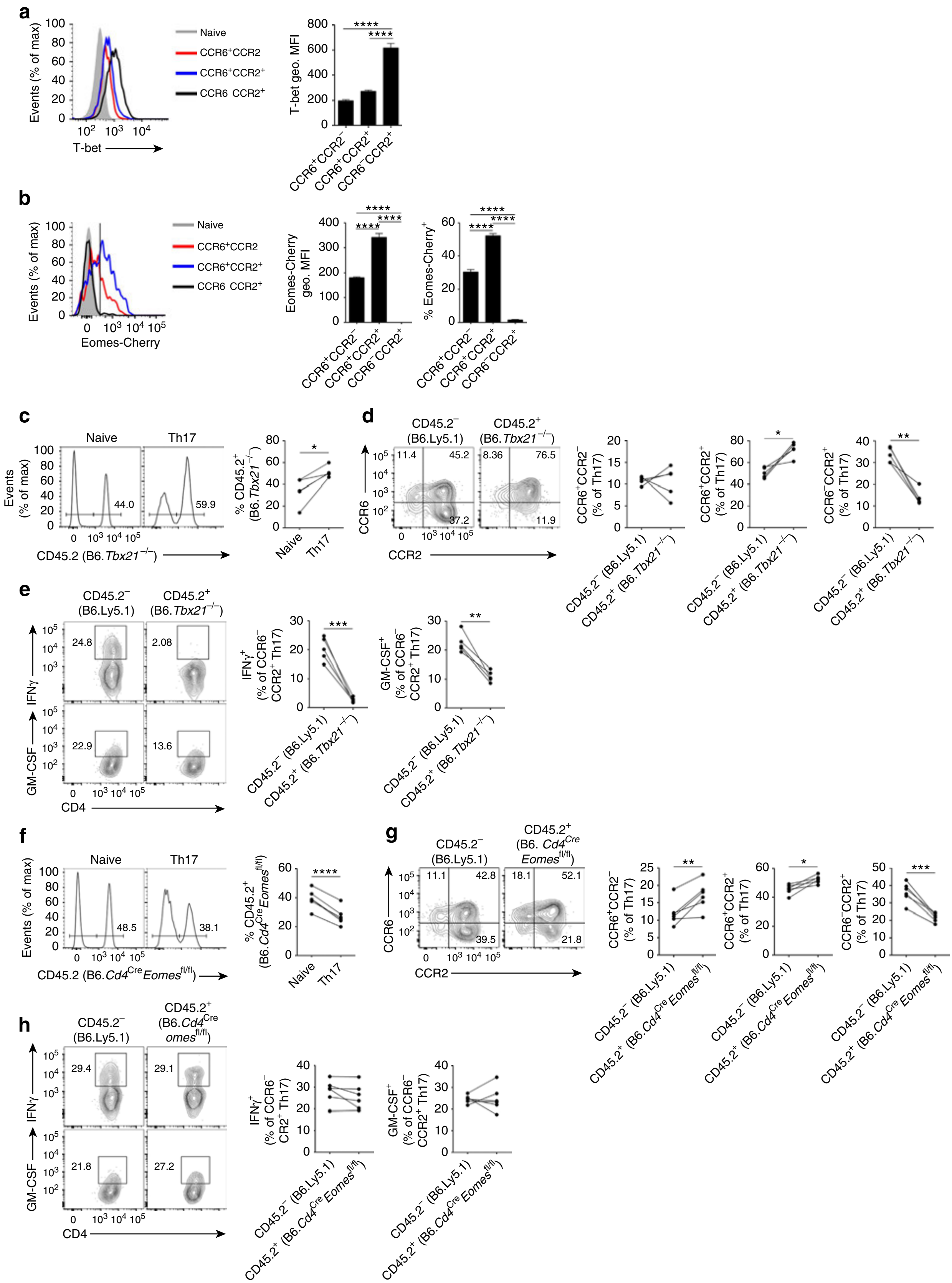

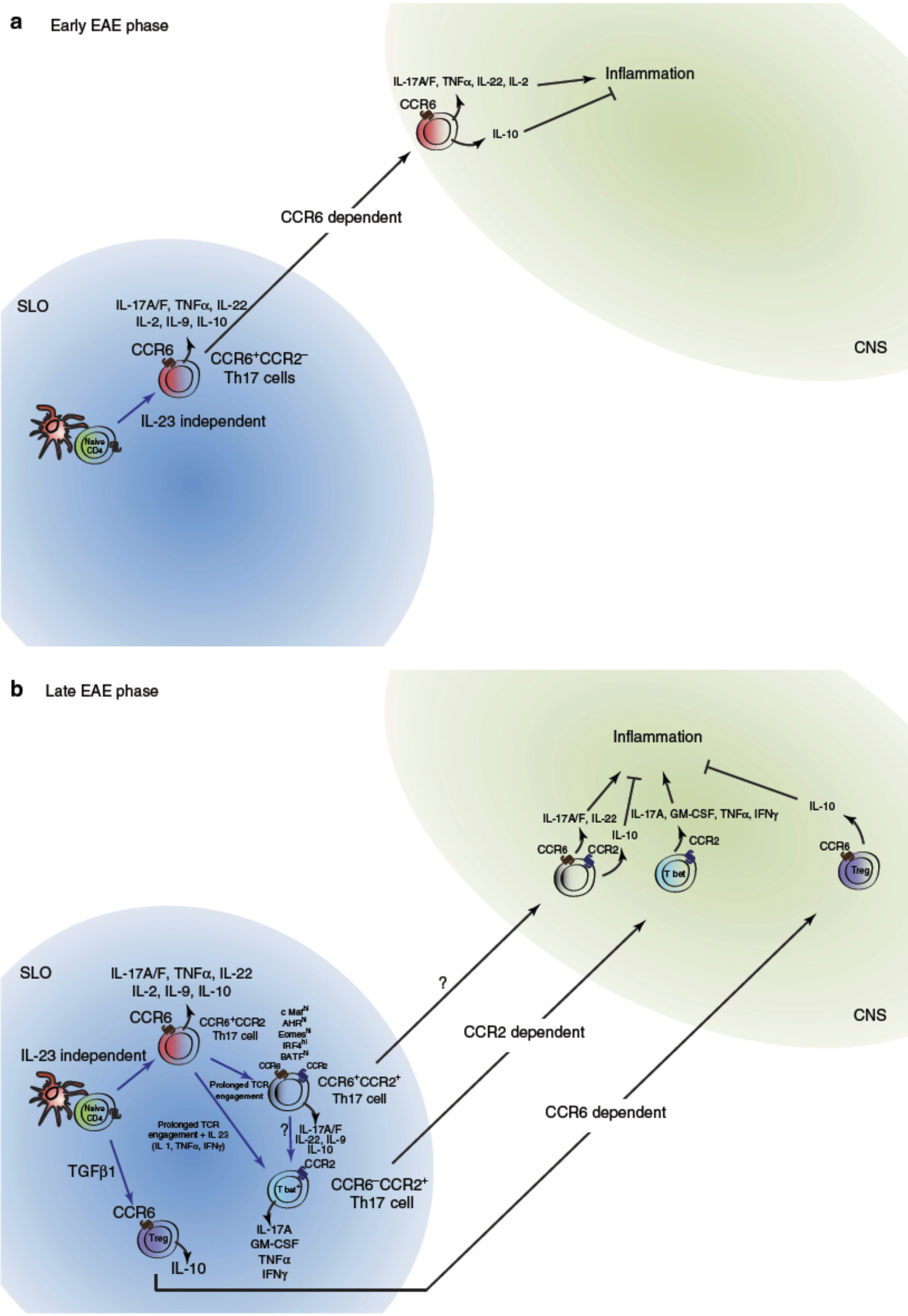

Figure 7 | Proposed model of Th17 cell development and homing in EAE. (**a**) Initial Th17 cell differentiation from naive precursors occurs independently of IL-23 and gives rise to CCR6$^+$CCR2$^-$ Th17 cells. These cells gain access to the CNS via CCR6 (first wave) and may contribute to the initiation of CNS inflammation via the provision of inflammatory cytokines including IL-17A/F, TNFα, IL-22 and IL-2. (**b**) Meanwhile in the SLOs, persistent antigen drives the emergence of CCR2$^+$ Th17 cell population whereby prolonged TCR stimulation gives rise to CCR6$^+$CCR2$^+$ Th17 cells, which express IL-10 and IL-9, whereas the presence of IL-23 and, to a lesser extent, IL-1, TNFα and IFNγ drives differentiation of GM-CSF/IFNγ-producing CCR6$^-$CCR2$^+$Th17 cells in a T-bet and Eomesodermin-dependent manner. Encephalitogenic Th17 cells gain access to the CNS via CCR2, independently of CCR6 (second wave), where the balance between CCR6$^+$CCR2$^+$ IL-10-producing Th17 cells, CCR6$^-$CCR2$^+$ GM-CSF/IFNγ-producing Th17 cells, other effector T cells (not depicted) and CCR6$^+$ Tregs determines the outcome of disease.

Human samples. Heparinized blood was collected following informed consent and rested for 4 h at 22 °C before peripheral blood mononuclear cell isolation using lymphocyte separation medium (MP Biomedicals). Peripheral blood mononuclear cells were frozen in 10% Dimethyl sulphoxide (Sigma) and stored at 80 °C before analysis. Properties of the study population are described in Supplementary Information (Supplementary Table 1). All experiments were conducted in accordance to the guidelines outlined by the ethics committee at the University of Leuven.

BM chimeras. B6.Ly5.1 mice were lethally irradiated with 1,000 Rads and reconstituted with 4 5×10^6 total BM cells intravenously (i.v.) of genotypes indicated in-text. A minimum of 8 weeks was allowed for reconstitution before experimentation.

Experimental autoimmune encephalomyelitis. Mice on the B6 background were immunized subcutaneously with 100 µg $MOG_{35\ 55}$ (GL Biochem) emulsified in 100 µl Complete Freund's Adjuvant (CFA) containing 85% mineral oil (Sigma), 15% mannide manooleate (Sigma) and 8.33 mg ml^{-1} *Mycobacterium tuberculosis* strain H37RA (Difco Laboratories). SJL/J mice were immunized subcutaneously with 100 µg proteolipid protein $(PLP)_{139\ 151}$ emulsified in 100 µl CFA (as above with the addition of 0.5 mg ml^{-1} *Mycobacterium butyricum* (Difco Laboratories)). Mice received 300 ng pertussis toxin (List Biological Laboratories) intraperitoneally on days 0 and 2. For B6.*Rag1*$^{-/-}$ EAE experiments, 8×10^6 CD4$^+$ T cells (CD4$^+$ T-cell isolation kit, StemCell Technologies) from B6 or B6.*Ccr2*$^{-/-}$ mice were transferred i.v. into B6.*Rag1*$^{-/-}$ recipients, which were immunized for EAE the next day as described above.

Disease scores in $MOG_{35\ 55}$-induced and $PLP_{139\ 151}$-induced EAE were assigned as described previously[21,65]. Disease state in the SJL/J/$PLP_{139\ 151}$ model was assigned as follows: peak acute disease: score ≥ 2; remission: previously score ≥ 2, now score ≤ 1 for minimum of 2 days; relapse: reached peak acute disease and remission, and is now score ≥ 2. In Fig. 2c, mice in remission were randomly allocated to experimental groups by two independent researchers by drawing an experimental group number (at equal odds) in a blinded manner. EAE disease scores were assigned in a blinded manner by two independent researchers. For isolation of CNS leukocytes, mice were perfused through the left cardiac ventricle with PBS, the brain and spinal cord harvested and dissociated through 70-µm nylon filters (BD), followed by 40% Percoll gradient centrifugation.

***S. pneumoniae* nasopharyngeal colonization.** *S. pneumoniae* strain EF3030 (serotype 19F) was obtained from Professor David E. Briles (University of Alabama at Birmingham, USA). The EF3030 strain was chosen as it causes long-term nasopharyngeal colonization in mice, with no detectable bacteremia[66,67]. For mouse challenge, EF3030 was grown in serum broth (nutrient broth containing 10% vol/vol heat-inactivated horse serum) at 37 °C in 5% CO_2 to $A_{600}=0.17$ ($\sim5\times10^7$ CFU ml^{-1}). Serotype 19F-specific capsule production was confirmed by the Quellung reaction. Bacteria were harvested by centrifugation at 3000*g*, washed once in PBS and resuspended in PBS to 5×10^8 CFU ml^{-1}. Mice were challenged with 10 µl (5×10^6 CFU) of bacterial suspension by microtip instillation into both nares without anaesthesia. The challenge dose was confirmed retrospectively by serial dilution and plating of the inocula on blood agar.

***In vivo* neutralization/antagonism.** Mice were administered 100 µg $CCL2_{ala}$ (scrambled peptide control)[22,23], $CCL2_{9\ 76}$ (CCR2 receptor antagonist)[23] or $CCL20_{6\ 70}$ (CCR6 receptor antagonist)[21,22] intraperitoneally using the dosing regimen indicated in-text. Neutralizing antibodies to CCL2 (BioXCell; clone 2H5; 300 µg per dose), IFNγ (BioXCell; clone XMG1.2; 250 µg per dose) and IL-1R1 (BioXCell; clone JAMA-147; 250 µg per dose) were administered intraperitoneally using the dosing regimen indicated in-text.

Flow cytometry. Antibodies used in this study are described in Supplementary Information (Supplementary Tables 2 and 3). For assessment of intracellular cytokine expression in murine cells, cells were first stimulated with phorbol 12-myristate 13-acetate (PMA; 20 ng ml^{-1}) (Invitrogen), Ionomycin (1 µM) (Invitrogen) and GolgiStop (BD; as per the manufacturers' instructions) in complete IMDM for 4 5 h before surface staining. Dead cells were excluded using LIVE/DEAD fixable near-infrared dye (Molecular Probes). Cells were stained in PBS containing 0.04% sodium azide and 1% BSA (Sigma) or 2% FCS. Fc receptors were blocked before surface staining with 1 mg ml^{-1} murine γ-globulin (Rockland). For detection of CCR2, 10^6 cells were stained with 5.5 µg ml^{-1} purified rat anti-mouse CCR2 (Clone MC21). Goat anti-rat IgG-Alexa Fluor 647 (Life Technologies) secondary antibody pre-adsorbed in 1% normal mouse serum and murine γ-globulin (0.5 mg ml^{-1}; Rockland) was used to detect primary rat antibody. Following secondary antibody staining, cells were incubated in rat γ-globulin (1 mg ml^{-1}; Rockland) before directly conjugated surface antibodies. Intracellular staining was performed using the BD Cytofix/Cytoperm kit (staining cytokines only) or eBioscience Foxp3/Transcription Factor Staining Buffer Set (transcription factor and cytokine staining) as per the manufacturers' instructions. For detection of transcription factors (excluding Foxp3), antibodies were pre-adsorbed in 2% normal mouse serum and 2% normal rat serum for 20 min before staining. Data were acquired on BD LSRII, BD FACSCanto, BD FACSAria or BD LSRFortessa flow cytometers. BD FACSAria was used for sorting experiments. For assessment of cytokine expression in human cells, thawed cells were stimulated for 5 h in 1 × Cell Stimulation Cocktail (plus protein transport inhibitors) (eBioscience). Stimulated cells were surface stained, then fixed and permeabilized using Cytofix/Cytoperm (BD) before staining for cytokines. Data were acquired on a BD FACSCantoII. All data were analysed using FlowJo software (Treestar).

***Ex vivo* MOG-reactive Th17 cell culture and T-cell transfers.** Splenocytes from d5 MOG/CFA-immunized mice were cultured (10^6 cells per ml) in complete IMDM (Gibco) containing $MOG_{35\ 55}$ (10 µg ml^{-1}; GL Biochem), anti-IFNγ (10 µg ml^{-1}; Clone XMG1.2, BioXCell) and anti-IL-4 (10 µg ml^{-1}; Clone 11B11, BioXCell) with the addition of either no cytokines, TGFβ1 (2 ng ml^{-1}; eBioscience) and IL-6 (20 ng ml^{-1}; eBioscience), or IL-23 (10 ng ml^{-1}; eBioscience). Cells were analysed after 3 days of culture. For transfer experiments, donor mice were immunized subcutaneously with 100 µg $MOG_{35\ 55}$/CFA in footpads and hind flanks. Popliteal and inguinal lymph nodes were harvested 10 days post immunization and MOG-reactive Th17 cells expanded *ex vivo* in complete IMDM (Gibco) containing $MOG_{35\ 55}$ (10 µg ml^{-1}; GL Biochem) and IL-23 (3 ng ml^{-1}; eBioscience) at a cell density of 10^6 cells per ml for 3 days. Before transfer, numbers of MOG-reactive Th17 (TCRβ$^+$CD4$^+$IL-17A$^+$) cells in culture were determined following restimulation with PMA/Ionomycin/GolgiStop in complete IMDM for 4 5 h using flow cytometry. MOG-reactive Th17 cells (3×10^5) were adoptively transferred i.v. into pre-immunized congenic recipient mice as described in text.

***Ex vivo* chemotaxis assays.** Splenocytes from d10 $MOG_{35\ 55}$/CFA-immunized mice were rested at 37 °C in complete RPMI 1640 for 3 4 hr. Chemokines (recombinant mouse CCL20 or recombinant mouse CCL2; kindly provided by the late Professor Ian Clark-Lewis) diluted in 150 µl chemotaxis buffer (RPMI 1640 with 0.5% BSA and 20 mM HEPES) were added to lower chambers of 96-well Transwell chemotaxis plates (5-µm pore size; Corning). Rested cells were extensively washed in chemotaxis buffer and loaded into the upper chambers at 2×10^6 cells per well in 50 µl of chemotaxis buffer and incubated for 3 h at 37 °C. To enumerate Th17, Th1 and Treg cell migration, cells were harvested from the bottom chambers, restimulated in complete IMDM containing PMA/Ionomycin/GolgiStop as described above for 4 h before flow cytometric analyses. Cells of interest were gated as follows: Th1: CD3$^+$CD4$^+$Foxp3$^-$IL-17A$^-$IFNγ$^+$; Th17: CD3$^+$CD4$^+$Foxp3$^-$IL-17A$^+$; Treg: CD3$^+$CD4$^+$IL-17A$^-$IFNγ$^-$Foxp3$^+$. Migration index was calculated by dividing the number of positive events in test wells by the number of positive events in which no chemokine was added to the bottom chamber. Migrated cells of interest were enumerated using CaliBRITE beads (BD) as an internal reference.

Quantitative PCR. Primer sequences used in this study are described in Supplementary Information (Supplementary Table 4). RNA was harvested from cells using the Qiagen microRNeasy kit with on-column DNase treatment as per the manufacturers' instructions. cDNA synthesis was performed using the Transcriptor First Strand cDNA synthesis kit (Roche) and used as template in reactions using LightCycler 480 SYBR Green master mix I (Roche) according to the manufacturers' instructions. Relative abundance of transcript was calculated as $2^{-\Delta CT}$, that is, $\Delta CT = (CT_{Target}\quad CT_{Rplp0})$.

ELISA. Supernatants from homogenized CNS samples were stored at 80 °C in PBS containing a protease inhibitor cocktail (Sigma) until the day of analysis. ELISA were conducted as previously described[65]. CCL2 and CCL20 ELISA: capture and detection antibody from R&D; IL-10 and IFNγ ELISA: capture and detection antibody from eBioscience; IL-17A ELISA: capture antibody, purified clone TC11-18H10 from BD; and detection antibody, biotinylated clone TC11-8H4 from BD were used.

Statistics. Data were analysed with Prism 6 (GraphPad Software) using two-tailed unpaired or paired Student's *t*-tests, one-way or two-way analysis of variances with appropriate post tests as indicated in text. For all analyses, $P\leq0.05$ was considered significant. Sample or experiment sizes were determined empirically for sufficient statistical power. No statistical tests were used to predetermine the size of experiments. No data points were excluded from statistical tests. Statistical analysis was performed on groups with similar variance. Limited variance was observed within sample groups.

References

1. Peters, A., Lee, Y. & Kuchroo, V. K. The many faces of Th17 cells. *Curr. Opin. Immunol.* **23,** 702 706 (2011).
2. McGeachy, M. J. *et al.* TGF-beta and IL-6 drive the production of IL-17 and IL-10 by T cells and restrain T(H)-17 cell-mediated pathology. *Nat. Immunol.* **8,** 1390 1397 (2007).

3. Ghoreschi, K. *et al.* Generation of pathogenic T(H)17 cells in the absence of TGF-beta signalling. *Nature* **467,** 967 971 (2010).
4. Lee, Y. *et al.* Induction and molecular signature of pathogenic TH17 cells. *Nat. Immunol.* **13,** 991 999 (2012).
5. Esplugues, E. *et al.* Control of TH17 cells occurs in the small intestine. *Nature* **475,** 514 518 (2011).
6. El-Behi, M. *et al.* The encephalitogenicity of T(H)17 cells is dependent on IL-1- and IL-23-induced production of the cytokine GM-CSF. *Nat. Immunol.* **12,** 568 575 (2011).
7. Codarri, L. *et al.* RORgammat drives production of the cytokine GM-CSF in helper T cells, which is essential for the effector phase of autoimmune neuroinflammation. *Nat. Immunol.* **12,** 560 567 (2011).
8. McGeachy, M. J. *et al.* The interleukin 23 receptor is essential for the terminal differentiation of interleukin 17-producing effector T helper cells in vivo. *Nat. Immunol.* **10,** 314 324 (2009).
9. Langrish, C. L. *et al.* IL-23 drives a pathogenic T cell population that induces autoimmune inflammation. *J. Exp. Med.* **201,** 233 240 (2005).
10. Haines, C. J. *et al.* Autoimmune memory T helper 17 cell function and expansion are dependent on interleukin-23. *Cell Rep.* **3,** 1378 1388 (2013).
11. Hirota, K. *et al.* Fate mapping of IL-17-producing T cells in inflammatory responses. *Nat. Immunol.* **12,** 255 263 (2011).
12. Gaffen, S. L., Jain, R., Garg, A. V. & Cua, D. J. The IL-23-IL-17 immune axis: from mechanisms to therapeutic testing. *Nat. Rev. Immunol.* **14,** 585 600 (2014).
13. Hirota, K. *et al.* Plasticity of Th17 cells in Peyer's patches is responsible for the induction of T cell-dependent IgA responses. *Nat. Immunol.* **14,** 372 379 (2013).
14. Chackerian, A. A. *et al.* Neutralization or absence of the interleukin-23 pathway does not compromise immunity to mycobacterial infection. *Infect. Immun.* **74,** 6092 6099 (2006).
15. Kleinschek, M. A. *et al.* IL-23 enhances the inflammatory cell response in *Cryptococcus neoformans* infection and induces a cytokine pattern distinct from IL-12. *J. Immunol.* **176,** 1098 1106 (2006).
16. Yamazaki, T. *et al.* CCR6 regulates the migration of inflammatory and regulatory T cells. *J. Immunol.* **181,** 8391 8401 (2008).
17. Comerford, I. *et al.* An immune paradox: how can the same chemokine axis regulate both immune tolerance and activation?: CCR6/CCL20: a chemokine axis balancing immunological tolerance and inflammation in autoimmune disease. *Bioessays* **32,** 1067 1076 (2010).
18. Reboldi, A. *et al.* C-C chemokine receptor 6-regulated entry of TH-17 cells into the CNS through the choroid plexus is required for the initiation of EAE. *Nat. Immunol.* **10,** 514 523 (2009).
19. Elhofy, A., Depaolo, R. W., Lira, S. A., Lukacs, N. W. & Karpus, W. J. Mice deficient for CCR6 fail to control chronic experimental autoimmune encephalomyelitis. *J. Neuroimmunol.* **213,** 91 99 (2009).
20. Villares, R. *et al.* CCR6 regulates EAE pathogenesis by controlling regulatory CD4+ T-cell recruitment to target tissues. *Eur. J. Immunol.* **39,** 1671 1681 (2009).
21. Liston, A. *et al.* Inhibition of CCR6 function reduces the severity of experimental autoimmune encephalomyelitis via effects on the priming phase of the immune response. *J. Immunol.* **182,** 3121 3130 (2009).
22. Kara, E. E. *et al.* Distinct chemokine receptor axes regulate Th9 cell trafficking to allergic and autoimmune inflammatory sites. *J. Immunol.* **191,** 1110 1117 (2013).
23. Gong, J. H., Ratkay, L. G., Waterfield, J. D. & Clark-Lewis, I. An antagonist of monocyte chemoattractant protein 1 (MCP-1) inhibits arthritis in the MRL-lpr mouse model. *J. Exp. Med.* **186,** 131 137 (1997).
24. Fife, B. T., Huffnagle, G. B., Kuziel, W. A. & Karpus, W. J. CC chemokine receptor 2 is critical for induction of experimental autoimmune encephalomyelitis. *J. Exp. Med.* **192,** 899 905 (2000).
25. Izikson, L., Klein, R. S., Charo, I. F., Weiner, H. L. & Luster, A. D. Resistance to experimental autoimmune encephalomyelitis in mice lacking the CC chemokine receptor (CCR)2. *J. Exp. Med.* **192,** 1075 1080 (2000).
26. Gaupp, S., Pitt, D., Kuziel, W. A., Cannella, B. & Raine, C. S. Experimental autoimmune encephalomyelitis (EAE) in CCR2(-/-) mice: susceptibility in multiple strains. *Am. J. Pathol.* **162,** 139 150 (2003).
27. Wang, Y. *et al.* The transcription factors T-bet and Runx are required for the ontogeny of pathogenic interferon-gamma-producing T helper 17 cells. *Immunity* **40,** 355 366 (2014).
28. Wilson, R. *et al.* Protection against *Streptococcus pneumoniae* lung infection after nasopharyngeal colonization requires both humoral and cellular immune responses. *Mucosal Immunol.* **8,** 627 639 (2015).
29. Zhang, Z., Clarke, T. B. & Weiser, J. N. Cellular effectors mediating Th17-dependent clearance of pneumococcal colonization in mice. *J. Clin. Invest.* **119,** 1899 1909 (2009).
30. Palaniappan, R. *et al.* Differential PsaA-, PspA-, PspC-, and PdB-specific immune responses in a mouse model of pneumococcal carriage. *Infect. Immun.* **73,** 1006 1013 (2005).
31. Kebir, H. *et al.* Preferential recruitment of interferon-gamma-expressing TH17 cells in multiple sclerosis. *Ann. Neurol.* **66,** 390 402 (2009).
32. Rasouli, J. *et al.* Expression of GM-CSF in T cells is increased in multiple sclerosis and suppressed by IFN-beta therapy. *J. Immunol.* **194,** 5085 5093 (2015).
33. Awasthi, A. *et al.* Cutting edge: IL-23 receptor gfp reporter mice reveal distinct populations of IL-17-producing cells. *J. Immunol.* **182,** 5904 5908 (2009).
34. Sutton, C., Brereton, C., Keogh, B., Mills, K. H. & Lavelle, E. C. A crucial role for interleukin (IL)-1 in the induction of IL-17-producing T cells that mediate autoimmune encephalomyelitis. *J. Exp. Med.* **203,** 1685 1691 (2006).
35. Kimura, A., Naka, T. & Kishimoto, T. IL-6-dependent and -independent pathways in the development of interleukin 17-producing T helper cells. *Proc. Natl Acad. Sci. USA* **104,** 12099 12104 (2007).
36. Harrington, L. E. *et al.* Interleukin 17-producing CD4+ effector T cells develop via a lineage distinct from the T helper type 1 and 2 lineages. *Nat. Immunol.* **6,** 1123 1132 (2005).
37. Yeh, W. I., McWilliams, I. L. & Harrington, L. E. IFNgamma inhibits Th17 differentiation and function via Tbet-dependent and Tbet-independent mechanisms. *J. Neuroimmunol.* **267,** 20 27 (2014).
38. Lexberg, M. H. *et al.* IFN-gamma and IL-12 synergize to convert in vivo generated Th17 into Th1/Th17 cells. *Eur. J. Immunol.* **40,** 3017 3027 (2010).
39. Xu, J. *et al.* c-Maf regulates IL-10 expression during Th17 polarization. *J. Immunol.* **182,** 6226 6236 (2009).
40. Ciofani, M. *et al.* A validated regulatory network for Th17 cell specification. *Cell* **151,** 289 303 (2012).
41. Lazarevic, V. *et al.* T-bet represses T(H)17 differentiation by preventing Runx1-mediated activation of the gene encoding RORgammat. *Nat. Immunol.* **12,** 96 104 (2011).
42. Duhen, R. *et al.* Cutting edge: the pathogenicity of IFN-gamma-producing Th17 cells is independent of T-bet. *J. Immunol.* **190,** 4478 4482 (2013).
43. Allegretti, M., Cesta, M. C., Garin, A. & Proudfoot, A. E. Current status of chemokine receptor inhibitors in development. *Immunol. Lett.* **145,** 68 78 (2012).
44. Mack, M. *et al.* Expression and characterization of the chemokine receptors CCR2 and CCR5 in mice. *J. Immunol.* **166,** 4697 4704 (2001).
45. Sato, W., Aranami, T. & Yamamura, T. Cutting edge: Human Th17 cells are identified as bearing CCR2+CCR5- phenotype. *J. Immunol.* **178,** 7525 7529 (2007).
46. Mahad, D. J. & Ransohoff, R. M. The role of MCP-1 (CCL2) and CCR2 in multiple sclerosis and experimental autoimmune encephalomyelitis (EAE). *Semin. Immunol.* **15,** 23 32 (2003).
47. Kreymborg, K. *et al.* IL-22 is expressed by Th17 cells in an IL-23-dependent fashion, but not required for the development of autoimmune encephalomyelitis. *J. Immunol.* **179,** 8098 8104 (2007).
48. Haak, S. *et al.* IL-17A and IL-17F do not contribute vitally to autoimmune neuro-inflammation in mice. *J. Clin. Invest.* **119,** 61 69 (2009).
49. Frei, K. *et al.* Tumor necrosis factor alpha and lymphotoxin alpha are not required for induction of acute experimental autoimmune encephalomyelitis. *J. Exp. Med.* **185,** 2177 2182 (1997).
50. Gagliani, N. *et al.* Th17 cells transdifferentiate into regulatory T cells during resolution of inflammation. *Nature* **523,** 221 225 (2015).
51. Ichiyama, K. *et al.* Transcription factor Smad-independent T helper 17 cell induction by transforming-growth factor-beta is mediated by suppression of eomesodermin. *Immunity* **34,** 741 754 (2011).
52. Fontenot, J. D. *et al.* Regulatory T cell lineage specification by the forkhead transcription factor foxp3. *Immunity* **22,** 329 341 (2005).
53. Varona, R. *et al.* CCR6-deficient mice have impaired leukocyte homeostasis and altered contact hypersensitivity and delayed-type hypersensitivity responses. *J. Clin. Invest.* **107,** R37 R45 (2001).
54. Boring, L. *et al.* Impaired monocyte migration and reduced type 1 (Th1) cytokine responses in C-C chemokine receptor 2 knockout mice. *J. Clin. Invest.* **100,** 2552 2561 (1997).
55. Cua, D. J. *et al.* Interleukin-23 rather than interleukin-12 is the critical cytokine for autoimmune inflammation of the brain. *Nature* **421,** 744 748 (2003).
56. Magram, J. *et al.* IL-12-deficient mice are defective in IFN gamma production and type 1 cytokine responses. *Immunity* **4,** 471 481 (1996).
57. Mattner, F. *et al.* Genetically resistant mice lacking interleukin-12 are susceptible to infection with Leishmania major and mount a polarized Th2 cell response. *Eur. J. Immunol.* **26,** 1553 1559 (1996).
58. Huang, S. *et al.* Immune response in mice that lack the interferon-gamma receptor. *Science* **259,** 1742 1745 (1993).
59. Korner, H. *et al.* Distinct roles for lymphotoxin-alpha and tumor necrosis factor in organogenesis and spatial organization of lymphoid tissue. *Eur. J. Immunol.* **27,** 2600 2609 (1997).
60. Peschon, J. J. *et al.* TNF receptor-deficient mice reveal divergent roles for p55 and p75 in several models of inflammation. *J. Immunol.* **160,** 943 952 (1998).

61. Erickson, S. L. *et al.* Decreased sensitivity to tumour-necrosis factor but normal T-cell development in TNF receptor-2-deficient mice. *Nature* **372,** 560–563 (1994).
62. Finotto, S. *et al.* Development of spontaneous airway changes consistent with human asthma in mice lacking T-bet. *Science* **295,** 336–338 (2002).
63. Zhu, Y. *et al.* T-bet and eomesodermin are required for T cell-mediated antitumor immune responses. *J. Immunol.* **185,** 3174–3183 (2010).
64. Mombaerts, P. *et al.* Mutations in T-cell antigen receptor genes alpha and beta block thymocyte development at different stages. *Nature* **360,** 225–231 (1992).
65. Comerford, I. *et al.* The atypical chemokine receptor CCX-CKR scavenges homeostatic chemokines in circulation and tissues and suppresses Th17 responses. *Blood* **116,** 4130–4140 (2010).
66. van Ginkel, F. W. *et al.* Pneumococcal carriage results in ganglioside-mediated olfactory tissue infection. *Proc. Natl Acad. Sci. USA* **100,** 14363–14367 (2003).
67. Briles, D. E., Crain, M. J., Gray, B. M., Forman, C. & Yother, J. Strong association between capsular type and virulence for mice among human isolates of *Streptococcus pneumoniae*. *Infect. Immun.* **60,** 111–116 (1992).

Acknowledgements

We thank Professor Tracey Handel (University of California, La Jolla, USA) and the late Professor Ian Clark-Lewis for recombinant chemokines and chemokine receptor antagonists; Dr Josef Ngyuen (Royal Adelaide Hospital, Adelaide, Australia) for mouse irradiation; Professor Brigitta Stockinger (Medical Research Council National Institute for Medical Research, UK) for B6.$Il17a^{Cre}Rosa26^{eYFP}$ mice; Dr Christian Engwerda (QIMR Berghofer Medical Research Institute, Australia) for B6.$Ccr2^{-/-}$ mice; Professor Bernhard Baune (University of Adelaide, Australia) for B6.$Tnf^{-/-}$, B6.$Tnfrsf1a^{-/-}$ and B6.$Tnfrsf1b^{-/-}$ mice; Professor Carola Vinuesa (John Curtin School of Medical Research, Australia) for B6.$Tcra^{-/-}$ mice; Staff of the Laboratory Animal Services of the University of Adelaide for Animal Husbandry; and Staff of the Detmold Facility (IMVS, Australia) for some cell sorting experiments. This work was supported by funding held by S.R.M. and I.C. from National Health and Medical Research Council (NH&MRC) Grant 1066781. I.C. is supported by funds from Multiple Sclerosis Research Australia. M.J.S. is supported by an NH&MRC Research Fellowship (1078671). E.E.K. is supported by an Australian Postgraduate Award and the Norman and Patricia Polglase Scholarship.

Author contributions

E.E.K. designed, performed and analysed experiments, and wrote the manuscript. D.R.M., C.R.B. and C.E.G. performed experiments and edited the manuscript. K.A.F., D.R. and A.D.O. performed experiments. C.S. generated B6.$Eomes^{Cherry}$ reporter mice. M.M. provided the anti-mouse CCR2 antibody and edited the manuscript. B.D. provided peripheral blood samples from healthy and MS patient donors. A.L. supervised human Th17 cell experiments, critical discussions and edited the manuscript. J.C.P. provided the *S. pneumoniae* nasopharyngeal colonization model. K.P.A.M., G.T.B., M.J.S. and G.R.H. provided mice, critical discussions and edited the manuscript. I.C. and S.R.M. supervised the study and wrote the manuscript.

Additional information

Supplementary Information accompanies this paper at http://www.nature.com/naturecommunications

Competing financial interests: The authors declare no competing financial interests.

Reprints and permission information is available online at http://npg.nature.com/reprintsandpermissions/

How to cite this article: Kara, E. E. *et al.* CCR2 defines *in vivo* development and homing of IL-23-driven GM-CSF-producing Th17 cells. *Nat. Commun.* 6:8644 doi: 10.1038/ncomms9644 (2015).

SUPPLEMENTARY FIGURES

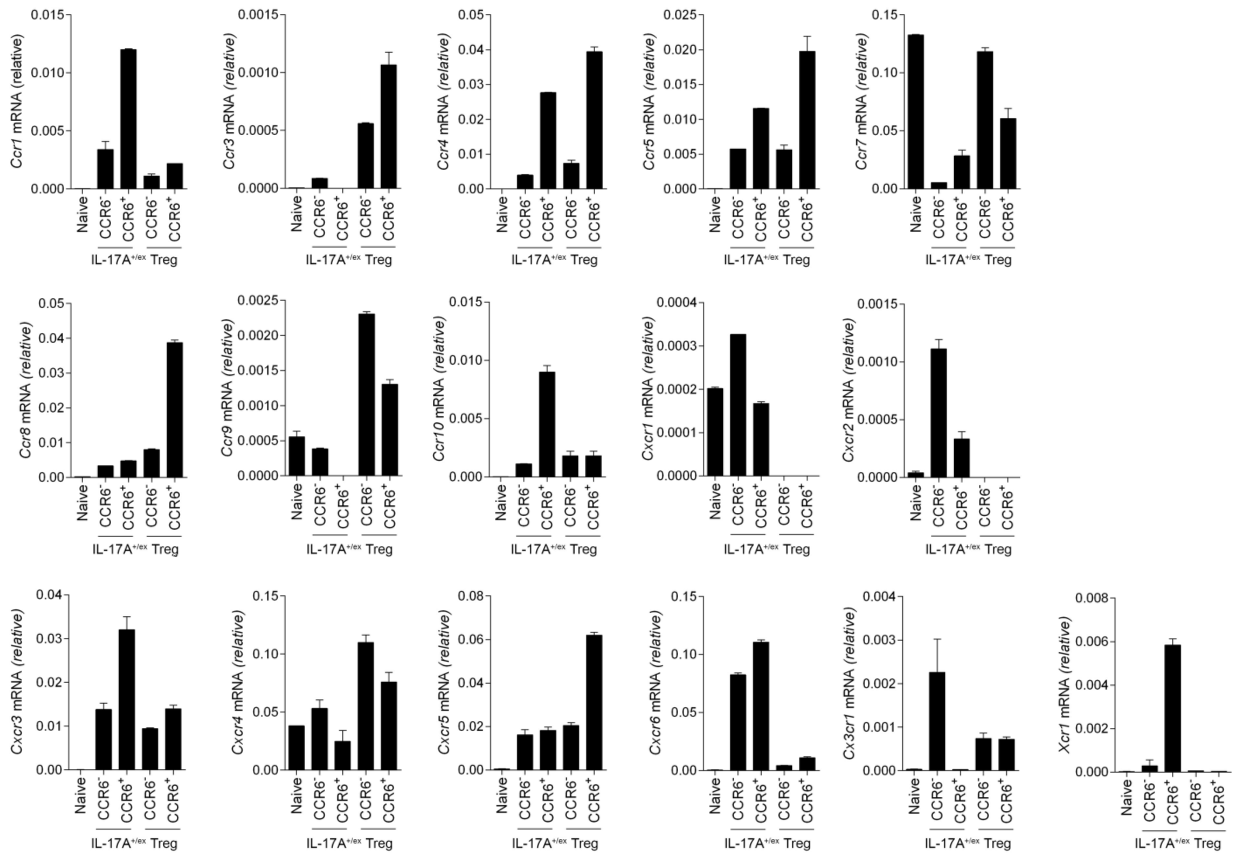

Supplementary Figure 1: Chemokine receptor expression profiles of CCR6^{+} and CCR6^{-} CD4^{+}IL-17A$^{+/ex}$ and Treg cells.

Quantitative PCR analysis of chemokine receptor transcript abundance in FACS-purified CCR6^{+} and CCR6^{-} subsets of CD4^{+}IL-17A$^{+/ex}$ cells (CD3^{+}CD4^{+}CD44^{hi}IL-17A-eYFP^{+} - B6.*Il17a*^{Cre}*Rosa26*^{eYFP} mice) and Tregs (CD3^{+}CD4^{+}Foxp3-GFP^{+} - B6.*Foxp3*^{GFP} mice) from pooled spleen and dLN of mice 10 days post MOG/CFA immunization. Data presented relative to *Rplp0* (mean ± SD).

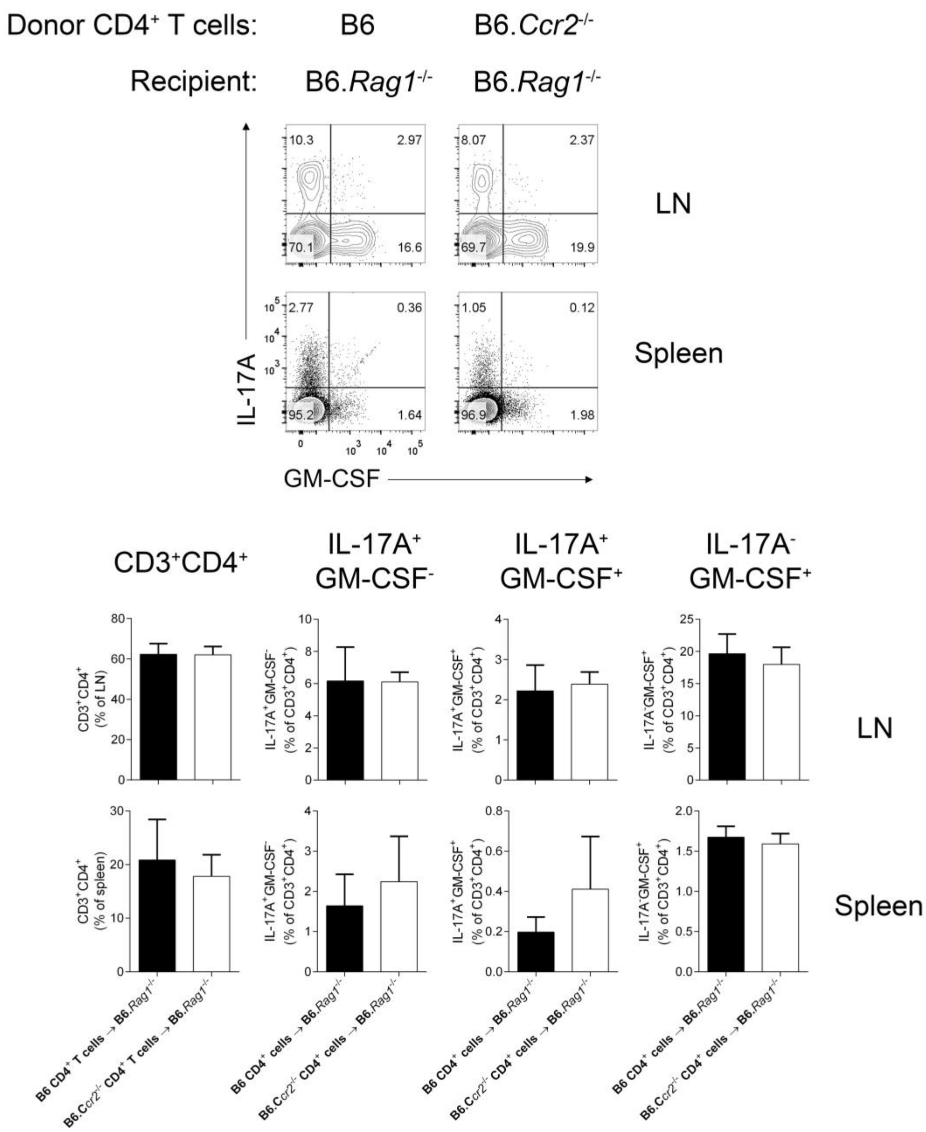

Supplementary Figure 2: *Ccr2*-deficiency on CD4$^+$ T cells does not alter Th17 cell of GM-CSF$^+$ Th cell generation in EAE-induced B6.*Rag1*$^{-/-}$ T cell-reconstituted mice.

8×10^6 MACS-purified CD4$^+$ T cells from B6 or B6.*Ccr2*$^{-/-}$ mice were transferred into B6.*Rag1*$^{-/-}$ recipients, which were immunised for EAE the next day. Representative flow cytometric analysis and quantitation of IL-17A and GM-CSF staining in CD3$^+$CD4$^+$ T cells from the lymph node (LN) and spleen 25 days post-immunisation.

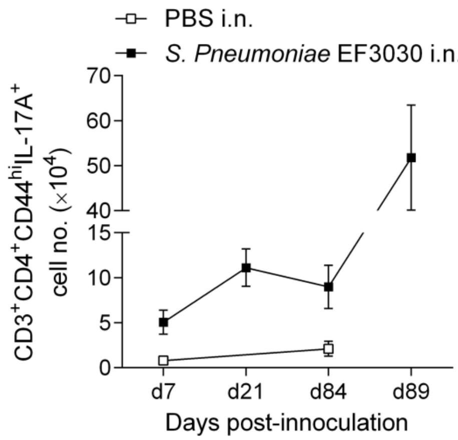

Supplementary Figure 3: Nasopharyngeal colonization with *S. pneumoniae* EF3030 induces splenic Th17 cell responses.

Mice were challenged with 5×10^6 CFU EF3030 or PBS by microtip instillation into both nares without anesthesia. Mice were sacrificed at various timepoints and Th17 cells ($CD3^+CD4^+CD44^{hi}IL\text{-}17A^+$) in the spleen enumerated over the course of infection by flow cytometry. On day 84 post-infection, mice were re-challenged i.n. with 5×10^6 CFU EF3030 and splenic Th17 cells enumerated 5 days post-secondary challenge (d89).

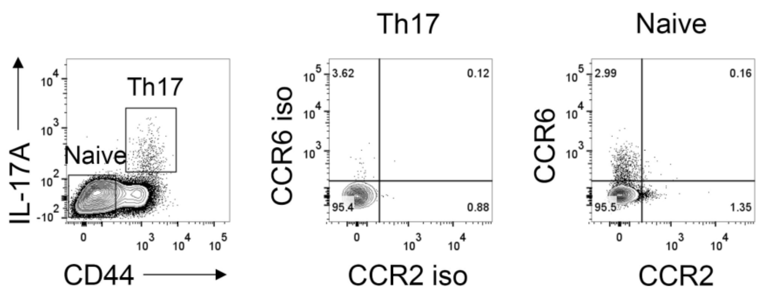

Supplementary Figure 4: Representative gating strategy relating to Fig. 5a.

Representative flow cytometric gating of naïve $CD4^+$ T cells ($CD4^+CD44^{lo}$) and Th17 cells ($CD4^+CD44^{hi}IL\text{-}17A^+$) related to Fig. 5a. Isotype staining on Th17 cells and CCR2/CCR6 expression on naïve $CD4^+$ T cells is shown.

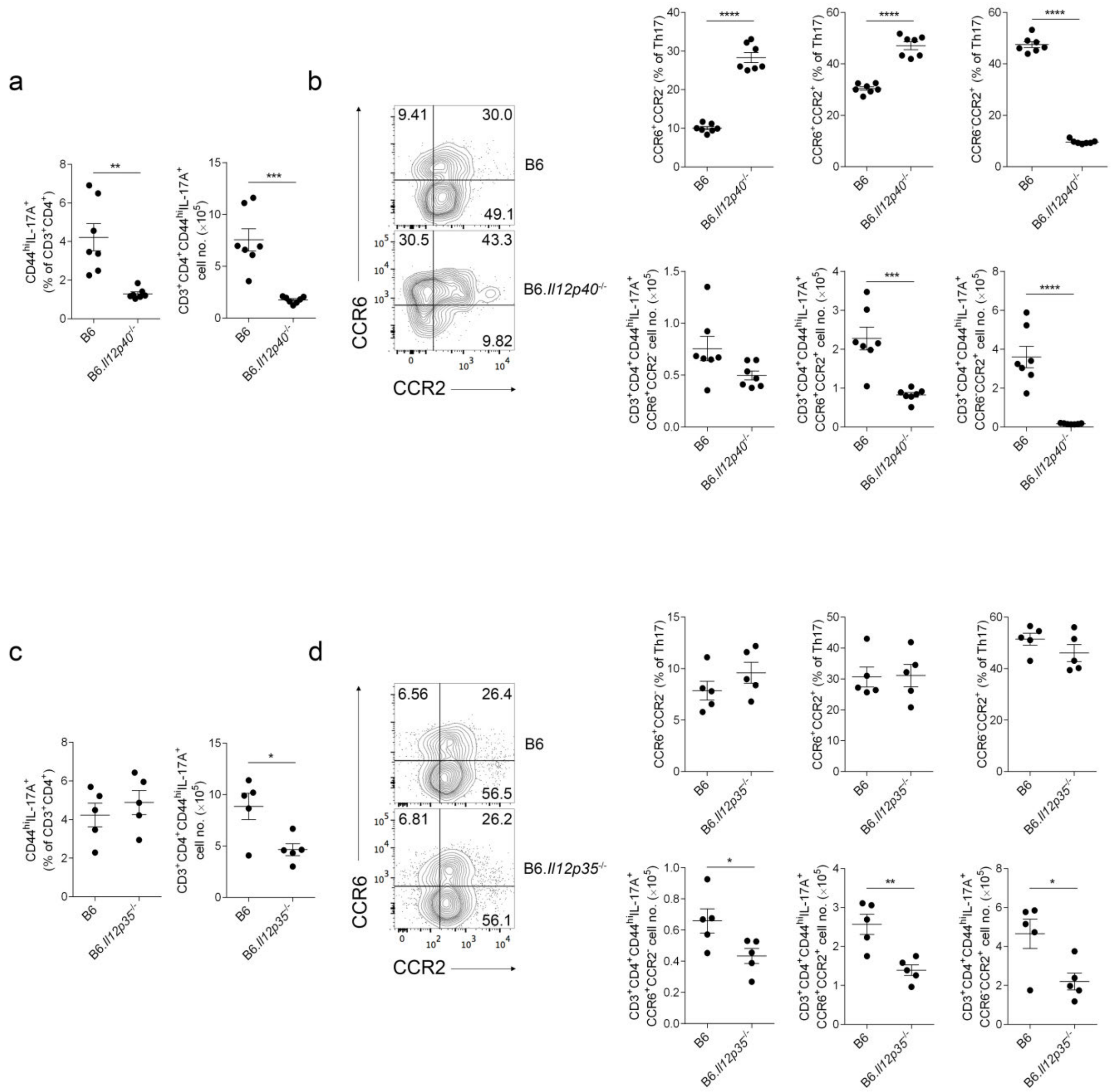

Supplementary Figure 5: Differentiation of CCR6$^-$CCR2$^+$ Th17 cells *in vivo* is independent of IL-12.

(**a, b**) Analysis of B6 (n=7) and B6.*Il12p40*$^{-/-}$ (n=7) mice d10 post MOG/CFA immunization. (**a**) Frequency and total number of Th17 cells in spleen; (**b**) representative flow cytometric analysis and quantitation of CCR6 and CCR2 staining on Th17 cells. (**c, d**) Analysis of B6 (n=5) and B6.*Il12p35*$^{-/-}$ (n=5) mice d10 post MOG/CFA immunization. (**c**) Frequency and total number of

Th17 cells in spleen; (**d**) representative flow cytometric analysis and quantitation of CCR6 and CCR2 staining on Th17 cells. (**a-d**) Each dot represents an individual mouse; data presented as mean ± SEM; * $p \leq 0.05$, ** $p \leq 0.01$, *** $p \leq 0.001$, **** $p \leq 0.0001$; unpaired two-tailed Student's *t*-test.

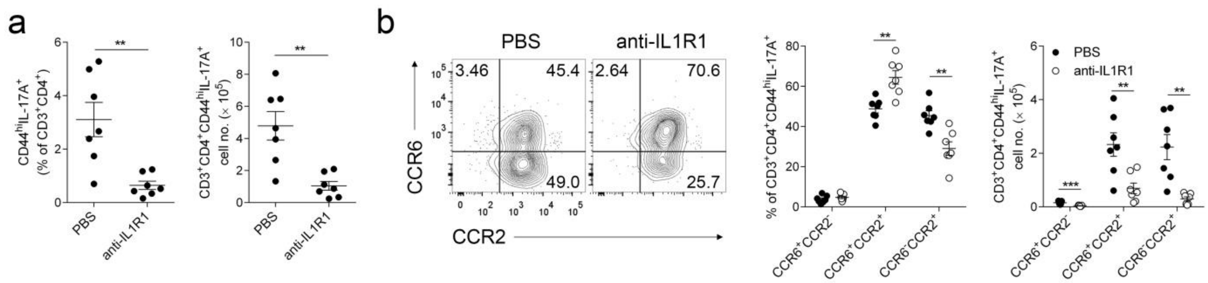

Supplementary Figure 6: IL-1 promotes CCR6$^-$CCR2$^+$ Th17 cell differentiation *in vivo*.

(**a, b**) Analysis of PBS (n=7) or neutralizing anti-IL-1R1 (n=7; 250 μg i.p. on d0 and every 48 hours thereafter) treated mice d10 post MOG/CFA immunization. (**a**) Frequency and total number of Th17 cells in spleen; (**b**) representative flow cytometric analysis and quantitation of CCR6 and CCR2 staining on Th17 cells. (**a, b**) Each dot represents an individual mouse; * $p \leq 0.05$, ** $p \leq 0.01$, *** $p \leq 0.001$; unpaired two-tailed Student's *t*-test; data presented as mean ± SEM.

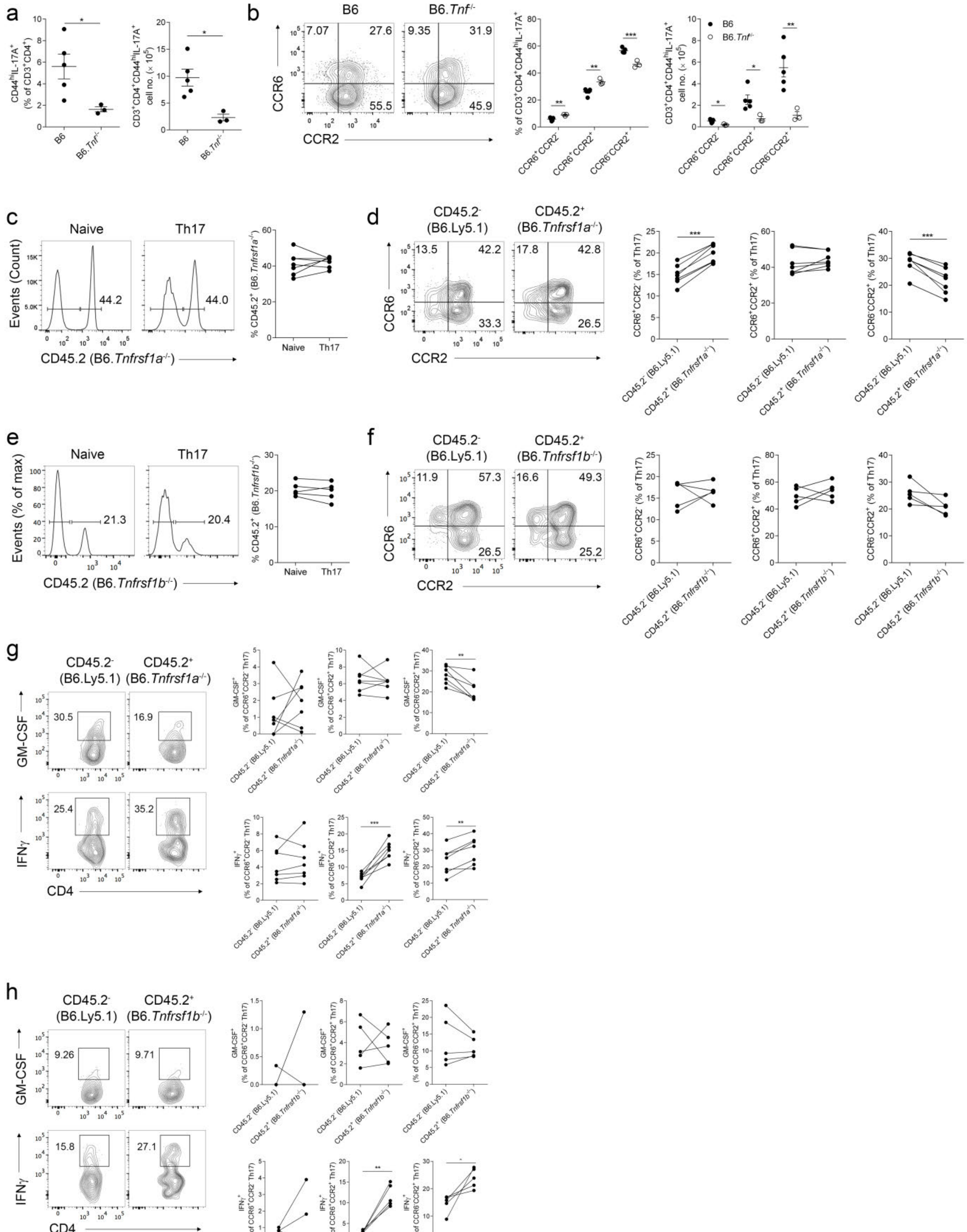

a
b
B6
B6.Tnf-/-
CCR6
CCR2
c
Naive
Th17
Events (Count)
CD45.2 (B6.Tnfrsf1a-/-)
d
CD45.2- (B6.Ly5.1)
CD45.2+ (B6.Tnfrsf1a-/-)
e
Events (% of max)
CD45.2 (B6.Tnfrsf1b-/-)
f
CD45.2+ (B6.Tnfrsf1b-/-)
g
GM-CSF
IFNγ
CD4
h

Supplementary Figure 7: T-cell expression of TNFR1 promotes $CCR6^{-}CCR2^{+}$ Th17 cell differentiation *in vivo*.

(**a ,b**) Analysis of B6 (n=5) and B6.*Tnf*$^{-/-}$ (n=3) mice d10 post MOG/CFA immunization. (**a**) Frequency and total number of Th17 cells in spleen; (**b**) representative flow cytometric analysis and quantitation of CCR6 and CCR2 staining on Th17 cells. Data are representative of 2 independent experiments. (**c, e**) Representative flow cytometric analysis and quantitation of $CD45.2^{+}$ cells within naïve $CD4^{+}$ ($CD3^{+}CD4^{+}CD44^{lo}$) and Th17 cells ($CD3^{+}CD4^{+}CD44^{hi}IL\text{-}17A^{+}$) in spleen of B6.*Tnfrsf1a*$^{-/-}$ (n=7) (**c**) and B6.*Tnfrsf1b*$^{-/-}$ (n=5) (**e**) mixed bone marrow chimeric mice on d10 post-MOG/CFA immunisation. (**d, f**) Representative flow cytometric analysis and quantitation of CCR6 and CCR2 staining on $CD45.2^{-}$ (B6.Ly5.1) and $CD45.2^{+}$ (**d** - B6.*Tnfrsf1a*$^{-/-}$; **f** - B6.*Tnfrsf1b*$^{-/-}$) Th17 cells in mixed bone marrow chimeras immunized with MOG/CFA 10 days prior. (**g, h**) Representative flow cytometric analysis of GM-CSF and IFNγ staining amongst $CD45.2^{-}$ (B6.Ly5.1) and $CD45.2^{+}$ (indicated KO) $CCR6^{-}CCR2^{+}$ Th17 cells in B6.*Tnfrsf1a*$^{-/-}$ (**g**, n=7) and B6.*Tnfrsf1b*$^{-/-}$ (**h**, n=5) mixed bone marrow chimeric mice 10 days post MOG/CFA immunization. Right, GM-CSF and IFNγ expression amongst CCR6/CCR2 Th17 cell populations in mixed bone marrow chimeras. (**a-h**) Each dot represents an individual mouse; * $p \leq 0.05$; ** $p \leq 0.01$; *** $p \leq 0.001$. (**a, b**) Data presented as mean ± SEM; unpaired two-tailed Student's *t*-test. (**c-h**) Paired two-tailed Student's *t*-test.

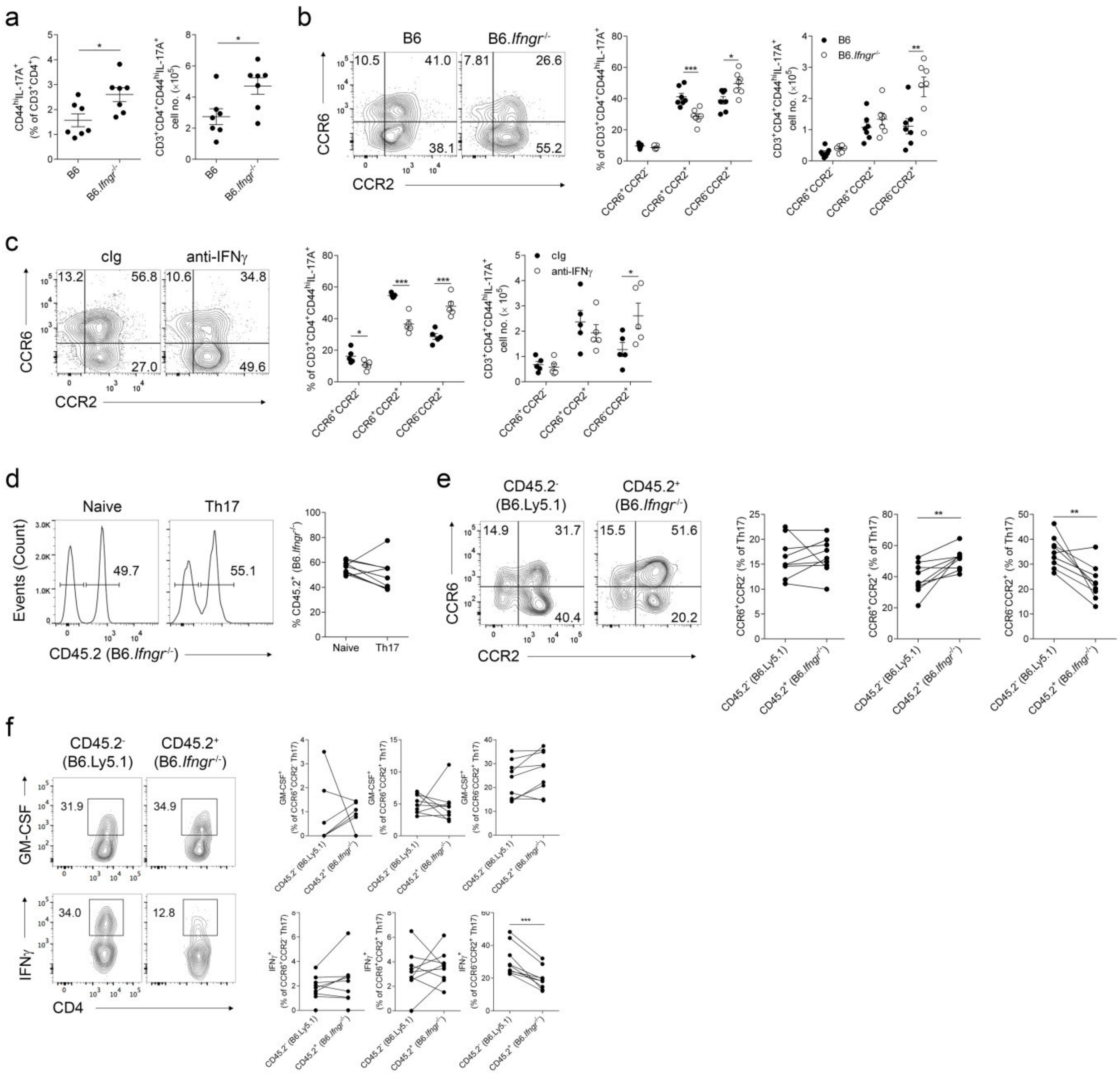

Supplementary Figure 8: T-cell intrinsic IFNγR signaling promotes CCR6^{-}CCR2^{+} Th17 cell development *in vivo*.

(**a, b**) Analysis of B6 (n=7) and B6.*Ifngr*$^{-/-}$ (n=7) mice d10 post MOG/CFA immunization. (**a**) Frequency and total number of Th17 cells in spleen; (**b**) representative flow cytometric analysis and quantitation of CCR6 and CCR2 staining on Th17 cells. (**c**) Representative flow cytometric analysis and quantitation of CCR6 and CCR2 staining on Th17 cells from control immunoglobulin (cIg) (n=5) or neutralizing anti-IFNγ treated (n=5; 250 μg i.p. on d0 and every 48 hours thereafter) mice d10 post MOG/CFA immunization. (**d**) Representative flow cytometric analysis and quantitation of CD45.2^{+} (B6.*Ifngr*$^{-/-}$) cells within naïve CD4^{+} (CD3^{+}CD4^{+}CD44^{lo}) and Th17 cells (CD3^{+}CD4^{+}CD44^{hi}IL-17A^{+}) in spleen of B6.*Ifngr*$^{-/-}$ mixed bone marrow chimeric mice (n=9) immunized with MOG/CFA 10 days prior. (**e**) Representative flow cytometric analysis and quantitation of CCR6 and CCR2 staining on CD45.2^{-} (B6.Ly5.1) and CD45.2^{+} (B6.*Ifngr*$^{-/-}$) Th17 cells in mixed bone marrow chimeras immunized with MOG/CFA 10 days prior. (**f**) Representative flow cytometric analysis of GM-CSF and IFNγ staining amongst CD45.2^{-} (B6.Ly5.1) and CD45.2^{+} (B6.*Ifngr*$^{-/-}$) CCR6^{-}CCR2^{+} Th17 cells in B6.*Ifngr*$^{-/-}$ (n=7) mixed bone marrow chimeric mice 10 days post MOG/CFA immunization. Right, GM-CSF and IFNγ expression amongst CCR6/CCR2 Th17 cell populations in B6.*Ifngr*$^{-/-}$ mixed bone marrow chimeras. (**a-f**) Each dot represents an individual mouse; * $p \leq 0.05$, ** $p \leq 0.01$, *** $p \leq 0.001$. (**a-c**) Data presented as mean ± SEM; unpaired two-tailed Student's *t*-test. (**d-f**) Paired two-tailed Student's *t*-test.

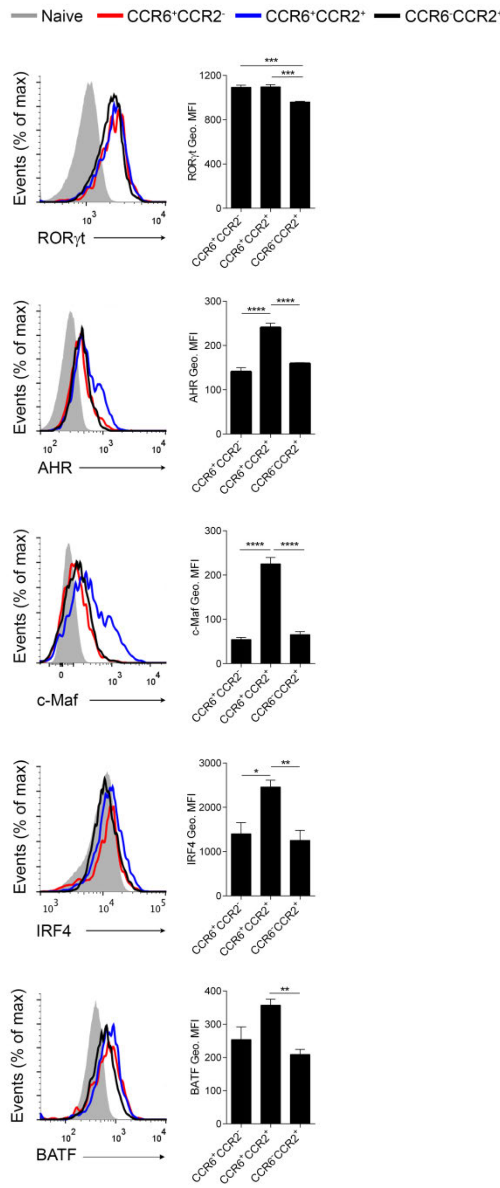

Supplementary Figure 9: Transcription factor expression by CCR6/CCR2-expressing Th17 cell populations.

Representative flow cytometric analysis and quantitation of RORγt, AHR, c-Maf, IRF4, and BATF expression in naïve $CD4^+$ T-cells (grey – filled; $CD3^+CD4^+CD44^{lo}$) and $CCR6^+CCR2^-$ (red - open), $CCR6^+CCR2^+$ (blue – open) and $CCR6^-CCR2^+$ (black – open) Th17 cells ($CD3^+CD4^+CD44^{hi}IL\text{-}17A^+$) from spleen d10 post MOG/CFA immunization. Geometric MFI (gMFI) of transcription factor staining in Th17 cell populations is presented after subtraction from concurrent naïve $CD4^+$ T-cell gMFI. Data representative of 2-3 independent experiments with n=4-5 mice/experiment. * $p \leq 0.05$, ** $p \leq 0.01$, *** $p \leq 0.001$; one-way ANOVA with Bonferroni multiple comparisons test.

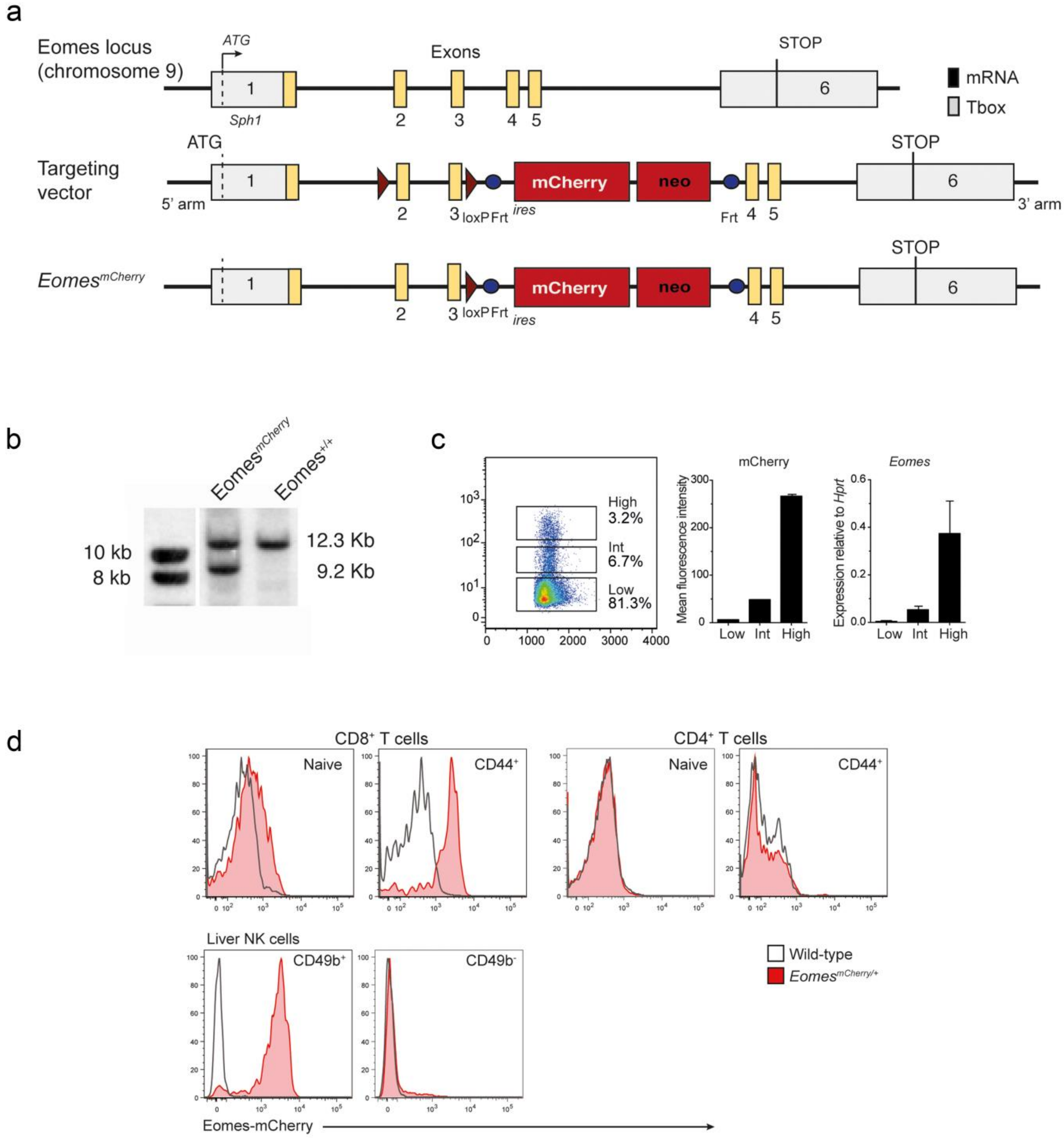

Supplementary Figure 10: B6.*Eomes*$^{\text{Cherry}}$ reporter mice.

(**a**) The genomic locus of Eomes. Exons are represented by boxes; introns are represented as black lines; coding regions are shaded yellow; non-translated regions are in white; arrows indicate the direction of translation. The alleles derived from the integration of the targeting vector and subsequent manipulations are shown. Circles, Frt sites; triangles, loxP sites. The

Eomes-mCherry reporter line was derived from an embryonic stem cell (ES) clone that lacked the 5’ loxP site and was identified by PCR. (**b**) Southern blot analysis using a 5’ probe of ES cell Sph1-digested DNA showing the wild-type (12.293 kb) and targeted (9.198 kb) alleles. (**c**) Quantitative analysis of *Eomes* mRNA expression relative to *Hprt* for the indicated transcripts of live (PI^-) cells from splenocytes purified on the basis of their expression of Eomes-mCherry. Data show the mean ± S.D. of two experiments. (**d**) Expression of Eomes-mCherry in splenic T cell (CD8 and CD4) and hepatic NK cell subsets from wild-type (B6) and B6.*Eomes*$^{Cherry/+}$ mice as indicated.

SUPPLEMENTARY TABLES

Supplementary Table 1: Properties of the human study population

	Controls	MS
Total number of participants (n)	7	12
Gender (% Female)	72	75
Age at onset (years; mean (range))	-	34 (21-50)
Age at sampling (years; mean (range))	36 (30-43)	50 (27-77)
Disease duration at sampling (years; mean (range))	-	16 (6-39)
Disease course MS (% RRMS)	-	75
Duration treatment at sampling (years; mean (range))	-	Untreated

Supplementary Table 2: Anti-mouse antibodies

Anti-mouse antibodies				
Anti-	**Fluorophore**	**Clone**	**Source**	**Final concentration**
CD3ε	FITC PE-Cy7 Biotin	145-2C11	BD eBiosciences eBiosciences	2.77 µg/ml 0.83 µg/ml 2.08 µg/ml
CD4	BV450 PerCP-Cy5.5 PE-Cy7 Alexa Fluor 647 PECF594	RM4-5	BD BD BD BD BD	0.83 µg/ml 0.83 µg/ml 0.83 µg/ml 0.83 µg/ml 0.83 µg/ml
CD8α	PE-Cy7	53-6.7	BD	0.83 µg/ml
TCRβ	PE	H57-597	eBiosciences	0.4 µg/ml
CD44	BV450 FITC Biotin	IM7	BD BD BD	0.83 µg/ml 2.08 µg/ml 0.83 µg/ml
CCR6	PE Purified Alexa Fluor 488	140706	R&D R&D R&D	8 µl neat 4.16 µg/ml 9 µl neat
CCR2	Purified	MC21	Prof. Matthias Mack, Universität Regensburg, Germany	5.5 µg/ml
CD11b	PE-Cy7	M1/70	BD	0.83 µg/ml
F4/80	FITC	BM8	eBiosciences	2.77 µg/ml
Gr-1	PE	RB6-8C5	BD	0.83 µg/ml
CD45	APC	30-F11	BD	0.83 µg/ml

CD45.2	FITC PerCP PerCP-Cy5.5 Biotin	104	BD Biolegend eBiosciences BD	2.08 µg/ml 2.08 µg/ml 0.83 µg/ml 2.08 µg/ml
IL-17A	BV510 PerCP-Cy5.5 PE	Tc11-18H10.1 eBio17B1 TC11-18H10	Biolegend eBiosciences BD	1.33 µg/ml 1.11 µg/ml 1.11 µg/ml
IFNγ	FITC PE-Cy7	XMG1.2	BD eBiosciences	2.77 µg/ml 1.11 µg/ml
GM-CSF	FITC	MP1-22E9	eBioscienes	2.77 µg/ml
TNFα	FITC	MP6-XT22	eBiosciences	2.77 µg/ml
IL-2	Alexa Fluor 488	JES6-5H4	eBiosciences	2.77 µg/ml
IL-9	PE	D9302C12	BD	1.66 µg/ml
IL-10	FITC	JES5-16E3	BD	4.0 µg/ml
IL-17F	Alexa Fluor 488	eBio18F10	eBiosciences	2.77 µg/ml
IL-22	PerCP-eFluor710	1H8PWSR	eBiosciences	1.66 µg/ml
Foxp3	PerCP-Cy5.5	FJK-16s	eBiosciences	1.66 µg/ml
T-bet	PerCP-Cy5.5	eBio4B10	eBiosciences	1.66 µg/ml
RORγt	PerCP-eFluor710	B2D	eBiosciences	1.66 µg/ml
AHR	Alexa Fluor 488	4MEJJ	eBiosciences	4.16 µg/ml
c-Maf	PerCP-eFluor710	symOF1	eBiosciences	5 µl neat
IRF4	PerCP-eFluor710	3E4	eBiosciences	1.66 µg/ml
BATF	PerCP-eFluor710	MBM7C7	eBiosciences	5 µl neat

Supplementary Table 3: Anti-human antibodies

Anti-human antibodies				
Anti-	**Fluorophore**	**Clone**	**Source**	**Final concentration**
CD4	APC-eFluor780	RPA-T4	eBioscience	8.33 μg/ml
CD8α	PerCP-eFluor710	SK1	eBioscience	0.20 μg/ml
IL-17A	FITC	eBio64DEC17	eBioscience	1.25 μg/ml
IFNγ	eFluor450	4S.B3	eBioscience	5.00 μg/ml
GM-CSF	APC	BVD2.21C11	Biolegend	5.00 μg/ml
CCR2	PE	K036C2	Biolegend	10.0 μg/ml
CCR6	PE-Cy7	G034E3	Biolegend	10.0 μg/ml

Supplementary Table 4: Primer sequences

Primer	Forward (5'-3')	Reverse (5'-3')
Rplp0	TGCAGATCGGGTACCCAACT	ACGCGCTTGTACCCATTGA
Ccr1	TGGGAGTTCACTCACCGTACCT	TCCACTGCTTCAGGCTCTTGT
Ccr2	GTTCATCCACGGCATACTATCAAC	GCCCCTTCATCAAGCTCTTG
Ccr3	TTGCCTACACCCACTGCTGTAT	TTTCCGGAACCTCTCACCAA
Ccr4	GCAACACTGCAAGAATGAGAAGA	GACCACCACGGCGAAGAT
Ccr5	CATCCGTTCCCCCTACAAGA	GGAACTGACCCTTGAAAATCCA
Ccr6	CCTGGGCAACATTATGGTGGT	CAGAACGGTAGGGTGAGGACA
Ccr7	CATTGCCTATGACGTCACCTACA	GAAGGCATACCAGAAAGGGTTGA
Ccr8	GCTCGCTCAGATAATTGGTCTTC	CGTGACGTTGGGCTCCAT
Ccr9	CAGTTCTGAGGAGGATGCTTGA	AACCCAGCTGCACTGATGATC
Ccr10	CCTCTACTCGGCCTCTTTCCA	CGGTCGGCGCTGATACAG
Cxcr1	TGTCCCACATATTTGGCTTCCT	GCCCGTAGCAGACCAGCAT
Cxcr2	GCCCTGACCTTGCCTGTCT	TGCACAGGGTTGAGCCAAA
Cxcr3	TACCTTGAGGTTAGTGAACGTCA	CGCTCTCGTTTTCCCCATAATC
Cxcr4	ACCTCTACAGCAGCGTTCTCATC	TGTTGGTGGCGTGGACAATA
Cxcr5	GGGCTCCATCACATACAATATGG	GAATCTCCGTGCTGTTACTGTAGAAG
Cxcr6	CCGGCAGGCTAAGTGGAA	CACCCAAATGAGCAAGCAAA
Cx3cr1	ATCAGCATCGACCGGTACCT	CTGCACTGTCCGGTTGTTCAT
Xcr1	CATGACCATCCACCGATACCT	GCTGCCCACACACATGATGT

CHAPTER THREE:

RESULTS -

'Regulation of activated B cell differentiation by atypical chemokine receptor 4'

Please refer to Appendix for published manuscript:

Kara EE *et al*. Atypical chemokine receptor 4 shapes activated B cell fate. *J. Exp. Med*. 5;215(3):801-813 doi: 10.1084/jem.20171067 (2018).

Statement of Authorship

Title of Paper	Atypical chemokine receptor 4 shapes activated B cell fate
Publication Status	☑ Published
Publication Details	Published in The Journal of Experimental Medicine: Kara E. E. *et al.*, Atypical chemokine receptor 4 shapes acticated B cell fate. *J Exp Med* 215(3):801-813 doi: 10.1084/jem.20171067.

Principal Author

Name of Principal Author (Candidate)	Ervin E. Kara		
Contribution to the Paper	Conceived the study, designed all experiments, performed most experiments, analysed all data, interpreted all data, wrote the manuscript		
Overall percentage (%)	80%		
Certification:	This paper reports on original research I conducted during the period of my Higher Degree by Research candidature and is not subject to any obligations or contractual agreements with a third party that would constrain its inclusion in this thesis. I am the primary author of this paper.		
Signature		Date	04/04/2018

Co-Author Contributions

By signing the Statement of Authorship, each author certifies that:

i. the candidate's stated contribution to the publication is accurate (as detailed above);

ii. permission is granted for the candidate in include the publication in the thesis; and

iii. the sum of all co-author contributions is equal to 100% less the candidate's stated contribution.

Name of Co-Author	Cameron R. Bastow		
Contribution to the Paper	Performed experiments		
Signature		Date	29/5/18

Name of Co-Author	Duncan R. McKenzie		
Contribution to the Paper	Performed experiments		
Signature		Date	27/4/2018

Name of Co-Author	Carly E. Gregor

Contribution to the Paper	Performed experiments
Signature	Date 27/4/18

Name of Co-Author	Kevin A. Fenix
Contribution to the Paper	Performed experiments
Signature	Date 27/4/18

Name of Co-Author	Rachelle Babb
Contribution to the Paper	Performed experiments
Signature	Date 27/4/2018

Name of Co-Author	Todd S. Norton
Contribution to the Paper	Performed experiments
Signature	Date 27.4.18

Name of Co-Author	Dimitra Zotos
Contribution to the Paper	Performed experiments
Signature	Date 27/4/2018

Name of Co-Author	Lauren B. Rodda
Contribution to the Paper	Performed experiments
Signature	Date 27/4/2018

Name of Co-Author	Jana R. Hermes

Contribution to the Paper	Provded reagents
Signature	Date 27/4/2018

Name of Co-Author	Katherine Bourne
Contribution to the Paper	Provided reagents
Signature	Date 27/4/2018

Name of Co-Author	Derek S. Gilchrist
Contribution to the Paper	Provided mice
Signature	Date 27/4/2018

Name of Co-Author	Robert J. Nibbs
Contribution to the Paper	Provded mice
Signature	Date 27/4/2018

Name of Co-Author	Mohammed Alsharifi
Contribution to the Paper	Critical discussions
Signature	Date 27/4/2018

Name of Co-Author	Carola G. Vinuesa
Contribution to the Paper	Provided mice, critical discussions
Signature	Date 27/4/2018

Name of Co-Author	David M. Tarlinton

Contribution to the Paper	Supervised experiments, critical discussions, edited manuscript		
Signature		Date	27/4/2018

Name of Co-Author	Robert Brink		
Contribution to the Paper	Provided key reagents, critical discussions, edited manuscript		
Signature		Date	27/4/2018

Name of Co-Author	Geoffrey R. Hill		
Contribution to the Paper	Provided key reagents		
Signature		Date	27/4/2018

Name of Co-Author	Jason G. Cyster		
Contribution to the Paper	Provided reagents, supervised experiments, critical discussions, edited manuscipt		
Signature		Date	27/4/2018

Name of Co-Author	Iain Comerford		
Contribution to the Paper	Co-supervised the study, analysed, designed and interpreted experiments, wrote the manuscript		
Signature		Date	27/4/18

Name of Co-Author	Shaun R. McColl		
Contribution to the Paper	Co-supervised the study, analysed, designed and interpreted experiments, wrote the manuscript		
Signature		Date	27/4/18

Title: Regulation of activated B cell differentiation by atypical chemokine receptor 4

Authors: Ervin E. Kara[1, †], Cameron R. Bastow[1], Duncan R. McKenzie[1], Carly E. Gregor[1], Kevin A. Fenix[1], Rachelle Babb[1], Todd S. Norton[1], Dimitra Zotos[2], Lauren B. Rodda[3], Jana R. Hermes[4], Katherine Bourne[4], Derek S. Gilchrist[5], Robert J. Nibbs[6], Mohammed Alsharifi[1], Carola G. Vinuesa[7], David M. Tarlinton[2,8], Robert Brink[4,9], Geoffrey R. Hill[10], Jason G. Cyster[3,11], Iain Comerford[1] and Shaun R. McColl[1,12].

Affiliations:

[1]Department of Molecular and Cellular Biology, School of Biological Sciences, University of Adelaide, Adelaide, SA 5005, Australia.

[2]Walter and Eliza Hall Institute of Medical Research, Parkville, VIC 3052, Australia.

[3]Department of Microbiology and Immunology, University of California, San Francisco, San Francisco, CA 94143, USA.

[4]Immunology Division, Garvan Institute of Medical Research, Darlinghurst, NSW 2010, Australia.

[5]Institute of Infection, Immunity and Inflammation, College of Medicine, Veterinary and Life Sciences, University of Glasgow, Glasgow G12 8QQ, United Kingdom.

[6]Institute of Infection, Immunity and Inflammation, College of Medicine, Veterinary and Life Sciences, University of Glasgow, Glasgow G12 8TA, United Kingdom.

[7]Department of Immunology and Infectious Disease, John Curtin School of Medical Research, Australian National University, Canberra, ACT 0200, Australia.

[8]Department of Immunology, Burnet Institute, Monash University, Melbourne, VIC 3145, Australia.

[9]St Vincent's Clinical School, University of New South Wales, Darlinghurst, NSW 2010, Australia.

[10]Centre for Immunotherapy and Vaccine Development, QIMR Berghofer Medical Research Institute, Brisbane, QLD, Australia.

[11]Howard Hughes Medical Institute, Department of Microbiology and Immunology, University of California, San Francisco, San Francisco, CA 94143, USA.

[12]Centre for Molecular Pathology, School of Biological Sciences, University of Adelaide, Adelaide, SA 5005, Australia.

*Correspondence to: Shaun McColl (shaun.mccoll@adelaide.edu.au) or Iain Comerford (iain.comerford@adelaide.edu.au)

[†]Present address: Laboratory of Molecular Immunology, The Rockefeller University, New York, NY 10065, USA.

Abstract: Upon activation, B cells dynamically regulate chemoattractant responsiveness enabling spatio-temporal access to distinct lymphoid niches that drive their proliferation and differentiation. Activated B cells can initially differentiate into three functionally-distinct fates: early plasmablasts (PB), germinal center B (GCB) or early memory B (EBM) cells by mechanisms that remain ill-defined. Here, we identify a new modality of B cell migration via atypical chemokine receptor 4 (ACKR4), a decoy receptor that binds and degrades CCR7 ligands CCL19/CCL21, that shapes the fate trifurcation of activated B cells. By restricting initial access to the splenic interfollicular zone (IFZ), ACKR4 limits the early proliferation of activated B cells, reducing their frequency available for subsequent differentiation. Consequently, ACKR4-deficiency enhanced early PB, GCB and EBM cell development in a CCL19/CCL21-dependent and B cell-intrinsic manner. Aberrant localization to the IFZ by ACKR4-deficient activated B cells enhanced interferon regulatory factor 4 expression guiding their preferential commitment to the early PB lineage. Our results reveal a novel regulatory mechanism of B cell trafficking via an atypical chemokine receptor that shapes activated B cell fate.

One Sentence Summary: The atypical chemokine receptor ACKR4 shapes early activated B cell migration and governs their differentiation fate.

Main Text:

Differentiation of activated B cells during T-dependent antibody responses proceeds down early plasmablast (PB), germinal center B (GCB) cell and/or early GC-independent memory B (EBM) cell pathways that differ in their spatio-temporal emergence, cellular longevity and function (*1*). Adoption of these fates is controlled to a large extent by B cell trafficking receptors, which are dynamically regulated following antigen-engagement, enabling access to antigen, interactions with T cells, and positioning in distinct lymphoid niches that support rapid or durable antibody production (*2*).

Recent evidence suggests that a subfamily of atypical chemokine receptors play a key role in regulation of cellular migration (*3*). These receptors are uncoupled from classical chemokine receptor signal transduction machinery, do not induce cell migration, are mainly expressed outside the hematopoietic compartment, and mediate chemokine removal or redistribution *in vivo (3)*. Atypical chemokine receptor 4 (ACKR4; gene: *Ccrl1*) binds CCR7 ligands CCL19/CCL21 and regulates their bioavailability *in vivo* (*4-7*). CCR7 has been well documented to drive early antigen-engaged B cell migration toward the T/B interface and interfollicular zone (also known as splenic marginal zone bridging channel) facilitating their interaction with cognate T cells (*8-10*). Despite a previous study indicating that ACKR4 is exclusively expressed in cells of non-hematopoietic origin from unimmunized mice (*11*), we identified abundant ACKR4 expression amongst GCB cells (Fig S1). However, the function of ACKR4 in development of T-dependent antibody responses is unknown.

To investigate hematopoietic ACKR4 function in humoral immunity, we studied bone-marrow (BM) chimeric mice with ACKR4-deficiency restricted to the hematopoietic compartment (H-*Ccrl1*$^{-/-}$ mice). Deletion of hematopoietic ACKR4 led to an enhanced hapten-specific IgG response 21 days following immunization with the T-dependent antigen 4-hydroxy-3-nitrophenyl acetyl (NP) conjugated to keyhole limpet hemocyanin (KLH) (Fig. 1A). In response to sheep red blood cell (SRBC) immunization, H-*Ccrl1*$^{-/-}$ mice formed increased frequencies of GCB cells, IgM$^+$ and switched PBs, GC-resident CD4$^+$ T cells (CXCR5^{hi}PD1^{hi}), but exhibited a normal ratio of T follicular helper (T_{FH}) to T follicular regulatory (T_{FR}) cells (Fig. 1B and Fig. S2). Unimmunized

H-*Ccrl1*$^{-/-}$ mice also contained greater frequencies of GCB cells and PBs in mesenteric lymph nodes, which are constitutively active due to chronic stimulation via gut flora (Fig. S3). Similar results were obtained in BM chimeric mice with ACKR4-deficiency restricted to B cells (Fig. 1C and Fig. S4). Consistent with exaggerated GC responses, GC output in the form of switched (IgD^{-}) memory B cells was also enhanced in the absence of B cell ACKR4 (Fig S5). We conclude that B cell expression of ACKR4 limits T-dependent humoral immune responses.

The prominent expression of ACKR4 on GCB cells (Fig. S1), and their expansion in immunized H-*Ccrl1*$^{-/-}$ mice, prompted investigation of ACKR4 function in GC biology. Using a combination of experimental approaches, we did not find a role for ACKR4 in regulation of GC morphology, CCL21 abundance surrounding established GCs, dark zone/light zone GCB cell segregation, somatic hypermutation or affinity maturation (Fig. 1D-H). Thus, in contrast with its elevated expression in the GC, ACKR4 plays a limited role in these key parameters of GC physiology. Nevertheless, absence of ACKR4 in B cells enhanced both GCB cell and early PB responses (Fig. 1), leading us to hypothesize that ACKR4 limits early antigen-engaged B cell responses prior to their initial differentiation. To test this, three independent approaches were utilized.

First, we investigated the cell-intrinsic requirement of ACKR4 in B cell differentiation using three complementary approaches. In mice reconstituted with an equal mixture of *Ccrl1*$^{-/-}$ and WT BM, ACKR4-deficiency enhanced GCB cell and early PB development relative to concurrently activated WT cells following SRBC immunization (Fig. 2A and Fig. S6). Thus, despite a lack of expression amongst early PBs, ACKR4 limits GCB cell and early PB responses in a B cell-intrinsic manner. These cell-intrinsic differences were independent of aberrant proliferation or apoptosis amongst *Ccrl1*$^{-/-}$ GCB cells and early PBs at the time of analysis as revealed by BrdU incorporation, DNA content and Annexin V analyses (Fig. S7). A cell-intrinsic role for ACKR4 was not evident in T_{FH} or T_{FR} development (Fig. S8), indicating that increases in these populations in H-*Ccrl1*$^{-/-}$ and B-cell specific *Ccrl1*$^{-/-}$ BM chimeric mice (Fig. S2, S4) were secondary to enhanced B cell responses. To confirm these results, we also studied SRBC-immunized μMT mice (which lack endogenous B cells) reconstituted with equivalent frequencies of WT and *Ccrl1*$^{-/-}$ FoB cells. In keeping with BM chimera analyses, *Ccrl1*$^{-/-}$ cells accumulated more favorably amongst GCB cells and early PBs (Fig. S9). The SW_{HEL} system was also utilized to assess a cell-intrinsic role for ACKR4 in antigen-specific PB, GCB and EBM cell development (*12*). SW_{HEL} B cells express a B cell receptor with high affinity to the model antigen hen egg lysozyme (HEL) (*12*). Genetically marked WT ($CD45.1^{+}CD45.2^{+}$) and *Ccrl1*$^{-/-}$ ($CD45.2^{+}$) SW_{HEL} B cells were co-transferred into $CD45.1^{+}$ recipients and immunized with the reduced affinity HEL mutant HEL^{2X} (*12*). By day 5, ACKR4-deficient SW_{HEL} B cells outcompeted WT in all (PB, GCB and EBM) differentiated compartments, most notably amongst SW_{HEL} PB responses (Fig. 2B). We conclude that B cell expression of ACKR4 limits early antigen-engaged B cell differentiation.

Second, we used an approach that allows the isolation of B cell activation and early PB differentiation in the absence of GCB cell development to determine whether ACKR4 influenced this differentiation pathway. Immunization with *Samonella enterica* induces an early T-dependent $IgG2c^{+}$ PB response, with GC development substantially delayed (~30-35 days) (*13, 14*). As reported (*13, 14*), GCs were not detected above background by day 7 of the response in either WT and *Ccrl1*$^{-/-}$ mice (Fig. S10A). At this time point, *Ccrl1*$^{-/-}$ mice contained increased frequencies of $IgG2c^{+}$ and IgM^{+} PBs in splenic bridging channels and red pulp, more serum anti-*Salmonella*

IgG2c, more $CXCR5^{+}PD1^{lo}$ pre-T_{FH} cells (*14*), but equivalent liver bacterial burden, indicating that ACKR4 limits early PB formation in this model, but does not influence peripheral effector T cell responses to infection (*14, 15*) (Fig. S10B-F).

Third, we reasoned that forced expression of ACKR4 prior to antigen-engaged B cell differentiation would limit their entry into both GCB cell and early PB compartments. To test this, we generated floxed conditional *Ccrl1* 'knock-in' mice downstream of the *Rosa26* locus ($Rosa26^{LSL\text{-}Ccrl1}$) and crossed these to mice in which Cre recombinase is driven by the FoB-specific gene *Cd23a* ($Cd23^{Cre}$) (*16*). FoB cells in $Cd23a^{Cre/+}.Rosa26^{LSL\text{-}Ccrl1/+}$ (hereafter $Cd23^{Cre}Ccrl1^{Tg}$) mice, expressed functional ACKR4 (Fig. S11A-D). Transgenic ACKR4 expression in FoB cells did not alter CCR7 or CXCR5 expression at rest nor after BCR-stimulation, but inhibited activated B cell migration toward CCL21, but not CXCL13 (a non-murine ACKR4 ligand (*17*)) (Fig. S11E), consistent with the proposed function of ACKR4 as a regulator of CCR7 biology (*4, 5*). Supporting the concept that ACKR4 negatively regulates activated B cell differentiation, in mixed BM chimeric mice reconstituted with $Cd23^{Cre}Ccrl1^{Tg}$ and WT BM, B cells with transgenic ACKR4 expression contributed less to both GCB cell and early PB compartments (Fig. 2C). This cell-intrinsic defect was independent of aberrant GCB cell or early PB proliferation or apoptosis at the time of analysis (Fig. S12). Assessment of *S. enterica*-immunized μMT mice reconstituted with equal frequencies of WT and $Ccrl1^{-/-}$ or $Ccrl1^{Tg}$ FoB cells also demonstrated that cell-intrinsic ACKR4-deficiency enhanced, whilst forced ACKR4 expression reduced, T-dependent switched PB development (Fig. S13). Taken together, these data indicate that ACKR4 functions in a B cell-intrinsic manner to limit early PB, GCB and EBM cell responses prior to the fate trifurcation of antigen-engaged B cells.

To examine ACKR4-dependent regulation of initial antigen-engaged B cell differentiation in more detail, we tracked early WT and $Ccrl1^{-/-}$ SW_{HEL} B cell responses to HEL^{2X} using mixed SW_{HEL} B cell transfers. CFSE (carboxyfluorescin succinimidyl ester) dilution profiling revealed a cell-intrinsic proliferative advantage for ACKR4-deficient SW_{HEL} B cells as early as d2 of the response (Fig. 3A & 3B), which became increasingly apparent by d3 (Fig. 3B). Importantly, the magnitude of this early advantage for ACKR4-deficient SW_{HEL} B cells was largely proportional to their advantage observed amongst established SW_{HEL} GCB and EBM cell compartments by day 5 of the response (Fig. 2B). In experiments where WT or $Ccrl1^{-/-}$ SW_{HEL} B cells were transferred into separate recipients, ACKR4-deficient SW_{HEL} B cells were detected at greater frequencies by d2.5, and remained more abundant over the first 5.5 days of the response (Fig. 3C). By d5.5, ACKR4-deficient SW_{HEL} B cells had a greater propensity to enter the PB compartment than WT (Fig. 3D, E and Fig. S14, S15), which was first apparent on d4.5 and translated to a greater serum anti-HEL IgM and IgG1 response (Fig. 3F & G), seemingly at the expense of GCB cell development (Fig. 3D, H and Fig. S14). Whilst ACKR4-deficient SW_{HEL} GCB cell responses appeared equivalent to WT when assessed as a frequency per spleen, greater numbers of SW_{HEL} GCB cells formed in the absence of ACKR4 (Fig. 3H). Analogous experiments using ACKR4-deficient $SW_{HEL(H)}$ B cells, which harbor the HyHEL10 heavy chain transgene which, when paired with random endogenous κ light chains, generate clones with varying affinities to HEL (*18*), yielded equivalent results (Fig. S14), indicating that preferential PB differentiation in the absence of ACKR4 also occurs in a system that more closely reflects a polyclonal repertoire. Together, these data indicate that ACKR4 limits early antigen-engaged B cell proliferation in a B-cell intrinsic manner, reducing the precursor frequency of antigen-engaged B cells available for subsequent PB, GCB and EBM cell differentiation. In addition, the limiting effect of ACKR4 on early PB responses is most prominent.

BCR affinity and avidity of BCR-mediated activation are key regulators of early PB expansion, and thus the durability of the early PB response (*19, 20*). In the SW_{HEL} system, immunization with high affinity HEL protein, or HEL conjugated to SRBCs at a high epitope density (modeling high avidity B cell activation) enhances SW_{HEL} PB expansion and prolongs the early PB response (*19, 20*). We reasoned that the enhanced early PB response in the absence of ACKR4 may result from two possibilities: i) ACKR4 limits the commitment of antigen-engaged B cell precursors to the early PB lineage; ii) ACKR4 limits the expansion, and thus durability, of an early PB response. To distinguish these mechanisms, we studied concurrent WT and *Ccrl1*$^{-/-}$ SW_{HEL} B cell responses to intermediate (HEL^{2X}) or low (HEL^{3X}) affinity HEL proteins conjugated to SRBCs at varying epitope densities (*20*). *Ccrl1*$^{-/-}$ SW_{HEL} B cells preferentially formed PBs and outcompeted WT cells in the GCB and EBM compartments 5 days post-immunization when either HEL^{2X} or HEL^{3X} of equivalent intermediate epitope densities were used (Fig. S15). Conversely, when the epitope density was reduced, both WT and *Ccrl1*$^{-/-}$ SW_{HEL} PB responses had abated by the same time point, however the cell-intrinsic advantage for ACKR4-deficient SW_{HEL} GCB and EBM cell development remained consistent (Fig. S15). These data indicate that B cell expression of ACKR4 suppresses early PB differentiation from antigen-engaged B cell precursors, rather than shaping the durability of this response.

Within hours of activation, antigen-engaged B cells reposition to the outer follicle via EBI2 (*21*), followed by CCR7-directed migration toward the T/B border, and distribution along this interface via EBI2/CXCR5/CCR7 to facilitate cognate interactions with pre-T_{FH} cells (*8-10, 21-26*). Here, CCR7 expression wanes, initiating EBI2-mediated migration to interfollicular zones by d2-3 of the response (*10, 19, 21-26*). Antigen-engaged B cell localization to the interfollicular zone, rich in cognate T cells and dendritic cells, promotes initial B cell proliferation and shapes B cell differentiation fate (*22, 24-32*). To examine whether ACKR4 influences early antigen-engaged B cell localization, positioning of ACKR4-deficient SW_{HEL} B cell during the evolution of the HEL^{2X} response was mapped using histology. Within 24 hours, WT SW_{HEL} B cells were positioned at the T/B interface or within the T cell zone (Fig. 4A and Fig. S16). By d2-2.5, the majority of WT SW_{HEL} B cells remained at the T/B interface, although some redistribution to interfollicular zones or follicle center was apparent (Fig. 4A and Fig. S16). In contrast, by 24 hours, a large proportion of ACKR4-deficient SW_{HEL} B cells were localized in interfollicular zones at the expense of T/B interface positioning (Fig. 4A and Fig. S16). On d2-2.5, the majority of ACKR4-deficient SW_{HEL} B cells remained localized in interfollicular zones, with a proportion repositioned to the T/B interface or follicle center (Fig. 4A and Fig. S16). ACKR4-deficient SW_{HEL} B cells were visibly more abundant than WT SW_{HEL} B cells by d2, which became increasingly apparent over the next 60 hours (Fig. 4A and Fig. S16). Whereas WT SW_{HEL} B cells largely remained in interfollicular zones and T/B interface on d3-3.5, a significant proportion of ACKR4-deficient SW_{HEL} B cells were distributed in the outer follicle with the appearance of large SW_{HEL} B cell clusters in the outer follicle and interfollicular zones, and emergence of cells exhibiting a PB phenotype in bridging channels as early as d3, which became more obvious by d3.5-4.5 (Fig. 4A and Fig. S16). Changes to the migratory patterns of ACKR4-deficient SW_{HEL} B cells were independent of defects in expression of other key chemoattractant receptors (Fig. S17). These processes were also independent of changes to costimulatory molecule CD40, anti-apoptotic Bcl-2 expression, apoptosis or receptors for IL-4, IL-6 or IL-21 (Fig. S18, S19). Thus, in the absence of ACKR4, antigen-engaged B cells preferentially home to the interfollicular zone early during the humoral immune response.

ACKR4 scavenges CCR7 ligands CCL19/CCL21 *in vitro* and *in vivo* (*4-7*). To determine whether ACKR4-mediated regulation of early B cell responses was dependent on CCL19/CCL21, these ligands were neutralized in mixed BM chimeras. This revealed that the advantage of ACKR4-deficient B cells to enter GCB cell and early PB compartments was dependent, at least in part, on physiological CCL19/CCL21 (Fig. 4B).

B cell differentiation down early PB or GCB cell trajectories is dictated by the concentration-dependent activity of transcription factors interferon regulatory factor (IRF)4 and IRF8, respectively (*33*). As early as d1, ACKR4-deficient SW_{HEL} B cells expressed a higher ratio of IRF4:IRF8 relative to concurrent WT SW_{HEL} B cells, and this was maintained for the first 3 days of the response (Fig. 4C). The magnitude of enhanced IRF4:IRF8 content mirrored the duration of preferential positioning of responding ACKR4-deficient B cells in interfollicular zones over their WT counterparts (Fig. 4A), suggesting that this initial positioning defect contributes to enhanced PB formation in the absence of ACKR4. Together, these data suggest that in the absence of ACKR4, antigen-engaged B cells initially preferentially home to interfollicular zones at the expense of T/B interface positioning, resulting in enhanced proliferation, increased IRF4:IRF8 content and preferential early PB differentiation.

Our results identify a novel regulatory modality of B cell migration, via the atypical chemokine receptor ACKR4, that shapes the early fate trifurcation of activated B cells. Spatio-temporal regulation of chemoattractant responsiveness following antigen-engagement guides the activation, proliferation and differentiation of rare antigen-specific B cells, and thus governs success of humoral immunity (*2*). CCR7 drives activated B cell homing toward the T/B interface, but also contributes, together with EBI2, to the positioning of cells in interfollicular niches (*8-10*). Our data support a model in which ACKR4, a scavenger of CCR7 ligands CCL19 and CCL21, limits the initial localization of activated B cells to the interfollicular zone. ACKR4-dependent tuning of antigen-engaged B cell migration limits the early expansion of these cells and balances their subsequent distribution into early PB, GCB and EBM cell fates. We speculate that such a mechanism may serve to restrict clonal dominance early during the response, preserving the clonal diversity of activated B cell precursors available to seed these differentiated compartments. Further, our data support recent reports that describe the interfollicular zone as an important niche that fosters early PB commitment by mechanisms that remain unknown (*22, 30*). Our results are the first, to our knowledge, to describe an *in vivo* cell-intrinsic role for an atypical chemokine receptor in lymphocyte biology, and further our understanding of the cellular events that govern antibody production, which is critical moving forward toward the rational design of protective vaccines with higher therapeutic indices.

References and Notes:

1. J. J. Taylor, M. K. Jenkins, K. A. Pape, Heterogeneity in the differentiation and function of memory B cells. *Trends Immunol* **33**, 590-597 (2012).
2. J. P. Pereira, L. M. Kelly, J. G. Cyster, Finding the right niche: B-cell migration in the early phases of T-dependent antibody responses. *Int Immunol* **22**, 413-419 (2010).
3. R. J. Nibbs, G. J. Graham, Immune regulation by atypical chemokine receptors. *Nat Rev Immunol* **13**, 815-829 (2013).

4. I. Comerford, S. Milasta, V. Morrow, G. Milligan, R. Nibbs, The chemokine receptor CCX-CKR mediates effective scavenging of CCL19 in vitro. *Eur J Immunol* **36**, 1904-1916 (2006).
5. I. Comerford *et al.*, The atypical chemokine receptor CCX-CKR scavenges homeostatic chemokines in circulation and tissues and suppresses Th17 responses. *Blood* **116**, 4130-4140 (2010).
6. M. H. Ulvmar *et al.*, The atypical chemokine receptor CCRL1 shapes functional CCL21 gradients in lymph nodes. *Nat Immunol* **15**, 623-630 (2014).
7. S. A. Bryce *et al.*, ACKR4 on Stromal Cells Scavenges CCL19 To Enable CCR7-Dependent Trafficking of APCs from Inflamed Skin to Lymph Nodes. *J Immunol* **196**, 3341-3353 (2016).
8. K. Reif *et al.*, Balanced responsiveness to chemoattractants from adjacent zones determines B-cell position. *Nature* **416**, 94-99 (2002).
9. T. Okada *et al.*, Antigen-engaged B cells undergo chemotaxis toward the T zone and form motile conjugates with helper T cells. *PLoS Biol* **3**, e150 (2005).
10. D. Gatto, K. Wood, R. Brink, EBI2 operates independently of but in cooperation with CXCR5 and CCR7 to direct B cell migration and organization in follicles and the germinal center. *J Immunol* **187**, 4621-4628 (2011).
11. K. Heinzel, C. Benz, C. C. Bleul, A silent chemokine receptor regulates steady-state leukocyte homing in vivo. *Proc Natl Acad Sci U S A* **104**, 8421-8426 (2007).
12. R. Brink *et al.*, The SW(HEL) system for high-resolution analysis of in vivo antigen-specific T-dependent B cell responses. *Methods Mol Biol* **1291**, 103-123 (2015).
13. A. F. Cunningham *et al.*, Salmonella induces a switched antibody response without germinal centers that impedes the extracellular spread of infection. *J Immunol* **178**, 6200-6207 (2007).
14. S. K. Lee *et al.*, B cell priming for extrafollicular antibody responses requires Bcl-6 expression by T cells. *The Journal of experimental medicine* **208**, 1377-1388 (2011).
15. J. Hess, C. Ladel, D. Miko, S. H. Kaufmann, Salmonella typhimurium aroA- infection in gene-targeted immunodeficient mice: major role of CD4+ TCR-alpha beta cells and IFN-gamma in bacterial clearance independent of intracellular location. *J Immunol* **156**, 3321-3326 (1996).
16. K. Kwon *et al.*, Instructive role of the transcription factor E2A in early B lymphopoiesis and germinal center B cell development. *Immunity* **28**, 751-762 (2008).
17. J. R. Townson, R. J. Nibbs, Characterization of mouse CCX-CKR, a receptor for the lymphocyte-attracting chemokines TECK/mCCL25, SLC/mCCL21 and MIP-3beta/mCCL19: comparison to human CCX-CKR. *Eur J Immunol* **32**, 1230-1241 (2002).
18. M. Thien *et al.*, Excess BAFF rescues self-reactive B cells from peripheral deletion and allows them to enter forbidden follicular and marginal zone niches. *Immunity* **20**, 785-798 (2004).
19. T. D. Chan *et al.*, Antigen affinity controls rapid T-dependent antibody production by driving the expansion rather than the differentiation or extrafollicular migration of early plasmablasts. *J Immunol* **183**, 3139-3149 (2009).
20. D. Paus *et al.*, Antigen recognition strength regulates the choice between extrafollicular plasma cell and germinal center B cell differentiation. *J Exp Med* **203**, 1081-1091 (2006).

21. L. M. Kelly, J. P. Pereira, T. Yi, Y. Xu, J. G. Cyster, EBI2 guides serial movements of activated B cells and ligand activity is detectable in lymphoid and nonlymphoid tissues. *J Immunol* **187**, 3026-3032 (2011).
22. D. Gatto, D. Paus, A. Basten, C. R. Mackay, R. Brink, Guidance of B cells by the orphan G protein-coupled receptor EBI2 shapes humoral immune responses. *Immunity* **31**, 259-269 (2009).
23. J. P. Pereira, L. M. Kelly, Y. Xu, J. G. Cyster, EBI2 mediates B cell segregation between the outer and centre follicle. *Nature* **460**, 1122-1126 (2009).
24. S. Hannedouche *et al.*, Oxysterols direct immune cell migration via EBI2. *Nature* **475**, 524-527 (2011).
25. T. Yi *et al.*, Oxysterol gradient generation by lymphoid stromal cells guides activated B cell movement during humoral responses. *Immunity* **37**, 535-548 (2012).
26. C. Liu *et al.*, Oxysterols direct B-cell migration through EBI2. *Nature* **475**, 519-523 (2011).
27. F. Coffey, B. Alabyev, T. Manser, Initial clonal expansion of germinal center B cells takes place at the perimeter of follicles. *Immunity* **30**, 599-609 (2009).
28. S. M. Kerfoot *et al.*, Germinal center B cell and T follicular helper cell development initiates in the interfollicular zone. *Immunity* **34**, 947-960 (2011).
29. M. Kitano *et al.*, Bcl6 protein expression shapes pre-germinal center B cell dynamics and follicular helper T cell heterogeneity. *Immunity* **34**, 961-972 (2011).
30. C. P. Chappell, K. E. Draves, N. V. Giltiay, E. A. Clark, Extrafollicular B cell activation by marginal zone dendritic cells drives T cell-dependent antibody responses. *J Exp Med* **209**, 1825-1840 (2012).
31. C. Garcia De Vinuesa *et al.*, Dendritic cells associated with plasmablast survival. *Eur J Immunol* **29**, 3712-3721 (1999).
32. E. Mohr *et al.*, Dendritic cells and monocyte/macrophages that create the IL-6/APRIL-rich lymph node microenvironments where plasmablasts mature. *J Immunol* **182**, 2113-2123 (2009).
33. H. Xu *et al.*, Regulation of bifurcating B cell trajectories by mutual antagonism between transcription factors IRF4 and IRF8. *Nature immunology* **16**, 1274-1281 (2015).
34. B. J. Quah, H. S. Warren, C. R. Parish, Monitoring lymphocyte proliferation in vitro and in vivo with the intracellular fluorescent dye carboxyfluorescein diacetate succinimidyl ester. *Nat Protoc* **2**, 2049-2056 (2007).
35. W. C. McFarland, B. A. Stocker, Effect of different purine auxotrophic mutations on mouse-virulence of a Vi-positive strain of Salmonella dublin and of two strains of Salmonella typhimurium. *Microb Pathog* **3**, 129-141 (1987).
36. M. D. Bunting *et al.*, CCX-CKR deficiency alters thymic stroma impairing thymocyte development and promoting autoimmunity. *Blood* **121**, 118-128 (2013).
37. I. Clark-Lewis, B. Dewald, M. Loetscher, B. Moser, M. Baggiolini, Structural requirements for interleukin-8 function identified by design of analogs and CXC chemokine hybrids. *J Biol Chem* **269**, 16075-16081 (1994).
38. K. G. Smith *et al.*, bcl-2 transgene expression inhibits apoptosis in the germinal center and reveals differences in the selection of memory B cells and bone marrow antibody-forming cells. *J Exp Med* **191**, 475-484 (2000).
39. A. Ehlich, V. Martin, W. Muller, K. Rajewsky, Analysis of the B-cell progenitor compartment at the level of single cells. *Curr Biol* **4**, 573-583 (1994).

40. M. G. McHeyzer-Williams, G. J. Nossal, P. A. Lalor, Molecular characterization of single memory B cells. *Nature* **350**, 502-505 (1991).
41. E. E. Kara *et al.*, Distinct chemokine receptor axes regulate Th9 cell trafficking to allergic and autoimmune inflammatory sites. *J Immunol* **191**, 1110-1117 (2013).
42. T. G. Phan *et al.*, B cell receptor-independent stimuli trigger immunoglobulin (Ig) class switch recombination and production of IgG autoantibodies by anergic self-reactive B cells. *J Exp Med* **197**, 845-860 (2003).
43. E. E. Kara *et al.*, CCR2 defines in vivo development and homing of IL-23-driven GM-CSF-producing Th17 cells. *Nat Commun* **6**, 8644 (2015).
44. D. Gatto *et al.*, The chemotactic receptor EBI2 regulates the homeostasis, localization and immunological function of splenic dendritic cells. *Nature immunology* **14**, 446-453 (2013).

Acknowledgments:

We thank Dr. Josef Nguyen (Royal Adelaide Hospital, Adelaide, Australia) for mouse irradiation; Staff of Laboratory Animal Services, University of Adelaide for animal husbandry; Prof. Meinrad Busslinger for permission to use B6.Cd23-Cre mice; Prof. Renato Morono (University of Adelaide, Adelaide, Australia) for the *Salmonella* strain (originally from Prof. David E Briles). This work was supported in part by an NNH&MRC grant (APP1105312) to SRM, JGC and IC. JGC is an Investigator of the Howard Hughes Medical Institute.

EEK was supported by an Australian Postgraduate Award, The Norman and Patricia Polglase Scholarship and an NHMRC CJ Martin – Overseas Biomedical Fellowship.EEK conceived the study, designed, performed and analyzed experiments and wrote the manuscript. CRB, DRM, CEG, KAF, RB, TSN, DZ, LBR, JRH and KB performed experiments; DSG and RJN generated B6.*Ccrl1*^{Tg} mice; DMT, CGV, MA, RB, GH and JGC provided key reagents, critical discussions and edited the manuscript; IC and SRM conceived the study, designed experiments, supervised the project and wrote the manuscript.

Figures and Figure Legends (Main Text):

Fig. 1

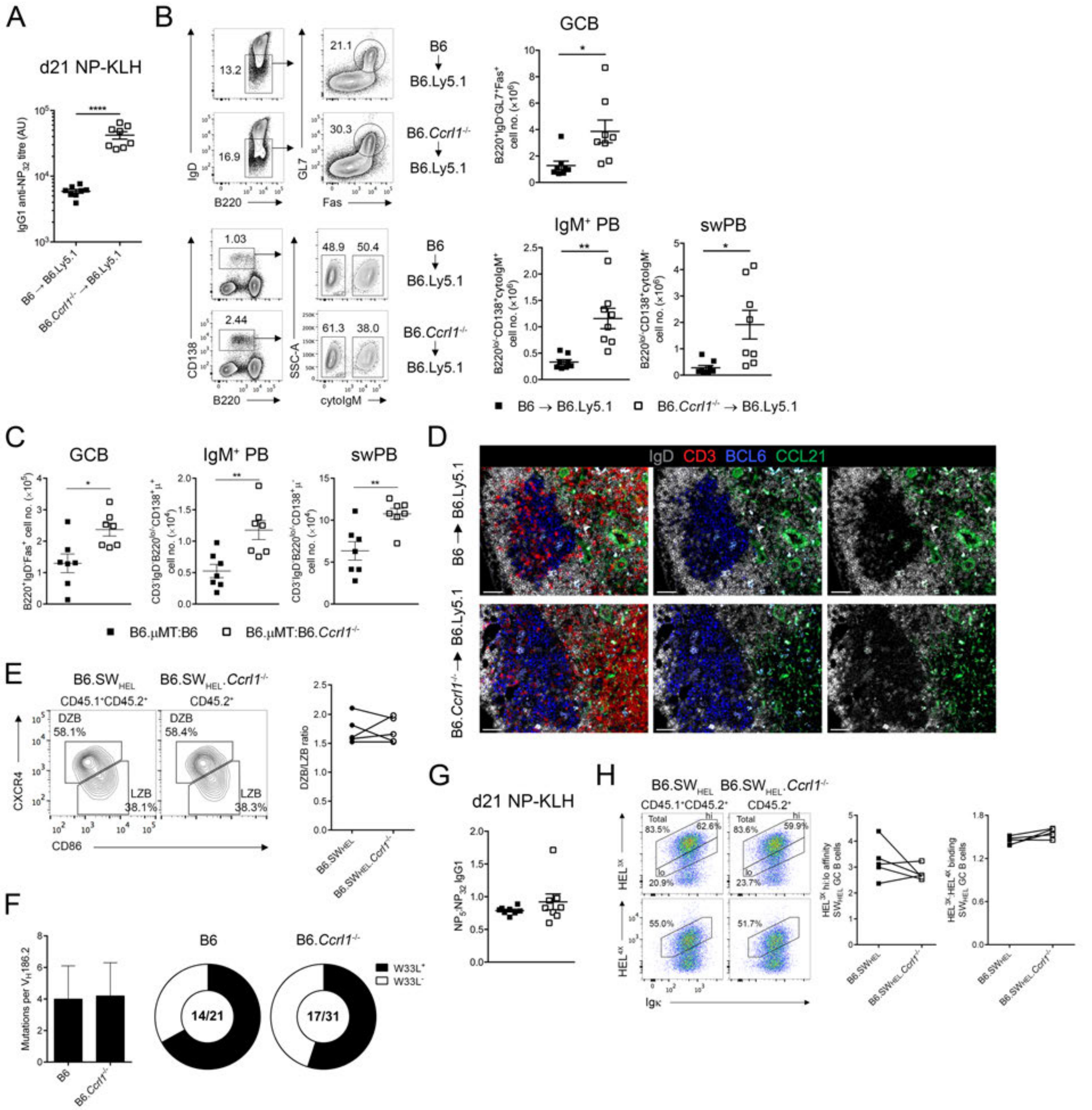

Fig. 1. **B cell expression of ACKR4 limits T-dependent humoral immunity. (A)** Serum NP-specific IgG1 responses day 21 post NP-KLH immunization in lethally-irradiated B6.Ly5.1 mice reconstituted with B6 (H-WT) or B6.*Ccrl1*$^{-/-}$ (H-*Ccrl1*$^{-/-}$) bone marrow (BM). **(B)** GCB cell, IgM^{+} and switched PB responses in H-WT and H-*Ccrl1*$^{-/-}$ mice immunized with SRBC. **(C)** GCB cell, IgM^{+} and switched PB responses in lethally-irradiated B6.Ly5.1 mice reconstituted with a mixture of BM derived from B6.μMT (80%) and B6 (20%; B6.μMT:B6) or B6.*Ccrl1*$^{-/-}$ (20%; B6.μMT:B6.*Ccrl1*$^{-/-}$) immunized with SRBC. **(D)** GC morphology or surrounding CCL21 abundance is unaltered in the absence of hematopoietic ACKR4. Representative histology of BCL-6^{+} GCs (blue) amongst IgD^{+} (white) B cell follicles and CD3^{+} (red) T cell zones in mesenteric LNs

of H-WT and H-*Ccrl1*$^{-/-}$ mice. Right, IgD and CCL21 staining; Middle, IgD, BCL6 and CCL21 staining; Left, all stains merged. 20X magnification. **(E)** WT ($CD45.1^{+}CD45.2^{+}$) and *Ccrl1*$^{-/-}$ ($CD45.2^{+}$) SW_{HEL} B cells were co-transferred into B6.Ly5.1 ($CD45.1^{+}$; n=5) recipients, immunized with HEL^{3X}-SRBC and analyzed 9 days later. Representative flow cytometric analyses of concurrent WT and *Ccrl1*$^{-/-}$ SW_{HEL} GCB cell ($CD45.2^{+}B220^{+}CD138^{-}Ig\kappa^{+}HEL^{+}GL7^{+}$) dark zone (DZB; $CXCR4^{hi}CD86^{lo}$) and light zone (LZB; $CXCR4^{lo}CD86^{hi}$) phenotypes. DZB:LZB ratio of each genotype per recipient. **(F)** Total mutation (left) and high affinity W33L mutation (right) frequency per $V_{H}186.2$ gene segment in individual WT and *Ccrl1*$^{-/-}$ $NP^{+}IgG1^{+}$ GCB cells d14 post NP-KLH immunization. **(G)** Serum NP_{32} and NP_{5} specific IgG1 responses expressed as an NP_{5}:NP_{32} ratio (3000^{-1} sera dilution) from mice in (A). **(H)** WT ($CD45.1^{+}CD45.2^{+}$) and *Ccrl1*$^{-/-}$ ($CD45.2^{+}$) SW_{HEL} B cells were co-transferred into B6.Ly5.1 ($CD45.1^{+}$) mice, immunized with HEL^{3X}-SRBC and analyzed d9 post-immunization. Plots show concurrent WT and *Ccrl1*$^{-/-}$ $Ig\kappa^{+}$ SW_{HEL} GCB cells with high (top diagonal gate) and low (bottom diagonal gate) affinity to HEL^{3X} (top); or HEL^{4X}-binding which reflects high affinity responding GCB cells to HEL^{3X} (bottom).

Paired analyses of HEL^{3X} high affinity:global affinity (left) and HEL^{3X}:HEL^{4X}-binding (right) is shown.

Fig. 2

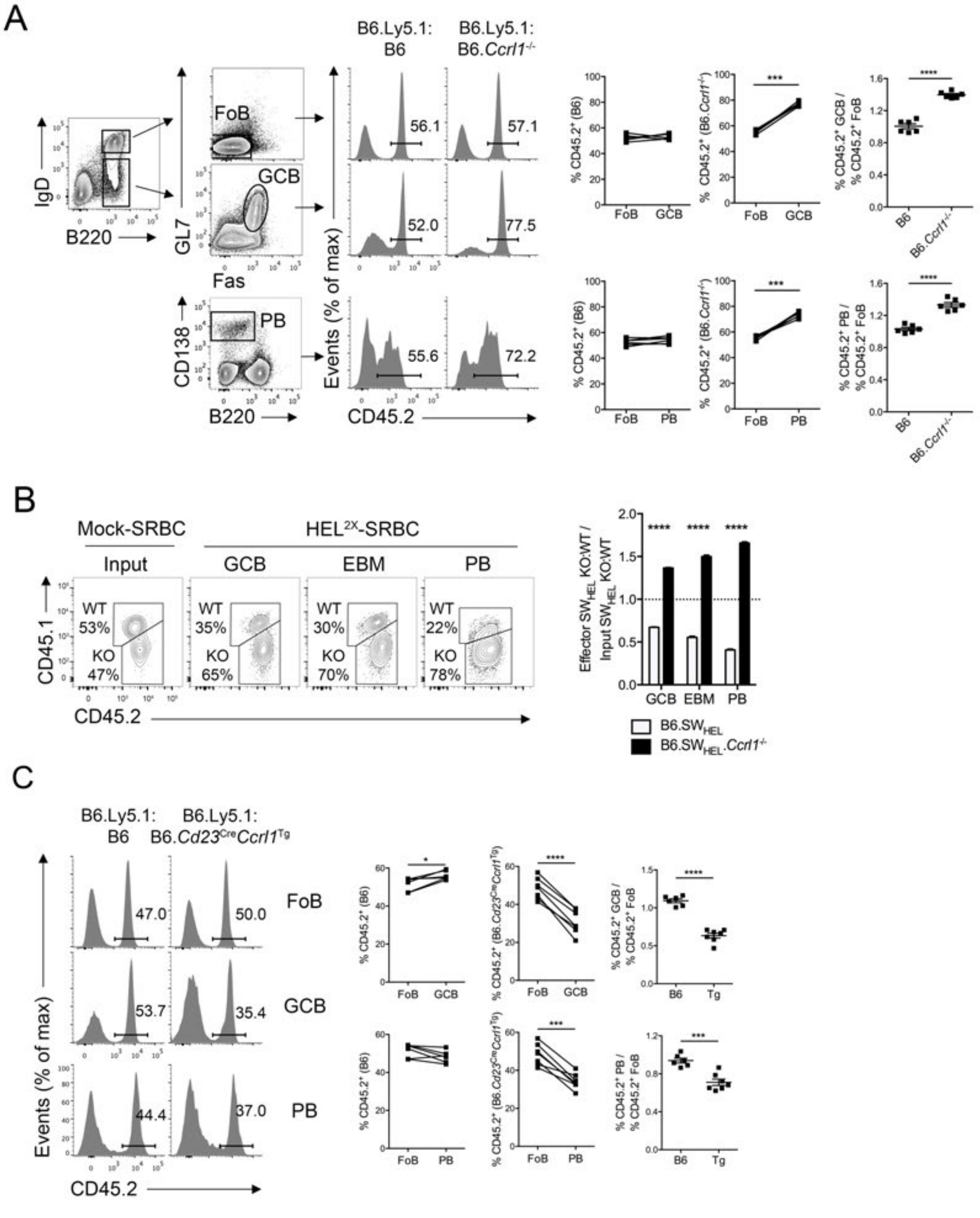

Fig. 2. ACKR4 limits early B cell differentiation in a B cell-intrinsic manner. (A) Mixed BM chimeras were generated with an equal mixture of B6.Ly5.1 ($CD45.1^+$) and B6 ($CD45.2^+$) or B6.*Ccrl1*$^{-/-}$ ($CD45.2^+$) BM. Representative plots of $CD45.2^+$ cells amongst FoB cell, GCB cell and early PB post SRBC immunization. Graphs show the contribution of $CD45.2^+$ cells amongst GCB or PB populations relative to $CD45.2^+$ cells amongst concurrent FoB cells. **(B)** WT ($CD45.1^+CD45.2^+$) and *Ccrl1*$^{-/-}$ ($CD45.2^+$) SW_{HEL} B cells were co-transferred into B6.Ly5.1 ($CD45.1^+$) mice and immunized with HEL^{2X}-SRBC (n=4) or mock-conjugated SRBCs (Mock-SRBC; n=3). Contribution of WT and *Ccrl1*$^{-/-}$ cells to SW_{HEL} GCB ($CD45.2^+CD138^-$

$B220^+Ig\kappa^+HEL^+GL7^+$), EBM $CD45.2^+CD138^-B220^+Ig\kappa^+HEL^{hi}GL7^-$) cells, and PB ($CD45.2^+CD138^+B220^{lo/-}Ig\kappa^+HEL^+$) populations d5 post immunization. Mean KO:WT input ratio was determined from Mock-SRBC immunized mice. Graph shows KO:WT ratio amongst SW_{HEL} GCB, EBM and PB divided by KO:WT input ratio. **(C)** Mixed BM chimeras were generated with an equal mixture of B6.Ly5.1 ($CD45.1^+$) and B6 ($CD45.2^+$) or B6.*Cd23*^{Cre}*Ccrl1*^{Tg} ($CD45.2^+$) and analyzed as in (A). **(A and C)** Each dot represents an individual mouse; *middle graphs*: paired two-tailed Student's *t*-test, *right graph*: unpaired two-tailed Student's *t*-test. **(B)** Unpaired two-tailed Student's *t*-test. **(A-C)** Data are representative of at least 2 independent experiments; *$p<0.05$; ***$p<0.001$; ****$p<0.0001$.

Fig. 3

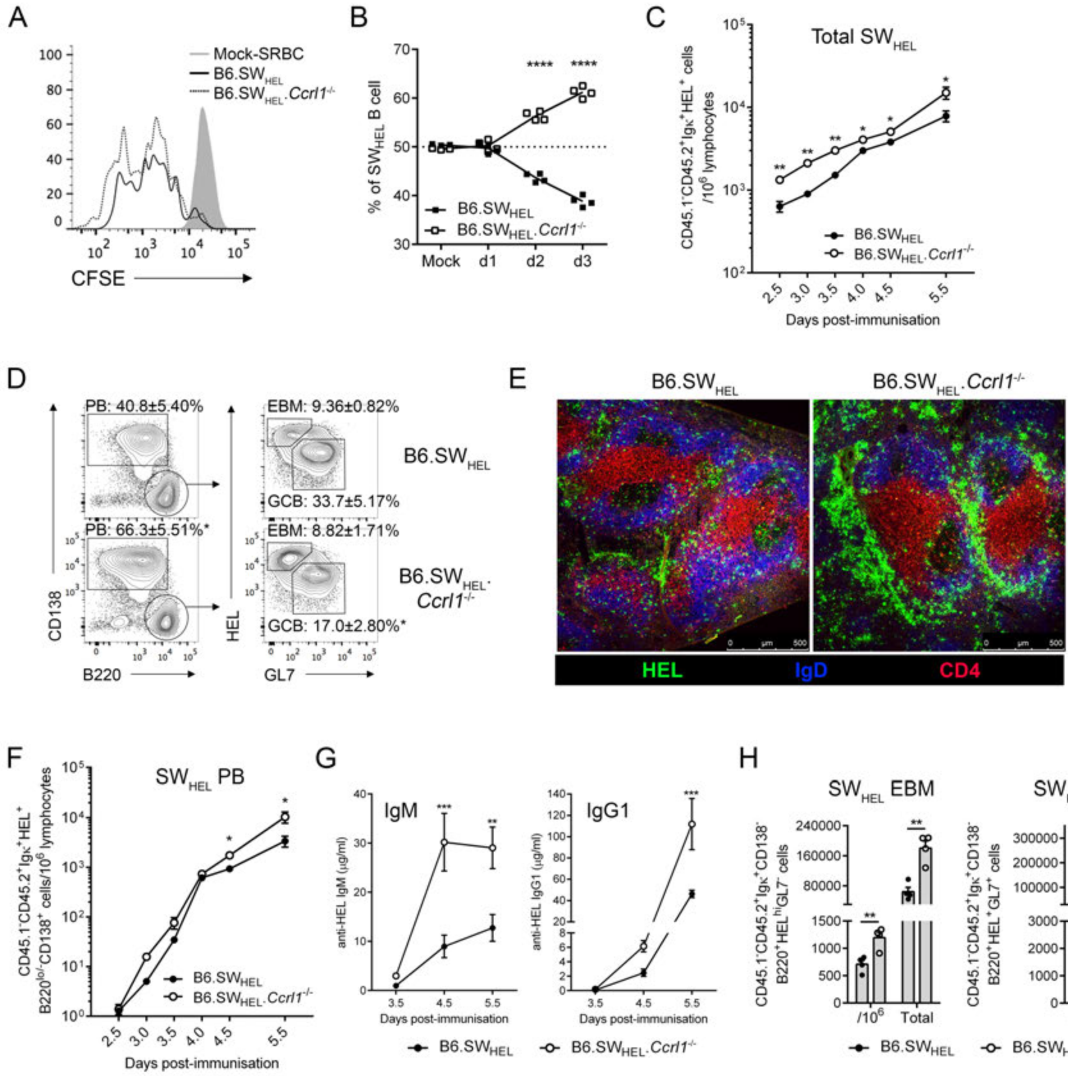

Fig. 3. ACKR4 shapes the fate trifurcation of activated B cells. (A and B) WT ($CD45.1^+CD45.2^+$) and *Ccrl1*$^{-/-}$ ($CD45.2^+$) SW_{HEL} B cells were co-transferred into B6.Ly5.1 ($CD45.1^+$) mice and immunized with HEL^{2X}-SRBC. **(A)** CFSE dilution profiles of concurrent WT and *Ccrl1*$^{-/-}$ SW_{HEL} B cells ($CD45.2^+CD138^-B220^+Ig\kappa^+HEL^+$) day (d) 2 post immunization (n=5). Undivided cells were analyzed from Mock-SRBC immunized recipients. **(B)** WT:*Ccrl1*$^{-/-}$ SW_{HEL} B cell ratio over the first 3 days of the HEL^{2X}-SRBC response. **(C-H)** WT or *Ccrl1*$^{-/-}$ ($CD45.2^+$) SW_{HEL} B cells were transferred into B6.Ly5.1 ($CD45.1^+$) mice and immunized with HEL^{2X}-SRBC. **(C)** Frequency of SW_{HEL} B cells ($CD45.2^+Ig\kappa^+HEL^+$) per 10^6 splenocytes. **(D)** Representative plots of SW_{HEL} PB, GCB and EBM cell responses d5.5 post immunization. Plots are pre-gated $CD45.2^+Ig\kappa^+HEL^+$. Numbers indicate the frequency of total SW_{HEL} B cells (mean±s.e.m.). **(E)** Representative histology of the SW_{HEL} B cell response d5.5 post immunization; 10X magnification. **(F)** Frequency of SW_{HEL} PBs per 10^6 splenocytes. **(G)** Anti-HEL IgM and IgG1 serum concentration as determined by ELISA. **(H)** Frequency per 10^6 splenocytes and total number

of SW_{HEL} EBM and GCB cell responses d5.5 post immunization. **(A-H)** Data are representative of 2 independent experiments; mean±s.e.m.; unpaired two-tailed Student's *t*-test. $^{*}p<0.05$; $^{**}p<0.01$; $^{***}p<0.001$.

Fig. 4

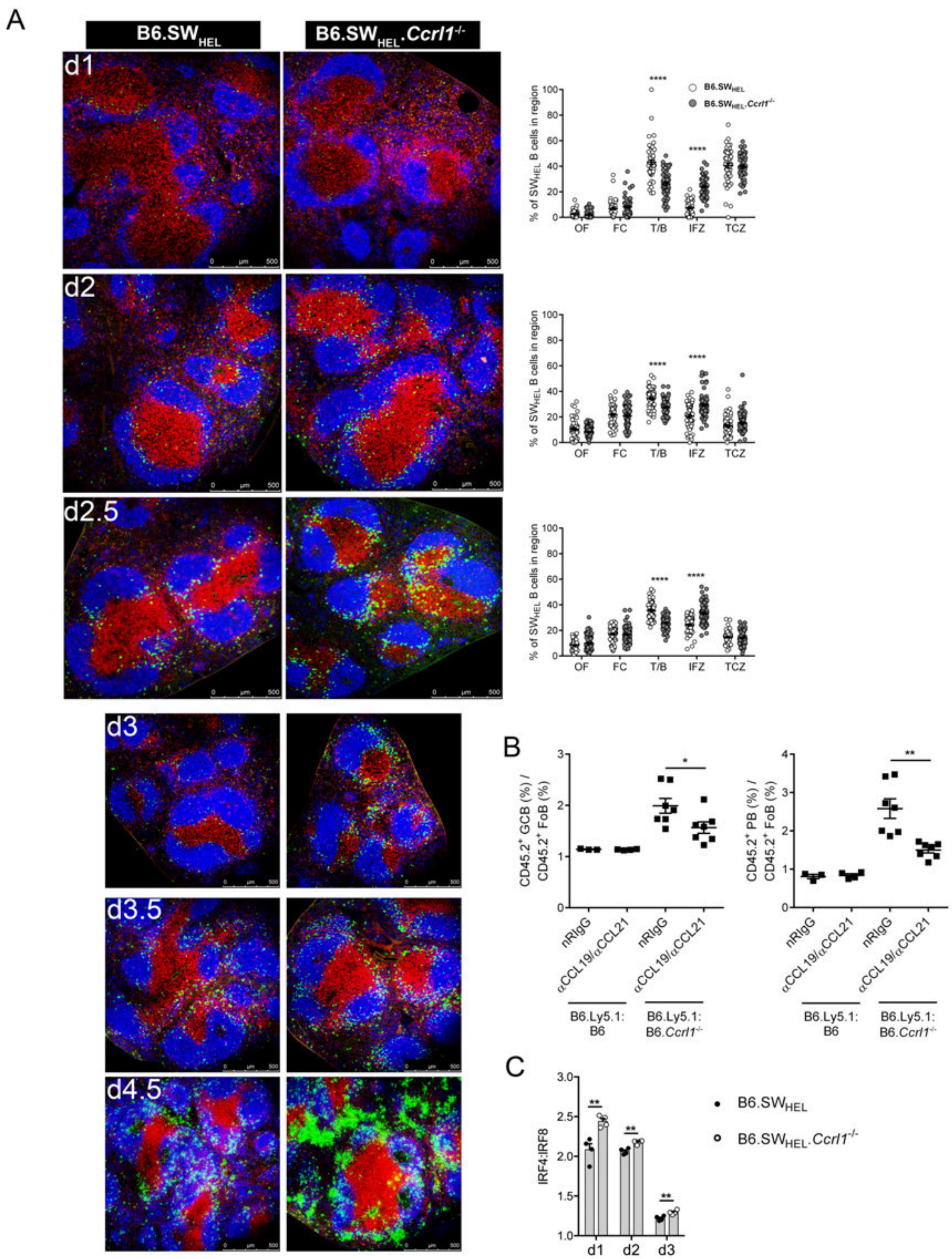

Fig. 4. ACKR4 shapes early antigen-engaged B cell migration and differentiation via CCL19/CCL21. (A) WT or *Ccrl1*$^{-/-}$ SW_{HEL} B cells were transferred into B6.Ly5.1 recipients and immunized with HEL^{2X}-SRBC. Representative histology of responding SW_{HEL} B cells in the

spleen days 1, 2, 2.5, 3, 3.5 and 4.5 post immunization. Quantification of SW_{HEL} B cell frequency per splenic region is shown for days 1, 2 and 2.5 as described in Online Methods. Magnification 10X. Blue = IgD, Green = HEL-binding, Red = CD4. **(B)** WT ($CD45.1^+CD45.2^+$) and *Ccrl1*$^{-/-}$ ($CD45.2^+$) SW_{HEL} B cells were co-transferred into B6.Ly5.1 ($CD45.1^+$) mice and immunized with HEL^{2X}-SRBC. *Left, middle graphs*: Fold change in geometric MFI of IRF4 and IRF8 staining between WT or *Ccrl1*$^{-/-}$ SW_{HEL} B cells ($CD45.2^+B220^+Ig\kappa^+HEL^+$) and concurrent endogenous FoB ($CD45.2^-CD45.1^+B220^+IgD^{hi}$). *Right graph*: IRF4:IRF8 ratio was calculated as described in Online Methods. **(C)** Mixed BM chimeras were generated with 80% BM derived from B6.Ly5.1 ($CD45.1^+$) and 20% BM derived from B6 ($CD45.2^+$) or B6.*Ccrl1*$^{-/-}$ ($CD45.2^+$). Mice were administered polyclonal rabbit sera containing 500 µg anti-CCL19 and 500 µg anti-CCL21 or 1 mg normal rabbit IgG (NRIgG) intraperitoneally on days -1, 0, 2 and 4. Mice were intraperitoneally immunized with SRBC on day 0 and analyzed 5 days later. Frequency of $CD45.2^+$ cells amongst GCB cells or early PB divided by the frequency of $CD45.2^+$ cells amongst concurrent FoB cells. **(B and C)** Each dot represents an individual mouse; mean±s.e.m.; unpaired two-tailed Student's *t*-test; *$p<0.05$; **$p<0.01$; ***$p<0.001$; ****$p<0.0001$.

Supplementary Information:

Materials and Methods, Figures S1-S19, References (*34*-*44*)

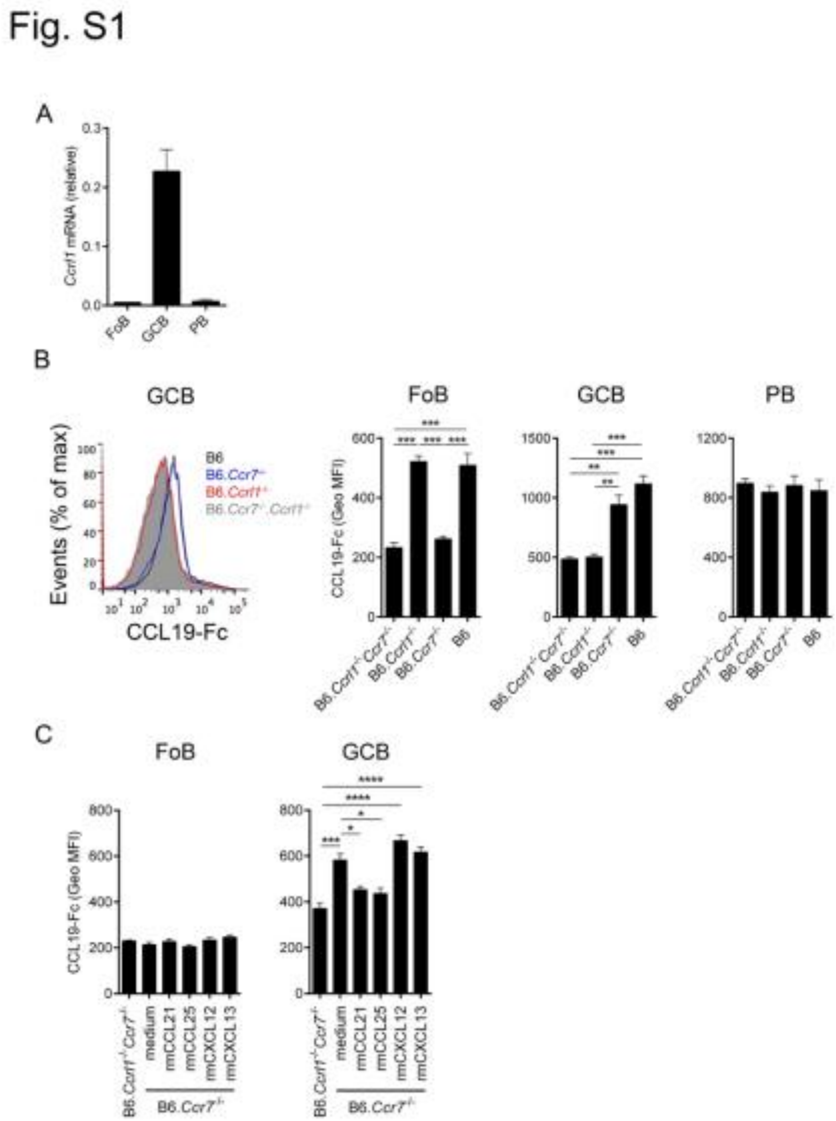

Fig. S1: GCB cells express ACKR4. (A) Quantitative PCR analysis of *Ccrl1* transcript abundance in sorted FoB, GCB cells and early PB d5 post SRBC immunization (mean±s.e.m.; n=5). Data are presented relative to housekeeping gene *Rplp0* and are representative of 3 independent experiments. **(B)** GCB cells express surface ACKR4. Representative histogram of CCL19-Fc staining on GCB cells from d5 SRBC immunized B6 (ACKR4 and CCR7 staining), B6.*Ccr7*$^{-/-}$ (ACKR4 staining), B6.*Ccrl1*$^{-/-}$ (CCR7 staining) and B6.*Ccr7*$^{-/-}$.*Ccrl1*$^{-/-}$ (no ACKR4/CCR7 staining). Geometric mean fluorescence intensity (Geo. MFI) of CCL19-Fc staining on FoB, GCB and early PB is shown. **(C)** Confirmation of CCL19-Fc strategy to detect surface ACKR4. Geo. MFI of CCL19-Fc staining on B6.*Ccr7*$^{-/-}$ (n=5) GCB cells pre-incubated with the ACKR4 ligands CCL21/CCL25, or the non-ACKR4 ligands CXCL12/CXCL13 relative to B6.*Ccr7*$^{-/-}$.*Ccrl1*$^{-/-}$ (n=5) GCB cells. **(B and C)** Representative of 2 independent experiments; mean±s.e.m.; one-way ANOVA with Bonferroni multiple comparisons test; *p<0.05; **p<0.01; ***p<0.001; ****p<0.0001.

Fig. S2

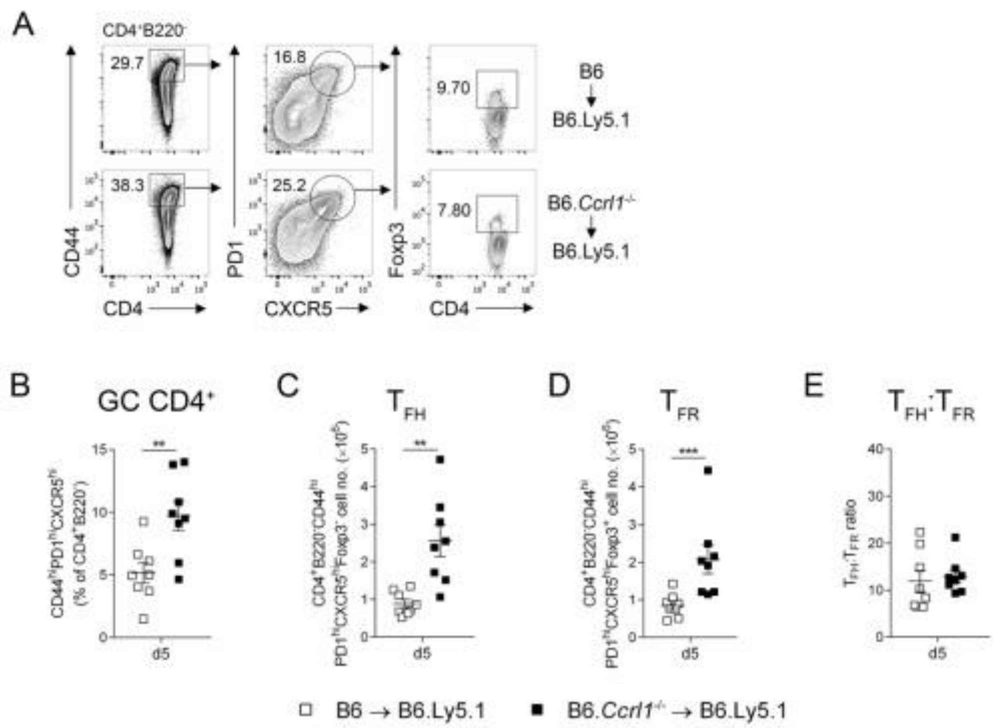

Fig. S2: Hematopoietic ACKR4 limits GC CD4$^+$ T cell responses. (A and B) Representative flow cytometric analysis (A) and quantitation (B) of germinal center CD4$^+$ T helper (GC CD4$^+$) cells (B220$^-$CD4$^+$CD44^{hi}CXCR5^{hi}PD1^{hi}), segregated into Foxp3$^-$ T_{FH} and Foxp3$^+$ T_{FR} cell populations in H-WT (n=8) and H-*Ccrl1*$^{-/-}$ (n=8) BM chimeric mice (generated as in Fig. 1A) d5 post SRBC immunization. **(C and D)** Total number of T_{FH} (C) and T_{FR} (D) cells. **(E)** T_{FH}:T_{FR} ratio per mouse. **(A-D)** Representative of 2 independent experiments; each dot represents an individual mouse; mean±s.e.m.; unpaired two-tailed Student's *t*-test; *p<0.05; **p<0.01; ***p<0.001.

Fig. S3

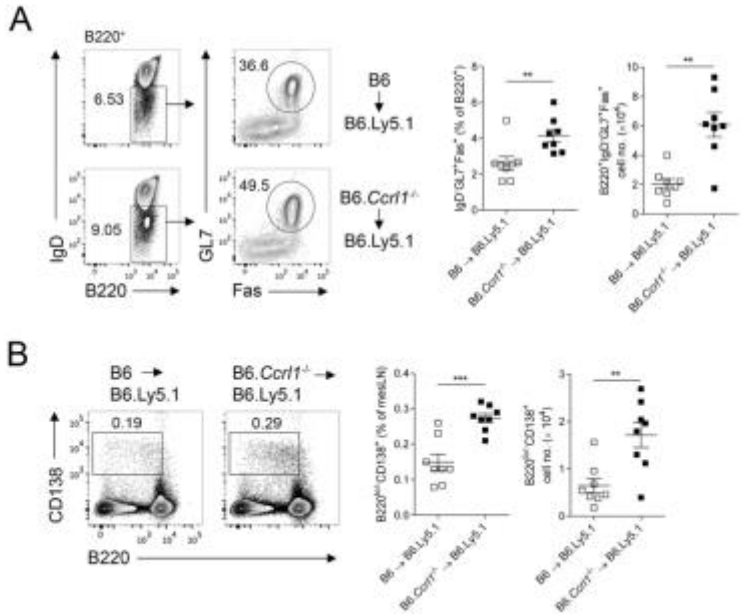

Fig. S3: Hematopoietic ACKR4 limits chronic GCB cell and PB responses in mesenteric lymph nodes. (A and B) Representative flow cytometric analysis and quantitation of GCB cells (A) and PB (B) in mesenteric lymph nodes (mesLN) of H-WT (n=8) and H-*Ccrl1*$^{-/-}$ (n=8) BM chimeric mice (generated as in Fig. 1A). Representative of 2 independent experiments; each dot represents an individual mouse; mean±s.e.m.; unpaired two-tailed Student's *t*-test; **p<0.01; ***p<0.001.

Fig. S4

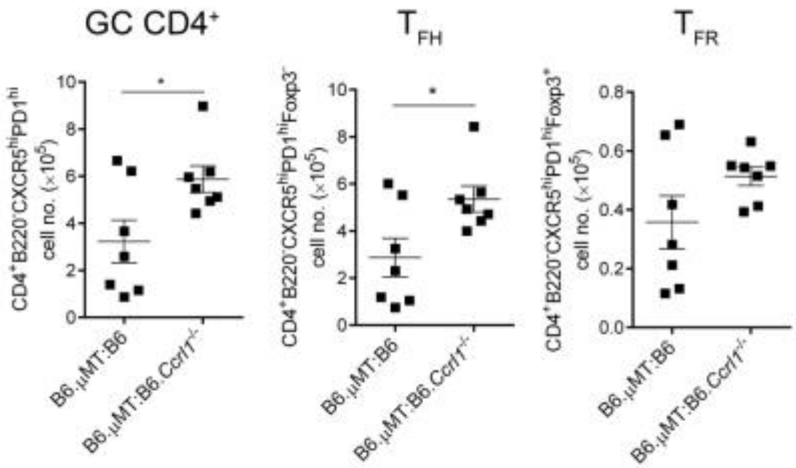

Fig. S4: B cell ACKR4 limits GC CD4$^+$ T cell responses. (A-C) Number of GC CD4$^+$ T helper (B220$^-$CD4$^+$CD44^{hi}CXCR5^{hi}PD1^{hi}) cells (A), Foxp3$^-$ T_{FH} (B) and Foxp3$^+$ T_{FR} (C) cells in B6.µMT:B6 (n=7) and B6.µMT:B6.*Ccrl1*$^{-/-}$ (n=7) BM chimeric mice (generated as in Fig. 1C) d5 post SRBC immunization. Representative of 2 independent experiments; each dot represents an individual mouse; mean±s.e.m.; unpaired two-tailed Student's *t*-test; *p<0.05.

Fig. S5

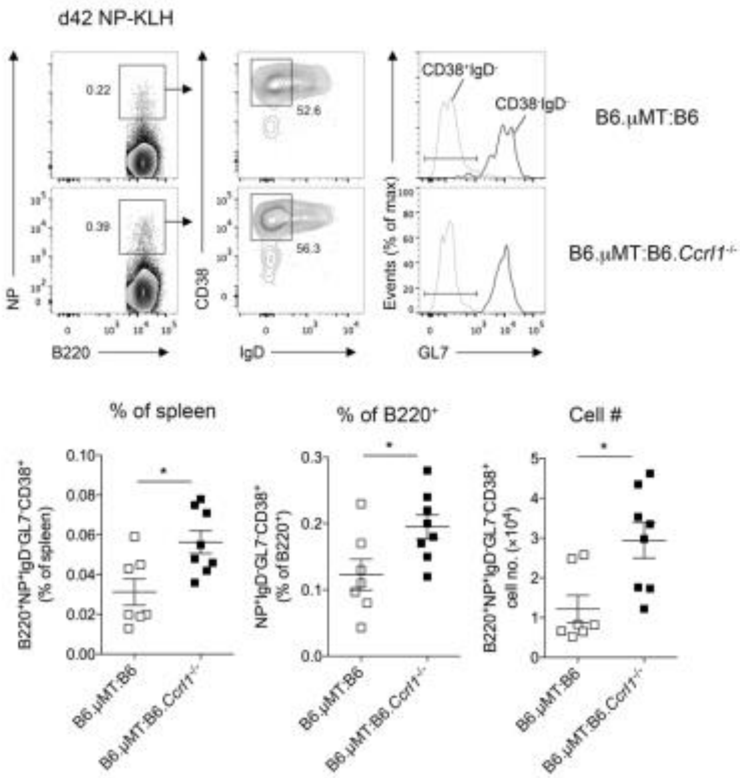

Fig. S5: B cell ACKR4 limits memory B cell generation. B6.µMT:B6 (n=7) and B6.µMT:B6.*Ccrl1*$^{-/-}$ (n=8) BM chimeric mice were generated as described in Fig. 1C and immunized with NP-KLH i.p.. Representative flow cytometric analysis of splenic NP-specific memory B cells ($B220^{+}NP^{+}CD38^{+}IgD^{-}GL7^{-}$) 42 days post immunization. Graphs show the frequency of NP-specific memory B cells per spleen (left), amongst all $B220^{+}$ cells (middle) and total number. Representative of 2 independent experiments; each dot represents an individual mouse; mean±s.e.m.; unpaired two-tailed Student's *t*-test; *p<0.05.

Fig. S6

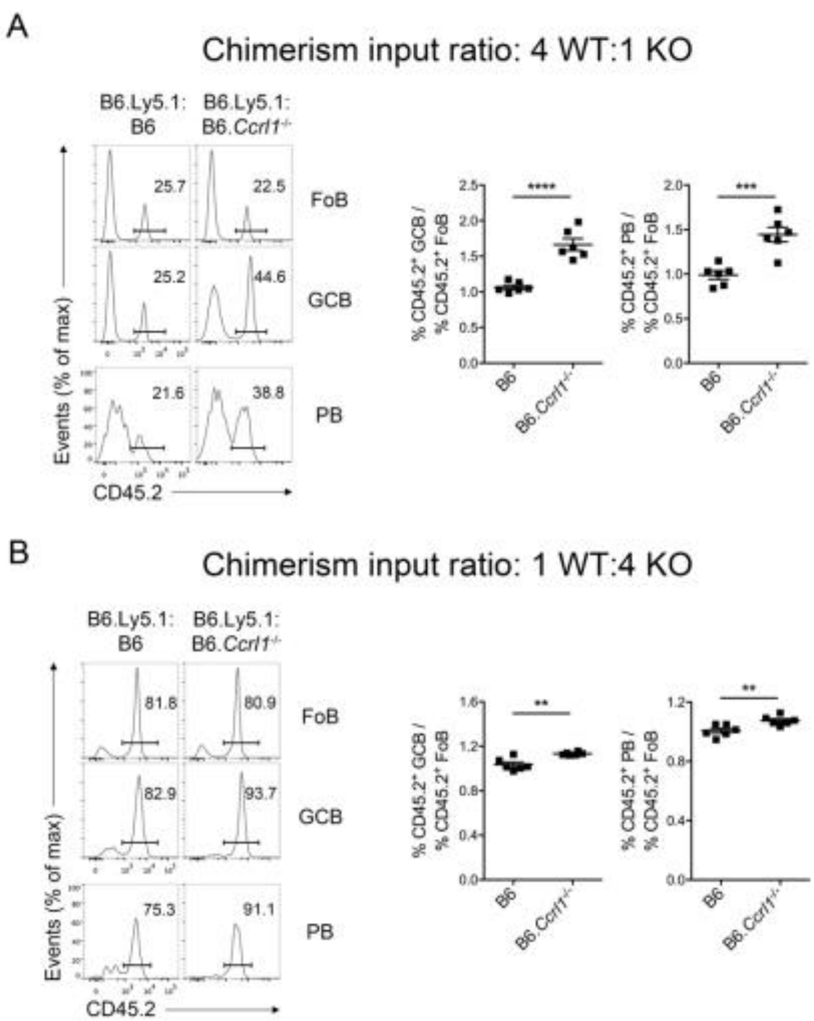

Fig. S6: ACKR4 limits early B cell differentiation in a B cell-intrinsic manner. (A) Mixed BM chimeric mice were generated by transferring 80% BM derived from B6.Ly5.1 ($CD45.1^+$) with 20% from B6 or B6.*Ccrl1*$^{-/-}$ ($CD45.2^+$) into lethally-irradiated B6.Ly5.1 recipients (input chimerism ratio - 4:1 WT:KO). Representative histograms of $CD45.2^+$ cells amongst concurrent FoB cell ($B220^+IgD^{hi}GL7^-Fas^-$), GCB cell ($B220^+IgD^-GL7^+Fas^+$) and early PB ($B220^{lo/-}CD138^+$) compartments d5 post SRBC immunization. Graphs show the frequency of $CD45.2^+$ cells amongst GCB (left) or PB (right) divided by $CD45.2^+$ cells amongst concurrent FoB cells. **(B)** Mixed BM chimeric mice were generated and analyzed as in (A) using 20% BM derived from B6.Ly5.1 with 80% from B6 or B6.*Ccrl1*$^{-/-}$ (input chimerism ratio – 1:4 WT:KO). **(A-B)** Each dot represents an individual mouse; n=6 per group; unpaired two-tailed Student's *t*-test; **p<0.01; ***p<0.001; ****p<0.0001.

Fig. S7

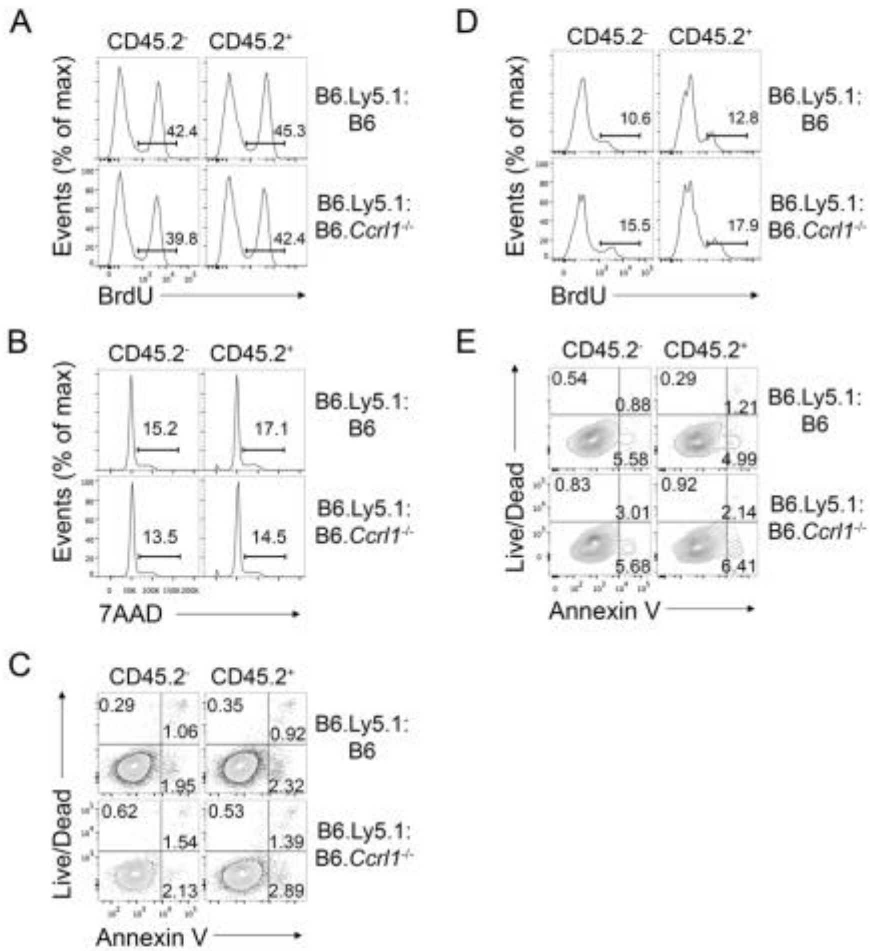

Fig. S7: ACKR4 does not alter GCB cell or early PB proliferation and apoptosis. 1:1 WT:KO mixed BM chimeric mice were immunized with SRBCs. On day 5, mice were administered 2 mg BrdU i.p. 5 hours prior to euthanasia. **(A)** Representative flow cytometric analysis of BrdU$^+$ cells amongst concurrent CD45.2$^-$ (B6.Ly5.1) and CD45.2$^+$ (B6 or B6.*Ccrl1*$^{-/-}$) GCB cells. **(B)** Representative flow cytometric analysis of DNA content (7AAD) in concurrent CD45.2$^-$ (B6.Ly5.1) and CD45.2$^+$ (B6 or B6.*Ccrl1*$^{-/-}$) GCB cells. Gated are cells in S-G2-M phase of the cell-cycle. **(C)** Representative flow cytometric analysis of Annexin V and Live/Dead staining amongst concurrent CD45.2$^-$ (B6.Ly5.1) and CD45.2$^+$ (B6 or B6.*Ccrl1*$^{-/-}$) GCB cells. AV$^+$LD$^+$ - apoptosed; AV$^+$LD$^-$ apoptotic at time of analysis. **(D)** Representative flow cytometric analysis of BrdU$^+$ cells amongst concurrent CD45.2$^-$ (B6.Ly5.1) and CD45.2$^+$ (B6 or B6.*Ccrl1*$^{-/-}$) PB. **(E)** Representative flow cytometric analysis of Annexin V and Live/Dead staining amongst concurrent CD45.2$^-$ (B6.Ly5.1) and CD45.2$^+$ (B6 or B6.*Ccrl1*$^{-/-}$) PB. AV$^+$LD$^+$ - apoptosed; AV$^+$LD$^-$ apoptotic at time of analysis. **(A-D)** Data are representative of 6 chimeric mice per experimental group. Data are representative of 2 independent experiments.

Fig. S8

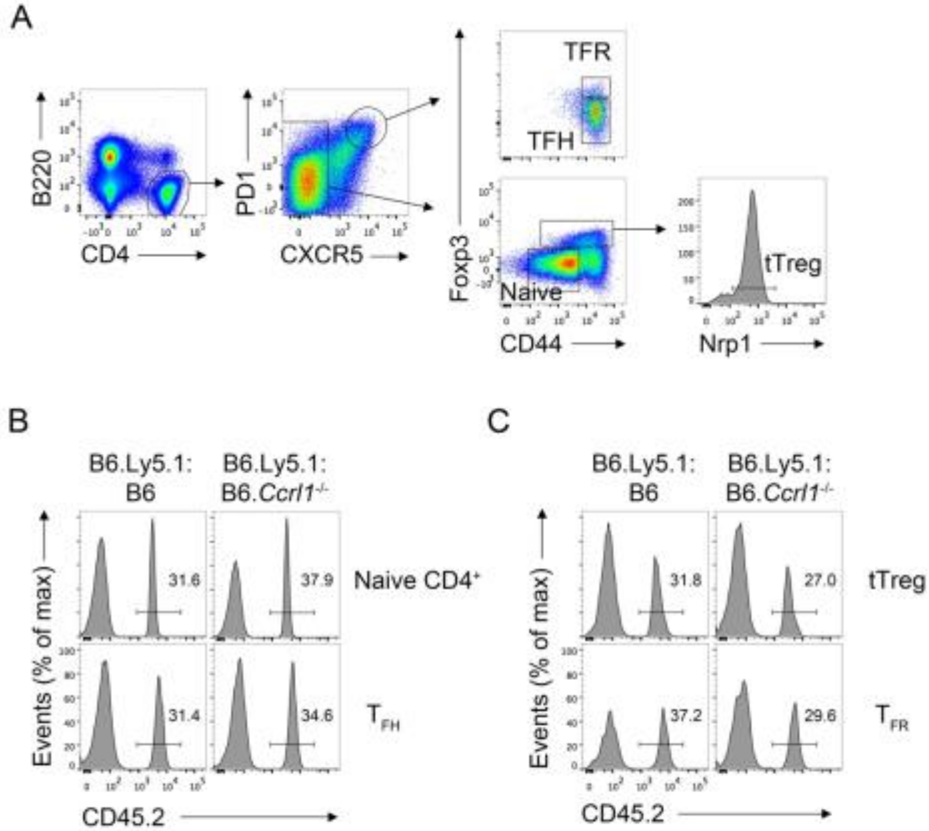

Fig. S8: ACKR4 does not alter GC CD4$^+$ T cell responses cell-autonomously. Mixed BM chimeric mice were established as described in Fig. 2A. **(A)** Representative flow cytometric gating strategy identifying naïve CD4$^+$ T cells (B220$^-$CD4$^+$CXCR5$^-$CD44^{lo}Foxp3$^-$), thymic-derived T regulatory (tTreg) cells (B220$^-$CD4$^+$CXCR5$^-$Foxp3$^+$Nrp1$^+$), T follicular helper (T_{FH}) cells (B220$^-$CD4$^+$CXCR5^{hi}PD1^{hi}CD44^{hi}Foxp3$^-$) and T follicular regulatory (T_{FR}) cells (B220$^-$CD4$^+$CXCR5^{hi}PD1^{hi}CD44^{hi}Foxp3$^+$). **(B)** Representative histograms of CD45.2$^+$ cells amongst concurrent naïve CD4$^+$ T cell and T_{FH} compartments d5 post SRBC immunization. **(C)** Representative histograms of CD45.2$^+$ cells to concurrent tTreg cell and T_{FR} compartments d5 post SRBC immunization. **(A-C)** Data are representative of 6 chimeric mice per experimental group. Data are representative of 2 independent experiments.

Fig. S9

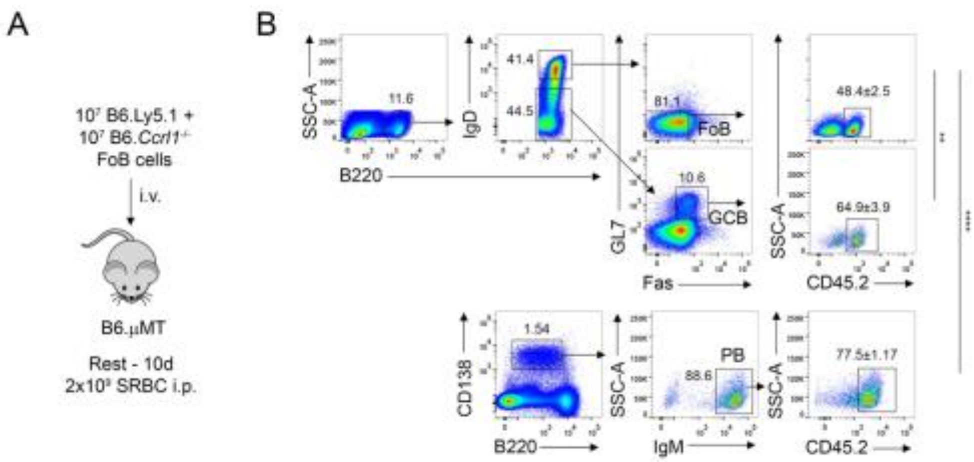

Fig. S9: ACKR4 limits GCB cell and early PB formation in a mixed FoB cell reconstitution chimeric model. (A) Schematic of experimental protocol. Splenocytes containing equivalent frequencies of B6.Ly5.1 ($CD45.1^+$) and B6 or B6.*Ccrl1*$^{-/-}$ ($CD45.2^+$) FoB cells (10^7/genotype) were transferred into B cell-deficient B6.µMT mice and immunized 10 day(d)s later with SRBCs. **(B)** Representative flow cytometric analysis of $CD45.2^+$ cells amongst concurrent FoB cells ($B220^+IgD^{hi}GL7^-Fas^-$), GCB cells ($B220^+IgD^-GL7^+Fas^+$) and PB ($B220^{lo/-}CD138^+\mu^+$) d5 post SRBC immunization. Numbers indicate mean±s.e.m. Paired two-tailed Student's *t*-test; **p<0.01; ***p<0.001.

Fig. S10

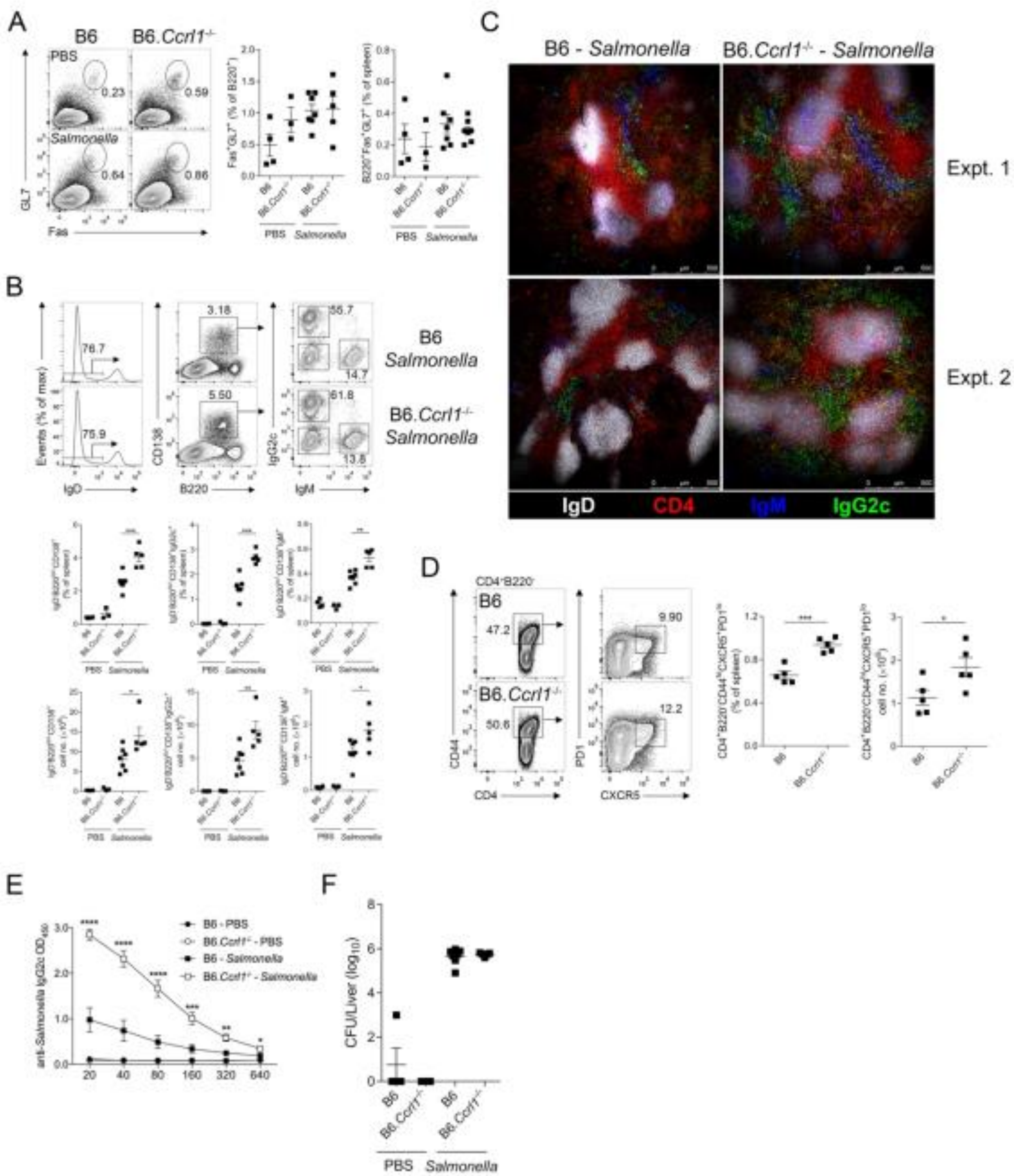

Fig. S10: ACKR4 limits early PB responses to *Salmonella enterica* infection. WT and *Ccrl1*$^{-/-}$ mice were challenged intraperitoneally with 10^6 CFU log-phase *Salmonella enterica* or vehicle (PBS) and analyzed 7 days later (unless otherwise indicated). **(A)** Representative flow cytometric analysis and quantitation of splenic GCB cells. **(B)** Representative flow cytometric analysis and quantitation (% of spleen and total number) of splenic IgM$^+$ and IgG2c$^+$ PBs. **(C)** Representative histology (representative image per independent experiment) of IgG2c$^+$ and IgM$^+$ PB responses. 10X magnification. **(D)** Serum anti-*Salmonella* IgG2c as determined by ELISA. **(E)**

Representative flow cytometric analysis and quantitation of splenic pre-T_{FH} cells ($B220^{-}CD4^{+}CD44^{hi}PD1^{lo}CXCR5^{+}$). **(F)** Liver bacterial burden (CFU/liver) day 12 post challenge. **(A-F)** Representative of 2 independent experiments. **(A-D and F)** PBS – B6: n=4, *Ccrl1*$^{-/-}$: n=3, *Salmonella* – B6: n=7, *Ccrl1*$^{-/-}$: n=5. **(E)** Samples pooled from 2 independent experiments. PBS – B6: n=8, *Ccrl1*$^{-/-}$: n=7, *Salmonella* – B6: n=14, *Ccrl1*$^{-/-}$: n=11. **(A, B, E and F)** Each dot represents an individual mouse. **(A, B and D-F)** Mean±s.e.m.; unpaired two-tailed Student's *t*-test; *p<0.05; **p<0.01; ***p<0.001.

Fig. S11

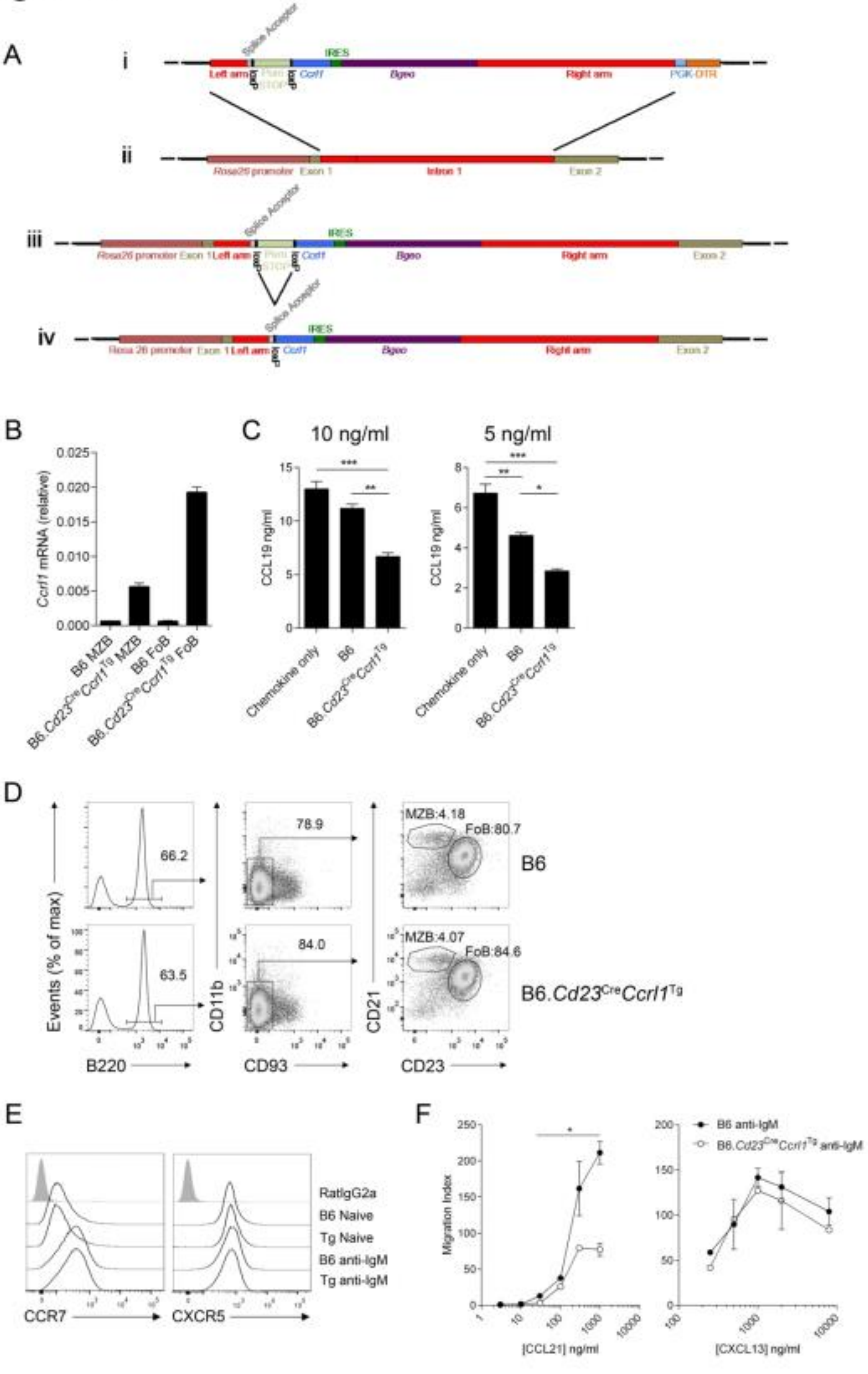

A
i
ii
iii
iv
Splice Acceptor
IRES
Left arm
Puro STOP
loxP
Ccrl1
Bgeo
Right arm
PGK-DTR
Rosa26 promoter
Exon 1
Intron 1
Exon 2
B
Ccrl1 mRNA (relative)
B6 MZB
B6.Cd23CreCcrl1Tg MZB
B6 FoB
B6.Cd23CreCcrl1Tg FoB
C
10 ng/ml
5 ng/ml
CCL19 ng/ml
Chemokine only
B6
B6.Cd23CreCcrl1Tg
D
66.2
63.5
78.9
84.0
MZB:4.18
FoB:80.7
MZB:4.07
FoB:84.6
B6
B6.Cd23CreCcrl1Tg
Events (% of max)
CD11b
CD21
B220
CD93
CD23
E
RatIgG2a
B6 Naive
Tg Naive
B6 anti-IgM
Tg anti-IgM
CCR7
CXCR5
F
Migration Index
[CCL21] ng/ml
[CXCL13] ng/ml
B6 anti-IgM
B6.Cd23CreCcrl1Tg anti-IgM

Fig. S11: Generation and validation of *Cd23a*$^{\text{Cre/+}}$.*Rosa26*$^{\text{LSL-}\textit{Ccrl1}\text{/+}}$ (*Cd23*$^{\text{Cre}}$*Ccrl1*$^{\text{Tg}}$) mice. (A) B6.*Ccrl1*$^{\text{Tg}}$ targeting strategy. *(i) Ccrl1*$^{\text{Tg}}$ construct; *(ii)* WT *Rosa26* locus; *(iii)* Targeted *Rosa26* locus; *(iv)* Targeted *Rosa26* locus after *Cd23*-Cre-mediated recombination. loxP:loxP - targets for Cre-mediated recombination; Puro-STOP – puromycin resistence gene followed by STOP cassette (transcriptional pause sequence with 2 polyA sites); IRES – internal ribosome entry site; *Bgeo* – fusion of β-gal and neomycin resistance cDNA; PGK-DTR – diphtheria toxin receptor control by the PGK promoter. **(B)** Quantitative PCR analysis of *Ccrl1* transcript abundance in FACS-purified marginal zone B (MZB) cells and follicular B (FoB) cells (gated as shown in (D)) from B6 and B6.*Cd23*$^{\text{Cre}}$*Ccrl1*$^{\text{Tg}}$ mice (mean±s.e.m.; n=3). Data presented relative to housekeeping gene *Rplp0*. **(C)** CCL19 scavenging assay. Purified FoB cells from B6 (n=3) or B6.*Cd23*$^{\text{Cre}}$*Ccrl1*$^{\text{Tg}}$ (n=3) mice were incubated with 10 or 5 ng/ml recombinant CCL19 for 3 hours at 37 degrees. CCL19 concentration in cell-free supernatants were determined by ELISA. Samples with no addition of cells (chemokine only) were used to determine input CCL19 concentration. One-way ANOVA with Bonferroni multiple comparisons test. **(D)** Forced ACKR4 in B cells does not alter MZB and FoB cell frequency. Representative flow cytometric analysis of MZB and FoB cell frequency in spleen of B6 (n=3) and B6.*Cd23*$^{\text{Cre}}$*Ccrl1*$^{\text{Tg}}$ (n=3). **(E)** Representative flow cytometric analysis of CCR7 and CXCR5 expression on unstimulated (rested overnight) and BCR-stimulated (anti-IgM 5 µg/ml; 24 hours) B6 and B6.*Cd23*$^{\text{Cre}}$*Ccrl1*$^{\text{Tg}}$ B cells. **(F)** BCR-stimulated B6 and B6.*Cd23*$^{\text{Cre}}$*Ccrl1*$^{\text{Tg}}$ B cell transwell chemotaxis to CCL21 and CXCL13. Unpaired two-tailed Student's t-test. **(C and F)** *$p<0.05$; **$p<0.01$; ***$p<0.001$.

Fig. S12

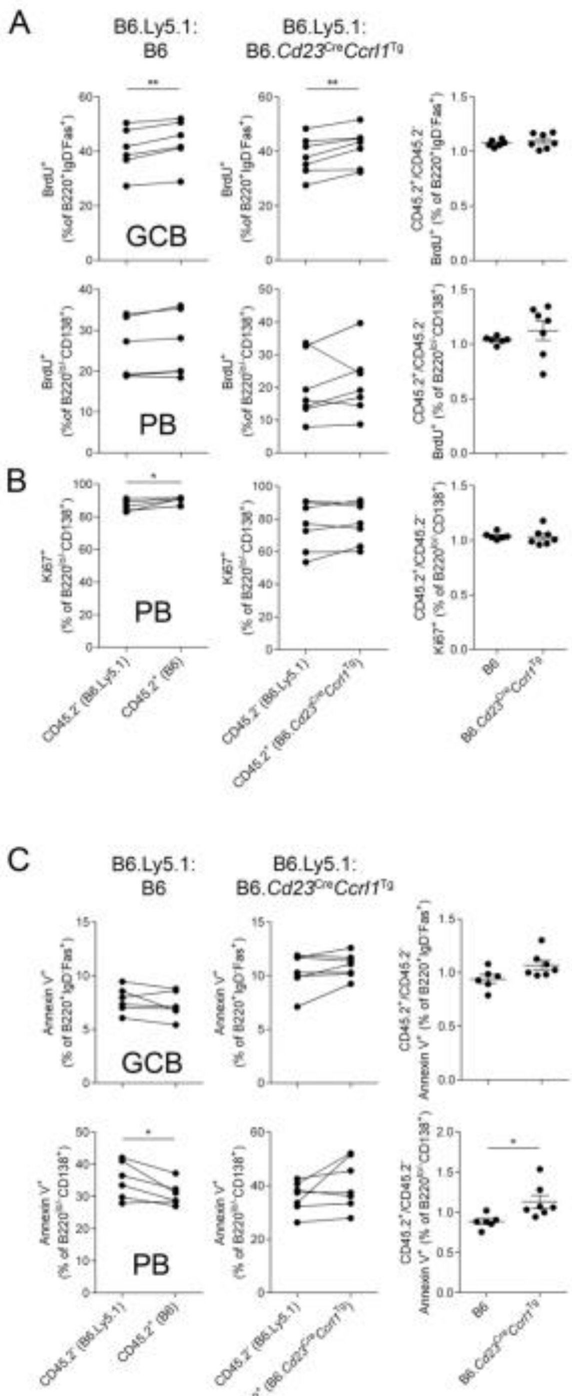

Fig. S12: Aberrant proliferation/apoptosis does not account for reduced GCB cell and early PB responses in ACKR4 transgenic B cells

(A) Proliferation of *Cd23*^{Cre}*Ccrl1*^{Tg} and control GCB cells and early PB was assessed by administering a single dose of BrdU (2 mg/mouse i.p.) to mixed bone marrow (BM) chimeras (from Fig. 2C) 5 hours prior to euthanasia. *Left and middle graphs:* $BrdU^+$ cells amongst *Cd23*^{Cre}*Ccrl1*^{Tg} and control GCB cell (top) and early PBs (bottom). *Right graph*: data are presented as % $BrdU^+$ amongst $CD45.2^+$ GCB cells or early PBs divided by % $BrdU^+$ amongst concurrent $CD45.2^-$ GCB cells or early PBs. **(B)** *Left and middle graphs*: $Ki67^+$ cells amongst *Cd23*^{Cre}*Ccrl1*^{Tg} and control early PBs from mixed BM chimeras. *Right graph*: data are presented as % $Ki67^+$ amongst $CD45.2^+$ early PBs divided by % $Ki67^+$ amongst concurrent $CD45.2^-$ early PBs. **(C)** *Left and middle graphs*: Annexin V $(AV)^+$ cells amongst *Cd23*^{Cre}*Ccrl1*^{Tg} and control GCB cells (top) and early PBs (bottom) from mixed BM chimeras. *Right graph*: data are presented as % AV^+ amongst $CD45.2^+$ GCB cells or early PBs divided by % AV^+ amongst concurrent $CD45.2^-$. Each dot represents an individual mouse; mean±s.e.m.; paired (left and middle graphs) or unpaired (right graph) two-tailed Student's *t*-test; *p<0.05; **p<0.01.

Fig. S13

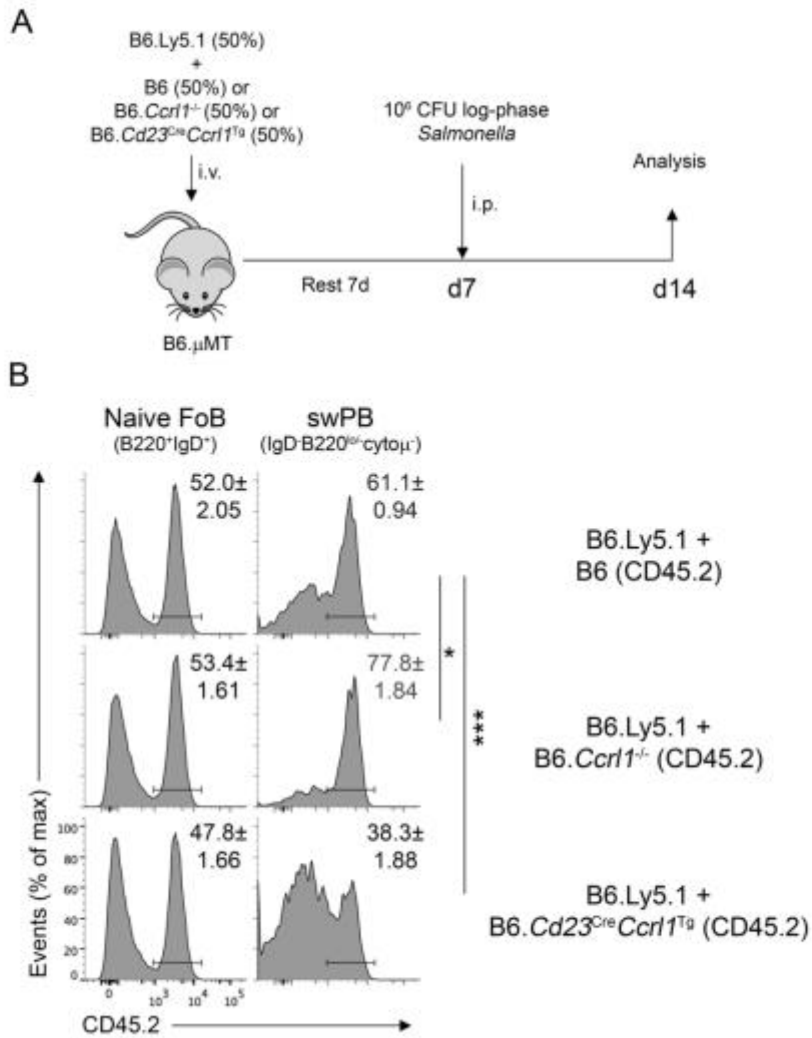

Fig. S13: ACKR4 shapes early PB responses to *Salmonella enterica* infection in a B cell-intrinsic manner. (A) Schematic of experimental protocol. Splenocytes containing equivalent frequencies of B6.Ly5.1 ($CD45.1^+$) and B6, B6.*Ccrl1*$^{-/-}$ or B6.*Cd23*^{Cre}*Ccrl1*^{Tg} ($CD45.2^+$; n=5/genotype) FoB cells (10^7/genotype) were transferred into B cell-deficient mice (B6.µMT) and challenged intraperitoneally 7 days later with 10^6 CFU log-phase *Salmonella enterica*. **(B)** Representative flow cytometric analysis of $CD45.2^+$ cells amongst FoB cells and switched plasmablasts (swPB) 7 days post challenge. Numbers indicate mean±s.e.m.. Data were analyzed using the following formula: % $CD45.2^+$ amongst swPB/% $CD45.2^+$ amongst concurrent FoB. These values were then statistically examined using a one-way ANOVA with Dunnett's multiple comparison test relative to B6.Ly5.1:B6 control group. *p<0.05; ***p<0.001.

Fig. S14

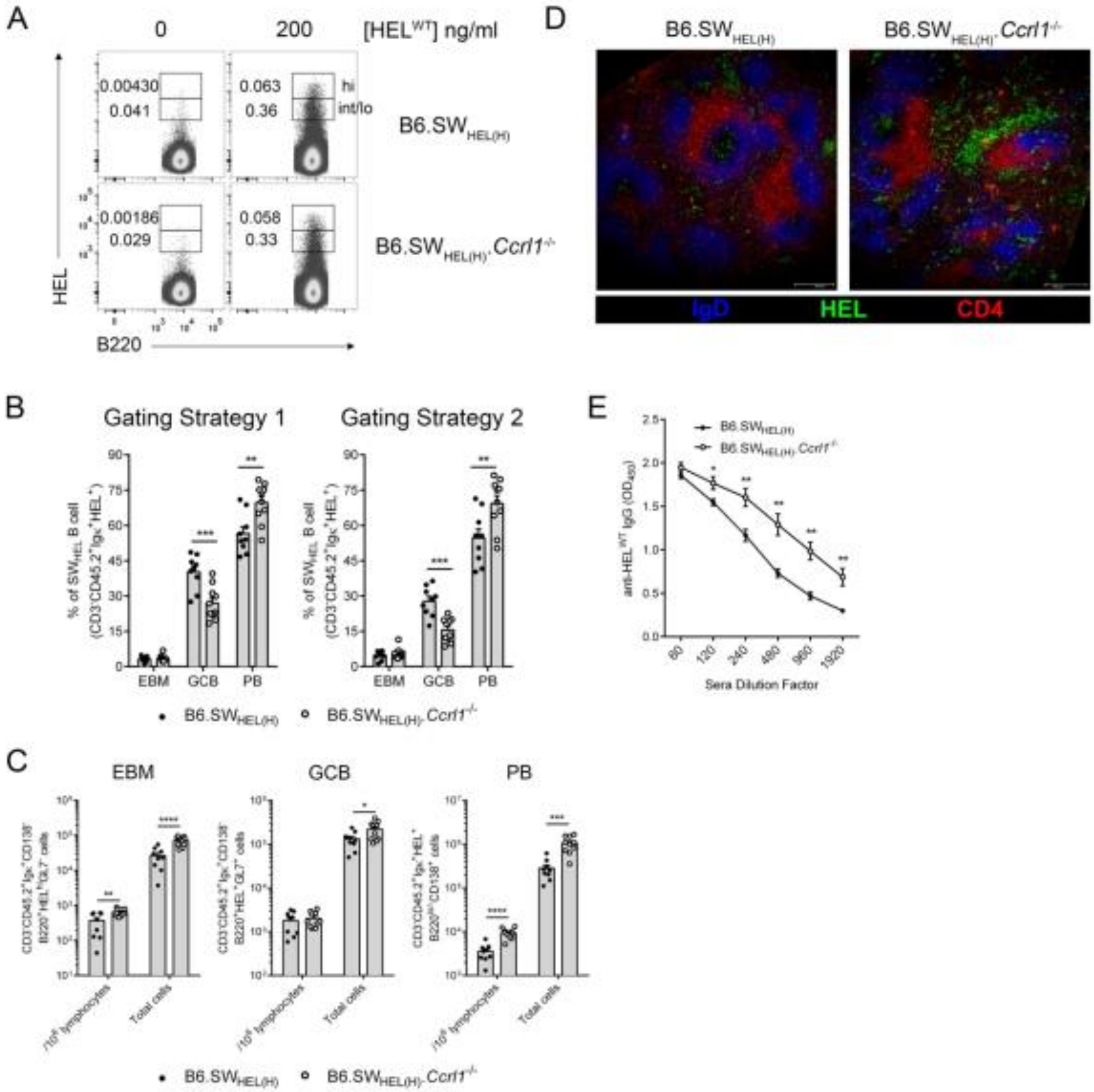

Fig. S14: ACKR4 limits SW$_{HEL(H)}$ B cell responses. (A) Splenocytes from unimmunized B6.SW$_{HEL(H)}$ (n=4) and B6.SW$_{HEL(H)}$.*Ccrl1*$^{-/-}$ (n=4) mice were incubated with HEL^{WT} (200 ng/ml) prior to detection of HEL-binding cells using HyHEL9 monoclonal antibody. Representative plots illustrate equivalent frequencies of high (top gate) and intermediate/low (bottom gate) affinity SW$_{HEL(H)}$ B cells between WT and *Ccrl1*$^{-/-}$ SW$_{HEL(H)}$ mice. **(B-E)** WT or *Ccrl1*$^{-/-}$ SW$_{HEL(H)}$ B cells (CD45.2^{+}) were transferred into B6.Ly5.1 (CD45.1^{+}) recipients, immunized with HEL^{WT}-SRBC and analyzed 5 days later. **(B)** Frequency of SW$_{HEL(H)}$ B cells (CD3^{-}CD45.2^{+}Igκ^{+}HEL^{+}) in EBM cell, GCB cell and early PB compartments determined using two flow cytometric gating strategies. *Gating strategy 1:* EBM: (CD3^{-}CD45.2^{+}CD138^{-}B220^{+}Igκ^{+}HEL^{hi}GL7^{-}), GCB: (CD3^{-}CD45.2^{+}CD138^{-}B220^{+}Igκ^{+}HEL^{+}GL7^{+}), PB: (CD3^{-}CD45.2^{+}Igκ^{+}HEL^{+}CD138^{+}B220$^{lo/-}$); *Gating strategy 2:* EBM: (CD3^{-}CD45.2^{+} Igκ^{+}B220^{+}HEL^{hi}), GCB: (CD3^{-}CD45.2^{+}Igκ^{+}B220^{+}HEL^{lo}), PB:

($CD3^{-}CD45.2^{+}Ig\kappa^{+}$ $B220^{lo/-}HEL^{+}$). **(C)** Frequency of SW_{HEL} EBM cell, GCB cell and PBs (gating strategy 1) per 10^6 splenocytes and total number per spleen. **(D)** Representative histology of WT and *Ccrl1*$^{-/-}$ $SW_{HEL(H)}$ B cell responses. 10X magnification. **(E)** Serum anti-HEL^{WT} IgG responses as determined by ELISA. **(B-F)** Data pooled from 2 independent experiments B6.$SW_{HEL(H)}$: n=9, B6.$SW_{HEL(H)}$.*Ccrl1*$^{-/-}$: n=10. **(B and C)** Each dot represents an individual mouse. **(B, C and E)** Mean±s.e.m; unpaired two-tailed Student's *t*-test; *p<0.05; **p<0.01; ***p<0.001; ****p<0.0001.

Fig. S15

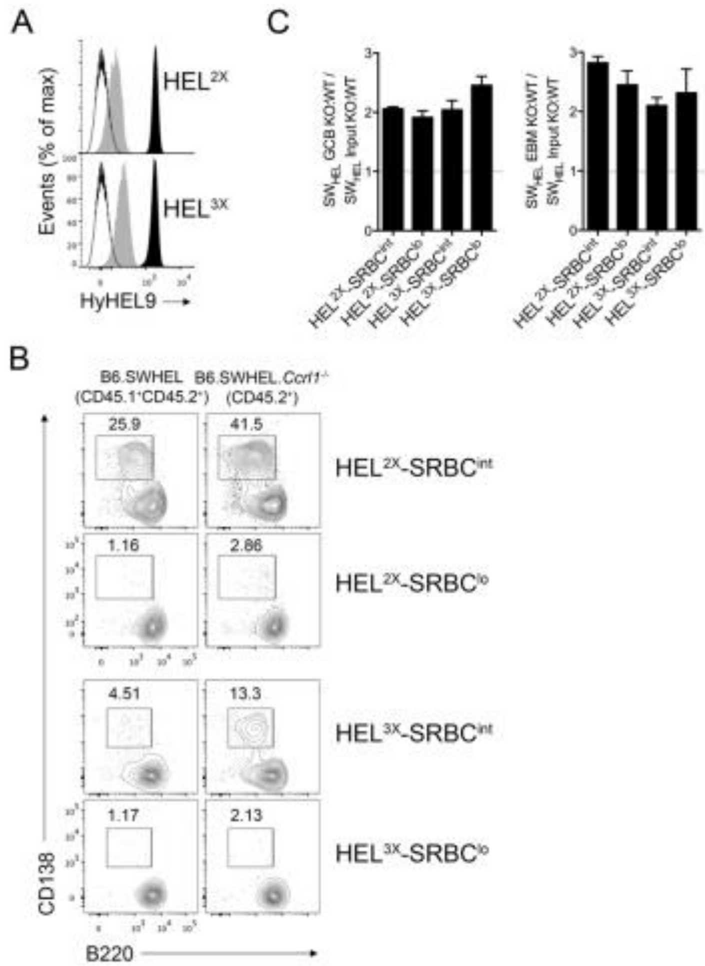

Fig. S15: ACKR4 limits early PB differentiation. WT ($CD45.1^+CD45.2^+$) and *Ccrl1*$^{-/-}$ ($CD45.2^+$) were co-transferred into B6.Ly5.1 ($CD45.1^+$) recipients and immunized with HEL^{2X} (intermediate affinity) or HEL^{3X} (low affinity) conjugated to SRBCs at varying epitope densities. Input ratio was determined from Mock-SRBC immunized mice. **(A)** HEL^{2X} or HEL^{3X} were conjugated to SRBCs at intermediate (black histogram; 100 µg/ml; $SRBC^{int}$) and low (grey histogram; 5 µg/ml; $SRBC^{lo}$) epitope densities and detected using HyHEL9 monoclonal antibody. Mock-conjugated SRBCs (open histogram) are shown for comparison. **(B)** Representative flow cytometric analysis of SW_{HEL} PB responses 5 days post immunization. **(C)** Fold differences between concurrent *Ccrl1*$^{-/-}$ and WT SW_{HEL} B cell responses was determined by dividing the KO:WT ratio amongst SW_{HEL} EBM ($CD45.2^+Igk^+$ $CD138^-B220^+HEL^{hi}GL7^-$) or GCB ($CD45.2^+Igk^+CD138^-B220^+HEL^+GL7^+$) cells from HEL-SRBC immunized mice (day 5) with the input KO:WT ratio from Mock-SRBC immunized mice. **(B and C)** n=4/condition; mean±s.e.m.; one-way ANOVA with Bonferroni multiple comparisons test.

Fig. S16

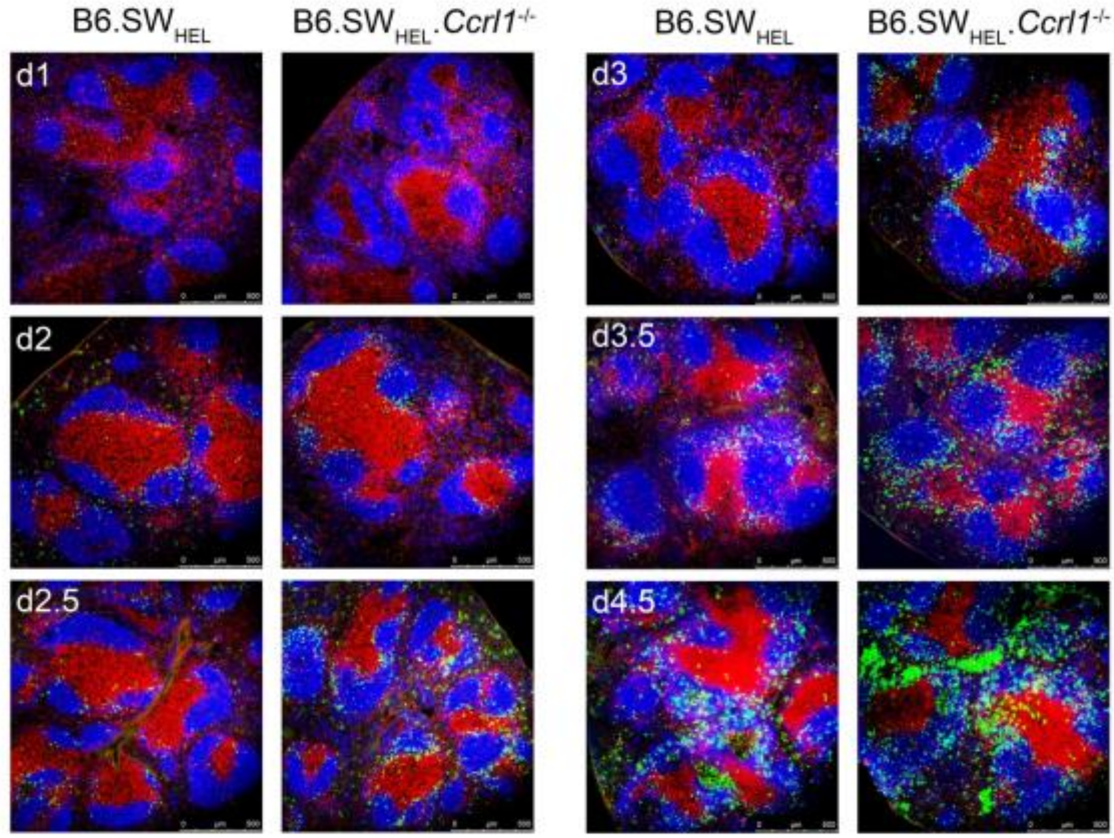

Fig. S16: *Ccrl1*$^{-/-}$ SW$_{HEL}$ B cells favorably localize to interfollicular zones early during the evolution of the HEL^{2X}-SRBC response (related to Fig. 4A). Additional representative images of WT and *Ccrl1*$^{-/-}$ SW$_{HEL}$ B cell responses day (d) 1, d2, d2.5, d3, d3.5 and d4.5 post HEL^{2X}-SRBC immunization (related to Fig. 4A). 10X magnification. Blue = IgD, Green = HEL-binding, Red = CD4.

Fig. S17

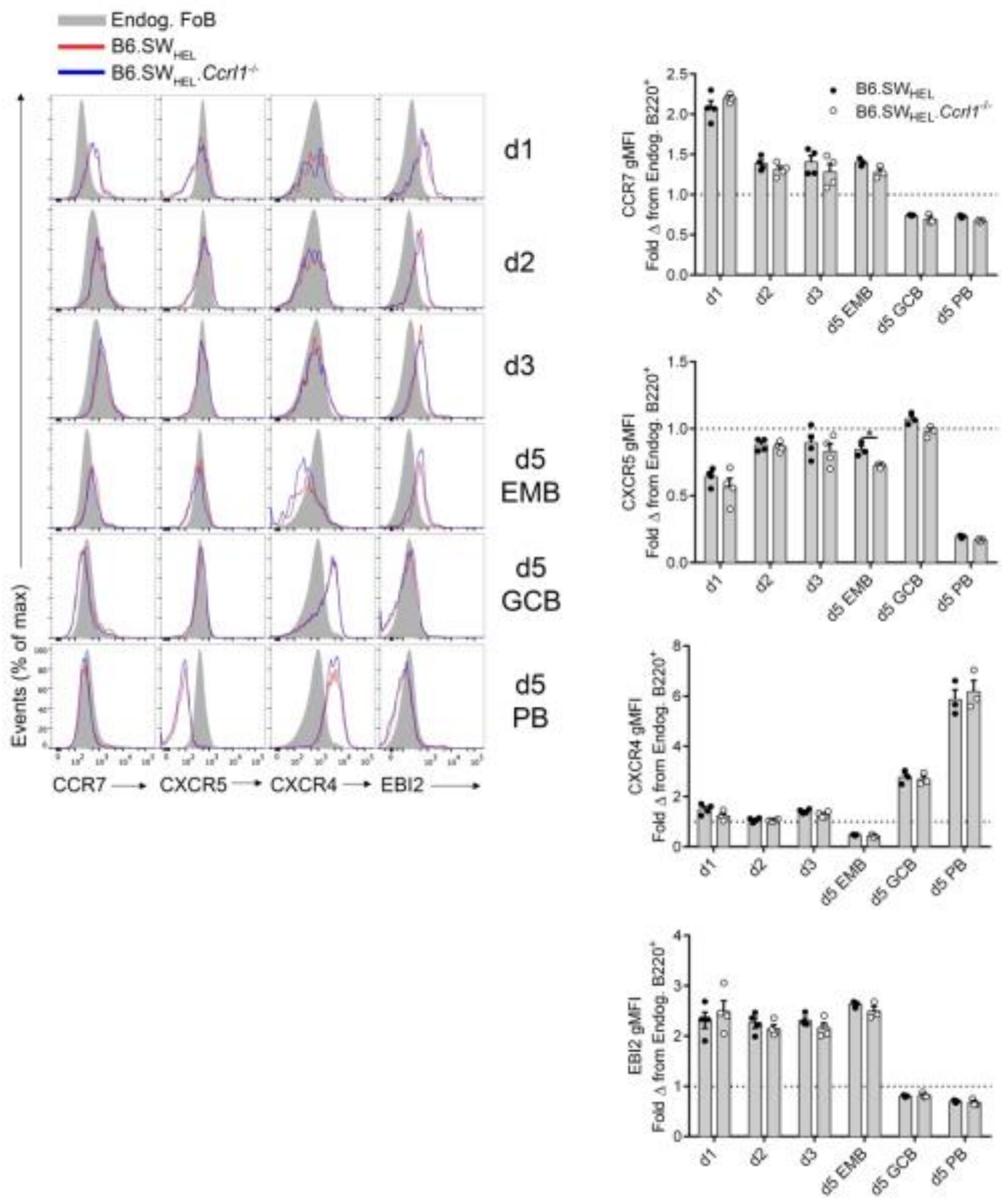

Fig. S17: ACKR4 does not alter antigen-engaged B cell expression of key chemoattractant receptors. WT ($CD45.1^{+}CD45.2^{+}$) and *Ccrl1*$^{-/-}$ ($CD45.2^{+}$) SW_{HEL} B cells were co-transferred into B6.Ly5.1 ($CD45.1^{+}$) recipients and immunized with HEL^{2X}-SRBC. *Day 1-3*: Representative histograms of concurrent WT (red) and *Ccrl1*$^{-/-}$ (blue) SW_{HEL} B cell ($CD45.2^{+}B220^{+}Ig\kappa^{+}HEL^{+}$) expression of CCR7, CXCR5, CXCR4 and EBI2 relative to concurrent endogenous FoB cells ($CD45.2^{-}CD45.1^{+}B220^{+}IgD^{hi}$; filled grey). *Day 5*: chemoattractant receptor expression on SW_{HEL} PB, EBM and GCB cells. Graphs show fold change in geometric mean fluorescence intensity (Geo. MFI) of chemoattractant receptor expression between WT or *Ccrl1*$^{-/-}$ SW_{HEL} B cells and concurrent endogenous FoB cells. Each dot represents an individual mouse (n=4); mean±s.e.m.; unpaired two-tailed Student's *t*-test. *$p<0.05$.

Fig. S18

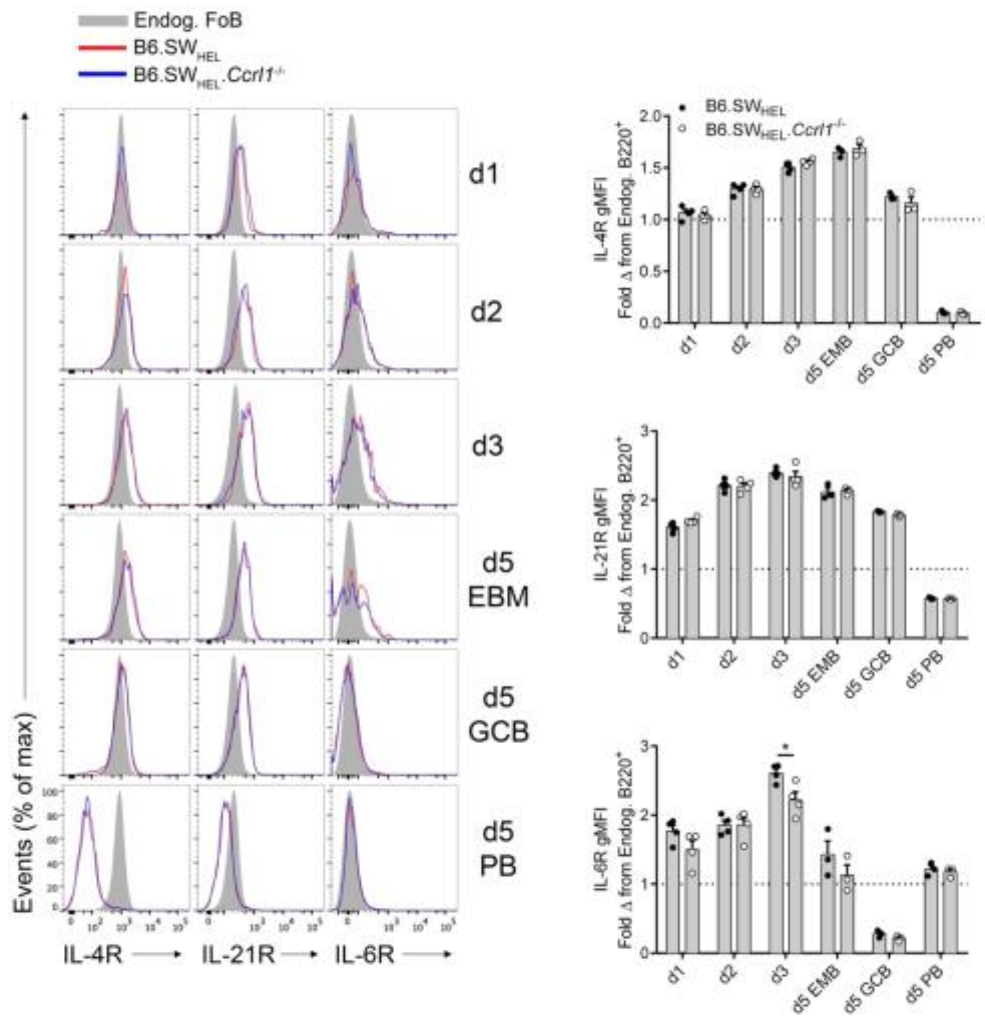

Fig. S18: ACKR4 does not alter IL-4, IL-6 or IL-21 receptor expression on antigen-engaged B cells. WT ($CD45.1^+CD45.2^+$) and *Ccrl1*$^{-/-}$ ($CD45.2^+$) SW_{HEL} B cells were co-transferred into B6.Ly5.1 ($CD45.1^+$) recipients and immunized with HEL^{2X}-SRBC. *Day 1-3*: Representative histograms of concurrent WT (red) and *Ccrl1*$^{-/-}$ (blue) SW_{HEL} B cell ($CD45.2^+B220^+Ig\kappa^+HEL^+$) expression of IL-4R (CD124), IL-6R (CD126) and IL-21R (CD360) relative to concurrent endogenous FoB cells ($CD45.2^-CD45.1^+B220^+IgD^{hi}$; filled grey). *Day 5*: cytokine receptor expression on SW_{HEL} PB, EBM and GCB cells. Graphs show fold change in geometric mean fluorescence intensity (Geo. MFI) of cytokine receptor expression between WT or *Ccrl1*$^{-/-}$ SW_{HEL} B cells and concurrent endogenous FoB cells. Each dot represents an individual mouse (n=4); mean±s.e.m.; unpaired two-tailed Student's *t*-test; *p<0.05.

Fig. S19

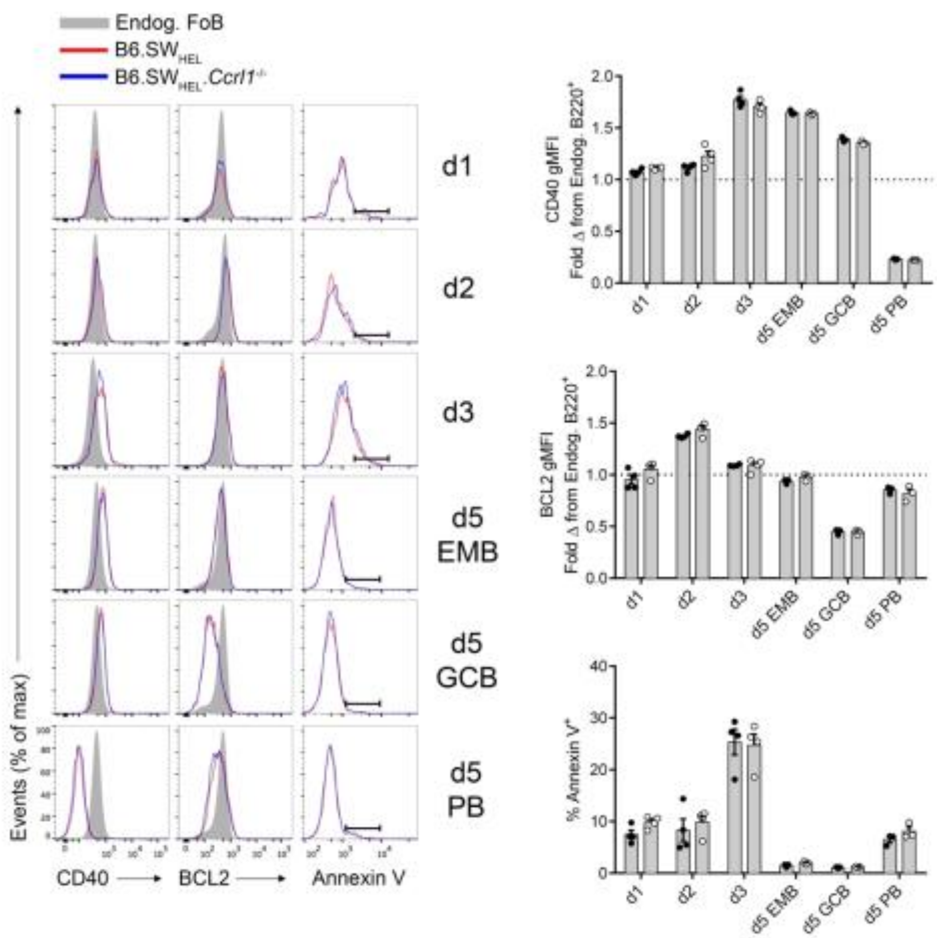

Fig. S19: Measures of early B cell activation and apoptosis are not altered by ACKR4. WT ($CD45.1^{+}CD45.2^{+}$) and *Ccrl1*$^{-/-}$ ($CD45.2^{+}$) SW_{HEL} B cells were co-transferred into B6.Ly5.1 ($CD45.1^{+}$) recipients and immunized with HEL^{2X}-SRBC. **(A)** *Day 1-3*: Representative histograms of concurrent WT (red) and *Ccrl1*$^{-/-}$ (blue) SW_{HEL} B cell expression of CD40, B cell lymphoma (BCL)2 and Annexin V (AV) relative to concurrent endogenous FoB cells ($CD45.2^{-}CD45.1^{+}B220^{+}IgD^{hi}$; filled grey). *Day 5*: CD40, BCL2 and AV staining on SW_{HEL} PB, EBM and GCB cells. *CD40 and BCL2*: Graphs show fold change in geometric mean fluorescence (Geo. MFI) intensity of CD40 and BCL2 expression between WT or *Ccrl1*$^{-/-}$ SW_{HEL} B cells and concurrent endogenous FoB cells. *AV*: Graphs show frequency of indicated population that are AV^{+}. Each dot represents an individual mouse (n=4); mean±s.e.m.; unpaired two-tailed Student's *t*-test.

Materials and Methods:

Mice

All mice were on the C57Bl/6J background and housed in a specific pathogen-free environment at Laboratory Animal Services, University of Adelaide (unless indicated otherwise). C57Bl/6 (B6) and B6.Ly5.1 were purchased from the Animal Resource Center (WA, Australia) or were from internal colonies. B6.*Ccrl1*$^{-/-}$, B6.*Ccr7*$^{-/-}$, B6.SW$_{HEL}$ (provided by R. Brink) and B6.µMT mice were from internal colonies. B6.*Ccr7*$^{-/-}$.*Ccrl1*$^{-/-}$, B6.SW$_{HEL}$.Ly5.1/Ly5.2 (CD45.1^{+}CD45.2^{+}) and B6.SW$_{HEL}$.*Ccrl1*$^{-/-}$ mice were generated and maintained in house. B6.*Cd23*^{Cre} mice were provided by D. Tarlinton (with permission from M. Busslinger). B6.*Cd23*^{Cre}*Ccrl1*^{Tg} mice were crossed and maintained in house. B6.SW$_{HEL(H)}$ and B6.SW$_{HEL(H)}$.*Ccrl1*$^{-/-}$ mice were generated by breeding out the Vκ10 light chain transgene from B6.SW$_{HEL}$ and B6.SW$_{HEL}$.*Ccrl1*$^{-/-}$ mice, respectively. Male and female mice between the ages of 6-12 weeks were used in experiments. Mice in each experiment were age and gender matched. All experiments were conducted in accordance to the guidelines outlined by the Animal Ethics Committee at the University of Adelaide.

Bone-marrow chimeras

Recipient mice were lethally irradiated with 1000 Rads (2 doses, 500 Rads) and reconstituted with 4-5×10^{6} total bone marrow cells i.v. of genotypes indicated in-text. A minimum of 8 weeks was allowed for reconstitution prior to experimentation.

Transfers, immunizations and BrdU treatment

T-dependent humoral immune responses were induced using 2×10^{9} sheep red blood cells (SRBC; Applied Biological Products) or 50 µg NP-KLH (Biosearch Technologies) precipitated in alum (AnalaR) i.p..

HEL^{2X} (R73$_{HEL}$E, D101$_{HEL}$R mutant) and HEL^{3X} (R21$_{HEL}$Q, R73$_{HEL}$E, D101$_{HEL}$R mutant) with varying affinities to HyHEL10 (*12*) were obtained from R. Brink. HEL^{WT} was purchased from Sigma. Conjugation of HEL to SRBCs was performed as described previously (*12*). Unless otherwise indicated, HEL conjugation to SRBCs was performed using 100 µg/ml HEL. Successful conjugation was confirmed using HyHEL9 monoclonal antibody (*12*) prior to immunization. Unless otherwise indicated, splenocytes or MACS-purified FoB cells (CD43 Negative Isolation Kit, Miltyeni Biotech) from B6.SW$_{HEL}$ or B6.SW$_{HEL}$.*Ccrl1*$^{-/-}$ mice containing 10^{5} HEL-binding B cells were transferred i.v. into B6.Ly5.1 recipient mice. The next day, recipient mice were immunized i.v. with 10^{9} HEL conjugated SRBCs. For SW$_{HEL(H)}$ experiments, splenocytes containing 5×10^{4} HEL-binding B cells from B6.SW$_{HEL(H)}$ or B6.SW$_{HEL(H)}$.*Ccrl1*$^{-/-}$ mice were transferred i.v. into B6.Ly5.1 recipient mice which were immunized the next day with 5×10^{8} HEL^{WT}-SRBCs i.v..

For B6.µMT reconstitution experiments, splenocytes containing 10^{7} FoB cells of each genotype were transferred i.v. and allowed to reconstitute for 7-10 days prior to immunization.

For assessment of proliferation in the SW_{HEL} system, splenocytes containing SW_{HEL} B cells were CFSE loaded as previously described (*34*) prior to transfer and immunisation as described above.

For BrdU experiments, 2 mg BrdU (Sigma-Aldrich) in 0.85% saline was injected i.p. 5 hours prior to euthanasia.

Salmonalla enterica immunization

Salmonella enterica serovar Dublin strain SL5440, an avirulent *aroA* deletion derivative of wild type *S. eneterica* serovar Dublin strain SL2972 (*35*), was obtained from Prof. Renato Morona (University of Adelaide, Australia). SL5440 was grown in Luria-Bertani (LB) medium overnight (37°C, 5% CO_2). Mice were immunized with 10^6 CFU (from log-phase culture) i.p.. Inoculation dose was confirmed retrospectively by serial dilution and plating of inocula on LB agar overnight. Control groups were administered endotoxin-free PBS. Liver bacterial load was measured by homogenising livers in Ceramic Bead Tubes (2.8 mm; MoBio) containing LB medium and plating in serial dilutions onto LB agar.

Histology

For assessment of SW_{HEL} B cell responses by histology (days 1-2.5), 5×10^5 HEL-binding B cells from B6.SW_{HEL} or B6.SW_{HEL}.*Ccrl1*$^{-/-}$ mice were transferred i.v. into B6.Ly5.1, which were immunized with 2×10^9 HEL^{2X}-SRBC i.v. the next day.

For assessment of SW_{HEL} B cell responses by histology (days 2.5-5.5), 2×10^5 HEL-binding B cells from B6.SW_{HEL} or B6.SW_{HEL}.*Ccrl1*$^{-/-}$ mice were transferred i.v. into B6.Ly5.1, which were immunized with 10^9 HEL^{2X}-SRBC i.v. the next day.

Organs were frozen in Tissue-Tek OCT embedding medium (Sakura Finetek). Cryostat sections (8 µm) were fixed in ice-cold acetone and stained as previously described (*36*). For detection of HEL-binding B cells, sections were first blocked with 30% normal horse serum and incubated with HEL^{WT} (100 ng/ml; Sigma-Aldrich), which was detected using unconjugated rabbit anti-HEL (Rockland; polyclonal) and goat anti-rabbit Ig Alexa Fluor 488 (Life Technologies). SW_{HEL} histology: Antibodies to IgD (11-26c; eBiosciences) and CD4 (RM4-5; BD) were used. *S. enterica* histology: Antibodies to IgD, CD4, IgM (R6-60.2; eBiosciences) and IgG2c (5.7; BD) were used. GC stain (Fig. 1D): IgD, CD3 (145-2C11; BD), BCL-6 (K112-91; BD) and CCL21 (goat polyclonal; R&D) were used.

To enumerate transferred SW_{HEL} B cell positioning in spleen sections, the outer follicle, follicle center, T/B interface, interfollicular zone and T cell zone per white pulp region was first defined (*10*) in a blinded manner on images stained with IgD/CD4 with HEL binding fluorescence removed. HEL binding fluorescence was then merged with these images and the total number of HEL-binding cells per white pulp area and HEL-binding cells in defined regions enumerated by 4 independent researchers in a blinded manner. Mean values across these 4 independent data sets are presented.

In vivo CCL19/CCL21 neutralization

Affinity-purified anti-mouse (m) CCL21 was generated and purified in house as described (*5*). Anti-mCCL19 antibodies were raised in New Zealand white rabbits by immunization with full-length synthetically manufactured chemokine (*37*) that was active in calcium mobilization and chemotaxis assays. Serum IgG was purified from pre-immunized bleeds (normal rabbit IgG (NRIgG) and mCCL19 or mCCL21 immunized rabbits using Protein A columns (Millipore). The CCL19 or CCL21 neutralizing ability of these antibodies was confirmed in chemotaxis assays prior to their use *in vivo*. Recipient mixed BM chimeric mice were administered 500 µg affinity-purified rabbit anti-mCCL21 and 500 µg affinity-purified rabbit anti-mCCL19 or 1 mg NRIgG intraperitoneally on days -1, 0, 2 and 4. Mice were immunized with SRBCs i.p. on day 0 and analyzed 5 days later.

V_H gene sequencing analysis of NP^+IgG1^+ germinal center B cells

Single NP^+IgG1^+ GCB cells were sorted from NP-KLH immunized (d14) B6 and B6.*Ccrl1*$^{-/-}$ mice using a BD FACSAria cell sorter. Two rounds of PCR were performed on cDNA using a single proximal 5' primer for the J558 V_H gene family (*38, 39*) together with nested primers specific for Cγ1 (*38, 40*). Bands of expected size were purified, sequenced and analyzed for V_H186.2-containing sequences as described. For $V_H186.2^+$ clones, the region encoding amino acids 10-96 were compared in detail with the germline V_H186.2 sequence as described (*38*).

Chemotaxis assay

MACS-purified FoB cells (CD43 Negative Isolation Kit, Miltyeni Biotech) were activated with 10 µg/ml goat anti-mouse IgM (Jackson ImmunoResearch) for 24 hours or rested overnight (unstimulated control). Various dilutions of recombinant mouse CCL21 (kindly provided by the late Prof. Ian Clark-Lewis) or CXCL13 (PeproTech) in 150 µl chemotaxis buffer (RPMI 1640 with 0.5% BSA and 20 mM HEPES) were added to lower chambers of Transwell Chemotaxis Plates (96-well; 5 µm pore size; Corning). Cells were extensively washed in chemotaxis buffer and loaded into upper chambers at 10^5 cells/well in 50 µl chemotaxis buffer and incubated for 3 hours at 37◦C. To enumerate B cell migration, cells were harvested from bottom chambers and $B220^+$ cells assessed by flow cytometry using a defined number of CaliBRITE beads (BD) as an internal reference. Migration index was calculated as described (*41*).

Scavenging Assay

FACS-sorted FoB cells (2×10^5) were incubated in RPMI 1640 medium containing 5 or 10 ng/ml recombinant mouse CCL19 (R&D Systems) at 37˚C for 3 hours with inversion every 30 minutes. 100 µL of cell-free supernatants was then assessed for CCL19 concentration by ELISA as described (*5*).

ELISA

Serum HEL-specific IgM and IgG1 concentrations were quantified using HyHEL10 IgM and IgG1 standards (obtained from R. Brink) as described (*42*). NP-specific IgG1 was detected using NP_5-

BSA or NP_{32}-BSA (10 µg/ml; Biosearch Technologies) coating antigen. Anti-*Salmonella* IgG2c ELISAs were conducted using 10 µg/ml *Salmonella* whole-cell lysate as described (*13*).

Quantitative PCR

RNA was harvested using the Qiagen microRNeasy Kit with on-column DNase treatment. cDNA synthesis was performed using Transcriptor First Strand cDNA Synthesis Kit (Roche) and used as template in reactions using LightCycler 480 SYBR Green Master Mix I (Roche). Relative *Ccrl1* transcript abundance was calculated with reference to the housekeeping gene *Rplp0* using the formula: $2^{-\Delta CT}$ ($\Delta CT = CT_{Ccrl1} - CT_{Rplp0}$). *Rplp0*: Forward – 5' AGATGCAGCAGATCCGCAT 3' and Reverse – 5' CAGTGAGCTTCCCGTTCAG 3'; *Ccrl1*: Forward – 5' AGATGCAGCAGATCCGCAT 3' and Reverse – 5' CAGTGAGCTTCCCGTTCAG 3'.

Flow Cytometry and Sorting

Cells were stained as described (*43*) using the following antibodies to CD45.2 (104), B220 (RA3-6B2), IgD (11-26c), IgD^b (217-170), Fas (Jo2), GL7, CD86 (GL1), CD138 (281-2), Igκ (RMK-45), IgM (R6-60.2), IgG2c (5.7), IgG1 (x56), CD93 (AA4.1), CD21 (7G6), CD23 (B3B4), CD11b (M1/70), CD40 (3/23), CD3 (145-2C11), CD4 (RM4-5), CD44 (IM7), PD-1 (J43), CXCR5 (2G8), CCR7 (4B12; in-house), EBI2 (polyclonal; obtained from R. Brink (*44*)), CXCR4 (2B11/CXCR4), Nrp-1 (3E12), Bcl2 (BCL/10C4), IRF4 (3E4), IRF8 (W3GYWCH) and Foxp3 (FJK-16s). Unconjugated/biotinylated antibodies were detected using goat anti-rat IgG (Life Technologies), goat anti-human IgG-Fcγ fragment specific (Jackon Immunoresearch), Streptavidin-PE (Jackson Immunoresearch), -Alexa Fluor 647 (Jackson Immunoresearch), -BV510, -BV421 or -BV450. All antibodies and secondary reagents were from BD, eBioscience or Biolegend unless otherwise indicated. Dead cells were excluded using LIVE/DEAD fixable near-infrared dye (Molecular Probes). 7AAD (eBiosciences) was used to detect DNA content. NP binding was detected using NIP-PE reagent (generated in-house) as described (*38*). CCL19-Fc is a mouse CCL19 fused to human IgG1 constant region chimeric protein (*8*) and was obtained from J. Cyster. Annexin V Apoptosis Detection Kit (eBioscience) was used to detect Annexin V. Cytofix/Cytoperm Kit (BD) was used to detect cytoplasmic IgM. Foxp3/TF Staining Buffer Set (eBioscience) was used to detect transcription factors. For detection of HEL-binding cells, 2×10^6 splenocytes were incubated with soluble HEL (saturating 200 ng/ml; or sub-saturating – 50 ng/ml), followed by detection of BCR-bound HEL using monoclonal antibody HyHEL9 conjugated to Alexa Fluor 647 (obtained from R. Brink) as described (*12*). Data were acquired on BD LSR II, BD FACSAria or BD LSRFortessa flow cytometers. For sorting experiments, BD FACSAria was used. Data were analyzed using FlowJo software (Tree Star).

Statistics

Data were analyzed with Prism (GraphPad Software) using two-tailed unpaired/paired Student's *t*-tests or one-way ANOVA with appropriate post-tests as indicated in text. For all analyses, $p<0.05$ was considered significant. Sample or experiment sizes were determined empirically for sufficient statistical power. No statistical tests were used to predetermine the size of experiments. No data points were excluded from statistical tests. Statistical analysis was performed on groups with similar variance.

CHAPTER FOUR:

DISCUSSION

4.1: CCR2 defines *in vivo* development and homing of IL-23-driven GM-CSF-producing Th17 cells *in vivo*

Th17 cells form an important component of protective immunity in the context of extracellular bacterial and fungal infection. However, when misdirected, Th17 cells have been shown to contribute to pathogenesis of numerous murine models of autoimmunity and are implicated as drivers of inflammation in certain human autoimmune disorders. Advances in the field of Th17 biology have revealed the existence of a spectrum of Th17 cellular phenotypes that differ in their inflammatory potential and differentiation requirements. Like most effector T cell subsets, Th17 cells must gain access to the site of inflammation to execute their effector function. A detailed understanding of the differentiation requirements of Th17 cells that vary in their inflammatory potential, how Th17 cells migrate to inflammatory lesions and whether types of Th17 cells differ in their migratory potential *in vivo* was assessed in chapter 2 of this thesis.

At the time of this study, how Th17 cells gained access to the CNS after the initiation of EAE was not clearly understood. Reboldi et al., demonstrated the importance of CCR6 for the early recruitment of Th17 cells to the uninflamed CNS for the initiation of inflammation in EAE. However, subsequent waves of CNS-infiltrating Th17 cells were shown to traffic in a manner that was independent of CCR6 function (*37*). The results shown in chapter 2 are in agreement with those of Reboldi et al. (*37*), and confirm the importance of CCR6 in the early recruitment of Th17 cells to the uninflamed CNS. Building on this model, CCR2 was identified as an important receptor driving encephalitogenic Th17 cell recruitment to the inflamed CNS. In this chapter it was shown that mice with T cells that lack CCR2 develop a weaker form of EAE relative to mice with WT T cells, and this was accompanied by a reduction in CNS-infiltrating GM-CSF-producing Th17 cells. However, the development of CNS inflammation in the absence of T cell expression of CCR2 points to the involvement of other mechanisms in control of Th17 cell trafficking. Our results, and those of others, indicate that Th17 cells also express CCR4 (*107-109*), CXCR3 (*107, 109*), CX3CR1 (*110*) and XCR1, the ligands of which have been shown to be variously expressed in the inflamed CNS during EAE (*111-114*). Experiments that aim to address the function of these receptors on Th17 cells will be important to obtain a more complete understanding of trafficking mechanisms that Th17 cells utilize to gain access to sites of inflammation. This knowledge will be important from a clinical perspective as manipulation of the chemokine receptor system presents as a tractable target for therapeutic intervention of misdirected Th17 cell responses in numerous pathological settings (*2*).

Many lines of evidence, including the identification that IL-23 is the critical regulator of T-cell-driven CNS autoimmunity (*24, 115*), and the demonstration that IL-23-dependent Th17 cell-derived GM-CSF is indispensable for EAE development (*23, 25*), have established IL-23-driven inflammatory Th17 cells as the key driver of murine CNS autoimmunity. These cells differ from Th17 cells with a limited inflammatory potential which have been shown to derive from the polarizing cytokines TGFβ1 and IL-6, which induce co-expression of IL-17A and the immunoregulatory cytokine IL-10 (*18-20*). Whilst the importance of IL-23 for driving the pathogenicity of Th17 cells is established, the differentiation requirements of these cells is less clear with reports that these cells derive from TGFβ1/IL-6-driven Th17 cell precursors via IL-23 (*23, 25, 26, 33*), and an alternative model in which these cells differentiate directly from naïve precursors independently of TGFβ1 in an IL-6, IL-1β and IL-23-dependent manner (*19*). By restricting *Il23r*-deficiency to a small number of transferred antigen-specific naïve T-cells, McGeachy et al. (*33*) reported a less prominent role for IL-23 in initial Th17 cell differentiation *in vivo*. However, IL-23R signaling was shown to be critical for subsequent Th17 cell expansion, maturation and acquisition of an inflammatory cytokine secreting repertoire. These data suggest that initial Th17 specification from naïve precursors *in vivo* occurs independently of IL-23 and give rise to cells of limited inflammatory potential, which subsequently expand and develop into 'pathogenic' Th17 cells via IL-23. The results of this chapter reveal the first non-invasive means to identify IL-23-driven Th17 cells, and provide data consistent with these cells developing from IL-23-independent initial Th17 cell precursors *in vivo*.

The data presented in chapter 2 of this thesis indicate that initial Th17 cells differentiate in an IL-23-independent manner, bear a $CCR6^+CCR2^-$ cell surface phenotype, and are recruited to the uninflamed CNS via CCR6. Given the importance of TGFβ1 for CCR6 induction on T-cells (*36*), it is likely that these cells represent previously described TGFβ1/IL-6-induced early (or 'intermediate') Th17 effector cells (*33*). Accordingly, *in vivo* TGFβ neutralization or deficiency in *Il6* abrogated initial $CCR6^+$ Th17 cell generation and prevented the cascade of events leading to $CCR2^+$ Th17 cell development in secondary lymphoid orangs following MOG/CFA immunization (data not shown). In keeping with the model proposed by Reboldi et al. (*37*), it is likely that this first wave of $CCR6^+CCR2^-$ Th17 cells contributes to the initiation of CNS inflammation. $CCR6^+CCR2^-$ Th17 cells express a unique cytokine profile including cytokines with proinflammatory (IL-17A/IL-17F/TNFα/IL-22/IL-2/IL-9) and regulatory (IL-10/IL-9) function. Genetic deficiency in *Il17a*, *Il22* or *Tnf* does not alter the incidence or severity of EAE (*116-118*), suggesting that these factors in isolation play a redundant role in the establishment of CNS autoimmunity. However, it is possible that these inflammatory cytokines elicited by the earliest CNS invading $CCR6^+$ Th17 cells function synergistically to initiate CNS inflammation in EAE, although this remains to be tested.

During the evolution of EAE, $CCR2^+$ populations of Th17 cells emerge in SLOs, giving rise to Th17 cells that bear $CCR6^+CCR2^+$ and $CCR6^-CCR2^+$ cell surface phenotypes. $CCR6^+CCR2^+$ Th17 cells express less proinflammatory TNFα relative to $CCR6^+CCR2^-$ Th17 cells, produce the immunomodulatory cytokines IL-10 and IL-9, and negligible amounts of GM-CSF and IFNγ, consistent with published descriptions of Th17 cells with a limited inflammatory potential (*18-20, 22*). Conversely, $CCR6^-CCR2^+$ Th17 cells phenotypically resemble descriptions of 'pathogenic' Th17 cells, with abundant expression of the inflammatory cytokines GM-CSF, IFNγ and TNFα, and undetectable expression of IL-10 or IL-9 (*19, 20, 23, 25, 28, 29, 33*). Deletion of IL-23 or its receptor specifically curtailed generation of $CCR6^-CCR2^+$ Th17 cells suggesting that the $CCR6^-CCR2^+$ cell surface phenotype labels IL-23-driven Th17 cells and that these cells represents an advanced differentiated state of Th17 cells *in vivo*.

Evidence for a step-wise model of Th17 cell differentiation further lies with the observations with respect to the function of IL-1 and IFNγ. IL-1 is critical for initial Th17 differentiation from naïve precursors (*119*), inducing IRF4 which reinforces RORγt expression (*120*), and promoting mTOR activity which enhances the metabolic fitness of Th17 cells during their rapid turnover (*121, 122*). Moreover, IL-1 promotes the pathogenicity of Th17 cells via its actions on committed TGFβ1- and IL-6-driven Th17 cell precursors by promoting their expansion and driving expression of GM-CSF and IFNγ (*23*). In keeping with these reports, the data presented in chapter 2 of this thesis confirm the important role of IL-1 in Th17 cell differentiation and demonstrate that IL-1 promotes differentiation of each Th17 subset ($CCR6^+CCR2^-$, $CCR6^+CCR2^+$ and $CCR6^-CCR2^+$), exerting its most potent effect on the emergence of the $CCR6^-CCR2^+$ population. Furthermore, a similar dual 'temporal' function has been described for IFNγ in Th17 cell biology with reports indicating that this cytokine inhibits Th17 cell differentiation from naïve $CD4^+$ T cells in a STAT1-dependent manner (*3, 123*), but also promotes, in synergy with IL-12, the development of IFNγ-producing 'pathogenic' Th17 cells from IFNγ-negative Th17 cell precursors (*124*). The results in this thesis are in keeping with these observations and indicate that that initial Th17 cell differentiation is inhibited by T cell-intrinsic IFNγ signaling, whereas Th17 cells that develop in the absence of IFNγ signaling specifically lack the emergence of $CCR6^-CCR2^+$ Th17 cells. These findings, together with the demonstration of the critical requirement of IL-23/IL-23R for $CCR6^-CCR2^+$ Th17 cell generation, which is not required for Th17 cell specification from naïve precursors but critical for their expansion and terminal differentiation, suggest that $CCR6^-CCR2^+$ Th17 cells represent an advanced differentiation stage of Th17 cells that arise from CCR6-expressing Th17 cell precursors. Further, Hirota et al. demonstrated that transfer of *in vivo*-derived $CCR6^+$ MOG-specific 2D2 TCR transgenic Th17 cells into MOG/CFA pre-immunized *Rag1*-deficient recipients resulted in their downregulation of CCR6 and concomitant induction of T-bet and IFNγ in both SLOs and CNS (*28*). The same report, in which the IL-17A-fate mapping mice utilized in the present study were generated, demonstrated that the terminally-differentiated state of a Th17 cell in chronic inflammatory settings, such as EAE, is IL-23-driven conversion to an $IL\text{-}17A^-IFN\gamma^+$ Th1-like phenotype (termed 'ex-Th17' cells). Accordingly, experiments using these mice demonstrated that IL-17A- and IFNγ-expressing Th17 cells and IFNγ-expressing ex-Th17 cells bear a $CCR6^-CCR2^+$ phenotype, whilst $IFN\gamma^-$ Th17 cells bear a $CCR6^+CCR2^{+/-}$ phenotype *in vivo* (data not shown). To specifically address whether $CCR6^-CCR2^+$ Th17 cells stem from CCR6-expressing Th17 cell precursors which are temporally generated prior to the appearance of these cells, experiments were attempted that aimed to track the fate of sorted $CCR6^+CCR2^-$ Th17 cells after adoptive transfer into pre-immunized CD45.1 congenic recipients. However, despite numerous attempts, difficulties were encountered in collecting sufficient cells for meaningful analyses given the rarity of Th17 cells early during EAE. To circumvent these limitations, mice in which Cre recombinase is driven by *Ccr6* promoter activity and crossing these to the *Rosa26*$^{LSL\text{-}eYFP}$ line used in this study, generating mice in which *Ccr6* expression is reported irrespective of its current expression status could be generated. Assessment of these mice in EAE would determine whether the $CCR6^{-}CCR2^{+}$ Th17 cells that emerge after disease onset originate from canonical $CCR6^{+}$ Th17 cell precursors or from distinct naive precursors that do not express CCR6 following activation.

The results also establish T-bet and Eomesodermin as transcriptional regulators of $CCR6^{-}CCR2^{+}$ Th17 cell differentiation *in vivo*. Accumulating evidence points to a dual role for T-bet in Th17 cell biology. T-bet inhibits Th17 cell differentiation from naïve precursors via formation of T-bet/Runx1 complexes which inhibit Runx1-mediated transactivation of *Rorc* (*29, 125*), and scavenge 'free' Runx1 to prevent formation of transcriptionally-active Runx1/RORγt complexes critical for Th17 cell specification (*125*). The function of T-bet in 'pathogenic' Th17 cell biology is controversial with reports indicating that these cells develop independently of T-bet (*126, 127*), and conflicting data which define 'pathogenic' Th17 cells as $ROR\gamma t^{+}T\text{-}bet^{+}$ (*28*), and identify IL-23/IL-12 as inducers of T-bet which, in collaboration with Runx1, promote conversion of Th17 cell precursors into inflammatory IFNγ-producing Th17 cells (*28, 29*). Using mixed BM chimeric systems, an approach that specifically addresses T cell-intrinsic function of T-bet in Th17 cells and excludes T cell-extrinsic effects accompanied with *Tbx21*-deficiency, it was observed that in the absence of T-bet, Th17 cell generation was enhanced but cells with the $CCR6^{-}CCR2^{+}$ phenotype were selectively curtailed. These data implicate a key role for T-bet in inflammatory Th17 cell generation *in vivo*. The function of Eomes in Th17 cell biology is less clear. TGFβ1-mediated repression of Eomes is required for TGFβ1/IL-6-driven Th17 differentiation from naïve precursors *in vitro* (*128*). *Eomes* is induced in committed TGFβ1/IL-6-driven Th17 cells in the presence of inflammatory cytokines such as IL-12 (*29*), however ectopic expression of *Eomes* does not promote generation of IFNγ-producing Th17 cells *in vitro* (*29*). The results of this thesis indicate that amongst Th17 cells, Eomes expression is restricted to CCR6-expressing Th17 cell populations, but is not required for their development *in vivo*. *Eomes*-deficiency however, led to a selective defect in $CCR6^{-}CCR2^{+}$ Th17 cell generation, implicating Eomes as a key regulator of inflammatory Th17 cell differentiation *in vivo*. These data are consistent with the notion that $CCR6^{+}$ Th17 cell populations serve as precursors to $CCR6^{-}CCR2^{+}$ Th17 cells. Eomes directly repress *Rorc* and *Il17a* transcription (*128*). Thus, it is likely that Eomes and T-bet are drivers of Th17 differentiation and plasticity by implementing changes to the transcriptional landscape of Th17 cells, such as repression of *Rorc* and *Il17a*, and induction of *Ifng* and *Csf2* (GM-CSF), as

Th17 cells differentiate from IL-17A$^+$ CCR6$^+$ Th17 cells, through IL-17A$^+$ CCR6$^-$CCR2$^+$ Th17 cells, toward an 'ex-Th17' cell phenotype in chronic inflammatory environments.

The results cannot exclude the possibility that the 'switch' in Th17 phenotype from CCR6 toward CCR2 expression and induction of GM-CSF/IFNγ occurs in the CNS. Indeed, cells in the CNS of EAE mice are capable of producing IL-23 in response to GM-CSF and other stimuli (*129, 130*). However, the observation that that the IL-23-driven 'switch' occurred within SLOs prior to the appearance of these cells in the CNS, and that T cell-specific deletion of *Ccr2* reduced the frequency of CNS-infiltrating GM-CSF$^+$ Th17 cells without altering their generation in SLOs suggest that this phenomenon is predominantly regulated at the level of immune priming.

Taken together, the results of this chapter identify CCR2 as a key driver of inflammatory Th17 cell recruitment to the CNS in EAE, a murine model of the human autoimmune disorder multiple sclerosis. The data indicated that the earliest detectable Th17 cells generated during EAE express CCR6 and lacked CCR2 expression. As the response evolved, CCR2-expressing populations of Th17 cells became evident in lymphoid organs and CNS. Using EAE and *S. pneumoniae* infection models, it was found that inflammatory GM-CSF- and IFNγ-producing Th17 cells display a CCR6$^-$ CCR2$^+$ cell surface phenotype in mice, and in humans. Conversely, Th17 cells that express CCR6 and CCR2 (CCR6$^+$CCR2$^+$) were found to express a cytokine-secreting repertoire consistent with Th17 cells with a more limited inflammatory potential, including IL-10. Using these cell surface signatures, it was found that a IL-23/IL-1/IFNγ/TNF/T-Bet/Eomes-driven circuit drives the emergence of CCR6$^-$CCR2$^+$ GM-CSF/IFNγ-producing Th17 cell development *in vivo*. Thus, the results of this chapter identify a unique cell surface signature and developmental features of GM-CSF/IFNγ producing Th17 cells *in vivo* and address the question regarding the molecular control of inflammatory Th17 cell trafficking to the CNS in EAE.

Clearly however, CCR6-expressing and CCR6$^-$CCR2$^+$ Th17 cell types did not evolve for the purposes of initiating or propagating autoimmune reactions. What is not clear from the results of this chapter is the functional relevance of these populations of Th17 cells in the context of protective immunity. It has been hypothesized that Th17 cells with a limited inflammatory potential may serve a more important role in the maintenance of barrier tissue integrity (*18, 22,* *131*), whereas inflammatory subsets of Th17 cells amplify inflammation during persistent extracellular bacterial or fungal infection (*7, 132*). Using a persistent strain of the extracellular pathogen *S. pneumoniae*, the results presented in chapter 2 of this thesis demonstrate that the earliest detectable Th17 cells formed in response to infection were largely $CCR6^+$ and lacked expression of the inflammatory cytokines GM-CSF or IFNγ. During the evolution of the response it was found that $CCR6^-CCR2^+$ Th17 cells emerge in SLO and encompass the GM-CSF/IFNγ-producing subset of Th17 cells. The temporal kinetics of these distinct populations of Th17 cells formed in response to a chronic bacterial infection were similar to those obtained in the EAE model and are in keeping with hypotheses that inflammatory Th17 cell responses are mobilized in settings where antigen is chronic (*7, 132*). Distinguishing the roles of CCR6-expressing and $CCR6^-CCR2^+$ Th17 cells in the context of extracellular bacterial infection would be important toward ascertaining a complete understanding of how these subsets of Th17 cells contribute to protection, and from a broader perspective give context to why such populations of Th17 cells with differing inflammatory potentials exist.

4.2: Regulation of activated B cell differentiation by Atypical Chemokine Receptor 4

Clonally selected B cells must gain access to distinct lymphoid niches with appropriate temporal dynamics to support their expansion and differentiation (*40, 41*). To achieve this, B cells sequentially alter chemoattractant receptor expression following antigen engagement, coordinating their movements to these niches in a timely manner. Following initial expansion, activated B cells trifurcate into three functionally-distinct subsets: early plasmablasts (PB), germinal center (GC) B cells and early memory (EM) B cells (*56, 57*). The molecular and cellular cues that govern this fate decision are essential to our understanding of how T-dependent humoral immunity manifests, but remain largely unknown.

The results of this chapter identified a previously unrecognized modality of activated B cell migration, via an atypical chemokine receptor, that influences the differentiation fate of activated B cells. The data presented in chapter 3 of this thesis indicated that atypical chemokine receptor 4 (ACKR4), a chemokine receptor that degrades CCR7 ligands CCL19/CCL21 without initiating cell migration, shaped activated B cell migration and differentiation fate. Monoclonal Ig transgenic

ACKR4-deficient activated B cells aberrantly localize to the splenic interfollicular zone (IFZ) early during the response, enhancing their initial proliferation and increasing the abundance of these cells available for subsequent differentiation into PB, GCB and/or EBM cells. The results demonstrate that the limiting effect of ACKR4 on humoral immunity is dependent on physiological CCL19/CCL21, occurs in a B cell-intrinsic manner, and is most prominent amongst early PB differentiation by shaping the balance of interferon regulator factor (IRF) 4 (pro-PB fate) and IRF8 (pro-GCB fate) expression in early activated B cells.

These data build additional complexity into the current model of the molecular control of B cell positional dynamics following antigen recognition. To summarize the current model, BCR-engaged B cells rapidly reposition to the outer follicle via EBI2, drawing the cells nearer to the source of antigen which is hypothesized to consolidate their activation (*43, 46*). Here, EBI2 expression wanes but remains functional, CXCR5 expression remains unaltered, and cell surface CCR7 is induced, enabling CCR7-dependent migration toward the T/B interface via a CCL19/CCL21 gradient that emanates from the T cell zone (*42, 43, 46, 49, 50*). EBI2, CXCR5 and CCR7 coordinate the lateral spreading of activated B cells along this T/B interface hypothesized to maximize interactions with pre-Tfh cells (*42, 43, 46, 47, 49, 50*). Cognate interactions with T cells at this interface induces CD40-dependent EBI2-mediated migration to the IFZ and outer follicular regions where activated cells begin to expand (*42, 43, 46, 47, 55, 62*). The results of this study indicate that ACKR4 is operational during these early events of activated B cell migration. Gatto *et al.* demonstrated that transfer of *Cxcr5*-deficient activated B cells results in their exclusion from B cell follicles and accumulation in marginal zone bridging channels. However, compound deletion of both *Cxcr5* and *Ccr7* positioned cells away from this niche and toward the outer regions of the B cell follicle (*43*). These data indicate that in addition to its established role as driving activated B cell migration toward the T cell zone (*49, 50*), CCR7 also contributes to the positioning of activated B cells in interfollicular and bridging zones. In this thesis, experiments with SW_{HEL} B cells indicate that deletion of ACKR4, a scavenger of CCR7 ligands, promotes responding B cell migration to splenic IFZs. Further, no compensatory changes in expression of CCR7, EBI2 or CXCR5 in the absence of ACKR4 early after activation were detected. These data support the notion that ACKR4 may function to 'tune' early CCR7-dependent cues in a proportion of responding B cells, limiting their CCR7-driven homing to splenic IFZs.

The finding that physiological CCL19 and CCL21 were required, at least in part, for ACKR4-dependent changes to early PB and GC B cell responses supports a relationship between ACKR4 and CCR7 function in the regulation of activated B cell responses.

Increased IFZ localization by ACKR4-deficient activated SW_{HEL} B cells was associated with their preferential entry into the early PB compartment. This phenotype is reminiscent of data reported by Gatto *et al.,* which demonstrated that forced expression of EBI2 in SW_{HEL} B cells aberrantly draws activated cells to the IFZ resulting in their preferential entry into the early PB compartment (*47*). In the same study, the authors demonstrate that EBI2-deficient SW_{HEL} B cells are defective in their ability to access splenic IFZ and in their ability to form robust early PB responses following immunization (*47*). Together, these data point to migration to the splenic IFZ as a key determinant of activated B cell fate, by an as yet to be determined mechanism. The splenic IFZ is rich in cognate T cells and specialized DCs that uniquely express the cell-surface lectin DCIR2 (also known as CLEC4A) (*54, 62, 89, 133*). Using a monoclonal antibody to target a T-cell dependent antigen to these DCIR2$^+$ DCs, Chappell *et al.*, demonstrated that their uptake and display of antigen to B cells results in a rapid and robust early PB response that occurs in a T cell-independent manner (*89*). DCIR2$^+$ DCs have been shown to produce IL-6 and B-cell-activating factor (BAFF), which are known activators of STAT3 and NF-κB1 signaling pathways in B cells (*134, 135*). STAT3 and NF-κB1 occupy and activate the *Irf4* promoter (*136, 137*), the induction of which promotes PB differentiation via direct transactivation of the PB master transcriptional regulator BLIMP-1 and antagonism of the pro-GC transcription factor IRF8 (*138, 139*). Preferential localization in the IFZ by ACKR4-deficient activated B cells was associated with their enhanced proliferation and increased IRF4:IRF8 content, possibly as a result of enhanced interactions with DCIR2$^+$ DCs in this area of the spleen early in the response. To test this hypothesis, mice that express a loxP-STOP-loxP (LSL) cassette protecting expression of the diphtheria toxin receptor (DTR) downstream of the *Clec4a* locus (*Clec4a*$^{\text{LSL-DTR}}$) could be engineered. Crossing these to *Zbtb46*-Cre mice, in which Cre recombinase expression is restricted to all classical DCs (encompassing DCIR2$^+$ DCs) (*140*), would result in the ability to selectively ablate DCIR2$^+$ DCs upon administration of diphtheria toxin (final genotype: *Zbtb46*$^{\text{Cre}}$.*Clec4a*$^{\text{LSL-DTR}}$). Co-transfer of genetically marked WT and ACKR4-deficient SW_{HEL} B cells into these mice with prior administration of DT would serve as an appropriate model to: a) formally address the function of

DCIR2$^+$ DCs in humoral immunity; and b) assess whether any subsequent phenotypes associated with preferential localization to the IFZ in the absence of ACKR4 are dependent on DCIR2$^+$ DCs.

In this study, it was observed that competition of ACKR4-deficient and –sufficient monoclonal Ig transgenic B cells resulted in an early proliferative advantage for ACKR4-deficient activated B cells. This early proliferative advantage of activated B cells at an undifferentiated stage appeared to contribute to the enhanced effector B cell responses in the absence of ACKR4. Thus, in a monoclonal system, ACKR4 restricts the early expansion of activated B cells prior to their differentiation. Using a combination of photoactivation to isolate single GCs, and Ig sequencing on single GCB cells from therein, Tas *et al.,* demonstrated that early GCs are clonally diverse with predictions of up to 200 distinct B cell clones seeding an individual GC in response to the complex antigen chicken gamma globulin (CGG) (*141*). These data revealed that early GCs were more clonally diverse than was previously predicted based largely on studies of early GCs in response to NP, a single epitope hapten (*141, 142*). Further, experiments that tracked the fate of a single antigen-specific B cell in a polyclonal reaction demonstrated that a single naïve precursor can differentiate into all three fates of an activated B cell (*58*). Importantly, the capacity of a single B cell to enter all three fates was shown to be enriched amongst clonal populations that had divided extensively and resisted apoptosis. These previous studies raise the proposition that ACKR4 functions in the polyclonal system to limit initial expansion of activated B cell clones, preserving the clonal diversity of antigen-specific cells available to seed early PB, GCB and EBM cell compartments. Technology to test this hypothesis was not available at the time this work was conducted, however this proposition could be addressed by performing single cell Ig heavy chain sequencing on GCB cell and early PB populations isolated from mixed BM chimeras immunized with a complex antigen such as chicken gamma globulin. If this hypothesis was supported, this would indicate that ACKR4 plays an important role in regulation of the clonal diversity of B cells that seed these compartments. How ACKR4 shapes the clonality of early GCs is of particular importance from a clinical perspective, as the ability to guide rare and non-immunodominant epitope-specific B cells into GCs remains a major hurdle for vaccines against complex pathogens such as HIV and influenza (*143, 144*).

Contemporary views of GC dynamics describe a T cell-centric governance of antibody affinity maturation (*65*), wherein LZ B cells compete for help from a limited number of T cells on the basis of their surface peptide (p)-MHC-II abundance which reflects their intrinsic BCR affinity (*78, 82, 83, 145, 146*). T cell-mediated selection on the basis of pMHC-II abundance results in mTORC1 activation (*147*) and Myc induction (*84, 148*), which metabolically 'charges' LZ cells and initiates their entry into the cell-cycle prior to their migration to the DZ where they proliferate and hypermutate their Ig genes in a process referred to as 'clonal bursting' (*78, 82, 83, 141*). By a mechanism that remains to be determined, DZ cells stop proliferating and re-enter the FDC rich regions of the GC to test their new BCRs (*65*). Iterative rounds of affinity-based LZ selection and DZ proliferation/hypermutation drives affinity maturation in a process referred to as the cyclic re-entry model of affinity maturation (*65, 141*). The results presented in chapter 3 of this thesis indicate that GCB cells express ACKR4, however, ACKR4-deficient GCs cells proliferate and accumulate high affinity mutations in their Ig genes at a similar rate to an ACKR4-sufficient GC reaction. These data indicate that despite influencing the size of the GC reaction, ACKR4 does not influence the processes of LZ affinity-based selection, GCB cell expansion and the processes of somatic hypermutation. Accordingly, ACKR4-deficiency was shown to enhance the magnitude of serum NP-specific IgG responses that was of equivalent affinity to WT. Importantly, assessment of these parameters of GC biology flow from experiments using the NP hapten model, which is a useful tool to experimentally measure the parameters of affinity maturation described above. Specifically, the evolution of the anti-NP GC response uniformly selects for a W33L mutation that endows a tenfold increase in affinity amongst NP-reactive GCB cells that can be measured using single-cell Ig sequencing (Fig. 1F) (*149*). Further, assays that utilize different NP haptenation ratios to conjugated proteins are available to assess the magnitude and affinity of serum NP-specific antibody by ELISA (Fig. 1A, G). Together, these tools allow for instantaneous measures of whether the processes of affinity maturation are operating appropriately at any given time of the NP-specific response. However, NP is a single epitope that triggers a clonally-restricted GC response largely dominated by clones that carry a V_H186.2 Ig heavy chain coupled to a lambda Ig light chain (B6 mice) (*150-153*). The results of the present study specifically show that despite the formation of larger GCs in the absence of ACKR4, NP-reactive VH186.2$^+$IgL$^+$ GCB cells ascertain the high affinity W33L mutation at a similar rate to a WT reaction. A possible explanation for these data is that enhanced early VH186.2$^+$IgL$^+$ precursor cell proliferation in the absence of

ACKR4 was controlled for in the GC by a proportional increase in T cells (Supplementary Figure 2, 4, 8) available to implement affinity based-selection (*154*). Given the clonally restricted nature of the anti-NP response, whether ACKR4 truly influences the processes of affinity maturation in more complex GCs that are colonized by diverse precursors of varying affinity and epitope specificity remains to be determined.

Experiments that aim to isolate the study of ACKR4 function specifically in the GC would require the circumvention of any ACKR4-dependent phenotype early in the reaction. Generating *Ccrl1*-floxed (*Ccrl1*$^{\text{fl/fl}}$) mice would be a useful tool to address this question. Crossing these to *S1pr2*$^{\text{CreERT2}}$ BAC transgenic mice that also report Cre activity with expression of red fluorescent protein (final genotype: *S1pr2*$^{\text{CreERT2}}$.*Rosa26*$^{\text{LSL-tdTomato/+}}$.*Ccrl1*$^{\text{fl/fl}}$) would allow for the temporal control of ACKR4 deletion (permanently marked by RFP) in mature GCB cells (*155*). Studying GC reactions in these mice would allow for the assessment of B cell intrinsic and/or extrinsic ACKR4 function specifically in the GC.

In summary, the results of this chapter identify a role for ACKR4 in regulation of early activated B cell migration and differentiation. In a monoclonal system, ACKR4 restricts the early localization of activated B cells to the IFZ, limits their early expansion and negatively regulates their entry into the PB compartment. Accordingly, absence of ACKR4 on B cells enhanced early PB, GCB and EBM cell responses. Many questions, however, remain regarding the role of ACKR4 in the GC reaction. Addressing the questions outlined above will be required to better understand the mechanism of how ACKR4 shapes the earliest events of B cell migration, how ACKR4 affects the clonality of early GCs during a polyclonal reaction and how ACKR4 functions in established GC structures.

REFERENCES

1. E. E. Kara *et al.*, Tailored immune responses: novel effector helper T cell subsets in protective immunity. *PLoS Pathog* **10**, e1003905 (2014).
2. I. Comerford, E. E. Kara, D. R. McKenzie, S. R. McColl, Advances in understanding the pathogenesis of autoimmune disorders: focus on chemokines and lymphocyte trafficking. *Br J Haematol* **164**, 329 341 (2014).
3. L. E. Harrington *et al.*, Interleukin 17 producing CD4+ effector T cells develop via a lineage distinct from the T helper type 1 and 2 lineages. *Nat Immunol* **6**, 1123 1132 (2005).
4. H. Park *et al.*, A distinct lineage of CD4 T cells regulates tissue inflammation by producing interleukin 17. *Nat Immunol* **6**, 1133 1141 (2005).
5. Ivanov, II *et al.*, The orphan nuclear receptor RORgammat directs the differentiation program of proinflammatory IL 17+ T helper cells. *Cell* **126**, 1121 1133 (2006).
6. X. O. Yang *et al.*, T helper 17 lineage differentiation is programmed by orphan nuclear receptors ROR alpha and ROR gamma. *Immunity* **28**, 29 39 (2008).
7. S. L. Gaffen, R. Jain, A. V. Garg, D. J. Cua, The IL 23 IL 17 immune axis: from mechanisms to therapeutic testing. *Nat Rev Immunol* **14**, 585 600 (2014).
8. J. J. Yu, S. L. Gaffen, Interleukin 17: a novel inflammatory cytokine that bridges innate and adaptive immunity. *Front Biosci* **13**, 170 177 (2008).
9. Y. Lee, V. Kuchroo, Defining the functional states of Th17 cells. *F1000Res* **4**, 132 (2015).
10. M. Veldhoen, R. J. Hocking, C. J. Atkins, R. M. Locksley, B. Stockinger, TGFbeta in the context of an inflammatory cytokine milieu supports de novo differentiation of IL 17 producing T cells. *Immunity* **24**, 179 189 (2006).
11. P. R. Mangan *et al.*, Transforming growth factor beta induces development of the T(H)17 lineage. *Nature* **441**, 231 234 (2006).
12. L. Zhou *et al.*, IL 6 programs T(H) 17 cell differentiation by promoting sequential engagement of the IL 21 and IL 23 pathways. *Nat Immunol* **8**, 967 974 (2007).
13. M. Ciofani *et al.*, A validated regulatory network for Th17 cell specification. *Cell* **151**, 289 303 (2012).
14. X. O. Yang *et al.*, STAT3 regulates cytokine mediated generation of inflammatory helper T cells. *J Biol Chem* **282**, 9358 9363 (2007).
15. T. J. Harris *et al.*, Cutting edge: An in vivo requirement for STAT3 signaling in TH17 development and TH17 dependent autoimmunity. *J Immunol* **179**, 4313 4317 (2007).
16. L. Wei, A. Laurence, K. M. Elias, J. J. O'Shea, IL 21 is produced by Th17 cells and drives IL 17 production in a STAT3 dependent manner. *J Biol Chem* **282**, 34605 34610 (2007).
17. R. Nurieva *et al.*, Essential autocrine regulation by IL 21 in the generation of inflammatory T cells. *Nature* **448**, 480 483 (2007).
18. M. J. McGeachy *et al.*, TGF beta and IL 6 drive the production of IL 17 and IL 10 by T cells and restrain T(H) 17 cell mediated pathology. *Nat Immunol* **8**, 1390 1397 (2007).
19. K. Ghoreschi *et al.*, Generation of pathogenic T(H)17 cells in the absence of TGF beta signalling. *Nature* **467**, 967 971 (2010).
20. Y. Lee *et al.*, Induction and molecular signature of pathogenic TH17 cells. *Nat Immunol* **13**, 991 999 (2012).
21. J. Xu *et al.*, c Maf regulates IL 10 expression during Th17 polarization. *J Immunol* **182**, 6226 6236 (2009).

22. E. Esplugues *et al.*, Control of TH17 cells occurs in the small intestine. *Nature* **475**, 514 518 (2011).
23. M. El Behi *et al.*, The encephalitogenicity of T(H)17 cells is dependent on IL 1 and IL 23 induced production of the cytokine GM CSF. *Nat Immunol* **12**, 568 575 (2011).
24. C. L. Langrish *et al.*, IL 23 drives a pathogenic T cell population that induces autoimmune inflammation. *J Exp Med* **201**, 233 240 (2005).
25. L. Codarri *et al.*, RORgammat drives production of the cytokine GM CSF in helper T cells, which is essential for the effector phase of autoimmune neuroinflammation. *Nat Immunol* **12**, 560 567 (2011).
26. C. J. Haines *et al.*, Autoimmune memory T helper 17 cell function and expansion are dependent on interleukin 23. *Cell Rep* **3**, 1378 1388 (2013).
27. A. L. Croxford *et al.*, The Cytokine GM CSF Drives the Inflammatory Signature of CCR2+ Monocytes and Licenses Autoimmunity. *Immunity* **43**, 502 514 (2015).
28. K. Hirota *et al.*, Fate mapping of IL 17 producing T cells in inflammatory responses. *Nat Immunol* **12**, 255 263 (2011).
29. Y. Wang *et al.*, The transcription factors T bet and Runx are required for the ontogeny of pathogenic interferon gamma producing T helper 17 cells. *Immunity* **40**, 355 366 (2014).
30. E. D. Ponomarev *et al.*, GM CSF production by autoreactive T cells is required for the activation of microglial cells and the onset of experimental autoimmune encephalomyelitis. *J Immunol* **178**, 39 48 (2007).
31. H. Kebir *et al.*, Preferential recruitment of interferon gamma expressing TH17 cells in multiple sclerosis. *Ann Neurol* **66**, 390 402 (2009).
32. J. Rasouli *et al.*, Expression of GM CSF in T Cells Is Increased in Multiple Sclerosis and Suppressed by IFN beta Therapy. *J Immunol* **194**, 5085 5093 (2015).
33. M. J. McGeachy *et al.*, The interleukin 23 receptor is essential for the terminal differentiation of interleukin 17 producing effector T helper cells in vivo. *Nat Immunol* **10**, 314 324 (2009).
34. I. Comerford *et al.*, An immune paradox: how can the same chemokine axis regulate both immune tolerance and activation?: CCR6/CCL20: a chemokine axis balancing immunological tolerance and inflammation in autoimmune disease. *Bioessays* **32**, 1067 1076 (2010).
35. N. Manel, D. Unutmaz, D. R. Littman, The differentiation of human T(H) 17 cells requires transforming growth factor beta and induction of the nuclear receptor RORgammat. *Nat Immunol* **9**, 641 649 (2008).
36. K. Hirota *et al.*, Preferential recruitment of CCR6 expressing Th17 cells to inflamed joints via CCL20 in rheumatoid arthritis and its animal model. *J Exp Med* **204**, 2803 2812 (2007).
37. A. Reboldi *et al.*, C C chemokine receptor 6 regulated entry of TH 17 cells into the CNS through the choroid plexus is required for the initiation of EAE. *Nat Immunol* **10**, 514 523 (2009).
38. A. Elhofy, R. W. Depaolo, S. A. Lira, N. W. Lukacs, W. J. Karpus, Mice deficient for CCR6 fail to control chronic experimental autoimmune encephalomyelitis. *J Neuroimmunol* **213**, 91 99 (2009).
39. R. Villares *et al.*, CCR6 regulates EAE pathogenesis by controlling regulatory CD4+ T cell recruitment to target tissues. *Eur J Immunol* **39**, 1671 1681 (2009).

40. D. Gatto, R. Brink, B cell localization: regulation by EBI2 and its oxysterol ligand. *Trends Immunol* **34**, 336 341 (2013).
41. J. P. Pereira, L. M. Kelly, J. G. Cyster, Finding the right niche: B cell migration in the early phases of T dependent antibody responses. *Int Immunol* **22**, 413 419 (2010).
42. L. M. Kelly, J. P. Pereira, T. Yi, Y. Xu, J. G. Cyster, EBI2 guides serial movements of activated B cells and ligand activity is detectable in lymphoid and nonlymphoid tissues. *J Immunol* **187**, 3026 3032 (2011).
43. D. Gatto, K. Wood, R. Brink, EBI2 operates independently of but in cooperation with CXCR5 and CCR7 to direct B cell migration and organization in follicles and the germinal center. *J Immunol* **187**, 4621 4628 (2011).
44. T. Yi *et al.*, Oxysterol gradient generation by lymphoid stromal cells guides activated B cell movement during humoral responses. *Immunity* **37**, 535 548 (2012).
45. S. Hannedouche *et al.*, Oxysterols direct immune cell migration via EBI2. *Nature* **475**, 524 527 (2011).
46. J. P. Pereira, L. M. Kelly, Y. Xu, J. G. Cyster, EBI2 mediates B cell segregation between the outer and centre follicle. *Nature* **460**, 1122 1126 (2009).
47. D. Gatto, D. Paus, A. Basten, C. R. Mackay, R. Brink, Guidance of B cells by the orphan G protein coupled receptor EBI2 shapes humoral immune responses. *Immunity* **31**, 259 269 (2009).
48. J. G. Cyster, B cell follicles and antigen encounters of the third kind. *Nat Immunol* **11**, 989 996 (2010).
49. K. Reif *et al.*, Balanced responsiveness to chemoattractants from adjacent zones determines B cell position. *Nature* **416**, 94 99 (2002).
50. T. Okada *et al.*, Antigen engaged B cells undergo chemotaxis toward the T zone and form motile conjugates with helper T cells. *PLoS Biol* **3**, e150 (2005).
51. N. M. Haynes *et al.*, Role of CXCR5 and CCR7 in follicular Th cell positioning and appearance of a programmed cell death gene 1high germinal center associated subpopulation. *J Immunol* **179**, 5099 5108 (2007).
52. P. Schaerli *et al.*, CXC chemokine receptor 5 expression defines follicular homing T cells with B cell helper function. *J Exp Med* **192**, 1553 1562 (2000).
53. D. Breitfeld *et al.*, Follicular B helper T cells express CXC chemokine receptor 5, localize to B cell follicles, and support immunoglobulin production. *J Exp Med* **192**, 1545 1552 (2000).
54. J. Li, E. Lu, T. Yi, J. G. Cyster, EBI2 augments Tfh cell fate by promoting interaction with IL 2 quenching dendritic cells. *Nature* **533**, 110 114 (2016).
55. T. D. Chan *et al.*, Antigen affinity controls rapid T dependent antibody production by driving the expansion rather than the differentiation or extrafollicular migration of early plasmablasts. *J Immunol* **183**, 3139 3149 (2009).
56. J. J. Taylor, M. K. Jenkins, K. A. Pape, Heterogeneity in the differentiation and function of memory B cells. *Trends Immunol* **33**, 590 597 (2012).
57. D. Gatto, R. Brink, The germinal center reaction. *J Allergy Clin Immunol* **126**, 898 907; quiz 908 899 (2010).

58. J. J. Taylor, K. A. Pape, H. R. Steach, M. K. Jenkins, Humoral immunity. Apoptosis and antigen affinity limit effector cell differentiation of a single naive B cell. *Science* **347**, 784 787 (2015).
59. A. L. Shaffer *et al.*, BCL 6 represses genes that function in lymphocyte differentiation, inflammation, and cell cycle control. *Immunity* **13**, 199 212 (2000).
60. K. Basso, R. Dalla Favera, Roles of BCL6 in normal and transformed germinal center B cells. *Immunol Rev* **247**, 172 183 (2012).
61. M. Kitano *et al.*, Bcl6 protein expression shapes pre germinal center B cell dynamics and follicular helper T cell heterogeneity. *Immunity* **34**, 961 972 (2011).
62. S. M. Kerfoot *et al.*, Germinal center B cell and T follicular helper cell development initiates in the interfollicular zone. *Immunity* **34**, 947 960 (2011).
63. C. D. Allen *et al.*, Germinal center dark and light zone organization is mediated by CXCR4 and CXCR5. *Nat Immunol* **5**, 943 952 (2004).
64. J. A. Green *et al.*, The sphingosine 1 phosphate receptor S1P(2) maintains the homeostasis of germinal center B cells and promotes niche confinement. *Nat Immunol* **12**, 672 680 (2011).
65. G. D. Victora, M. C. Nussenzweig, Germinal centers. *Annu Rev Immunol* **30**, 429 457 (2012).
66. N. K. Jerne, A study of avidity based on rabbit skin responses to diphtheria toxin antitoxin mixtures. *Acta Pathol Microbiol Scand Suppl* **87**, 1 183 (1951).
67. H. N. Eisen, G. W. Siskind, Variations in Affinities of Antibodies during the Immune Response. *Biochemistry* **3**, 996 1008 (1964).
68. M. G. Weigert, I. M. Cesari, S. J. Yonkovich, M. Cohn, Variability in the lambda light chain sequences of mouse antibody. *Nature* **228**, 1045 1047 (1970).
69. A. K. Szakal, R. L. Gieringer, M. H. Kosco, J. G. Tew, Isolated follicular dendritic cells: cytochemical antigen localization, Nomarski, SEM, and TEM morphology. *J Immunol* **134**, 1349 1359 (1985).
70. E. A. Goidl, W. E. Paul, G. W. Siskind, B. Benacerraf, The effect of antigen dose and time after immunization on the amount and affinity of anti hapten antibody. *J Immunol* **100**, 371 375 (1968).
71. K. Suzuki, I. Grigorova, T. G. Phan, L. M. Kelly, J. G. Cyster, Visualizing B cell capture of cognate antigen from follicular dendritic cells. *J Exp Med* **206**, 1485 1493 (2009).
72. F. D. Batista, D. Iber, M. S. Neuberger, B cells acquire antigen from target cells after synapse formation. *Nature* **411**, 489 494 (2001).
73. F. D. Batista *et al.*, The role of integrins and coreceptors in refining thresholds for B cell responses. *Immunol Rev* **218**, 197 213 (2007).
74. S. Moriyama *et al.*, Sphingosine 1 phosphate receptor 2 is critical for follicular helper T cell retention in germinal centers. *J Exp Med* **211**, 1297 1305 (2014).
75. C. D. Allen, T. Okada, J. G. Cyster, Germinal center organization and cellular dynamics. *Immunity* **27**, 190 202 (2007).
76. M. E. Meyer Hermann, P. K. Maini, D. Iber, An analysis of B cell selection mechanisms in germinal centers. *Math Med Biol* **23**, 255 277 (2006).
77. D. Depoil *et al.*, Immunological synapses are versatile structures enabling selective T cell polarization. *Immunity* **22**, 185 194 (2005).

78. G. D. Victora *et al.*, Germinal center dynamics revealed by multiphoton microscopy with a photoactivatable fluorescent reporter. *Cell* **143**, 592 605 (2010).
79. S. Han *et al.*, Cellular interaction in germinal centers. Roles of CD40 ligand and B7 2 in established germinal centers. *J Immunol* **155**, 556 567 (1995).
80. D. Zotos *et al.*, IL 21 regulates germinal center B cell differentiation and proliferation through a B cell intrinsic mechanism. *J Exp Med* **207**, 365 378 (2010).
81. M. A. Linterman *et al.*, IL 21 acts directly on B cells to regulate Bcl 6 expression and germinal center responses. *J Exp Med* **207**, 353 363 (2010).
82. A. D. Gitlin, Z. Shulman, M. C. Nussenzweig, Clonal selection in the germinal centre by regulated proliferation and hypermutation. *Nature* **509**, 637 640 (2014).
83. A. D. Gitlin *et al.*, HUMORAL IMMUNITY. T cell help controls the speed of the cell cycle in germinal center B cells. *Science* **349**, 643 646 (2015).
84. D. Dominguez Sola *et al.*, The proto oncogene MYC is required for selection in the germinal center and cyclic reentry. *Nat Immunol* **13**, 1083 1091 (2012).
85. D. Suan, C. Sundling, R. Brink, Plasma cell and memory B cell differentiation from the germinal center. *Curr Opin Immunol* **45**, 97 102 (2017).
86. D. C. Hargreaves *et al.*, A coordinated change in chemokine responsiveness guides plasma cell movements. *J Exp Med* **194**, 45 56 (2001).
87. D. R. Fooksman *et al.*, Development and migration of plasma cells in the mouse lymph node. *Immunity* **33**, 118 127 (2010).
88. C. Garcia De Vinuesa *et al.*, Dendritic cells associated with plasmablast survival. *Eur J Immunol* **29**, 3712 3721 (1999).
89. C. P. Chappell, K. E. Draves, N. V. Giltiay, E. A. Clark, Extrafollicular B cell activation by marginal zone dendritic cells drives T cell dependent antibody responses. *J Exp Med* **209**, 1825 1840 (2012).
90. J. J. Taylor, K. A. Pape, M. K. Jenkins, A germinal center independent pathway generates unswitched memory B cells early in the primary response. *J Exp Med* **209**, 597 606 (2012).
91. H. Toyama *et al.*, Memory B cells without somatic hypermutation are generated from Bcl6 deficient B cells. *Immunity* **17**, 329 339 (2002).
92. B. Schittek, K. Rajewsky, Natural occurrence and origin of somatically mutated memory B cells in mice. *J Exp Med* **176**, 427 438 (1992).
93. S. M. Anderson, M. M. Tomayko, A. Ahuja, A. M. Haberman, M. J. Shlomchik, New markers for murine memory B cells that define mutated and unmutated subsets. *J Exp Med* **204**, 2103 2114 (2007).
94. I. Dogan *et al.*, Multiple layers of B cell memory with different effector functions. *Nat Immunol* **10**, 1292 1299 (2009).
95. K. A. Pape, J. J. Taylor, R. W. Maul, P. J. Gearhart, M. K. Jenkins, Different B cell populations mediate early and late memory during an endogenous immune response. *Science* **331**, 1203 1207 (2011).
96. R. J. Nibbs, G. J. Graham, Immune regulation by atypical chemokine receptors. *Nat Rev Immunol* **13**, 815 829 (2013).
97. I. Comerford, W. Litchfield, Y. Harata Lee, R. J. Nibbs, S. R. McColl, Regulation of chemotactic networks by 'atypical' receptors. *Bioessays* **29**, 237 247 (2007).

98. E. Wendt, S. Keshav, CCR9 antagonism: potential in the treatment of Inflammatory Bowel Disease. *Clin Exp Gastroenterol* **8**, 119 130 (2015).
99. K. Heinzel, C. Benz, C. C. Bleul, A silent chemokine receptor regulates steady state leukocyte homing in vivo. *Proc Natl Acad Sci U S A* **104**, 8421 8426 (2007).
100. I. Comerford, S. Milasta, V. Morrow, G. Milligan, R. Nibbs, The chemokine receptor CCX CKR mediates effective scavenging of CCL19 in vitro. *Eur J Immunol* **36**, 1904 1916 (2006).
101. I. Comerford *et al.*, The atypical chemokine receptor CCX CKR scavenges homeostatic chemokines in circulation and tissues and suppresses Th17 responses. *Blood* **116**, 4130 4140 (2010).
102. M. D. Bunting *et al.*, CCX CKR deficiency alters thymic stroma impairing thymocyte development and promoting autoimmunity. *Blood* **121**, 118 128 (2013).
103. S. A. Bryce *et al.*, ACKR4 on Stromal Cells Scavenges CCL19 To Enable CCR7 Dependent Trafficking of APCs from Inflamed Skin to Lymph Nodes. *J Immunol* **196**, 3341 3353 (2016).
104. M. H. Ulvmar *et al.*, The atypical chemokine receptor CCRL1 shapes functional CCL21 gradients in lymph nodes. *Nat Immunol* **15**, 623 630 (2014).
105. W. Shi *et al.*, Transcriptional profiling of mouse B cell terminal differentiation defines a signature for antibody secreting plasma cells. *Nat Immunol* **16**, 663 673 (2015).
106. T. S. Heng, M. W. Painter, C. Immunological Genome Project, The Immunological Genome Project: networks of gene expression in immune cells. *Nat Immunol* **9**, 1091 1094 (2008).
107. H. W. Lim, J. Lee, P. Hillsamer, C. H. Kim, Human Th17 cells share major trafficking receptors with both polarized effector T cells and FOXP3+ regulatory T cells. *J Immunol* **180**, 122 129 (2008).
108. K. Moriguchi, K. Miyamoto, N. Tanaka, O. Yoshie, S. Kusunoki, The importance of CCR4 and CCR6 in experimental autoimmune encephalomyelitis. *J Neuroimmunol* **257**, 53 58 (2013).
109. E. V. Acosta Rodriguez *et al.*, Surface phenotype and antigenic specificity of human interleukin 17 producing T helper memory cells. *Nat Immunol* **8**, 639 646 (2007).
110. L. Dong *et al.*, T Cell CX3CR1 Mediates Excess Atherosclerotic Inflammation in Renal Impairment. *J Am Soc Nephrol* **27**, 1753 1764 (2016).
111. S. R. McColl *et al.*, Expression of rat I TAC/CXCL11/SCYA11 during central nervous system inflammation: comparison with other CXCR3 ligands. *Lab Invest* **84**, 1418 1429 (2004).
112. C. Ruland *et al.*, Chemokine CCL17 is expressed by dendritic cells in the CNS during experimental autoimmune encephalomyelitis and promotes pathogenesis of disease. *Brain Behav Immun* **66**, 382 393 (2017).
113. D. Sunnemark *et al.*, CX3CL1 (fractalkine) and CX3CR1 expression in myelin oligodendrocyte glycoprotein induced experimental autoimmune encephalomyelitis: kinetics and cellular origin. *J Neuroinflammation* **2**, 17 (2005).
114. E. H. Tran, W. A. Kuziel, T. Owens, Induction of experimental autoimmune encephalomyelitis in C57BL/6 mice deficient in either the chemokine macrophage inflammatory protein 1alpha or its CCR5 receptor. *Eur J Immunol* **30**, 1410 1415 (2000).
115. D. J. Cua *et al.*, Interleukin 23 rather than interleukin 12 is the critical cytokine for autoimmune inflammation of the brain. *Nature* **421**, 744 748 (2003).

116. K. Kreymborg *et al.*, IL 22 is expressed by Th17 cells in an IL 23 dependent fashion, but not required for the development of autoimmune encephalomyelitis. *J Immunol* **179**, 8098 8104 (2007).
117. S. Haak *et al.*, IL 17A and IL 17F do not contribute vitally to autoimmune neuro inflammation in mice. *J Clin Invest* **119**, 61 69 (2009).
118. K. Frei *et al.*, Tumor necrosis factor alpha and lymphotoxin alpha are not required for induction of acute experimental autoimmune encephalomyelitis. *J Exp Med* **185**, 2177 2182 (1997).
119. C. Sutton, C. Brereton, B. Keogh, K. H. Mills, E. C. Lavelle, A crucial role for interleukin (IL) 1 in the induction of IL 17 producing T cells that mediate autoimmune encephalomyelitis. *J Exp Med* **203**, 1685 1691 (2006).
120. Y. Chung *et al.*, Critical regulation of early Th17 cell differentiation by interleukin 1 signaling. *Immunity* **30**, 576 587 (2009).
121. M. F. Gulen *et al.*, The receptor SIGIRR suppresses Th17 cell proliferation via inhibition of the interleukin 1 receptor pathway and mTOR kinase activation. *Immunity* **32**, 54 66 (2010).
122. M. F. Gulen *et al.*, Inactivation of the enzyme GSK3alpha by the kinase IKKi promotes AKT mTOR signaling pathway that mediates interleukin 1 induced Th17 cell maintenance. *Immunity* **37**, 800 812 (2012).
123. W. I. Yeh, I. L. McWilliams, L. E. Harrington, IFNgamma inhibits Th17 differentiation and function via Tbet dependent and Tbet independent mechanisms. *J Neuroimmunol* **267**, 20 27 (2014).
124. M. H. Lexberg *et al.*, IFN gamma and IL 12 synergize to convert in vivo generated Th17 into Th1/Th17 cells. *Eur J Immunol* **40**, 3017 3027 (2010).
125. V. Lazarevic *et al.*, T bet represses T(H)17 differentiation by preventing Runx1 mediated activation of the gene encoding RORgammat. *Nat Immunol* **12**, 96 104 (2011).
126. R. Duhen *et al.*, Cutting edge: the pathogenicity of IFN gamma producing Th17 cells is independent of T bet. *J Immunol* **190**, 4478 4482 (2013).
127. R. A. O'Connor, H. Cambrook, K. Huettner, S. M. Anderton, T bet is essential for Th1 mediated, but not Th17 mediated, CNS autoimmune disease. *Eur J Immunol* **43**, 2818 2823 (2013).
128. K. Ichiyama *et al.*, Transcription factor Smad independent T helper 17 cell induction by transforming growth factor beta is mediated by suppression of eomesodermin. *Immunity* **34**, 741 754 (2011).
129. B. Becher, B. G. Durell, R. J. Noelle, IL 23 produced by CNS resident cells controls T cell encephalitogenicity during the effector phase of experimental autoimmune encephalomyelitis. *J Clin Invest* **112**, 1186 1191 (2003).
130. S. D. Miller, E. J. McMahon, B. Schreiner, S. L. Bailey, Antigen presentation in the CNS by myeloid dendritic cells drives progression of relapsing experimental autoimmune encephalomyelitis. *Ann N Y Acad Sci* **1103**, 179 191 (2007).
131. K. Hirota *et al.*, Plasticity of Th17 cells in Peyer's patches is responsible for the induction of T cell dependent IgA responses. *Nat Immunol* **14**, 372 379 (2013).

132. M. A. Kleinschek *et al.*, IL 23 enhances the inflammatory cell response in Cryptococcus neoformans infection and induces a cytokine pattern distinct from IL 12. *J Immunol* **176**, 1098 1106 (2006).
133. E. Lu, E. V. Dang, J. G. McDonald, J. G. Cyster, Distinct oxysterol requirements for positioning naive and activated dendritic cells in the spleen. *Sci Immunol* **2**, (2017).
134. I. MacLennan, C. Vinuesa, Dendritic cells, BAFF, and APRIL: innate players in adaptive antibody responses. *Immunity* **17**, 235 238 (2002).
135. S. Gardam, R. Brink, Non Canonical NF kappaB Signaling Initiated by BAFF Influences B Cell Biology at Multiple Junctures. *Front Immunol* **4**, 509 (2014).
136. H. Kwon *et al.*, Analysis of interleukin 21 induced Prdm1 gene regulation reveals functional cooperation of STAT3 and IRF4 transcription factors. *Immunity* **31**, 941 952 (2009).
137. E. Jacque *et al.*, IKK induced NF kappaB1 p105 proteolysis is critical for B cell antibody responses to T cell dependent antigen. *J Exp Med* **211**, 2085 2101 (2014).
138. U. Klein *et al.*, Transcription factor IRF4 controls plasma cell differentiation and class switch recombination. *Nat Immunol* **7**, 773 782 (2006).
139. H. Xu *et al.*, Regulation of bifurcating B cell trajectories by mutual antagonism between transcription factors IRF4 and IRF8. *Nat Immunol* **16**, 1274 1281 (2015).
140. J. Loschko *et al.*, Absence of MHC class II on cDCs results in microbial dependent intestinal inflammation. *J Exp Med* **213**, 517 534 (2016).
141. J. M. Tas *et al.*, Visualizing antibody affinity maturation in germinal centers. *Science* **351**, 1048 1054 (2016).
142. J. Jacob, J. Przylepa, C. Miller, G. Kelsoe, In situ studies of the primary immune response to (4 hydroxy 3 nitrophenyl)acetyl. III. The kinetics of V region mutation and selection in germinal center B cells. *J Exp Med* **178**, 1293 1307 (1993).
143. G. D. Victora, P. C. Wilson, Germinal center selection and the antibody response to influenza. *Cell* **163**, 545 548 (2015).
144. A. Escolano, P. Dosenovic, M. C. Nussenzweig, Progress toward active or passive HIV 1 vaccination. *J Exp Med* **214**, 3 16 (2017).
145. Z. Shulman *et al.*, Dynamic signaling by T follicular helper cells during germinal center B cell selection. *Science* **345**, 1058 1062 (2014).
146. T. A. Schwickert *et al.*, A dynamic T cell limited checkpoint regulates affinity dependent B cell entry into the germinal center. *J Exp Med* **208**, 1243 1252 (2011).
147. J. Ersching *et al.*, Germinal Center Selection and Affinity Maturation Require Dynamic Regulation of mTORC1 Kinase. *Immunity* **46**, 1045 1058 e1046 (2017).
148. D. P. Calado *et al.*, The cell cycle regulator c Myc is essential for the formation and maintenance of germinal centers. *Nat Immunol* **13**, 1092 1100 (2012).
149. D. Allen, T. Simon, F. Sablitzky, K. Rajewsky, A. Cumano, Antibody engineering for the analysis of affinity maturation of an anti hapten response. *EMBO J* **7**, 1995 2001 (1988).
150. T. Imanishi, O. Makela, Strain differences in the fine specificity of mouse anti hapten antibodies. *Eur J Immunol* **3**, 323 330 (1973).
151. R. S. Jack, T. Imanishi Kari, K. Rajewsky, Idiotypic analysis of the response of C57BL/6 mice to the (4 hydroxy 3 nitrophenyl)acetyl group. *Eur J Immunol* **7**, 559 565 (1977).

152. M. Reth, T. Imanishi Kari, K. Rajewsky, Analysis of the repertoire of anti (4 hydroxy 3 nitrophenyl)acetyl (NP) antibodies in C 57 BL/6 mice by cell fusion. II. Characterization of idiotopes by monoclonal anti idiotope antibodies. *Eur J Immunol* **9**, 1004 1013 (1979).
153. A. L. Bothwell *et al.*, Heavy chain variable region contribution to the NPb family of antibodies: somatic mutation evident in a gamma 2a variable region. *Cell* **24**, 625 637 (1981).
154. D. Baumjohann *et al.*, Persistent antigen and germinal center B cells sustain T follicular helper cell responses and phenotype. *Immunity* **38**, 596 605 (2013).
155. R. Shinnakasu *et al.*, Regulated selection of germinal center cells into the memory B cell compartment. *Nat Immunol* **17**, 861 869 (2016).

APPENDIX

LIST OF PUBLICATIONS ARISING FROM WORK CONDUCTED DURING MY Ph.D. CANDIATURE

i) Comerford I, Litchfield W, **Kara EE**, McColl SR. PI3Kγ drives priming and survival of autoreactive CD4(+) T cells during experimental autoimmune encephalomyelitis. ***PLoS One*** 7(9):e45095 (2012).

ii) Comerford I, Harata-Lee Y, Bunting MD, Gregor C, **Kara EE**, McColl SR. A myriad of functions and complex regulation of the CCR7/CCL19/CCL21 chemokine axis in the adaptive immune system. ***Cytokine Growth Factor Reviews*** 24(3):269-283 (2013).

iii) Weide F, Fromm PD, Comerford I, **Kara EE**, Bannan J, Schuh W, Ranasinghe C, Tarlinton D, Winkler T, McColl SR, Horner H. CCR6 is transiently upregulated after activation and modulates the germinal center reaction in the mouse. ***Immunology & Cell Biology*** 91(5):335-339 (2013).

iv) **Kara EE**, McColl SR, Comerford I. The basophil: resolved questions and new avenues of investigation. ***Bioessays*** 35(8):670 (2013).

v) **Kara EE**, Comerford I, Bastow CR, Fenix KA, Litchfield W, Handel TM, McColl SR. Distinct chemokine receptor axes regulate Th9 cell trafficking to allergic and autoimmune inflammatory sites. ***Journal of Immunology*** 191(3):1110-1117 (2013).

vi) Comerford I, **Kara EE**, McKenzie DR, McColl SR. Advances in understanding the pathogenesis of autoimmune disorders: focus on chemokine and lymphocyte trafficking. ***British Journal of Haematology*** 164(3): 329-341 (2014).

vii) **Kara EE**, Comerford I, Fenix KA, Bastow CR, Gregor CE, McKenzie DR, McColl SR. Tailored immune responses: novel effector helper T cell subsets in protective immunity. ***PLoS Pathogens*** 10(2):e1003905 (2014).

viii) Bunting MD, Comerford I, **Kara EE**, Korner H, McColl SR. CCR6 supports migration and differentiation of a subset of DN1 early thymocyte progenitors but is not required for thymic nTreg development. ***Immunology and Cell Biology*** 92(6):489-498 (2014).

ix) **Kara EE**, McKenzie DR, Bastow CR, Gregor CE, Fenix KA, Ogunniyi AD, Paton JC, Mack M, Pombal DR, Seillet C, Dubois B, Liston A, MacDonald KP, Belz GT, Smyth MJ, Hill GR, Comerford I, McColl SR. CCR2 defines in vivo development and homing of IL-23-driven GM-CSF-producing Th17 cells. ***Nature Communications*** 6:8644 doi: 10.1038/ncomms9644 (2015).

x) Babb R, Chen A, Hirst TR, **Kara EE**, McColl SR, Ogunniyi AD, Paton JC, Alsharifi M. Intranasal vaccination with γ-irradiated Streptococcus pneumoniae whole-cell vaccine provides serotype-independent protection mediated by B-cells and innate IL-17 responses. ***Clinical Science*** 130(9):697-710 (2016).

xi) Reimer D, Lee AY, Bannan J, Fromm P, **Kara EE**, Comerford I, McColl S, Weide F, Meilenz D, Korner H. Early CCR6 expression on B cells modulates germinal centre kinetics and efficient antibody responses. ***Immunology and Cell Biology*** 95(1):33-41 (2017).

xii) Babb R, Chen A, Ogunniyi AD, Hirst TR, **Kara EE**, McColl SR, Alsharifi M, Paton JC. Enhanced protective responses to a serotype-independent pneumococcal vaccine when combined with an inactivated influenza vaccine. ***Clinical Science*** 131(2):169-180 (2017).

xiii) McKenzie DR, **Kara EE**, Bastow CR, Tyllis TS, Fenix KA, Gregor CE, Wilson JJ, Babb R, Paton JC, Kallies A, Nutt SL, Brustle A, Mack M, Comerford I, McColl SR. IL-17-producing γδ T cells switch migratory patterns between resting and activated states. ***Nature Communications*** 8:15632 doi: 10.1038/ncomms15632 (2017).

xiv) **Kara EE**, Bastow CR, McKenzie DR, Gregor CE, Fenix KA, Babb R, Norton TS, Zotos D, Rodda LB, hermes JR, Bourne K, Gilchrist DS, Nibbs RJ, Alsharifi M, Vinuesa CG, Tarlinton DM, Brink R, Hill GR, Cyster JG, Comerford I, McColl SR. Atypical chemokine receptor 4 shapes activated B cell fate. ***Journal of Experimental Medicine*** 215(3):801-813 doi: 10.1084/jem.20171067 (2018).

JEM

Brief Definitive Report

Atypical chemokine receptor 4 shapes activated B cell fate

Ervin E. Kara,[1] Cameron R. Bastow,[1] Duncan R. McKenzie,[1] Carly E. Gregor,[1] Kevin A. Fenix,[1] Rachelle Babb,[1] Todd S. Norton,[1] Dimitra Zotos,[3] Lauren B. Rodda,[4] Jana R. Hermes,[6] Katherine Bourne,[6] Derek S. Gilchrist,[7] Robert J. Nibbs,[7] Mohammed Alsharifi,[1] Carola G. Vinuesa,[8] David M. Tarlinton,[3,9] Robert Brink,[6,10] Geoffrey R. Hill,[11] Jason G. Cyster,[4,5] Iain Comerford,[1] and Shaun R. McColl[1,2]

[1]Department of Molecular and Cellular Biology, School of Biological Sciences and [2]Centre for Molecular Pathology, School of Biological Sciences, University of Adelaide, Adelaide, South Australia, Australia
[3]Walter and Eliza Hall Institute of Medical Research, Parkville, Victoria, Australia
[4]Department of Microbiology and Immunology and [5]Howard Hughes Medical Institute, Department of Microbiology and Immunology, University of California, San Francisco, San Francisco, CA
[6]Immunology Division, Garvan Institute of Medical Research, Darlinghurst, New South Wales, Australia
[7]Institute of Infection, Immunity and Inflammation, College of Medicine, Veterinary and Life Sciences, University of Glasgow, Glasgow, Scotland, UK
[8]Department of Immunology and Infectious Disease, John Curtin School of Medical Research, Australian National University, Canberra, Australian Capital Territory, Australia
[9]Department of Immunology and Pathology, Monash University, Melbourne, Victoria, Australia
[10]St Vincent's Clinical School, University of New South Wales, Darlinghurst, New South Wales, Australia
[11]Immunology Department, QIMR Berghofer Medical Research Institute, Brisbane, Queensland, Australia

Activated B cells can initially differentiate into three functionally distinct fates—early plasmablasts (PBs), germinal center (GC) B cells, or early memory B cells—by mechanisms that remain poorly understood. Here, we identify atypical chemokine receptor 4 (ACKR4), a decoy receptor that binds and degrades CCR7 ligands CCL19/CCL21, as a regulator of early activated B cell differentiation. By restricting initial access to splenic interfollicular zones (IFZs), ACKR4 limits the early proliferation of activated B cells, reducing the numbers available for subsequent differentiation. Consequently, ACKR4 deficiency enhanced early PB and GC B cell responses in a CCL19/CCL21-dependent and B cell–intrinsic manner. Conversely, aberrant localization of ACKR4-deficient activated B cells to the IFZ was associated with their preferential commitment to the early PB linage. Our results reveal a regulatory mechanism of B cell trafficking via an atypical chemokine receptor that shapes activated B cell fate.

INTRODUCTION

Differentiation of activated B cells during the initial stages of T cell–dependent antibody responses proceeds simultaneously along pathways leading to early (extrafollicular) plasmablasts (PBs), germinal center (GC) B cells, and GC-independent, early memory B cells. These pathways differ in their spatiotemporal emergence, the longevity of their end products, their affinity for antigens, and their functional capacity (Taylor et al., 2012) and are considered important for establishing robust and diverse antibody responses. Adoption of these fates is controlled in part by B cell–trafficking receptors, which are dynamically regulated after antigen engagement to enable B cell access to antigens, interactions with T cells, and positioning in distinct lymphoid niches that foster the formation of immediate or long-lasting, antigen-specific antibody responses (Pereira et al., 2010). How antigen-activated B cells regulate their response to the several chemoattractants to which they may be simultaneously or sequentially exposed is uncertain. It is, however, potentially crucial as a mechanism in determining stoichiometry in the distribution of B cells along the differentiation pathways that generate the effector B cells of the immune response.

A key event in the initiation of T cell–dependent humoral immune responses is the CCR7-directed migration of antigen-engaged B cells toward, and subsequent EBI2/CXCR5/CCR7-dependent distribution along, the border between the T cell and B cell zones (Reif et al., 2002; Okada et al., 2005; Chan et al., 2009; Gatto et al., 2009, 2011; Pereira et al., 2009; Hannedouche et al., 2011; Kelly et al., 2011). Cognate T and B cell interactions at this interface drive EBI2-mediated relocalization to the interfollicular and outer follicular regions in which activated B cells initially proliferate (Chan et al., 2009; Gatto et al., 2009; Kelly et al., 2011; Kerfoot et al., 2011). Proliferating B cells subsequently trifurcate their differentiation trajectories, adopting a chemoattractant receptor profile that drives their positioning to lymphoid microenvironments that promote their effector function. Early PB differentiation is coupled with the induction of CXCR4

Correspondence to Iain Comerford: iain.comerford@adelaide.edu.au; Shaun R. McColl: shaun.mccoll@adelaide.edu.au

E.E. Kara's present address is Laboratory of Molecular Immunology, The Rockefeller University, New York, NY.

The Rockefeller University Press
J. Exp. Med. 2018 Vol. 215 No. 3 801–813
https://doi.org/10.1084/jem.20171067

Supplemental material can be found at:
http://doi.org/10.1084/jem.20171067

Journal of Experimental Medicine

and down-regulation of CXCR5 and CCR7, which repositions these cells in extrafollicular niches and the splenic red pulp (Hargreaves et al., 2001). These PBs are short lived and elicit the first line of antigen-specific antibody defense (Smith et al., 1996). GC-committed B cells down-regulate EBI2 (Gatto et al., 2009; Pereira et al., 2009) but maintain CXCR4 and CXCR5 expression (Allen et al., 2004), drawing them into the follicular dendritic cell–rich follicle center where GCs form. Another subset of B cells ultimately adopts a trafficking receptor profile that allows its continuous recirculation through the blood and secondary lymphoid organ follicles as early memory B cells, which retain their germline-encoded antibody. Whether the spatiotemporal control of B cell chemoattractant responsiveness, which is a crucial component of activated B cell differentiation, is stochastic or is intrinsic to the identified receptors and ligands and whether other receptors are involved remain unknown.

Recent studies have shown that a subfamily of atypical chemokine receptors regulates cellular migration (Nibbs and Graham, 2013). These receptors are uncoupled from the classic chemokine receptor–signal transduction machinery, do not induce cell migration, are mainly expressed outside the hematopoietic compartment, and mediate chemokine removal or redistribution in vivo (Nibbs and Graham, 2013). Atypical chemokine receptor 4 (ACKR4) binds CCR7 ligands CCL19 and CCL21 and the CCR9 ligand CCL25 and, thus, regulates their bioavailability in vivo without initiating cellular migration (Gosling et al., 2000; Comerford et al., 2006, 2010; Heinzel et al., 2007; Bunting et al., 2013; Ulvmar et al., 2014; Lucas et al., 2015; Bryce et al., 2016). However, despite the important role of CCR7 in the development of T cell–dependent antibody responses, the function of ACKR4 in this context is unknown. We now report an important, B cell–intrinsic role for ACKR4 in regulating B cell differentiation during the initial stages of the T cell–dependent humoral immune response.

RESULTS AND DISCUSSION

Although a previous study (Heinzel et al., 2007) concluded that ACKR4 is expressed exclusively by cells of nonhematopoietic origin in unimmunized mice, we detected ACKR4 transcripts and protein expression by GC B cells (Fig. 1, A and B). To investigate the possible functions for hematopoietic ACKR4 in T cell–dependent humoral immunity, we used bone marrow (BM) chimerism to generate mice in which ACKR4 deficiency was restricted to the hematopoietic compartment (H-*Ackr4*$^{-/-}$). We immunized these H-*Ackr4*$^{-/-}$ mice with sheep red blood cells (SRBCs) and observed an increased frequency of GC B cells at all time points assessed after immunization but most prominently on day 5 relative to hematopoietic WT (H-WT) mice (Fig. 1 C). The number of T follicular helper (TFH) cells, mediators of GC B cell selection and proliferation, and T follicular regulatory (TFR) cells, implicated in regulating the magnitude of the GC reaction, were also increased in immunized H-*Ackr4*$^{-/-}$ mice relative to controls (Fig. S1 A). The formation of early PBs, despite a lack of detectable ACKR4 expression, in H-*Ackr4*$^{-/-}$ mice was also enhanced on day 5 of the response (Fig. 1 D). These data reveal a negative regulatory role for ACKR4 expression in the hematopoietic compartment on early PB and GC B cell development. To determine whether this effect was intrinsic to B cell expression of ACKR4, we reconstituted lethally irradiated mice with a 4:1 mixture of BM recovered from B cell–deficient (μMT) mice that lack endogenous B cells (Kitamura et al., 1991) and either WT (B-WT) or *Ackr4*$^{-/-}$ (B-*Ackr4*$^{-/-}$) mice. Immunizing B-*Ackr4*$^{-/-}$ mice with SRBC reproduced the increased numbers of splenic GC B cells, TFH cells, and early PBs seen in immunized H-*Ackr4*$^{-/-}$ mice (Fig. 1, E and F; and Fig. S1 B). Collectively, these data reveal a B cell–intrinsic regulatory role for ACKR4 in the early stages of the B cell response to a T cell–dependent antigen.

ACKR4 expression by GC B cells (Fig. 1, A and B), and their disproportionate expansion in immunized H-*Ackr4*$^{-/-}$ and B-*Ackr4*$^{-/-}$ mice (Fig. 1, C and F), prompted us to investigate whether ACKR4 functioned in GC biology. ACKR4 internalizes and degrades CCR7 ligands without initiating cellular migration (Gosling et al., 2000; Townson and Nibbs, 2002; Comerford et al., 2006; Heinzel et al., 2007). However, CCL21 staining appeared to be normal around established *Ackr4*-deficient GCs in histologic sections of mesenteric LNs from H-*Ackr4*$^{-/-}$ mice (Fig. 2 A). This suggests that GC B cell expression of ACKR4 does not determine the abundance or localization of CCL21 outside GCs. GC B cells cycle between light zones (LZs) and dark zones (DZs) of the GCs, reflecting the iterative process of affinity-based selection, proliferation, and Ig somatic hypermutation that drives antibody affinity maturation (Victora and Nussenzweig, 2012). Flow cytometric assessment of DZ (CXCR4^{hi}CD86^{lo}) and LZ (CXCR4^{lo}CD86^{hi}) GC B cell phenotypes (Victora et al., 2010; Bannard et al., 2013) revealed no differences between H-WT and H-*Ackr4*$^{-/-}$ GCs (Fig. 2 B). Further, GC B cell proliferation and apoptosis were equivalent between H-WT and H-*Ackr4*$^{-/-}$ mice as measured by BrdU incorporation, DNA content, and Annexin V analyses (Fig. 2, C and D). Assessment of affinity maturation using Ig heavy chain–variable (V) region sequencing of individual (4-hydroxy-3-nitrophenyl) acetyl (NP)–specific IgG1$^+$ GC B cells revealed that overall somatic mutations and the affinity-enhancing W to L replacement at position V_H33 accumulated at similar rates in *Ackr4*-deficient and -sufficient GCs (Fig. 2 E). Serum antibody titers of NP-specific IgG were enhanced in H-*Ackr4*$^{-/-}$ mice at day 21 after immunization; however, the ratio of NP_5- (high affinity) to NP_{32}- (global affinity) reactive IgG was equivalent between H-WT and H-*Ackr4*$^{-/-}$ mice (Fig. 2 F). In addition, we addressed whether ACKR4 influenced GC B cell–affinity maturation in a cell-intrinsic manner. To do this, we crossed *Ackr4*$^{-/-}$ mice to SW_{HEL} Ig transgenic mice (SW_{HEL}.*Ackr4*$^{-/-}$) and measured GC B cell–affinity maturation in competition with WT SW_{HEL} B cells after transfer. SW_{HEL} B cells express a B cell receptor (BCR) derived

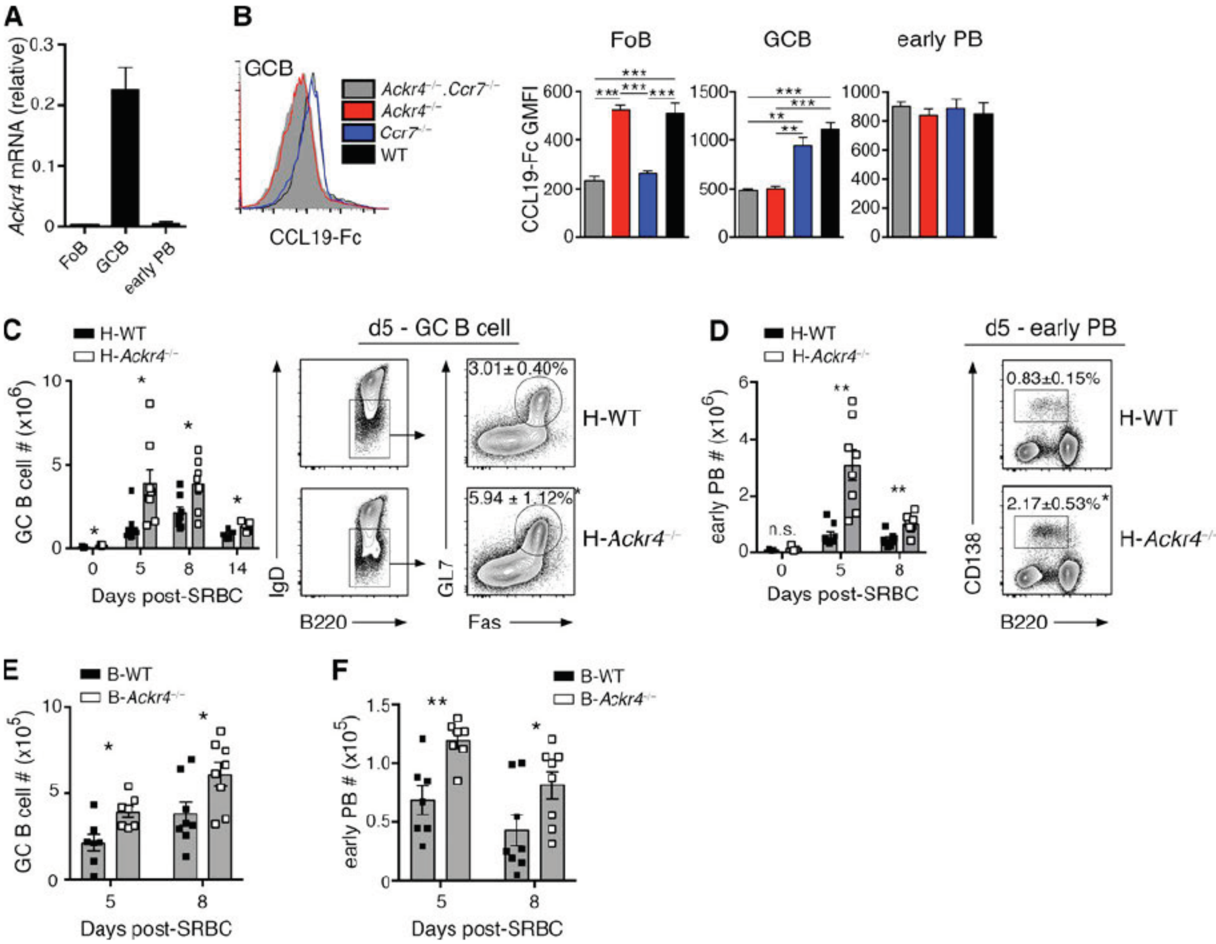

Figure 1. **B cell ACKR4 limits early PB and GC B cell responses. (A)** Quantitative PCR analysis of *Ackr4* transcript abundance in sorted Fo B cells ($B220^+IgD^+Fas^-GL7^-$), GC B cells ($B220^+IgD^-Fas^+GL7^+$), and early PB ($B220^{lo/-}CD138^+$) relative to the housekeeping gene *Rplp0* (means ± SD). **(B)** Representative histogram of CCL19–Fc staining on GC B cells from $Ackr4^{-/-}.Ccr7^{-/-}$ (cannot bind CCL19–Fc), $Ackr4^{-/-}$ (CCR7 staining), $Ccr7^{-/-}$ (ACKR4 staining), and WT (ACKR4/CCR7 staining) mice. Graphs plot geometric mean fluorescence intensity (GMFI) of CCL19–Fc staining on Fo B cells, GC B cells, and early PBs, gated as in A (n = 5 mice/genotype; means ± SEM). **(C and D)** H-$Ackr4^{-/-}$ and H-WT mice were generated by reconstituting lethally irradiated B6.Ly5.1 mice with BM from $Ackr4^{-/-}$ or WT mice, respectively. Representative plots of splenic GC B cell (C) and early PB (D) populations day 5 after SRBC immunization. Numbers in plots present the means ± SEM frequency of GC B cells per total $B220^+$ cells (C) or early PBs per spleen (D). Graphs present the total number of GC B cells (C) and early PB (D) per spleen on the days indicated after immunization. n = 3 (day 0); n = 8 (day 5); n = 8 (day 8); and n = 5 (day 14) mice/genotype; means ± SEM). **(E and F)** B cell–$Ackr4^{-/-}$ (B-$Ackr4^{-/-}$) and B-WT mice were generated by reconstituting lethally irradiated B6.Ly5.1 mice with a mixture of BM from µMT (80%) and $Ackr4^{-/-}$ mice or WT mice (20%), respectively. Graphs plot the total number of GC B cells (E) and early PB (F) per spleen on the days indicated after SRBC. (A–F) n = 7 (day 5) and n = 8 (day 8) mice/genotype; means ± SEM. Data are representative of two independent experiments. *, $P < 0.05$; **, $P < 0.01$; ***, $P < 0.001$. (B) One-way analysis of variance with the Bonferroni multiple-comparisons test. (C–F) Two-tailed, unpaired Student's t test or two-tailed, nonparametric Mann-Whitney test, as appropriate.

from the hen egg lysozyme (HEL)–specific HyHEL10 mAb (Brink et al., 2015). Immunization with the reduced-affinity HEL mutant HEL^{3X} (acid dissociation constant [K_a] = 1 × 10^7 M^{-1}) elicits a SW_{HEL} GC B cell response characterized by a Y53D substitution in the Ig heavy chain V region, which increases HyHEL10 affinity to HEL^{3X} by >100-fold (Paus et al., 2006; Chan et al., 2012; Brink et al., 2015). The additionally reduced affinity HEL mutant HEL^{4X} (K_a = 2.3 × 10^5 M^{-1}) does not bind the SW_{HEL} BCR in a physiologically relevant manner but can bind the Y53D mutant form of HyHEL10 selected during the SW_{HEL} GC response to HEL^{3X} (Chan et al., 2012), thereby providing a metric for affinity maturation in the anti–HEL^{3X} response. WT (CD45.1/2) and $Ackr4^{-/-}$ (CD45.2) SW_{HEL} B cells were cotransferred into CD45.1 congenic recipient mice and immunized with HEL^{3X}-SRBC (Fig. 2 G). On day 9, DZ/LZ phenotypes (Fig. 2 H) and the frequency of HEL^{4X}-binding GC B cells (Fig. 2 I) were equivalent between WT and $Ackr4^{-/-}$ SW_{HEL} GC B cells, indicating that, in this system, the absence of ACKR4 on GC B cells does not compromise the processes of affinity-based selection or establishment of DZ and LZ phenotypes in the presence of competing ACKR4-sufficient GC B cells. Collectively, these data show GC B cell proliferation, apoptosis, DZ/LZ phenotype ratio, somatic hypermutation, and affinity maturation to be unaltered in *Ackr4*-deficient GCs and suggest, instead, that B cell expression of ACKR4 negatively regulates, specifically, the pre-GC stages of development of the B cell response.

Our findings in H-*Ackr4*$^{-/-}$ and B-*Ackr4*$^{-/-}$ mice indicated that ACKR4 negatively regulates both early PB and GC B cell responses (Fig. 1, C–G). Recent evidence has indicated that a single B cell clone can enter all three possible differentiation fates, and that this positively correlates with the magnitude of their early proliferation and resistance to apoptosis (Taylor et al., 2015). Based on these observations and our data, we hypothesized that ACKR4 functions in undifferentiated, activated B cells to negatively regulate both early PB and GC B cell responses. This hypothesis predicts that *Ackr4*-deficient B cells will preferentially enter early PB and GC B compartments in an environment in which *Ackr4*$^{-/-}$ and WT B cells are in competition. To test this, we studied *Ackr4*$^{-/-}$ early PB and early GC B cell responses (day 5 after SRBC administration) in the context of mixed BM chimeras. In mice reconstituted with an equal mixture of *Ackr4*$^{-/-}$ and WT BM, ACKR4 deficiency enhanced early PB and early GC B cell responses relative to concurrently activated WT cells (Fig. 3 A). To extend these observations, we studied concurrent WT (CD45.1/2) and *Ackr4*$^{-/-}$ (CD45.2) SW_{HEL} B cell responses to the reduced affinity HEL mutant HEL^{2X} (K_a = 8×10^7 M^{-1}). This response forms early PBs, GC B cells, and a population of cells ($B220^+Ig[HEL]^{hi}GL7^-$) that likely encompass early memory B cells (Chan et al., 2009; Brink et al., 2015) by day 5 after immunization. At this time point, *Ackr4*$^{-/-}$ SW_{HEL} B cells outcompeted WT SW_{HEL} B cells in the early PB and GC B and $B220^+HEL^{hi}GL7^-$ cell populations, most prominently among SW_{HEL} early PBs (Fig. 3 B). We hypothesized further that enforced expression of ACKR4 prior to B cell activation by antigens may limit entry into early PB and GC B cell compartments. We tested this by generating *Ackr4* knockin mice (*Rosa26*$^{\text{LSL-}Ackr4}$; Fig. S2 A) and making expression conditional to follicular (Fo) B cells by introducing a Cre recombinase driven by the regulatory elements of *Cd23* (*Cd23*$^{\text{Cre}}$; Kwon et al., 2008). Fo B cells from *Cd23*$^{\text{Cre/+}}$.*Rosa26*$^{\text{LSL-}Ackr4/+}$ mice expressed functional ACKR4 (Fig. S2, B and C) and had frequencies of splenic Fo B cells and marginal-zone B cells that were equivalent to WT littermates (Fig. S2 D). Transgenic ACKR4 expression by Fo B cells did not alter CCR7 or CXCR5 expression at rest or after anti–IgM stimulation (Fig. S2 E), but, consistent with the known function of ACKR4 as a scavenger of CCR7 ligands (Comerford et al., 2006, 2010), inhibited anti-IgM–stimulated B cell migration toward CCL21, but not CXCL13, a non-ACKR4 ligand in mice (Townson and Nibbs, 2002; Fig. S2 F). Supporting the hypothesis that ACKR4 negatively regulates activated B cell differentiation, in mixed BM chimeric mice reconstituted with *Cd23*$^{\text{Cre/+}}$.*Rosa26*$^{\text{LSL-}Ackr4/+}$ and WT BM, ACKR4 transgenic B cells were less represented among early PB and GC B cells that form on day 5 of the SRBC response (Fig. 3 C). These data suggest that enforced ACKR4 expression in Fo B cells limits their ability to form early PB and GC B cells when in competition with WT cells. Collectively, we conclude that ACKR4 negatively regulates early PB and GC B cell responses in a B cell–intrinsic manner. Furthermore, these experiments did not reveal a cell-intrinsic role for ACKR4 in TFH or TFR development (Fig. S1 C), suggesting that the enhanced T cell responses observed in H-*Ackr4*$^{-/-}$ and B-*Ackr4*$^{-/-}$ mice (Fig. S1, A and B) are secondary to enhanced B cell responses, an observation that is in keeping with recent evidence, indicating that the magnitude of the TFH cell response is proportional to the magnitude of the GC B cell response (Baumjohann et al., 2013).

To examine ACKR4-dependent regulation of the initial antigen-engaged B cell differentiation in more detail, we tracked early WT and *Ackr4*$^{-/-}$ SW_{HEL} B cell responses to HEL^{2X} using mixed SW_{HEL} B cell transfers. Profiling CFSE dilution revealed a cell-intrinsic proliferative advantage for *Ackr4*$^{-/-}$ over WT SW_{HEL} B cells as early as day 2 (Fig. 4 A), which was increasingly apparent as the response progressed (Fig. 4 B). Notably, the magnitude of the advantage for *Ackr4*$^{-/-}$ SW_{HEL} B cells on day 3 of the reaction (KO:WT = 1.26 ± 0.01) was similar to their advantage among the day 5 GC B cell (KO:WT = 1.36 ± 0.01; Fig. 3 B) and $B220^+HEL^{hi}GL7^-$ cell (KO:WT = 1.49 ± 0.02; Fig. 3 B) populations. These findings suggest that enhanced early proliferation of responding *Ackr4*$^{-/-}$ SW_{HEL} B cells may contribute to their accumulation among the effector cell compartments by day 5 of the reaction (Fig. 3 B). In experiments in which WT or *Ackr4*$^{-/-}$ SW_{HEL} B cells were transferred into separate recipients, *Ackr4*$^{-/-}$ SW_{HEL} B cells were detected at greater frequencies by day 2.5, and remained more abundant during the first 5.5 d of the response (Fig. 4 C). By day 5.5, mice receiving *Ackr4*$^{-/-}$ SW_{HEL} B cells had an increased total number of early PBs, GC B cells, and $B220^+HEL^{hi}GL7^-$ cells per spleen compared with controls (Fig. 4 D). *Ackr4*$^{-/-}$ SW_{HEL} B cells showed a greater propensity to form early PBs (Fig. 4, E and F), which was apparent by flow cytometry on day 4.5 (Fig. 4 G) and translated to increased circulating anti–HEL IgM and IgG1 titers and kinetics (Fig. 4 H). Together, these findings suggest that ACKR4 limits early antigen-engaged B cell proliferation in a B cell–intrinsic manner, reducing the number of antigen-engaged B cell precursors available for early PB and GC B cell differentiation.

Comparisons of SW_{HEL} B cell responses elicited by HEL antigens that differ in their affinity for HyHEL10 (Paus et al., 2006; Chan et al., 2009), or conjugated to SRBCs at varying epitope densities (Paus et al., 2006), have revealed that affinity and/or avidity of initial BCR-mediated activation positively regulates the initial expansion of antigen-engaged B cells. To investigate whether ACKR4-dependent changes to activated B cell responses were congruent across different initiating affinities and/or avidities of BCR-mediated activation, we studied WT (CD45.1/2) and *Ackr4*$^{-/-}$ (CD45.2) SW_{HEL} B cell

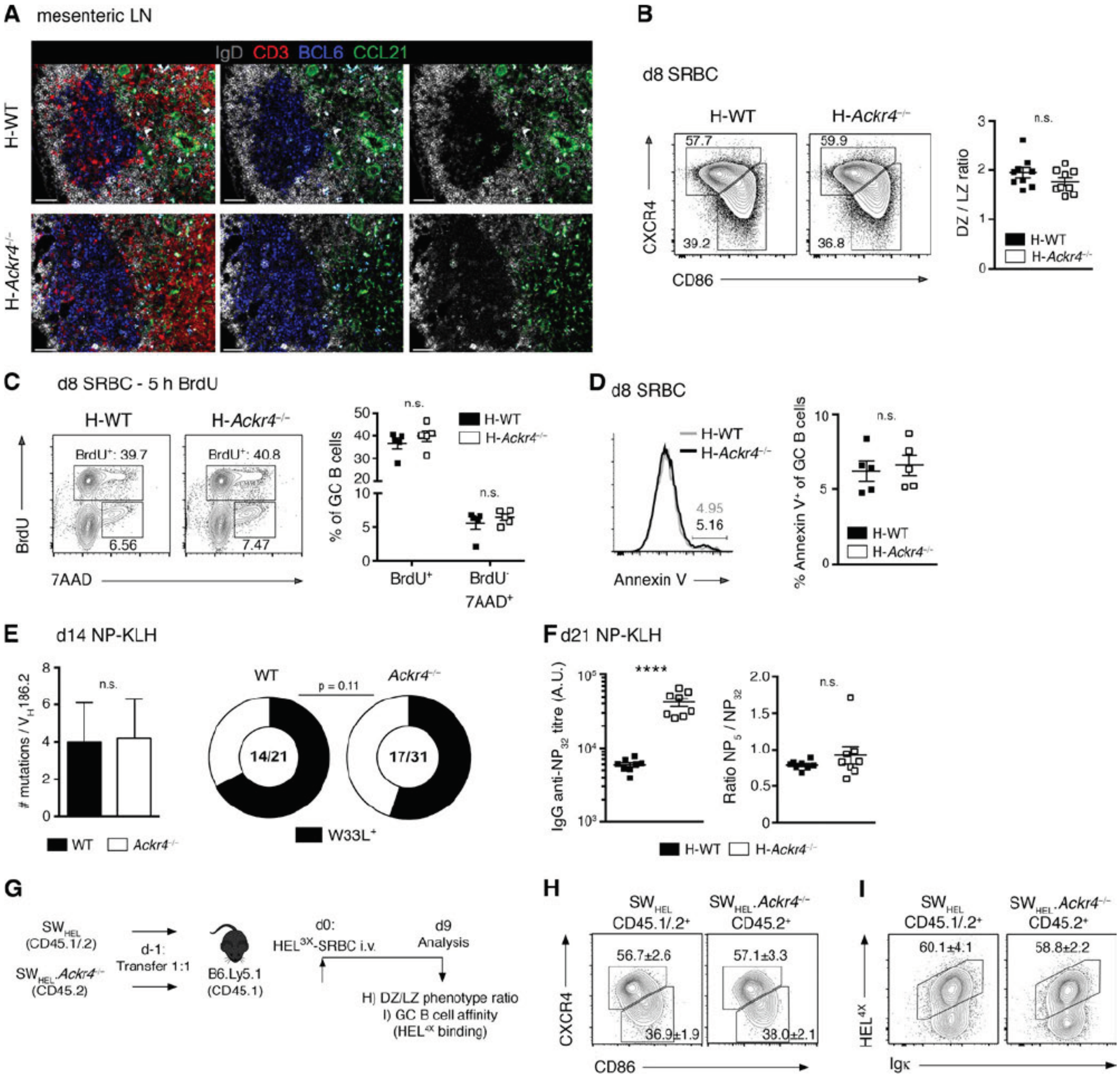

Figure 2. **ACKR4 in GC biology. (A)** Representative histology of CCL21 (green) abundance surrounding mesenteric LN GCs in H-WT and H-*Ackr4*$^{-/-}$ mice. BCL-6, blue; IgD, white; and CD3, red. Right: IgD and CCL21 staining. Middle: IgD, BCL6, and CCL21 staining. Left: All stains merged. Bars, 50 µm. n = 2–3 mice/genotype. **(B)** Representative DZ (CXCR4^{hi}CD86^{lo}) and LZ (CXCR4^{lo}CD86^{hi}) phenotype staining and ratios among splenic GC B cells (B220$^+$IgD$^-$Fas$^+$GL7$^+$) from H-WT and H-*Ackr4*$^{-/-}$ mice day 8 after SRBC. n = 8 mice/genotype (means ± SEM). **(C)** BrdU (2 mg) was administered i.p. 5 h before euthanasia. Representative BrdU and 7-aminoactinomycin D (DNA content) staining and quantitation of splenic GC B cells from H-WT and H-*Ackr4*$^{-/-}$ mice day 8 after SRBC. n = 5 mice/genotype (means ± SEM). **(D)** Representative staining and quantitation of Annexin V$^+$ splenic GC B cells day 8 after SRBC. n = 5 mice/genotype. **(E)** Total mutation (left; means ± SD) and high-affinity W33L mutation (right) frequency per V_H186.2 gene segment from single WT and *Ackr4*$^{-/-}$ NP$^+$IgG1$^+$ splenic GC B cells day 14 after NP-KLH immunization. Numbers in doughnut plots indicate the number of W33L$^+$ sequences of the total V_H186.2$^+$ sequences analyzed. **(F)** Total (NP$_{32}$) and the NP$_5$/NP$_{32}$ titer of serum NP-specific IgG antibodies in H-WT and H-*Ackr4*$^{-/-}$ mice day 21 after NP-KLH immunization. n = 8 mice/genotype (means ± SEM). **(G)** Experimental schematic. WT (CD45.1/2) and *Ackr4*$^{-/-}$ (CD45.2) SW$_{HEL}$ B cells were cotransferred into B6.Ly5.1 (CD45.1) mice and immunized the next day with HEL^{3X}-SRBC. **(H and I)** Representative flow cytometric DZ/LZ ratio (H) and HEL^{4X} (I; high-affinity) staining on concurrent WT and *Ackr4*$^{-/-}$ SW$_{HEL}$ GC B cells (B220$^+$HEL$^+$CD138$^-$GL7$^+$) on day 9. n = 5 mice. Numbers in plots present means ± SEM (A–I). Data are representative of one (A and E) and two (B–D and F–I) independent experiments. ****, $P < 0.0001$. (B–D and F) Two-tailed, unpaired Student's t test. (E) Two-tailed, unpaired Student's t test (left), Fisher's exact test (right, doughnut plots). (H and I) Two-tailed, unpaired Student's t test.

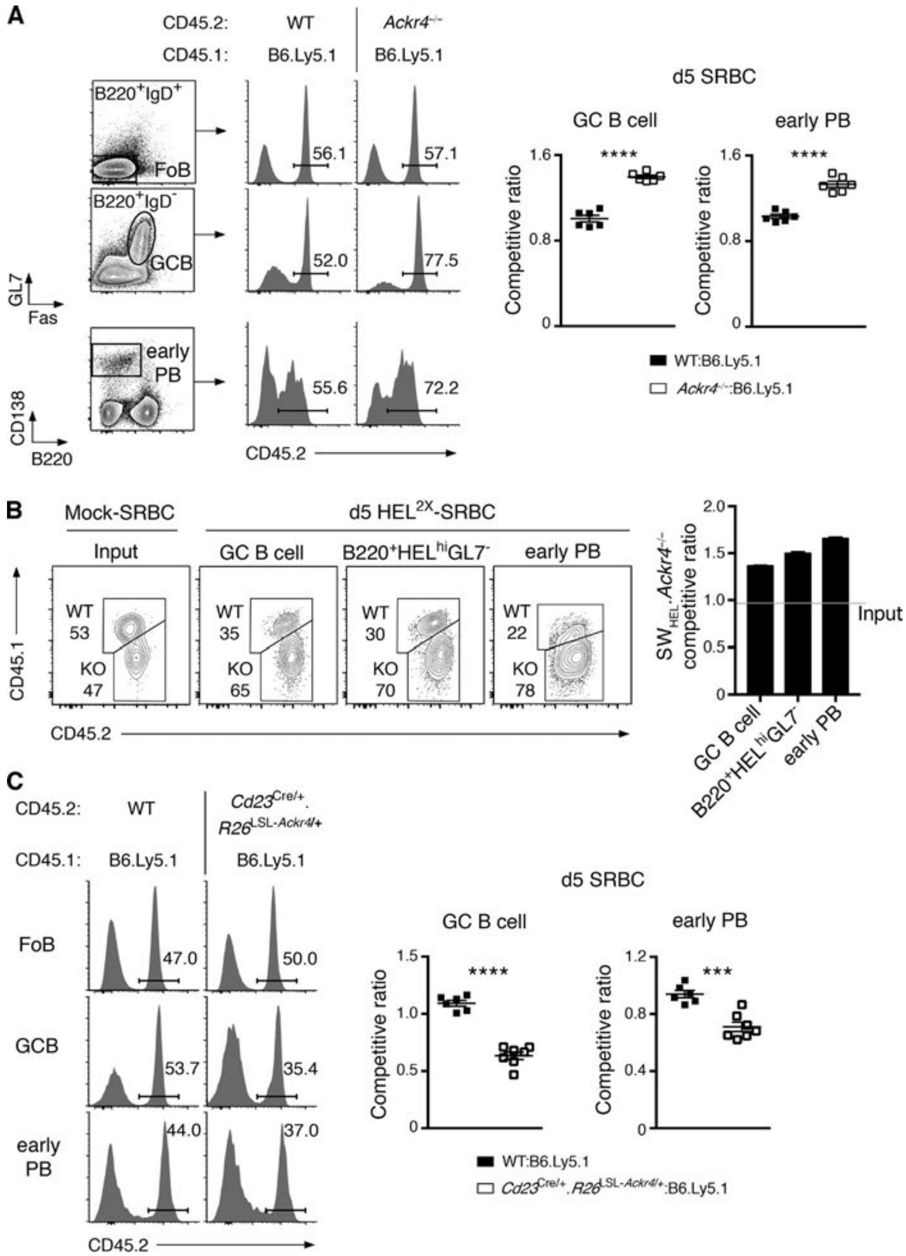

Figure 3. **ACKR4 limits early B cell responses in a B cell–intrinsic manner. (A)** Mixed BM chimeras were generated with an equal mixture of B6.Ly5.1 (CD45.1) and WT or *Ackr4*$^{-/-}$ (both CD45.2) BM. Representative plots of CD45.2^{+} cells among Fo B cells (B220^{+}IgD^{+}Fas^{-}GL7^{-}), GC B cells (B220^{+}IgD^{-}Fas^{+}GL7^{+}), and early PBs (B220$^{lo/-}$CD138^{+}) 5 d after SRBC. Gating of these populations is shown. Competitive ratios of GC B cells (left graph) and early PBs (right graph) are plotted as the frequencies of CD45.2^{+} cells in each compartment, normalized to the frequencies of CD45.2^{+} cells in the concurrent Fo B cell compartment. n = 6 mice/genotype (means ± SEM). **(B)** WT (CD45.1/2) and *Ackr4*$^{-/-}$ (CD45.2) SW$_{HEL}$ B cells were cotransferred into B6.Ly5.1 (CD45.1) mice and immunized with HEL^{2X}-SRBC (n = 4 mice) or mock-conjugated SRBCs (n = 3 mice). Contribution of WT and *Ackr4*$^{-/-}$ cells to SW$_{HEL}$ GC B cell (B220^{+}Igκ^{+}HEL^{int}GL7^{+}CD138^{-}), early PBs (B220$^{lo/-}$Igκ^{+}HEL^{+}CD138^{+}), and B220^{+}HEL^{hi}GL7^{-} (also Igκ^{+}CD138^{-}) cell populations 5 d after immunization. The SW$_{HEL}$.*Ackr4*$^{-/-}$ competitive ratio is plotted as the ratio of *Ackr4*$^{-/-}$ to WT among SW$_{HEL}$ effector cell compartments from day 5 HEL^{2X}-SRBC–immunized mice, normalized to the input ratio (as determined from mock-SRBC immunized mice analyzed on day 5 [means ± SEM]). **(C)** *Cd23*$^{Cre/+}$.*Rosa26*$^{LSL-Ackr4/+}$ mixed BM chimeras were generated and analyzed as in A (n = 6–7 mice/genotype; mean ± SEM). (A–C) Data are representative of two (B and C) and three (A) independent experiments. Two-tailed, unpaired Student's t test. ***, $P < 0.001$; ****, $P < 0.0001$.

responses to intermediate (HEL^{2X})- or low (HEL^{3X})-affinity HEL proteins conjugated to SRBCs at intermediate or low epitope densities (Fig. 4 I; Paus et al., 2006; Chan et al., 2009). *Ackr4*$^{-/-}$ SW$_{HEL}$ B cells preferentially formed early PBs (Fig. 4 J) and outcompeted WT cells in GC B cell and B220^{+}HEL^{hi}GL7^{-} cell compartments 5 d after immunization when either HEL^{2X} or HEL^{3X} of equivalent intermediate epitope densities were used (Fig. 4 K). Conversely, when the epitope density was reduced (low density), both WT and *Ackr4*$^{-/-}$ SW$_{HEL}$ PB responses were barely detectable by flow cytometry on day 5 (Fig. 4 J), but the cell-intrinsic advantage for *Ackr4*$^{-/-}$ SW$_{HEL}$ GC B cell and B220^{+}HEL^{hi}GL7^{-} cell development at that time point remained apparent (Fig. 4 K). These data indicate that ACKR4-dependent negative regulation of B cell responses is independent of the initiating affinity or avidity of BCR-mediated activation.

To explore the relationship between ACKR4 function as a regulator of CCR7-dependent cellular migration and its negative regulation of activated B cell responses, we studied the distribution of WT and *Ackr4*$^{-/-}$ SW$_{HEL}$ B cells within the spleen after HEL^{2X}-SRBC immunization using histology (Fig. 5 A). WT and *Ackr4*$^{-/-}$ SW$_{HEL}$ B cells were located throughout B cell follicles before immunization (unpublished data). Within 24 h, a proportion of WT SW$_{HEL}$ B cells had redistributed along the T/B border or had emigrated into the T cell zone. By days 2–2.5, most of the

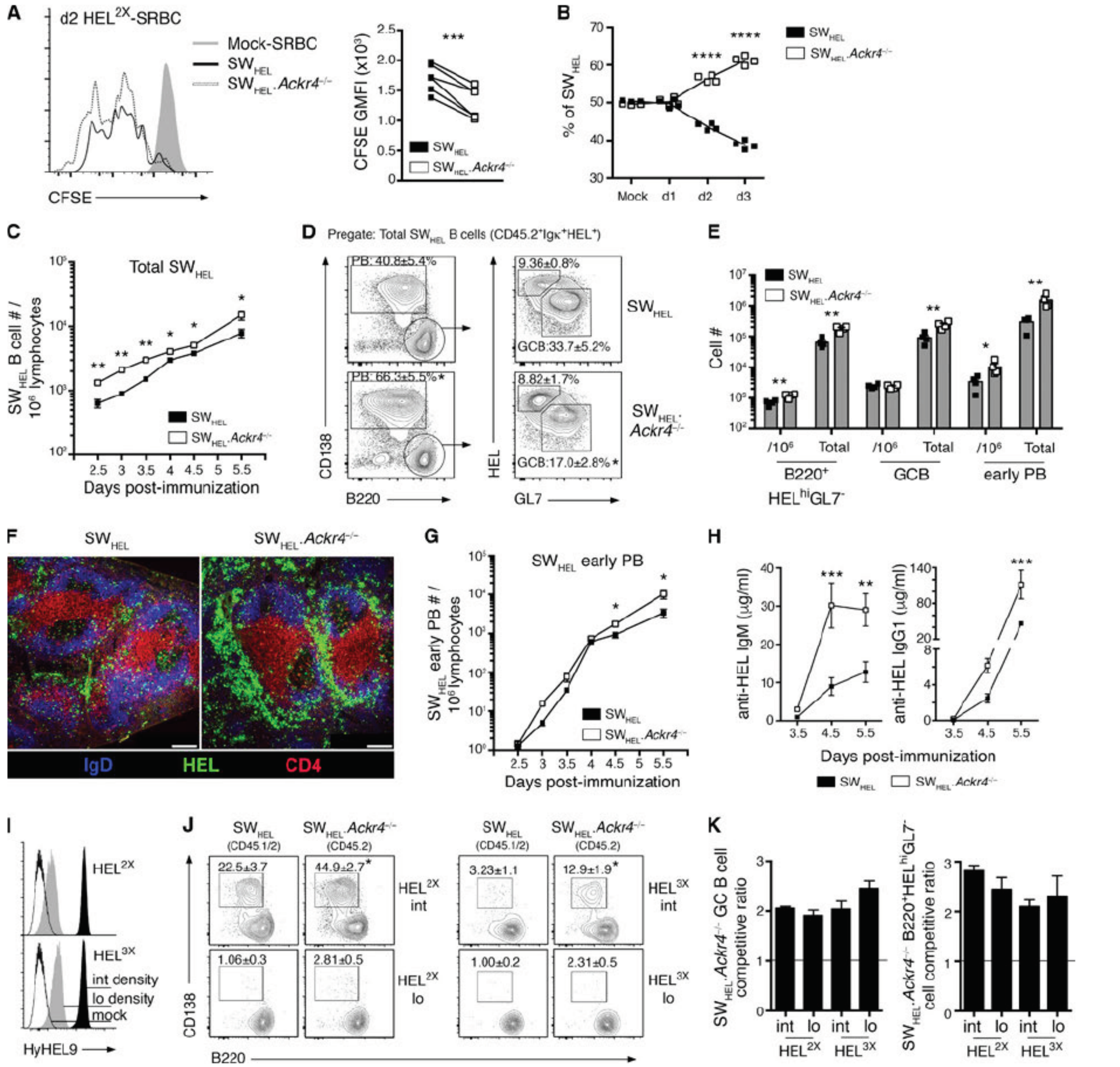

Figure 4. **ACKR4 limits early proliferation of antigen-engaged B cells and limits early PB responses. (A and B)** WT (CD45.1/2) and *Ackr4*$^{-/-}$ (CD45.2) SW_{HEL} B cells were cotransferred into B6.Ly5.1 (CD45.1) mice and immunized with HEL^{2X}-SRBC. (A) Representative flow-cytometric CFSE profiles and analysis of CFSE GMFI among responding SW_{HEL} B cells (B220$^+$Igκ$^+$HEL$^+$CD138$^-$) on day 2 (n = 6). Undivided SW_{HEL} B cells were analyzed from mock-SRBC–immunized recipients (n = 2). (B) Contribution of WT and *Ackr4*$^{-/-}$ among responding SW_{HEL} B cells (B220$^+$Igκ$^+$HEL$^+$CD138$^-$) over the first 3 d of the HEL^{2X}-SRBC response (n = 4 mice/time point). **(C–H)** WT or *Ackr4*$^{-/-}$ (both CD45.2) SW_{HEL} B cells were transferred into B6.Ly5.1 (CD45.1) mice and immunized with HEL^{2X}-SRBC (n = 4 mice/genotype per time point). (C) Frequency of total responding SW_{HEL} B cells (CD45.2$^+$Igκ$^+$HEL$^+$) per 10^6 splenocytes (means ± SEM). (D) Representative plots of early PB and GC B cell and B220$^+$HEL^{hi}GL7$^-$ cell responses as a frequency of total responding SW_{HEL} B cells (plots are pregated CD45.2$^+$Igκ$^+$HEL$^+$) on day 5.5. Numbers in plots represent the means ± SEM frequency of early PBs, GC B, or B220$^+$HEL^{hi}GL7$^-$ cells as the frequency of the total responding SW_{HEL} B cells. (E) Frequency of SW_{HEL} B220$^+$HEL^{hi}GL7$^-$ cells, GC B cells and early PBs (gated as shown in D) per 10^6 splenocytes and total number per spleen on day 5.5 (means ± SEM). (F) Representative histology of responding SW_{HEL} B cells on day 5.5 (n = 4 mice/genotype). Bar, 200 µm. HEL, green; IgD, blue; and CD4, red. (G) Frequency of SW_{HEL} early PBs (gated as in E) per 10^6 splenocytes (means ± SEM). (H) Anti-HEL IgM and IgG1 serum concentration as determined by ELISA (see Materials and methods; means ± SEM). **(I–K)** WT (CD45.1/2) and *Ackr4*$^{-/-}$ (CD45.2) were cotransferred into B6.Ly5.1 (CD45.1) recipients and immunized with HEL^{2X} (intermediate affinity) or HEL^{3X} (low affinity) conjugated to SRBCs at intermediate or low epitope densities (n = 4 mice/genotype per condition). (I) HEL^{2X} or HEL^{3X} were conjugated to SRBCs at intermediate (black histogram; 100 µg/ml; SRBC) and low (gray histogram; 5 µg/ml; SRBC) epitope densities and detected using HyHEL9 mAb. Mock-conjugated SRBCs (open histogram) are shown for comparison. (J) Representative plots of concurrent WT and *Ackr4*$^{-/-}$ SW_{HEL} early PBs on day 5 (pregated Igκ$^+$HEL$^+$ and CD45.1$^+$CD45.2$^+$ [WT] or CD45.1$^-$CD45.2$^+$ [*Ackr4*$^{-/-}$]). Numbers in plots represent the mean (± SEM) frequency of early PB as the frequency of total responding SW_{HEL} B cells. (K) SW_{HEL}.*Ackr4*$^{-/-}$ competitive ratio is plotted

WT SW_{HEL} B cells remained at the T/B border, although some redistribution to the interfollicular zone (IFZ; defined here as the lateral poles of the Fo B cell proximal to bridging regions, also referred to as the marginal-zone bridging channel) was apparent. In contrast, an increased proportion of *Ackr4*$^{-/-}$ SW_{HEL} B cells were localized in the IFZ early during the response. On days 2–2.5, a larger proportion of *Ackr4*$^{-/-}$ SW_{HEL} B cells were localized in the IFZ and were visibly more abundant than the WT SW_{HEL} B cell response at that time, which became increasingly apparent during the next 60 h of the response. Whereas most WT SW_{HEL} B cells were positioned in the IFZ and at the T/B border on days 3–3.5, a proportion of *Ackr4*$^{-/-}$ SW_{HEL} B cells were distributed in the outer follicle, with the emergence of SW_{HEL} B cell clusters in the outer follicular regions and the IFZ and the appearance of cells exhibiting a PB phenotype in the bridging channels on day 3, which became more obvious by days 3.5–4.5. These early ACKR4-dependent changes to the migratory patterns of SW_{HEL} B cells were independent of detectable cell-intrinsic defects in CCR7, CXCR5, CXCR4, or EBI2 expression during the first 3 d of this response (Fig. 5 B). Thus, in the absence of ACKR4, a proportion of activated B cells preferentially home to the splenic IFZ during the early stages of the humoral immune response. Favorable positioning to interfollicular niches was accompanied with the enhanced expansion of *Ackr4*$^{-/-}$ SW_{HEL} B cells in these zones and exaggerated early PB responses.

CCR7 guides activated B cell homing toward the T/B border but also contributes to the lateral spreading along that interface and positioning within the splenic IFZ (Reif et al., 2002; Okada et al., 2005; Gatto et al., 2011). To determine whether ACKR4-mediated regulation of early B cell responses was dependent on CCL19 and/or CCL21, these ligands were neutralized in mixed BM chimeras. This revealed that the advantage of ACKR4-deficient B cells to enter early PB and GC B cell compartments was dependent, at least in part, on physiological CCL19/CCL21 (Fig. 5 C).

Concluding remarks

Our findings establish ACKR4 as a B cell–intrinsic regulator of early PB and GC B cell responses. First, using ACKR4-deficient anti-HEL monoclonal B cells, we demonstrate that ACKR4 limits the early migration of antigen-engaged B cells to splenic interfollicular niches. Unrestricted access of activated B cells to these niches in the absence of ACKR4 was associated with their enhanced early expansion, which we propose increased the precursor pool of activated B cells available for subsequent differentiation into early PB and GC B cell fates. Further, we demonstrate that aberrant, splenic IFZ localization by antigen-engaged ACKR4-deficient anti-HEL B cells was accompanied by the preferential formation of early PB responses.

Existing evidence indicates that migration of activated B cells is predominantly shaped by their balanced responsiveness to CCR7, EBI2, CXCR5, and CXCR4 ligands (Pereira et al., 2010). Gatto et al. (2011) demonstrated that transfer of *Cxcr5*-deficient, activated B cells results in their exclusion from B cell follicles and accumulation in marginal-zone bridging channels; however, compound deletion of *Cxcr5* with *Ccr7* was shown to direct cells away from this niche and toward the outer regions of the follicle. These data indicate that, in addition to its established role as driving activated B cell migration toward the T cell zone (Reif et al., 2002), CCR7 also contributes to positioning activated B cells toward the IFZ and bridging zones of the spleen. Our experiments with SW_{HEL} B cells indicate that deletion of ACKR4, a scavenger of CCR7 ligands, promotes responding B cell migration to splenic IFZ. We speculate that ACKR4 may function to "tune" early CCR7-dependent cues on a proportion of responding B cells, limiting their CCR7-driven homing to splenic IFZ. Our findings that physiological CCL19 and CCL21 were required, at least in part, for ACKR4-dependent changes to early PB and GC B cell responses supports a relationship between ACKR4 and CCR7 function in the regulation of activated B cell responses.

Our results indicate that the propensity of ACKR4-deficient SW_{HEL} B cells to form early PB responses correlated with their favorable accumulation in the IFZ during the early stages of T cell–dependent humoral immunity. These data, together with published findings that (a) EBI2-deficient B cells, which are defective in their ability to access splenic IFZ and bridging channels, fail to form robust early PB responses (Gatto et al., 2009); (b) forced EBI2 expression on B cells promotes early PB responses (Gatto et al., 2009); and (c) targeted antigen delivery to splenic DCIR2^{+} dendritic cells, which localize to this niche, elicit robust early PB responses, and are implicated in promoting PB survival (García De Vinuesa et al., 1999; Chappell et al., 2012), support a model in which B cell migration at the early stages of activation has an important role in coordinating and balancing differentiation to early PB and GC B cell fates.

In summary, our results describe an in vivo, cell-intrinsic role for ACKR4 in shaping activated B cell differentiation and further our understanding of the cellular events that govern antibody production.

MATERIALS AND METHODS

Mice

All mice were on the C57BL/6J background and housed in specific pathogen-free conditions at Laboratory Animal

as the ratio of *Ackr4*$^{-/-}$ to WT among SW_{HEL} GC B cell (left) or B220^{+}HEL^{hi}GL7^{-} cell (right) compartments (gated as in D), normalized to the input ratio, as determined from mock-SRBC–immunized mice. *n* = 4 mice (means ± SEM) on day 5. (A–K) *, P < 0.05; **, P < 0.01; ****, P < 0.0001; data are representative of two independent experiments. (A and J) Two-tailed, paired Student's *t* test. (B and C–H) Two-tailed, unpaired Student's *t* test. (C–K) Means ± SEM.

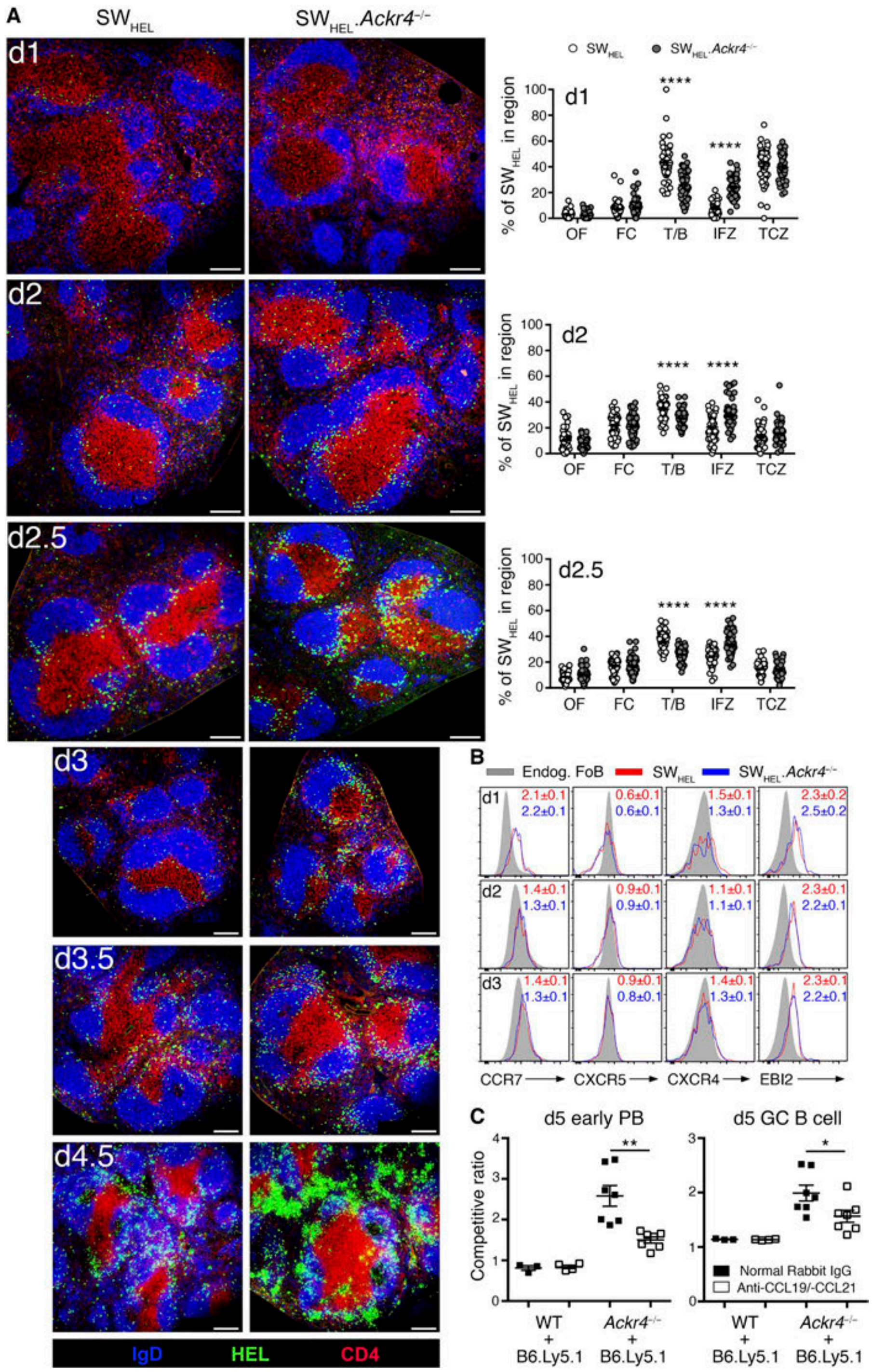

Figure 5. **ACKR4 limits early localization of antigen-engaged B cells to splenic IFZs.** **(A)** WT or *Ackr4*$^{-/-}$ SW_{HEL} B cells were transferred into WT recipients and immunized the next day with HEL^{2X}-SRBC (days 1–2.5 analysis, transfer of 5×10^5 SW_{HEL} B cells, immunization, 2×10^9 HEL^{2X}-SRBC; and days 3–4.5 analysis, transfer of 2×10^5 SW_{HEL} B cells, immunization, 10^9 HEL^{2X}-SRBC). Representative histology of responding SW_{HEL} B cells in the spleen on days 1, 2, 2.5, 3, 3.5, and 4.5 after immunization. Quantification of SW_{HEL} B cell frequency per splenic region is depicted for days 1, 2, and 2.5 (see Materials and methods; means ± SEM). Bar, 200 µm. Blue, IgD; green, HEL; red, CD4; OF, outer follicle; FC, follicle center; T/B, T/B border; TCZ, T cell zone. Images are representative of five mice/genotype per time point; two-tailed, unpaired Student's *t* test. **(B)** WT (CD45.1/2) and *Ackr4*$^{-/-}$ (CD45.2) SW_{HEL} B cells were cotransferred into B6.Ly5.1 (CD45.1) mice and immunized with HEL^{2X}-SRBC. Representative plots of CCR7, CXCR5, CXCR4, and EBI2 staining on responding SW_{HEL} B cells ($B220^+Ig\kappa^+HEL^+$) relative to endogenous Fo B cells ($CD45.1^+CD45.2^-B220^+IgD^{hi}$). Numbers indicate the fold change (means ± SEM) in surface receptor GMFI on WT and *Ackr4*$^{-/-}$ SW_{HEL} B cells relative to the concurrent endogenous Fo B cells (*n* = 5 mice/time point). **(C)** Mixed BM chimeras were generated with 80% BM from B6.Ly5.1 (CD45.1) and 20% from WT or *Ackr4*$^{-/-}$ (both CD45.2). Mice were administered polyclonal rabbit sera containing 500 µg anti–CCL19 and 500 µg anti–CCL21 or 1 mg normal rabbit IgG i.p. on days −1, 0, 2, and 4. Mice were immunized with SRBC on day 0 and analyzed on day 5. Competitive ratios of early PB (left; $B220^{lo/-}CD138^+$) and GC (right; $B220^+IgD^-Fas^+GL7^+$) B cells are plotted as the frequencies of $CD45.2^+$ cells in each compartment normalized to the frequency of $CD45.2^+$ cells in the concurrent Fo B cell ($B220^+IgD^{+-}Fas^-GL7^-$) compartment (*n* = 4–7 mice/genotype; means ± SEM). Two-tailed unpaired Student's *t* test. (A–C) Data are representative of two independent experiments. *, P < 0.05; **, P < 0.01; ****, P < 0.0001.

Services, University of Adelaide (unless indicated otherwise). C57BL/6 (WT) and B6.Ly5.1 (B6.SJL *Ptprca*) were purchased from the Animal Resource Center and bred in house. *Ackr4*$^{-/-}$, *Ccr7*$^{-/-}$, µMT, *Ackr4*$^{-/-}$.*Ccr7*$^{-/-}$ SW_{HEL} (CD45.2), SW_{HEL} (CD45.1/2), and SW_{HEL}.*Ackr4*$^{-/-}$ (CD45.2) mice were bred and maintained in house. *Cd23*^{Cre} mice were provided by M. Busslinger (Research Institute of Molecular Pathology, Vienna, Austria). *Cd23*^{Cre}.*Rosa26*$^{LSL\text{-}Ackr4/+}$ mice were generated by interbreeding and maintained in house. Mice used in experiments were gender- and age-matched animals and were between the ages of 6 and 12 wk. All animal experiments were approved by the Animal Ethics Committee of the University of Adelaide.

BM chimeras

Recipient mice were lethally irradiated with 1,000 rad (two doses of 500 rad) and reconstituted with 4–5 × 10^6 total BM cells i.v. of genotypes indicated in text. A minimum of 8 wk was allowed for reconstitution before experimentation.

Transfers, immunizations, and BrdU treatment

T cell–dependent humoral immune responses were induced with 2 × 10^9 SRBC (Applied Biological Products) or 50 µg NP-KLH (Biosearch Technologies) and precipitated in alum (Analar) i.p. HEL^{2X}, HEL^{3X}, and HEL^{4X}, with varying affinities to HyHEL10, as described (Brink et al., 2015). Conjugation of HEL proteins to SRBCs was performed as described (Brink et al., 2015). Unless otherwise indicated, HEL conjugation to SRBCs was performed using 300 µg/ml HEL. Successful conjugation was confirmed using HyHEL9 mAb (Brink et al., 2015) before immunization. Unless otherwise indicated, splenocytes or Fo B cells purified by magnetic-activated cell sorting (CD43 Negative Isolation kit; Miltenyi Biotech) from SW_{HEL} or SW_{HEL}.*Ackr4*$^{-/-}$ mice containing 10^5 HEL-binding B cells were transferred i.v. into B6.Ly5.1-recipient mice. The next day, recipient mice were immunized i.v. with 10^9 HEL-conjugated SRBCs. For assessment of SW_{HEL} B cell proliferation, splenocytes containing SW_{HEL} B cells were CFSE loaded, as described (Quah et al., 2007), before transfer and immunization the next day. For BrdU experiments, 2 mg BrdU (Sigma-Aldrich) in 0.85% saline was injected i.p. 5 h before euthanasia.

Histology

For assessment of SW_{HEL} B cell responses by histology (days 1–2.5), 5 × 10^5 HEL-binding B cells from SW_{HEL} or SW_{HEL}.*Ackr4*$^{-/-}$ mice were transferred i.v. into WT mice, which were immunized with 2 × 10^9 HEL^{2X}-SRBC i.v. the next day. For assessment of SW_{HEL} B cell responses by histology (days 3–5.5), 2 × 10^5 HEL-binding B cells from SW_{HEL} or SW_{HEL}.*Ackr4*$^{-/-}$ mice were transferred i.v. into WT mice, which were immunized with 10^9 HEL^{2X}-SRBC i.v. the next day. Organs were frozen in Tissue-Tek optimal cutting temperature–embedding medium (Sakura Finetek). Cryostat sections (8 µm) were fixed in ice-cold acetone and stained, as previously described (Bunting et al., 2013). For detection of HEL-binding B cells, sections were first blocked with 30% normal horse serum and incubated with HEL^{WT} (100 ng/ml; Sigma-Aldrich), which was detected using unconjugated rabbit anti–HEL (polyclonal; Rockland) and goat anti–rabbit Ig-Alexa Fluor 488 (Life Technologies). For SW_{HEL} histology, antibodies to IgD (11-26c; eBioscience) and CD4 (RM4-5; BD) were used. For the GC stain (Fig. 2 A), antibodies to IgD, CD3 (145-2C11; BD), BCL-6 (K112-91; BD), and CCL21 (goat polyclonal; R&D) were used. To enumerate transferred SW_{HEL} B cell positioning in spleen sections, the outer follicle, follicle center, T/B interface, IFZs, and T cell zone per white pulp region were first defined (Gatto et al., 2011) in a blinded manner on images stained with IgD/CD4, with HEL-binding fluorescence removed. HEL-binding fluorescence was then merged with these images, and the total number of HEL-binding cells per white pulp area and HEL-binding cells in defined regions were enumerated by four independent researchers. Means ± SEM values across those four independent data sets are presented.

In vivo CCL19/CCL21 neutralization

Affinity-purified anti–mouse (m) CCL21 was generated and purified in house as described (Comerford et al., 2010). Anti–mCCL19 antibodies were raised in New Zealand white rabbits by immunization with full-length, synthetically manufactured CCL19, which was active in calcium mobilization and chemotaxis assays (Clark-Lewis et al., 1994). Serum IgG was purified from preimmunized bleeds (normal rabbit IgG [NRIgG]) and mCCL19- or mCCL21-immunized rabbits using Protein A columns (Millipore). The CCL19- or CCL21-neutralizing ability of these antibodies was confirmed in chemotaxis assays before their use in vivo. Recipient, mixed-BM chimeric mice were administered 500 µg affinity-purified rabbit anti–mCCL21 and 500 µg affinity-purified, rabbit anti–mCCL19 or 1 mg NRIgG i.p. on days −1, 0, 2, and 4. Mice were immunized with SRBCs i.p. on day 0 and analyzed 5 d later.

V_H gene sequencing analysis of NP^+IgG1^+ GC B cells

Single NP^+IgG1^+ GC B cells were sorted from NP-KLH–immunized (day 14) mice using a BD FACSAria cell sorter. Two rounds of PCR were performed on cDNA using a single proximal 5′ primer for the J558 V_H gene family (Ehlich et al., 1994; Smith et al., 2000), together with nested primers specific for Cγ1 (McHeyzer-Williams et al., 1991; Smith et al., 2000). Bands of expected size were purified, sequenced, and analyzed for V_H186.2-containing sequences as described. For $V_H186.2^+$ clones, the region encoding amino acids 10–96 were compared in detail with the germline V_H186.2 sequence as described (Smith et al., 2000).

Chemotaxis assay

Fo B cells purified by magnetic-activated cell sorting were activated with 5 µg/ml goat anti–mouse IgM (Jackson ImmunoResearch) for 24 h or rested overnight (unstimulated control). Various dilutions of recombinant mouse CCL21 (provided by the late I. Clark-Lewis) or CXCL13 (PeproTech) in 150 µl chemotaxis buffer (RPMI-1640 with 0.5% BSA and 20 mM Hepes) were added to the lower chambers of Transwell chemotaxis plates (96-well, 5-µm pore size; Corning). Cells were extensively washed in chemotaxis buffer and loaded into the upper chambers at 10^5 cells/well in 50 µl chemotaxis buffer and incubated for 3 h at 37°C. To enumerate B cell migration, cells were harvested from the bottom chambers, and $B220^+$ cells were assessed by flow cytometry using a defined number of CaliBRITE beads (BD) as an internal reference. The migration index was calculated as described (Kara et al., 2013).

Chemokine-scavenging assay

FACS-sorted Fo B cells (2×10^5) were incubated in RPMI-1640 medium containing 5 or 10 ng/ml recombinant mouse CCL19 (R&D Systems) at 37°C for 3 h with inversion every 30 min. 100 µl of cell-free supernatant was then assessed for CCL19 concentration by ELISA as described previously (Comerford et al., 2010).

ELISA

Serum HEL-specific IgM and IgG1 concentrations were quantified using HyHEL10 IgM and IgG1 standards as described previously (Phan et al., 2003). NP-specific IgG was detected using NP_5-BSA or NP_{32}-BSA (10 µg/ml; Biosearch Technologies)–coating antigen. ELISAs were developed with 3,3′,5,5′-tetramethylbenzidine substrate.

Quantitative PCR

RNA was harvested using the Qiagen microRNeasy kit with on-column DNase treatment. cDNA synthesis was performed using Transcriptor First Strand cDNA synthesis kit (Roche) and used as the template in reactions with the LightCycler 480 SYBR Green Master Mix I (Roche). Relative *Ackr4* transcript abundance was calculated with reference to the housekeeping gene *Rplp0* using the formula: $2^{-\Delta CT}$ ($\Delta CT = CT_{Ackr4} - CT_{Rplp0}$); *Rplp0*, forward: 5′-AGATGCAGCAGATCCGCAT-3′, reverse: 5′-CAGTGAGCTTCCCGTTCAG-3′; *Ackr4*, forward: 5′-AGATGCAGCAGATCCGCAT-3′, reverse: 5′-CAGTGAGCTTCCCGTTCAG-3′.

Flow cytometry and sorting

Cells were stained as described previously (Kara et al., 2015) using antibodies specific for: CD45.2 (104), B220 (RA3-6B2), IgD (11-26c), IgD^b (217–170), Fas (Jo2), GL7, CD86 (GL1), CD138 (281–2), Igκ (RMK-45), CD93 (AA4.1), CD21 (7G6), CD23 (B3B4), CD11b (M1/70), CD3 (145-2C11), CD4 (RM4-5), CD44 (IM7), PD-1 (J43), CXCR5 (2G8), and CCR7 (4B12; in house); and EBI2 (chicken polyclonal; Gatto et al., 2013), CXCR4 (2B11/CXCR4), Nrp-1 (3E12), and Foxp3 (FJK-16s). Unconjugated/biotinylated antibodies were detected using goat anti–rat IgG (Life Technologies), goat anti–human IgG-Fcγ fragment specific (Jackson ImmunoResearch), streptavidin-PE (Jackson ImmunoResearch), -Alexa Fluor 647 (Jackson ImmunoResearch), -BV510, -BV421, or -BV450. All antibodies and secondary reagents were purchased from BD, eBioscience, or BioLegend unless otherwise indicated. Dead cells were excluded using LIVE/DEAD fixable near-infrared dye (Molecular Probes). 7-aminoactinomycin D (eBioscience) was used to detect DNA content. BrdU staining was conducted using the BrdU Flow kit (BD). NP-binding was detected using NP-PE made in house (Smith et al., 2000). CCL19-Fc is a chimeric protein of mouse CCL19 fused to human IgG1 constant region (Reif et al., 2002). The Annexin V apoptosis detection kit (eBioscience) was used to detect Annexin V. Foxp3/TF staining buffer set (eBioscience) was used to detect FoxP3. For detection of HEL-binding cells, 2×10^6 splenocytes were incubated with soluble HEL (200 ng/ml), followed by detection of BCR-bound HEL using mAb HyHEL9 conjugated to Alexa Fluor 647 as described (Brink et al., 2015). Data were acquired on BD LSR II, BD FACSAria, or BD LSRFortessa flow cytometers. For sorting experiments, a BD FACSAria was used. Data were analyzed using FlowJo software (Tree Star).

Statistics

Data were analyzed with Prism (GraphPad Software) using either two-tailed (unpaired or paired, as appropriate) Student's *t* tests (for normally distributed data sets comparing the mean of two samples), two-tailed nonparametric Mann-Whitney tests (for data sets that were determined by an *F* test not to have a normal distribution and where there was a comparison of the mean of two samples), or one-way analysis of variance with appropriate posttests as indicated in text (for comparisons of multiple samples). For all analyses, $P < 0.05$ was considered significant. Sample or experiment sizes were determined empirically for sufficient statistical power. No statistical tests were used to predetermine the size of experiments. No data points were excluded from statistical tests.

Online supplemental material

Fig. S1 shows that follicular T cell responses to SRBC immunization are enhanced in the absence of hematopoietic or B cell expression of ACKR4. Fig. S2 shows the generation and characterization of *Rosa26*$^{LSL\text{-}Ackr4}$ knockin mice.

ACKNOWLEDGMENTS

We thank Josef Nguyen (Royal Adelaide Hospital, Adelaide, Australia) for mouse irradiation; the staff of Laboratory Animal Services, University of Adelaide, for animal husbandry; Meinrad Busslinger for *Cd23*^{Cre} mice; and Harald Hartweger for comments on the manuscript.

This work was supported in part by a grant from the Australian National Health and Medical Research Council (APP1105312) to S.R. McColl, J.G. Cyster, and I. Comerford, J.G. Cyster is an investigator of the Howard Hughes Medical Institute. E.E. Kara is supported by an Australian postgraduate award, a Norman and Patricia Polglase scholarship, and a National Health and Medical Research Council C.J. Martin Overseas Biomedical fellowship.

The authors declare no competing financial interests.

Author contributions: E.E. Kara designed, performed, and analyzed experiments and wrote the manuscript. C.R. Bastow, D.R. McKenzie, C.E. Gregor, K.A. Fenix, R. Babb, T.S. Norton, D. Zotos, L.B. Rodda, J.R. Hermes, and K. Bourne performed experiments; D.S. Gilchrist and R.J. Nibbs generated *Rosa26*$^{LSL\text{-}Ackr4}$ mice; D.M. Tarlinton, C.G. Vinuesa, M. Alsharifi, R. Brink, G.R. Hill, and J.G. Cyster provided key reagents and critical discussions and edited the manuscript; I. Comerford and S.R. McColl conceptualized the project, designed the experiments, supervised the study, and wrote the manuscript.

Submitted: 13 June 2017

Revised: 18 October 2017

Accepted: 3 January 2018

REFERENCES

Allen, C.D., K.M. Ansel, C. Low, R. Lesley, H. Tamamura, N. Fujii, and J.G. Cyster. 2004. Germinal center dark and light zone organization is mediated by CXCR4 and CXCR5. *Nat. Immunol.* 5:943–952. https://doi.org/10.1038/ni1100

Bannard, O., R.M. Horton, C.D. Allen, J. An, T. Nagasawa, and J.G. Cyster. 2013. Germinal center centroblasts transition to a centrocyte phenotype according to a timed program and depend on the dark zone for effective selection. *Immunity.* 39:912–924. https://doi.org/10.1016/j.immuni.2013.08.038

Baumjohann, D., S. Preite, A. Reboldi, F. Ronchi, K.M. Ansel, A. Lanzavecchia, and F. Sallusto. 2013. Persistent antigen and germinal center B cells sustain T follicular helper cell responses and phenotype. *Immunity.* 38:596–605. https://doi.org/10.1016/j.immuni.2012.11.020

Brink, R., D. Paus, K. Bourne, J.R. Hermes, S. Gardam, T.G. Phan, and T.D. Chan. 2015. The SW(HEL) system for high-resolution analysis of in vivo antigen-specific T-dependent B cell responses. *Methods Mol. Biol.* 1291:103–123. https://doi.org/10.1007/978-1-4939-2498-1_9

Bryce, S.A., R.A. Wilson, E.M. Tiplady, D.L. Asquith, S.K. Bromley, A.D. Luster, G.J. Graham, and R.J. Nibbs. 2016. ACKR4 on Stromal Cells Scavenges CCL19 To Enable CCR7-Dependent Trafficking of APCs from Inflamed Skin to Lymph Nodes. *J. Immunol.* 196:3341–3353. https://doi.org/10.4049/jimmunol.1501542

Bunting, M.D., I. Comerford, N. Seach, M.V. Hammett, D.L. Asquith, H. Körner, R.L. Boyd, R.J. Nibbs, and S.R. McColl. 2013. CCX-CKR deficiency alters thymic stroma impairing thymocyte development and promoting autoimmunity. *Blood.* 121:118–128. https://doi.org/10.1182/blood-2012-06-434886

Chan, T.D., D. Gatto, K. Wood, T. Camidge, A. Basten, and R. Brink. 2009. Antigen affinity controls rapid T-dependent antibody production by driving the expansion rather than the differentiation or extrafollicular migration of early plasmablasts. *J. Immunol.* 183:3139–3149. https://doi.org/10.4049/jimmunol.0901690

Chan, T.D., K. Wood, J.R. Hermes, D. Butt, C.J. Jolly, A. Basten, and R. Brink. 2012. Elimination of germinal-center-derived self-reactive B cells is governed by the location and concentration of self-antigen. *Immunity.* 37:893–904. https://doi.org/10.1016/j.immuni.2012.07.017

Chappell, C.P., K.E. Draves, N.V. Giltiay, and E.A. Clark. 2012. Extrafollicular B cell activation by marginal zone dendritic cells drives T cell-dependent antibody responses. *J. Exp. Med.* 209:1825–1840. https://doi.org/10.1084/jem.20120774

Clark-Lewis, I., B. Dewald, M. Loetscher, B. Moser, and M. Baggiolini. 1994. Structural requirements for interleukin-8 function identified by design of analogs and CXC chemokine hybrids. *J. Biol. Chem.* 269:16075–16081.

Comerford, I., S. Milasta, V. Morrow, G. Milligan, and R. Nibbs. 2006. The chemokine receptor CCX-CKR mediates effective scavenging of CCL19 in vitro. *Eur. J. Immunol.* 36:1904–1916. https://doi.org/10.1002/eji.200535716

Comerford, I., R.J. Nibbs, W. Litchfield, M. Bunting, Y. Harata-Lee, S. Haylock-Jacobs, S. Forrow, H. Korner, and S.R. McColl. 2010. The atypical chemokine receptor CCX-CKR scavenges homeostatic chemokines in circulation and tissues and suppresses Th17 responses. *Blood.* 116:4130–4140. https://doi.org/10.1182/blood-2010-01-264390

Ehlich, A., V. Martin, W. Müller, and K. Rajewsky. 1994. Analysis of the B-cell progenitor compartment at the level of single cells. *Curr. Biol.* 4:573–583. https://doi.org/10.1016/S0960-9822(00)00129-9

García De Vinuesa, C., A. Gulbranson-Judge, M. Khan, P. O'Leary, M. Cascalho, M. Wabl, G.G. Klaus, M.J. Owen, and I.C. MacLennan. 1999. Dendritic cells associated with plasmablast survival. *Eur. J. Immunol.* 29:3712–3721. https://doi.org/10.1002/(SICI)1521-4141(199911)29:11<3712::AID-IMMU3712>3.0.CO;2-P

Gatto, D., D. Paus, A. Basten, C.R. Mackay, and R. Brink. 2009. Guidance of B cells by the orphan G protein-coupled receptor EBI2 shapes humoral immune responses. *Immunity.* 31:259–269. https://doi.org/10.1016/j.immuni.2009.06.016

Gatto, D., K. Wood, and R. Brink. 2011. EBI2 operates independently of but in cooperation with CXCR5 and CCR7 to direct B cell migration and organization in follicles and the germinal center. *J. Immunol.* 187:4621–4628. https://doi.org/10.4049/jimmunol.1101542

Gatto, D., K. Wood, I. Caminschi, D. Murphy-Durland, P. Schofield, D. Christ, G. Karupiah, and R. Brink. 2013. The chemotactic receptor EBI2 regulates the homeostasis, localization and immunological function of splenic dendritic cells. *Nat. Immunol.* 14:446–453. https://doi.org/10.1038/ni.2555

Gosling, J., D.J. Dairaghi, Y. Wang, M. Hanley, D. Talbot, Z. Miao, and T.J. Schall. 2000. Cutting edge: identification of a novel chemokine receptor that binds dendritic cell- and T cell-active chemokines including ELC, SLC, and TECK. *J. Immunol.* 164:2851–2856. https://doi.org/10.4049/jimmunol.164.6.2851

Hannedouche, S., J. Zhang, T. Yi, W. Shen, D. Nguyen, J.P. Pereira, D. Guerini, B.U. Baumgarten, S. Roggo, B. Wen, et al. 2011. Oxysterols direct immune cell migration via EBI2. *Nature.* 475:524–527. https://doi.org/10.1038/nature10280

Hargreaves, D.C., P.L. Hyman, T.T. Lu, V.N. Ngo, A. Bidgol, G. Suzuki, Y.R. Zou, D.R. Littman, and J.G. Cyster. 2001. A coordinated change in chemokine responsiveness guides plasma cell movements. *J. Exp. Med.* 194:45–56. https://doi.org/10.1084/jem.194.1.45

Heinzel, K., C. Benz, and C.C. Bleul. 2007. A silent chemokine receptor regulates steady-state leukocyte homing in vivo. *Proc. Natl. Acad. Sci. USA.* 104:8421–8426. https://doi.org/10.1073/pnas.0608274104

Kara, E.E., I. Comerford, C.R. Bastow, K.A. Fenix, W. Litchfield, T.M. Handel, and S.R. McColl. 2013. Distinct chemokine receptor axes regulate Th9 cell trafficking to allergic and autoimmune inflammatory sites. *J. Immunol.* 191:1110–1117. https://doi.org/10.4049/jimmunol.1203089

Kara, E.E., D.R. McKenzie, C.R. Bastow, C.E. Gregor, K.A. Fenix, A.D. Ogunniyi, J.C. Paton, M. Mack, D.R. Pombal, C. Seillet, et al. 2015. CCR2 defines in vivo development and homing of IL-23-driven GM-CSF-producing Th17 cells. *Nat. Commun.* 6:8644. https://doi.org/10.1038/ncomms9644

Kelly, L.M., J.P. Pereira, T. Yi, Y. Xu, and J.G. Cyster. 2011. EBI2 guides serial movements of activated B cells and ligand activity is detectable in lymphoid and nonlymphoid tissues. *J. Immunol.* 187:3026–3032. https://doi.org/10.4049/jimmunol.1101262

Kerfoot, S.M., G. Yaari, J.R. Patel, K.L. Johnson, D.G. Gonzalez, S.H. Kleinstein, and A.M. Haberman. 2011. Germinal center B cell and T follicular helper cell development initiates in the interfollicular zone. *Immunity.* 34:947–960. https://doi.org/10.1016/j.immuni.2011.03.024

Kitamura, D., J. Roes, R. Kühn, and K. Rajewsky. 1991. A B cell-deficient mouse by targeted disruption of the membrane exon of the immunoglobulin mu chain gene. *Nature.* 350:423–426. https://doi.org/10.1038/350423a0

Kwon, K., C. Hutter, Q. Sun, I. Bilic, C. Cobaleda, S. Malin, and M. Busslinger. 2008. Instructive role of the transcription factor E2A in early B lymphopoiesis and germinal center B cell development. *Immunity.* 28:751–762. https://doi.org/10.1016/j.immuni.2008.04.014

Lucas, B., A.J. White, M.H. Ulvmar, R.J. Nibbs, K.M. Sitnik, W.W. Agace, W.E. Jenkinson, G. Anderson, and A. Rot. 2015. CCRL1/ACKR4 is expressed in key thymic microenvironments but is dispensable for T lymphopoiesis at steady state in adult mice. *Eur. J. Immunol.* 45:574–583. https://doi.org/10.1002/eji.201445015

McHeyzer-Williams, M.G., G.J. Nossal, and P.A. Lalor. 1991. Molecular characterization of single memory B cells. *Nature.* 350:502–505. https://doi.org/10.1038/350502a0

Nibbs, R.J., and G.J. Graham. 2013. Immune regulation by atypical chemokine receptors. *Nat. Rev. Immunol.* 13:815–829. https://doi.org/10.1038/nri3544

Okada, T., M.J. Miller, I. Parker, M.F. Krummel, M. Neighbors, S.B. Hartley, A. O'Garra, M.D. Cahalan, and J.G. Cyster. 2005. Antigen-engaged B cells undergo chemotaxis toward the T zone and form motile conjugates with helper T cells. *PLoS Biol.* 3:e150. https://doi.org/10.1371/journal.pbio.0030150

Paus, D., T.G. Phan, T.D. Chan, S. Gardam, A. Basten, and R. Brink. 2006. Antigen recognition strength regulates the choice between extrafollicular plasma cell and germinal center B cell differentiation. *J. Exp. Med.* 203:1081–1091. https://doi.org/10.1084/jem.20060087

Pereira, J.P., L.M. Kelly, Y. Xu, and J.G. Cyster. 2009. EBI2 mediates B cell segregation between the outer and centre follicle. *Nature.* 460:1122–1126. https://doi.org/10.1038/nature08226

Pereira, J.P., L.M. Kelly, and J.G. Cyster. 2010. Finding the right niche: B-cell migration in the early phases of T-dependent antibody responses. *Int. Immunol.* 22:413–419. https://doi.org/10.1093/intimm/dxq047

Phan, T.G., M. Amesbury, S. Gardam, J. Crosbie, J. Hasbold, P.D. Hodgkin, A. Basten, and R. Brink. 2003. B cell receptor-independent stimuli trigger immunoglobulin (Ig) class switch recombination and production of IgG autoantibodies by anergic self-reactive B cells. *J. Exp. Med.* 197:845–860. https://doi.org/10.1084/jem.20022144

Quah, B.J., H.S. Warren, and C.R. Parish. 2007. Monitoring lymphocyte proliferation in vitro and in vivo with the intracellular fluorescent dye carboxyfluorescein diacetate succinimidyl ester. *Nat. Protoc.* 2:2049–2056. https://doi.org/10.1038/nprot.2007.296

Reif, K., E.H. Ekland, L. Ohl, H. Nakano, M. Lipp, R. Förster, and J.G. Cyster. 2002. Balanced responsiveness to chemoattractants from adjacent zones determines B-cell position. *Nature.* 416:94–99. https://doi.org/10.1038/416094a

Smith, K.G., T.D. Hewitson, G.J. Nossal, and D.M. Tarlinton. 1996. The phenotype and fate of the antibody-forming cells of the splenic foci. *Eur. J. Immunol.* 26:444–448. https://doi.org/10.1002/eji.1830260226

Smith, K.G., A. Light, L.A. O'Reilly, S.M. Ang, A. Strasser, and D. Tarlinton. 2000. bcl-2 transgene expression inhibits apoptosis in the germinal center and reveals differences in the selection of memory B cells and bone marrow antibody-forming cells. *J. Exp. Med.* 191:475–484. https://doi.org/10.1084/jem.191.3.475

Taylor, J.J., M.K. Jenkins, and K.A. Pape. 2012. Heterogeneity in the differentiation and function of memory B cells. *Trends Immunol.* 33:590–597. https://doi.org/10.1016/j.it.2012.07.005

Taylor, J.J., K.A. Pape, H.R. Steach, and M.K. Jenkins. 2015. Humoral immunity. Apoptosis and antigen affinity limit effector cell differentiation of a single naïve B cell. *Science.* 347:784–787. https://doi.org/10.1126/science.aaa1342

Townson, J.R., and R.J. Nibbs. 2002. Characterization of mouse CCX-CKR, a receptor for the lymphocyte-attracting chemokines TECK/mCCL25, SLC/mCCL21 and MIP-3beta/mCCL19: comparison to human CCX-CKR. *Eur. J. Immunol.* 32:1230–1241. https://doi.org/10.1002/1521-4141(200205)32:5<1230::AID-IMMU1230>3.0.CO;2-L

Ulvmar, M.H., K. Werth, A. Braun, P. Kelay, E. Hub, K. Eller, L. Chan, B. Lucas, I. Novitzky-Basso, K. Nakamura, et al. 2014. The atypical chemokine receptor CCRL1 shapes functional CCL21 gradients in lymph nodes. *Nat. Immunol.* 15:623–630. https://doi.org/10.1038/ni.2889

Victora, G.D., and M.C. Nussenzweig. 2012. Germinal centers. *Annu. Rev. Immunol.* 30:429–457. https://doi.org/10.1146/annurev-immunol-020711-075032

Victora, G.D., T.A. Schwickert, D.R. Fooksman, A.O. Kamphorst, M. Meyer-Hermann, M.L. Dustin, and M.C. Nussenzweig. 2010. Germinal center dynamics revealed by multiphoton microscopy with a photoactivatable fluorescent reporter. *Cell.* 143:592–605. https://doi.org/10.1016/j.cell.2010.10.032

SUPPLEMENTAL MATERIAL

Kara et al., https://doi.org/10.1084/jem.20171067

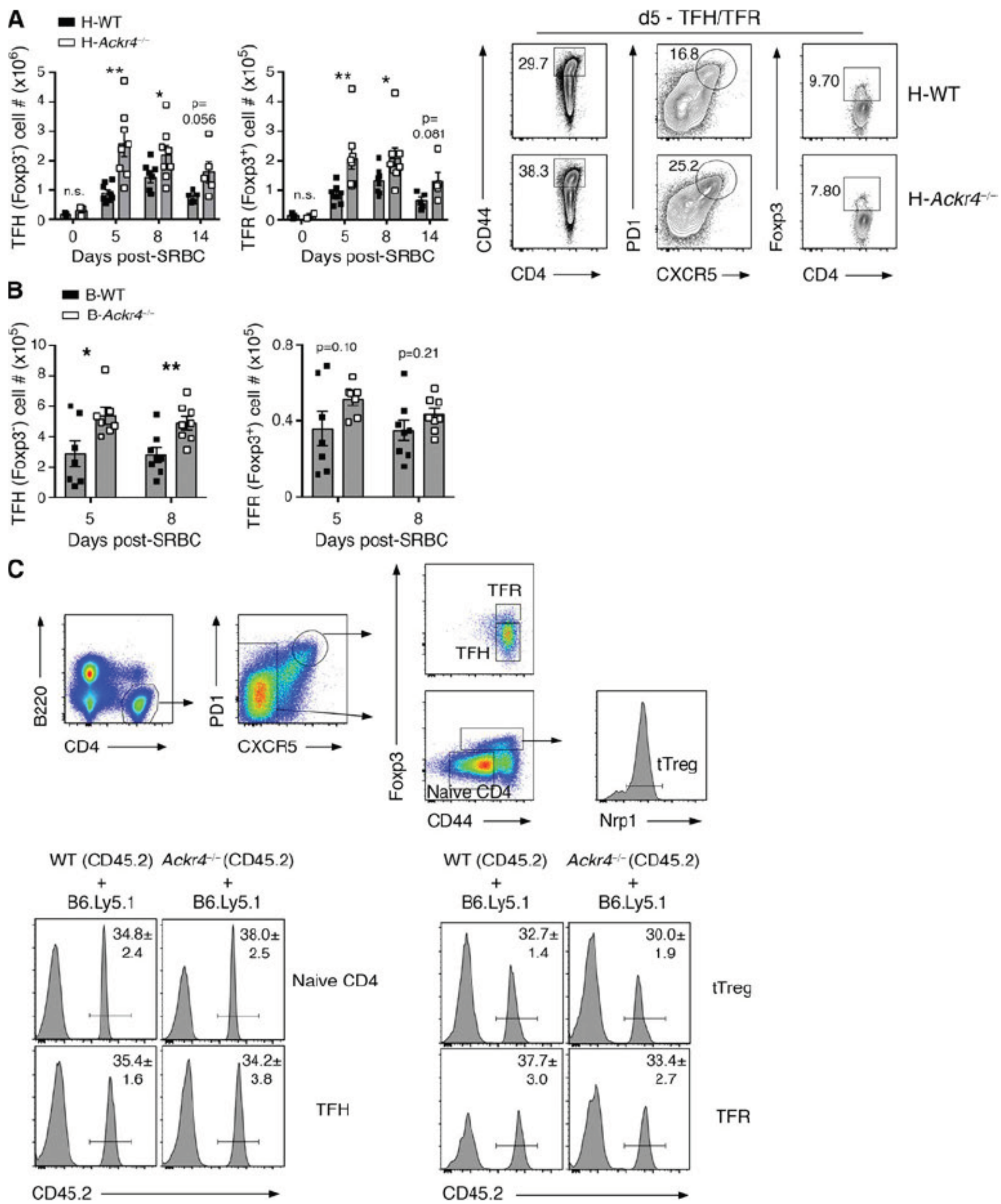

Figure S1. **Follicular T cell responses are enhanced in the absence of B cell ACKR4 (related to Figs. 1 and 3 A). (A)** TFH ($B220^{-}CD4^{+}CD44^{hi}PD1^{hi}CXCR5^{hi}Foxp3^{-}$) and TFR ($B220^{-}CD4^{+}CD44^{hi}PD1^{hi}CXCR5^{hi}Foxp3^{+}$) cell numbers in spleen of H-WT and H-*Ackr4*$^{-/-}$ mice after SRBC immunization as described in Fig. 1 (C and D; means ± SEM). Representative plots are from day 5 after SRBC immunization. Data were analyzed using a two-tailed, unpaired Student's *t* test or a two-tailed, nonparametric Mann-Whitney test. **(B)** TFH and TFR cell numbers in B-WT and B-*Ackr4*$^{-/-}$ mice described in Fig. 1 (E and F; means ± SEM). Data were analyzed using a two-tailed, unpaired Student's *t* test or a two-tailed, nonparametric Mann-Whitney test, as appropriate. **(C)** Representative flow-cytometric gating strategy identifying naive $CD4^{+}$ T cells, thymic-derived T regulatory (tTreg) cells, TFH, and TFR cells in mixed BM chimeras, as described in Fig. 3 A. Left: Representative histograms of $CD45.2^{+}$ cells among concurrent naive $CD4^{+}$ T cell and TFH compartments. Right: Representative histograms of $CD45.2^{+}$ cells among concurrent tTreg cell and TFR compartments. Numbers in plots indicate means ± SEM frequencies of $CD45.2^{+}$ cells among indicated cell populations (n = 6 mice/group). Data are representative of two independent experiments.

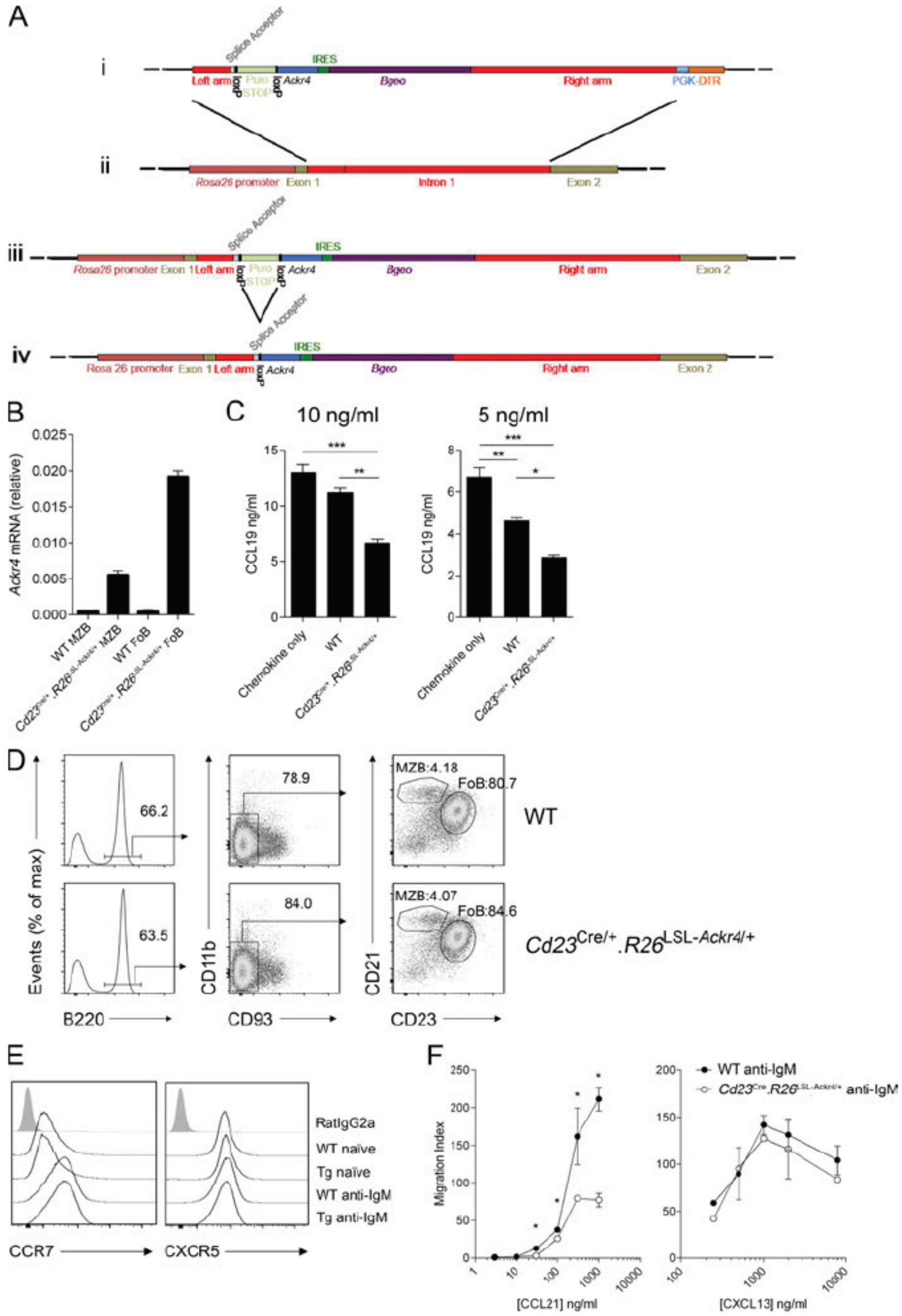

Figure S2. ***Cd23*^Cre/+^.*Rosa26*^LSL-Ackr4/+^ mice (related to Fig. 3 C).** **(A)** Rosa26 targeting strategy. (i) *Rosa26*^LSL-*Ackr4*^ targeting construct; (ii) WT *Rosa26* locus; (iii) targeted *Rosa26* locus; and (iv) targeted *Rosa26* locus after *Cd23*-Cre–mediated recombination. loxP:loxP, targets for Cre-mediated recombination; Puro-STOP, puromycin resistance gene, followed by STOP cassette (transcriptional pause sequence with two polyA sites); IRES, internal ribosome entry site; *Bgeo*, fusion of β-gal and neomycin resistance cDNA; PGK-DTR, diphtheria toxin receptor control by the PGK promoter. **(B)** Quantitative PCR analysis of *Ackr4* transcript abundance in sorted marginal zone B cells and Fo B cells (n = 3 mice/genotype; gated as shown in D). Data are presented relative to the housekeeping gene *Rplp0* (means ± SD). **(C)** CCL19 scavenging assay. Sorted Fo B cells from WT (n = 3) or $Cd23^{Cre/+}.Rosa26^{LSL\text{-}Ackr4/+}$ (n = 3) mice were incubated with 10 or 5 ng/ml recombinant CCL19 for 3 h at 37°C. CCL19 concentration in cell-free supernatants was determined by ELISA. Samples with no addition of cells (chemokine only) were used to determine input CCL19 concentration. One-way ANOVA with the Bonferroni multiple comparisons test (means ± SEM). **(D)** Representative flow cytometric analysis of marginal zone B cell ($B220^+CD11b^-CD93^-CD23^{lo/-}CD21^+$) and Fo B cell ($B220^+CD11b^-CD93^-CD23^+CD21^{lo/-}$) frequencies in spleen of WT (n = 3) and $Cd23^{Cre/+}.Rosa26^{LSL\text{-}Ackr4/+}$ (n = 3) mice. max, maximum. **(E)** Representative flow cytometric analysis of CCR7 and CXCR5 expression on unstimulated (rested overnight) and anti–IgM-stimulated (5 µg/ml; 24 h) WT and $Cd23^{Cre/+}•Rosa26^{LSL\text{-}Ackr4/+}$ B cells. **(F)** Anti–IgM-stimulated (24 h) WT and $Cd23^{Cre/+}.Rosa26^{LSL\text{-}Ackr4/+}$ B cell transwell chemotaxis to CCL21 and CXCL13 (means ± SEM). Unpaired, two-tailed Student's *t* test. (C and F) *, $P < 0.05$; **, $P < 0.01$; ***, $P < 0.001$.